UNIVERSITÀ
DEGLI STUDI
DI PADOVA

Head Office: *Università degli Studi di Padova*

Department of Industrial Engineering

Ph.D. COURSE IN: *Space Sciences, Technologies and Measurements*

CURRICULUM: *Sciences and Technologies for Aeronautics and Satellite Applications (STASA)*

SERIES *XXX*

NEW ENERGY ABSORBING MATERIALS AND THEIR USE IN PERSONAL PROTECTIVE EQUIPMENT

Thesis written with the financial contribution of the People Programme (Marie Sklodowska Curie Actions) of the European Union's Seventh Framework Programme FP7/2007-2013/ under REA grant agreement n° [FP7-PEOPLE-2013-ITN-608092].

Coordinator: *Prof. Giampiero Naletto*

Supervisor: *Prof. Ugo Galvanetto*

Ph.D. student: *Siamak Farajzadeh Khosroshahi*

To the global peace that I hope to see one day.

Abstract

Personal Protective Equipment (PPE) indicates protective clothing, helmets, goggles, or other garments or equipment designed to protect the wearer's body from injury, in particular they are used to dissipate the energy of the impact in case of accidents. Most of PPE items should pass certain standard criteria before being introduced into the market. Moreover, beside standards, biomechanical injury criteria can be used to compare different PPE items according to the human body tolerance against external loading.

Energy absorbing materials with higher capacity of energy dissipation can improve the injury mitigation capability of PPE items. Therefore, this thesis aims at studying the possibility of using new energy absorbing materials to optimize the protection level of protective devices, especially for motorcycle riders. The Finite Element Method (FEM) was mainly used to assess and compare the energy absorption capability of different materials and structures. However, experimental tests were carried out whenever possible for validation of FE models.

A computational method has been developed for partial optimization of the composite-shell of an helmet to mitigate the induced neck axial force due to the facial impact. The results of this optimization show that by varying the orientation of the chin bar plies, thus keeping the helmet mass constant, the neck axial force can be reduced by approximately 30% while ensuring that the helmet complies with the impact attenuation requirements prescribed in helmet standards adopted in Europe.

Moreover, the possibility of using addictively manufactured structures as the helmet liner has been studied. The results show that using a hierarchical lattice liner could reduce the risk of head injury significantly by comparison to a helmet with EPS liner and could potentially be considered as the new generation of energy absorbing liners for advanced helmets.

Furthermore, experimental tests were carried out to study the feasibility of using new polymeric fibres to make helmets lighter. The results of these tests show that such polymeric fibres may be used in conjunction with carbon fibres to mold hybrid laminates to build lighter helmets.

Finally, since there is no standard to design and test neck protective devices, the response of cervical vertebrae to direct impacts to the helmets in case of using such a device was studied numerically. The findings of this work show that using a neck brace designed to restrain the head-neck motion might increase the induced load in the neck and therefore the risk of cervical injuries, therefore the design of such devices needs more investigations and their assessment requires the introduction of the relevant standards.

Summary

Introduction

Energy absorbing or energy dissipative materials and structures are used in a wide range of applications like aerospace, defense and automotive industries, packaging, building construction, sports etc. They protect vulnerable and fragile products during shipment and human body parts during road accidents or dynamic sports against shock. Among all road users, motorcyclists are the most vulnerable. Accident data analysis shows that the risk of motorcycle riders' death is almost thirty times higher than that of car occupants in road traffic accidents, while head injury statistically is the principal cause of death and disability in motorcyclists [1–3]. Motorcycle helmets are to date the most effective item of protective equipment for head protection [4] and their energy absorption capability can further be improved to reduce the risk of head injuries. Therefore, present thesis aims at assessing the use of new energy absorbing materials in personal protective equipment (in particular helmets) to improve their protection level.

In the last years, the Finite Element Method (FEM) has been used as a powerful tool design protection equipment [5] and to study human body response during accidents. Therefore, the present work aims at assessing the use of new energy absorbing materials, by means of FEM, to improve PPE's protection capability.

Realistic material characterization of currently used energy absorbing materials

Expanded polystyrene (EPS) is the most widely used energy absorbing material in helmets and several researches have been carried out to study its capability of energy absorption using FEM. Even though the helmets may experience different impacts, including oblique impacts, many numerical simulations reported in the literature [5–8] made use only of the axial mechanical properties of EPS. The shearing response of EPS is a function of the axial strain and there was no experimental data in literature, which explicitly presented the shear stiffening of EPS due to axial compression. A part of this thesis is dedicated to present the empirical stress-strain curves for EPS, these experimental data can be used to improve in a decisive way the definition of the constitutive law of EPS foams for the simulation of helmets tests, especially in case of oblique impacts.

Assessment of neck protective devices

Neck protective devices have been recently introduced for motorcycle riders but there is no standard method to evaluate their performance. The goal of this study was to identify the response of the riders' cervical spine to direct impacts on the helmet with and without such a device. The methodology used was simulation by means of the finite element method. The finite element method was used to simulate three common types of cervical injury mechanisms i.e. hyperflexion, hyperextension and lateral bending [9]. The simulations were carried out for cases with and without the neck brace for the investigated loading conditions. The stress distribution at cervical vertebrae showed that using the investigated type of neck protective device could increase the risk of neck injury in some loading cases. The rotational movement of the head with respect to the torso and shearing and axial neck loads also showed that using the neck brace

could increase the force in the neck. The findings of the present work show that using a neck brace designed to restrain the head-neck motion might increase the induced load in the neck and therefore the risk of cervical injuries. Hence, the design of such devices needs more investigations and their assessment requires the introduction of the relevant standards.

Optimization of the helmet with respect to induced neck force

A numerical approach has been developed in the present work to optimize the chin bar of a composite-shell helmet with respect to the force induced at the connection between head and neck, a possible indicator of the most common type of injury among motorcycle riders, which is not clearly addressed in any standard. Basilar skull fracture (BSF) is one of the most common type of skull fractures sustained by motorcycle riders [10–13] and according to cadaveric tests, the neck tensile load at the base of the skull, which might be induced in case of a facial impact, is the most probable loading condition that can produce BSF [14]. Statistics showed that the chin bar of full-face helmets has the highest probability of impacts during accidents. Almost 50% of the severe impacts took place on the front of the helmet, involving the chin bar, and 40% of these impacts led to BSF [10]. Therefore, due to the high probability of basilar skull fracture related to chin bar impacts in motorcycle crashes and due to the lack of test methods that address chin bar design, in this thesis, a numerical method is presented to test whether it is possible to decrease the upper neck tensile force, a possible indicator of BSF, while meeting the standard requirements.

Feasibility study of using lattice structures as helmets' liner

Experimental and numerical investigations showed that using energy absorbing liners with varying mechanical properties (yield stress) through the thickness could improve the energy absorption capability of helmets [15,16]. Therefore, in the present thesis the feasibility of using a lattice structure which, provides varying mechanical properties though the thickness thanks to its hierarchical structure, has been investigated. Two different materials were used to print out the samples of the concept design, then the samples were tested for material characterization and material selection. A validated FE model of the hierarchical structure was developed according to the experimental results. Then the finite element method was used to study the capability of the concept model to reduce head accelerations. The results show that using the concept liner can reduce the linear and rotational accelerations of the center of gravity of the headfrom, compared to those obtained when using a liner made of EPS with similar mass. Moreover, simulations using a human body model (THUMS) showed that biomechanical indicators of brain injuries i.e. equivalent strain, stress and maximum shearing stress were reduced when the hierarchical lattice liner was used. These results show that additively manufactured materials could be used as new energy absorbing liners for the next generation of helmets.

Acknowledgement

I would like to thank my advisor Prof. Ugo Galvanetto for his advices throughout this research and my life. I will never forget his kind support, which I could always count on.

The work presented in this thesis received funding from the People Programme (Marie Sklodowska Curie Actions) of the European Union's Seventh Framework Programme FP7/2007-2013/ under REA grant agreement n° [FP7-PEOPLE-2013-ITN-608092].

I would like also to thank Dr. Mazdak Ghajari form Imperial College London for his advice and friendship.

I acknowledge Prof, Mirco Zaccariotto, Prof. Michele Modesti, Mr. Denis Hrelja, Prof. Giovanni Meneghetti and Prof. Mauro Ricotta from University of Padova, Mr. Alessandro Cernicchi form Dainese S.p.A., Mr. Antonio Bruco from Honeywell Co., Dr. Robin Olsson, Dr. Spyros Tsampas, Dr. Maciej Wysocki, Dr. Vasan Churchill and Mr. Peter Hellstrom all from SWEREA-SICOMP for their help and cooperation.

I would like to thank my friends Daniele Dipasquale, Giulia Sarego and Teo Mudric who helped me a lot especially during the first months after my arrival in Italy.

I would like to thank my parents for their love, dedication and encouragement throughout my life. I also thank my brothers for their support, love and their sense of humor that always makes my life fresh.

Finally, I would like to thank my wife, Razieh, whose love always keeps me going.

Publications

Journal papers:

- S. Farajzadeh Khosroshahi, U. Galvanetto, M. Ghajari, '*Optimization of the Chin Bar of a Composite-Shell Helmet to Mitigate the Upper Neck Force*', Applied Composite Materials, November 2016.
- M. Nasim, M. Brasca, S.F. Khosroshahi, U. Galvanetto, "*Understanding the impact properties of polymeric sandwich structures used for motorcyclists' back protectors*", Polymer Testing, 2017.
- S. Farajzadeh Khosroshahi, M. Ghajari, U. Galvanetto, "*Response of braced cervical spine in motorcycle accidents: A finite element study*", [Manuscript].
- S. Farajzadeh Khosroshahi, S. Tsampas, U. Galvanetto, "*Feasibility study of using a hierarchical lattice struructure as the helmet liner*", [Manuscript].
- S. Farajzadeh Khosroshahi, R. Olsson, U. Galvanetto, "*Biaxial behavior of EPS foams*", [under preparation].

Conference presentations and proceedings:

- S. Farajzadeh Khosroshahi, M. Ghajari, U. Galvanetto, "*A Numerical Approach for the Optimization of a Composite Chin Bar for Protection against Basilar Skull Fracture*", IRCOBI, Malaga, Spain, September 2016.
- S. Farajzadeh Khosroshahi, M. Ghajari, U. Galvanetto, "*Finite Element Simulation of Neck Brace Protective Equipment for Motorcycle Riders*", 1st International Conference on Impact Loading of Structures and Materials, Turin, Italy, May 2016.
- S. Farajzadeh Khosroshahi, M. Ghajari, U. Galvanetto, "*Assessment of Motorcycle Helmet's Chin Bar Design Criteria with Respect to Basilar Skull Fracture Using FEM*", LS-Dyna European Users Conference, Wurzburg, Germany, June 2015.

Other publications:

- S. Farajzadeh Khosroshahi, U. Galvanetto, "*New Energy Dissipative Materials*", Deliverable no. D.3.3, MOTORIST EU, 2016.
- S. Farajzadeh Khosroshahi, U. Galvanetto, "*Use of new dissipative materials in PPE*", Deliverable no. D.3.4, MOTORIST EU, 2017.

Table of Contents

List of figures

List of tables

1. Introduction

Over thirty thousand people die and more than 1.5 million people are injured every year in Europe because of road traffic accidents [17]. Motorcyclists are among the most vulnerable road users. Accident data analysis shows that motorcycle riders are in peril of death almost thirty times more than car occupants in road traffic accidents, with head injury being the leading cause of death and disability in motorcyclists [1–3]. Motorcycle helmets are the most effective item head protection [4]. In particular, the liner of the helmet is the main part of the helmet which dissipates the energy of the impact and mitigates the load transmitted to the head. Therefore, improving the material, which absorbs the impact energy, as much as possible, would improve the helmet's protection level.

Even though helmets already reduce the risk of fatality in motorcycle accidents, they could still be improved. Therefore, several researchers have been studying the effect of using different energy absorbing materials to increase the helmets' level of protection. Caserta et al. [18] studied the effect of using the honeycomb material in the liner and Coelho et al. [19] assessed the feasibility of using a composite liner made of EPS and cork, with the objective to reduce head linear acceleration.

Moreover, neck injuries are other types of common fatal injuries for motorcycle riders. Neck is made of seven cervical vertebrae, intervertebral discs and a complex muscular system, which supports the head and provides the capability of the four basic movements of the head-neck system, namely flexion, extension, lateral bending and rotation [20,21]. A wide range of injuries can occur at the cervical musculoskeletal system. Some types of neck injuries are vertebral fracture, intervertebral disk rupture, ligament disruption, vertebral dislocation, joint disruption, spinal cord laceration and vertebral artery laceration [11,22–27]. Therefore, Personal Protective Equipment (PPE) manufactures introduced neck braces which restrict the movement of the head-neck in order to reduce the risk of cervical injuries, but there is no specific standard for manufacturing and testing such devices.

According to what has been mentioned, various institutions and associations have financed research in the field of motorcyclists' safety in the last decade. The European Union is one of these communities which have contributed to research projects in the field of motorcycle's safety. MOTORIST (www.motorist-ptw.eu/) is a European network, which aims at improving the safety of motorcyclists. It is a multi disciplinary project, which has been involved in different fields namely, riders' training, active safety systems and passive safety. The present thesis is a part of the third work package of MOTORIST, that on PPE, and is focused on assessment and improvement of passive safety systems particularly for the head and the neck.

The innovative ideas of this thesis cover the following topics:

- Realistic material characterization of currently used energy absorbing materials.
- Assessment of neck protective devices.
- Optimization of the helmet with respect to induced neck force.

- Feasibility study of using hierarchical lattice structures as helmets' liner to reduce the risk of head injury.

Expanded Polystyrene (EPS) foam is the most widely used material for the safety helmets' liner. Moreover, FEM has been used as an accepted tool for testing helmets virtually [5,8], thus a reliable material characterization method for EPS, which is the most important energy absorbing of the helmet, should be adopted. Even though, the helmets may be subjected to oblique impacts and the liner may experience a multiaxial stress field, still a uniaxial compression test method is used for helmet's liner response characterization. Indeed, since currently used standards require direct impacts for helmets evaluation, uniaxial compression test for EPS characterization would provide reliable material properties for FE modeling of impact tests according to these standards. However, for more realistic FE simulations, especially in case of an oblique impact, a multiaxial stress filed in the EPS should be considered. Therefore, due to lack of realistic experimental data to replicate the liner's response accurately in the literature, a part of this thesis is dedicated to realistic material characterization of EPS foams. The result of this experimental tests are presented in Chapter 5.4. The tests were carried out at SWEREA-SICOMP by means of a multiaxial test rig and Dainese S.p.A. provided the EPS specimens. Both companies were partners of the MOTORIST network.

Moreover, in this thesis the neck axial load induced by facial impact on the helmet, which is a possible cause of Basilar Skull Fracture (BSF), has been addressed. This type of injury is not clearly addressed by standards despite it is the most common type of skull fracture among motorcyclists' accidents. Therefore, a numerical method has been developed in order to optimize the helmet's outer shell to mitigate the neck axial load. The optimization was carried out using validated finite element models of a motorcycle helmet, a head-neck model of Hybrid III 50 percentile male dummy and an ISO headfrom. The mechanism of injury and the optimization algorithm have been described in Chapters 2.1 and 8.1, respectively.

Since there is no specific standard for evaluation of neck protector devices for motorcycle riders, an assessment of a neck protector device was carried out within the present work. The assessment was done by means of finite element model. The model of a neck protective device has been generated and validated according to experimental tests. A Total HUman Model for Safety (THUMS) has been used as a human body surrogate. The result of this assessment is presented in Chapter 7.

The last part of this thesis is dedicated to the feasibility study of using new materials for helmets in order to improve their level of protection. SPECTRA, which was kindly provided by HONEYWELL Co., was studied to be used for the outer shell of the helmet and a hierarchical lattice structure was assessed to be used as the energy absorbing liner of the helmet. Experimental tests were carried out in order to compare SPECTRA with carbon fibre laminates, which are currently used in helmets' outer shell. A numerical-experimental method was used in order to compare the energy absorption capability of a lattice structure with an EPS foam and to study the effect of using such materials on the load transmitted to the head and brain. These are presented in Chapter 8.2 and 8.3.

Generally, the present thesis describes the mechanisms of head and neck injuries, and then introduces the head and neck protective devices and relevant standards. Later, the energy absorbing materials and the mechanisms of energy absorption are presented. Next, the assessment of the protective devices is presented and finally the feasibility of using new energy absorbing materials is discussed.

2. Injury mechanisms

2.1. Head Injuries

The human head consists of many different parts as shown in Figure 2-1 and Figure 2-2 but from a biomechanical point of view, some of them are more important: scalp, skull, blood vessels, meninges, cerebrospinal fluid (CSF), cerebrum, cerebellum and brain stem [28]. The inner surface of the cranial vault has a concave curvature with an irregular shaped bone forming the base. This base of skull contains a large hole, which is called foramen magnum through which the brainstem passes into the spinal cord. Moreover, basilar arteries also pass through foramen magnum [29].

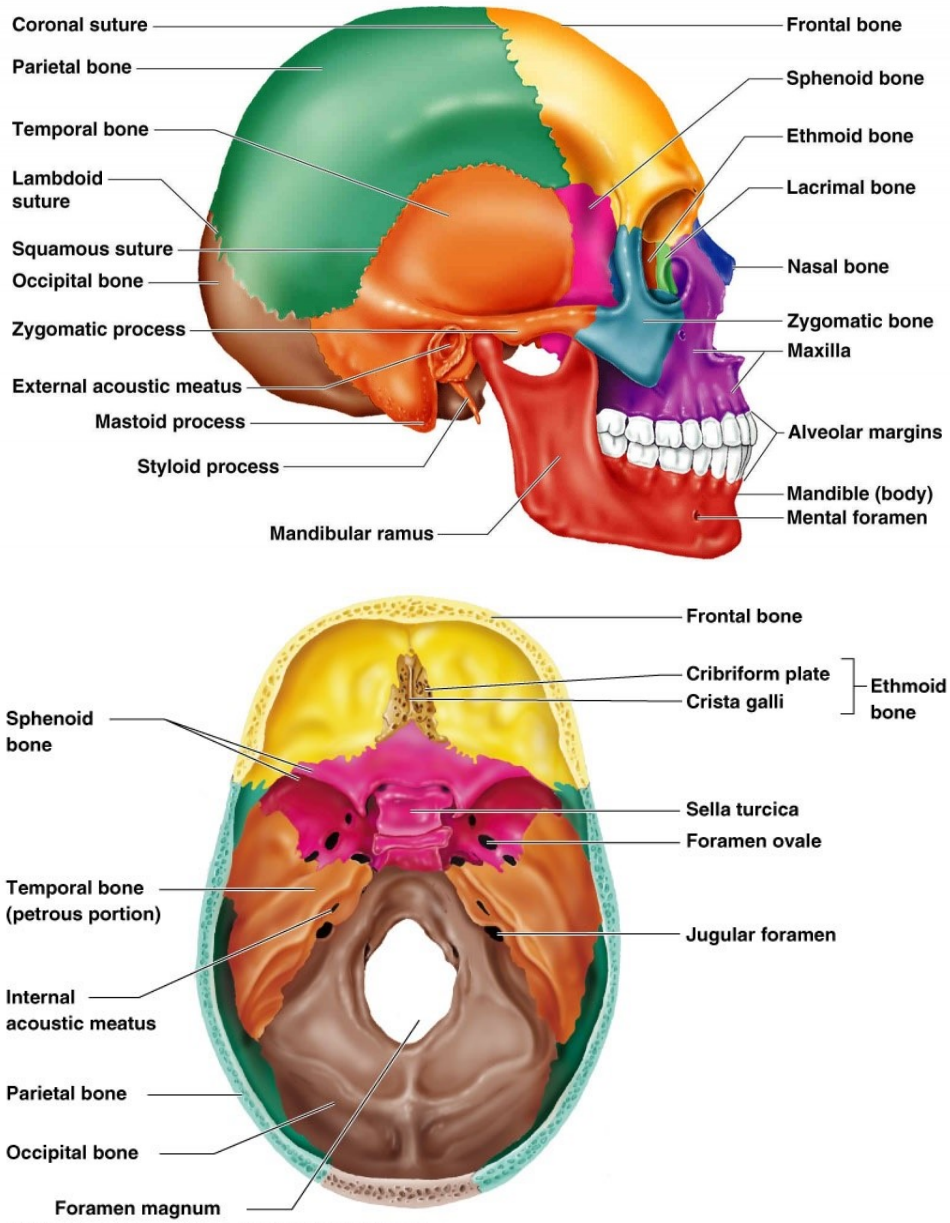

Figure 2-1 Skull anatomy, top: side view, bottom: superior view [30].

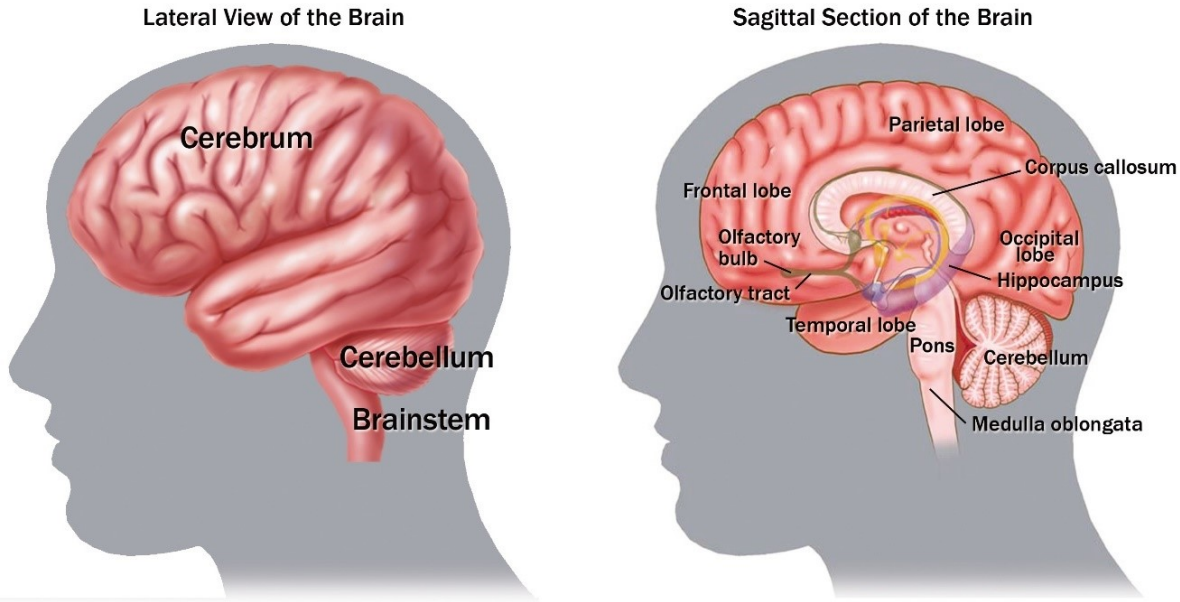

Figure 2-2 Brain anatomy [31].

Three membranes called the meninges, the dura mater, the arachnoidea mater, and the pia mater, protect and support the spinal cord and the brain and separate them from the surrounding bones (Figure 2-3). The dura mater is a tough, fibrous membrane, while the arachnoidea mater resembles a spider-web. Both membranes are separated by a narrow space, the subdural space. The subarachnoidal space separates the arachnoidea mater and the pia mater. The pia mater covers the surface of the brain, dipping well into its fissures. Cerebrospinal fluid (CSF) fills the subarachnoidal space and the ventricles of the brain and thus cushions the brain (and the spinal cord) from mechanical shock [29].

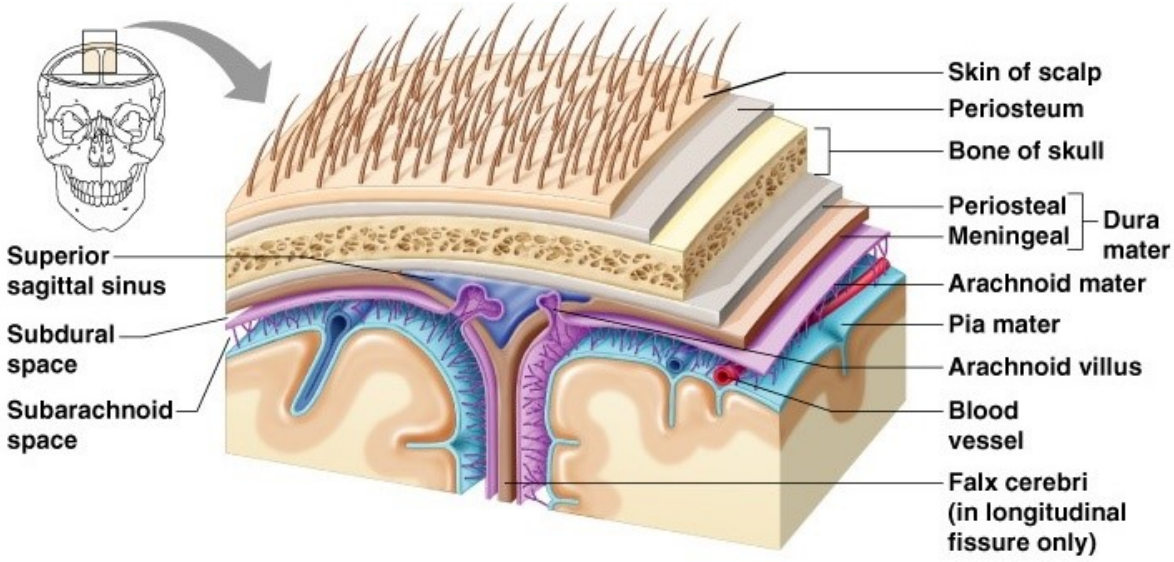

Figure 2-3 Meninges [32].

The most important types of head injuries are shown in Figure 2-4. Soft tissue injuries to the scalp and face, which include contusion and laceration, are considered minor injuries. Fractures are more severe head injuries. Head fractures can be categorized as follows: Facial, vault and basilar skull fractures [29]. Facial and cranial fractures usually happen due to an impact to the face or the vault but basilar skull fracture (BSF) is due to more complicated mechanisms. Moreover, BSF is one of the most common type of skull fractures sustained by motorcycle riders [10–13]. A clinical survey by Chee and Ali [13] revealed that 50% of patients suffering from BSF were motorcyclists. Dowdell et al. [10] studied 200 accidents involving helmeted motorcyclists and found that the chin bar of full-face helmets has the highest probability of impacts during accidents. According to this study, almost 50% of the severe impacts took place on the front of the helmet, involving the chin bar, and 40% of these impacts led to BSF. In a similar work, Whyte et al. [11] studied 47 cases of fatal motorcycle accidents and found that BSF was the most frequent type of head injury (31 cases), and interestingly in 15 cases suffering from BSF, there was no injury at the impact site. Another in depth injury analysis of non-fatal motorcycle accidents showed that almost 69% of cranium fractures took place at the base of skull [12].

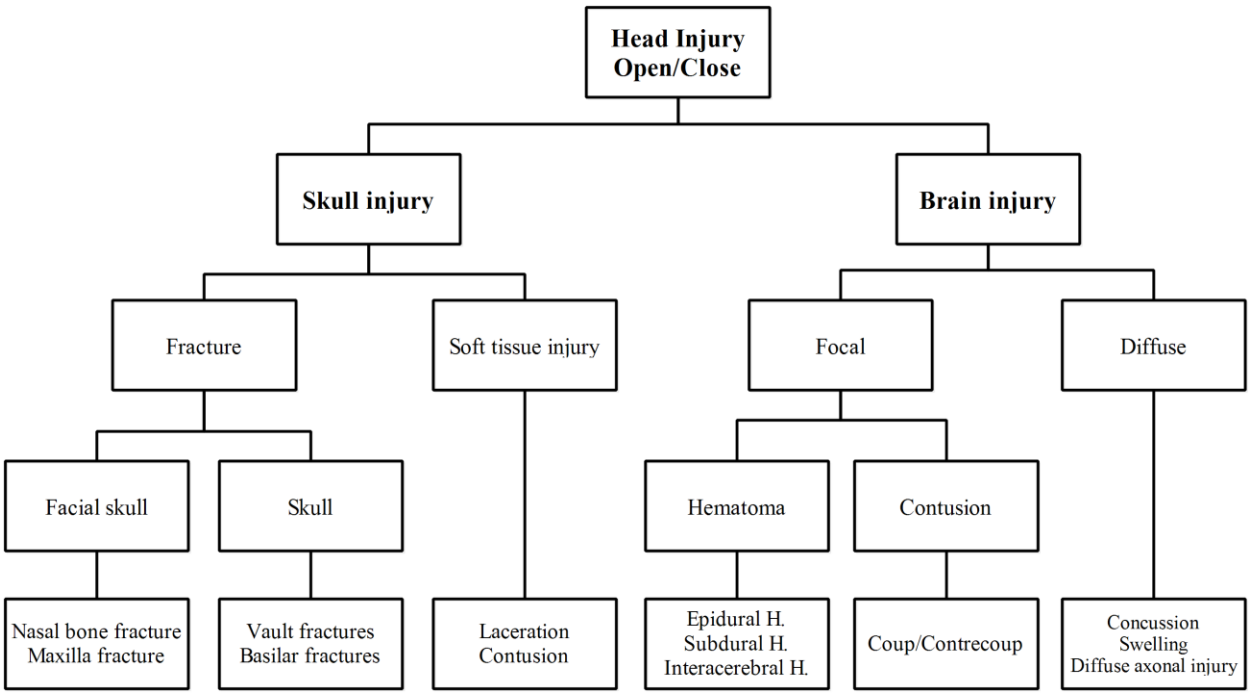

Figure 2-4 A possible classification of head injuries [29].

The base of the skull is its weakest region [33]. Any fracture occurring in this region or propagating to this region is called basilar skull fracture (see Figure 2-5) [34]. BSF can be caused by direct impacts at the base of the skull or by remote impacts [35,36], such as craniofacial impacts, which frequently occur in motorcycle accidents [10] and can lead to BSF [37,38]. Cooter and David [37] postulated that the impact load due to the blows on the full-face helmet's chin bar can be transmitted to the base of the skull via the chin strap and lead to BSF. Fracture at the skull base can lead to fatal injuries, such as damage to the carotid artery [39] or basilar artery

thrombosis [40]. The latter injury can occur even when brain or cervical injuries are mild [41,42].

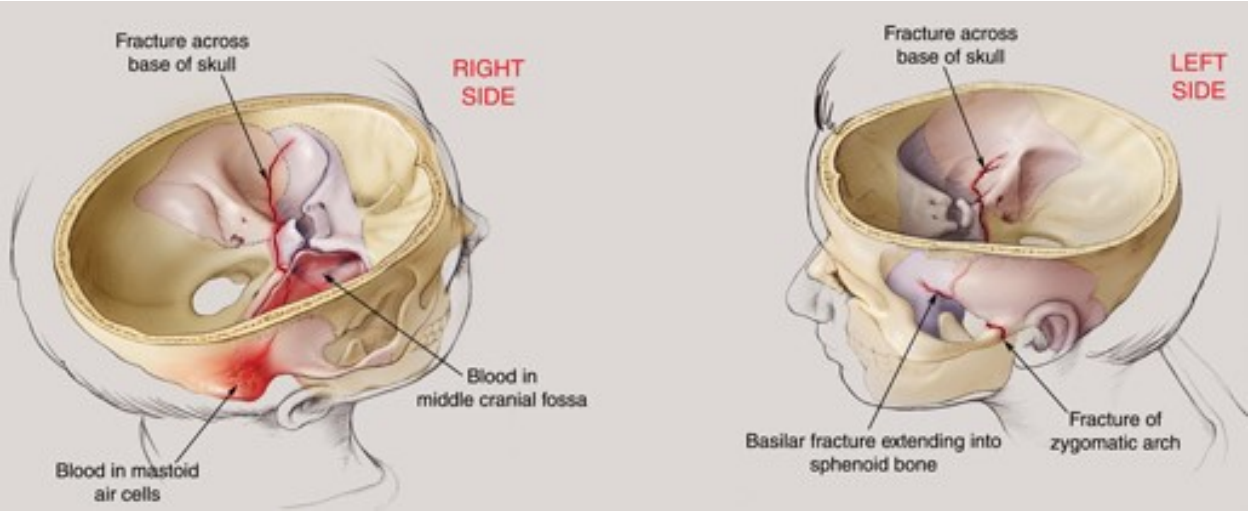

Figure 2-5 Skull base fracture [43].

Injuries to the brain can mainly be classified as diffuse injuries and focal injuries. The most common form of diffuse brain injury is mild concussion (fully reversible, no loss of consciousness). Particularly in sports, mild traumatic brain injury (mTBI) is often diagnosed. A more severe form of concussion is cerebral concussion, which is characterized by immediate loss of consciousness. The outcome of patients suffering from cerebral concussion strongly depends on whether there are associated brain injuries or not [44]. Diffuse axonal injury (DAI) describes disruption to the axons in the cerebral hemispheres and the subcortical white matter [29]. Focal brain injuries are local lesions in which the damaged area can be defined easily. Two possible types of focal injuries are hematoma and contusions. Contusion is the most frequently found lesion due to the head impact. In general, contusion may occur at the site of impact (coup contusion) and at site opposite to that of the impact (contrecoup contusion). Contrecoup contusions are considered more significant than coup-contusions [44]. There are three different types of hematoma, which could be distinguished depending on the site of the bleeding: epidural hematoma, subdural hematoma and intracerebral hematoma [29]. Figure 2-6 illustrates some types of brain injuries.

The head can get injured either under static loading (in which the load lasts more than 200 ms) or dynamic loading. In case of static loading, the head deforms until it reaches a maximum deformation and then the skull fractures. In case of dynamic loading, the injury can be due to contact or non-contact loading. An impact to the head can cause skull deformation, which may lead to direct or burst fracture. Furthermore, skull deformation can result in local brain injury like epidural hematoma or contusion as well as scalp injuries. Moreover, such a dynamic loading produces a stress wave, which propagates in the skull and the brain (see Figure 2-7). The wave propagation generates a pressure gradient in the brain with positive pressure at the site of impact (coup) and negative pressure on the opposite side of the impact (contrecoup) and such a pressure gradient may lead to focal brain injuries [29].

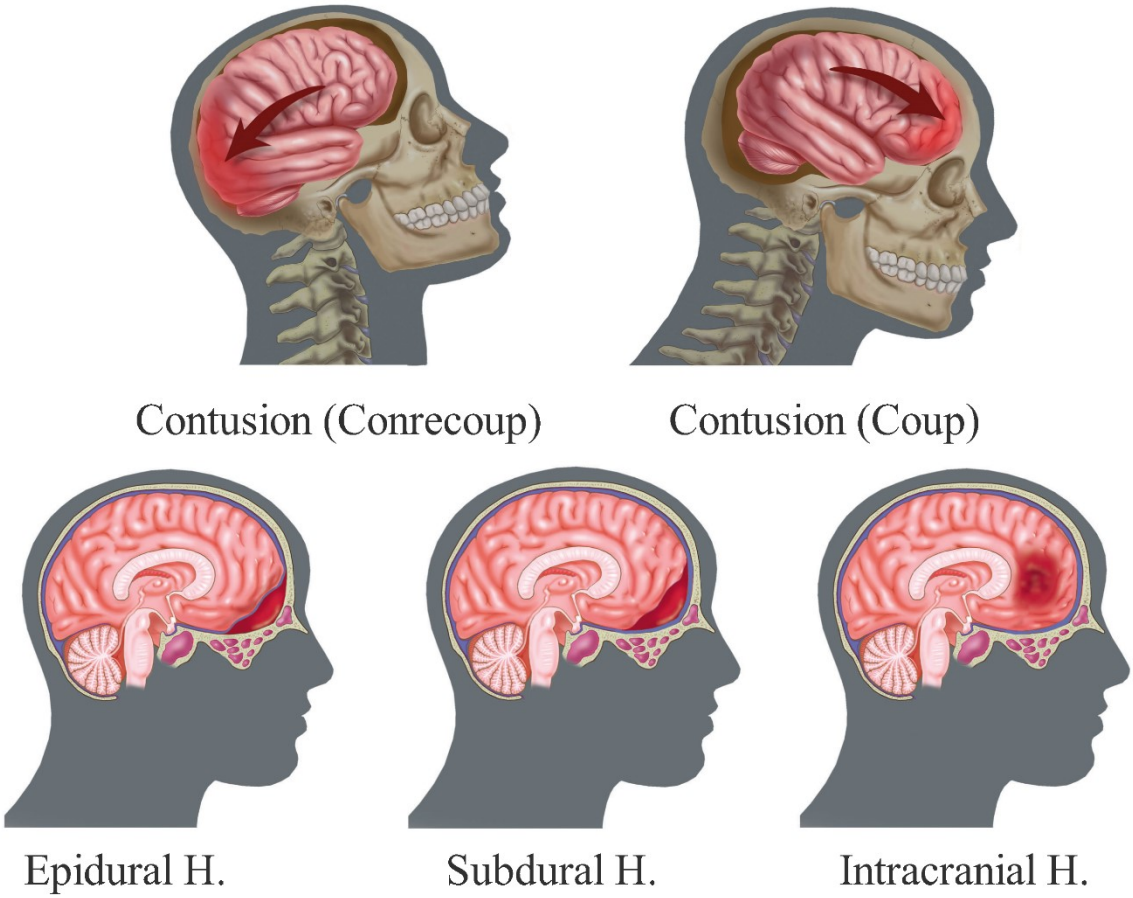

Figure 2-6 Some types of brain injury [31].

The head injuries can be due to induced inertial forces (acceleration or deceleration) without any direct contact. Acceleration can be either translational or rotational. Translational acceleration generally results in focal brain injury while rotational acceleration also causes diffuse brain injury. However, the injuries due to the induced acceleration can take place in case of direct impact to the head, as well [29].

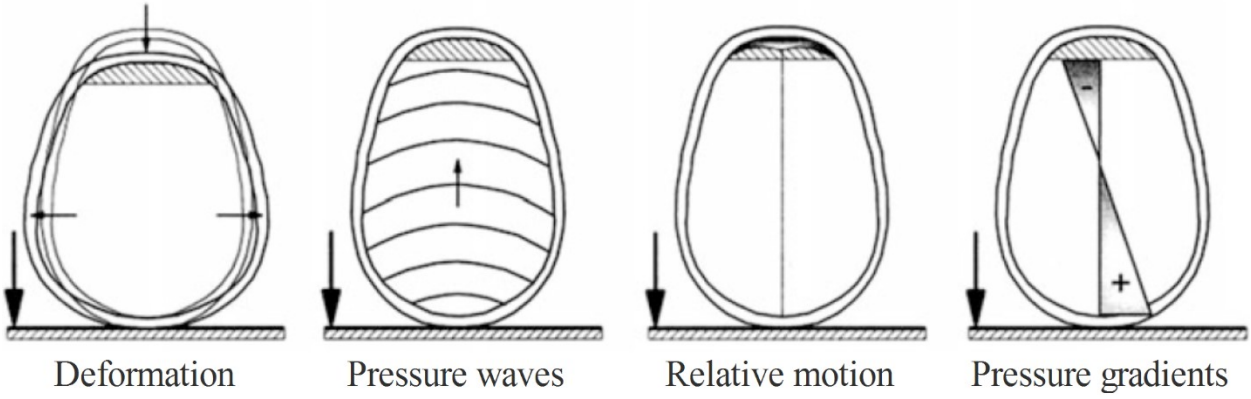

Figure 2-7 Mechanisms of head injuries due to an impact [29].

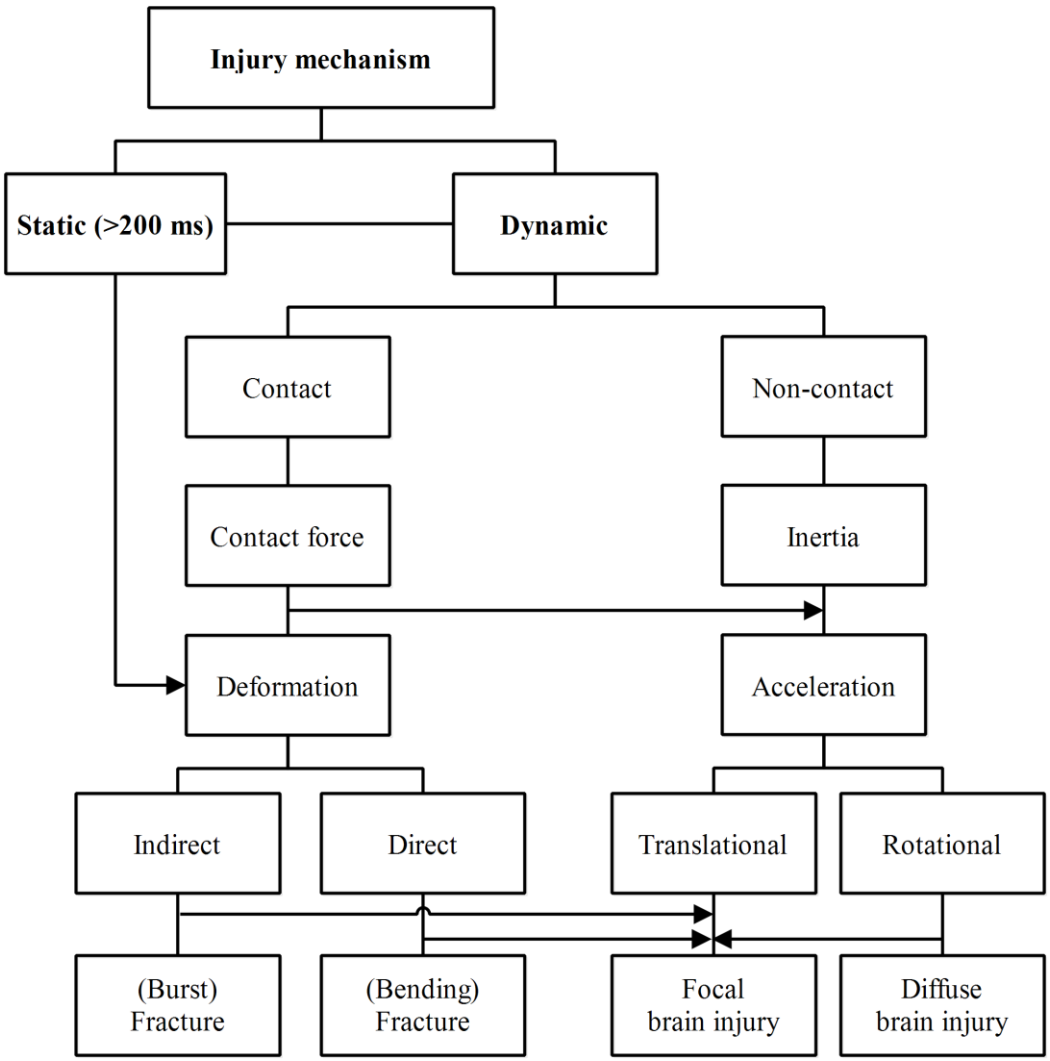

Figure 2-8 Possible mechanisms of head injuries [29].

According to clinical surveys, both compressive and tensile loading might cause BSF [45,46]. In case of compressive loading like cranial vault impact, it was thought that the cranium, due to its smooth curvature, could withstand the impact load and transmit the load to the base of skull, leading to BSF. In case of tensile loading, it was hypothesized that since the strength of the atlanto-occipital ligaments and musculature is higher than occipital bone's, the tensile loading, like in case of hyperextension, results in the skull base fracture instead of separation at the spine-skull junction [47,48]. McElhanney et al. [14] carried out an experimental study on cadavers to better understand the mechanisms of BSF. Three different types of loading were used in their work, as shown in Figure 2-9. The first type was direct loading of the mandible by dropping the head with mandible hitting a rigid anvil. The aim was to evaluate the effect of the load transferred through the temporomandibular joint to the base of the skull. In the second series of experiments, an un-embalmed head was subjected to a direct temporomandibular loading in conjunction with tensile neck loading. In the third series of tests, an intact head-neck, with a simulated torso mass, was dropped onto a rigid anvil in order to assess the effect of the compressive neck load on the skull base. It was found that the neck tensile load at the base of the

skull was the most probable loading condition that can produce BSF. They reported peak neck forces which led to ring basilar skull fractures from 2.74 kN to 4.72 kN. Therefore, the neck tensile load at the upper neck has been used as the indicator of BSF in the present study.

Due to the high probability of basilar skull fracture related to chin bar impacts in motorcycle crashes and the lack of test methods that address chin bar design for BSF mitigation, a part of this thesis is dedicated to optimize the motorcycle riders' helmet in order to mitigate the risk of BSF. The complete description of this optimization is presented in chapter 8.1.

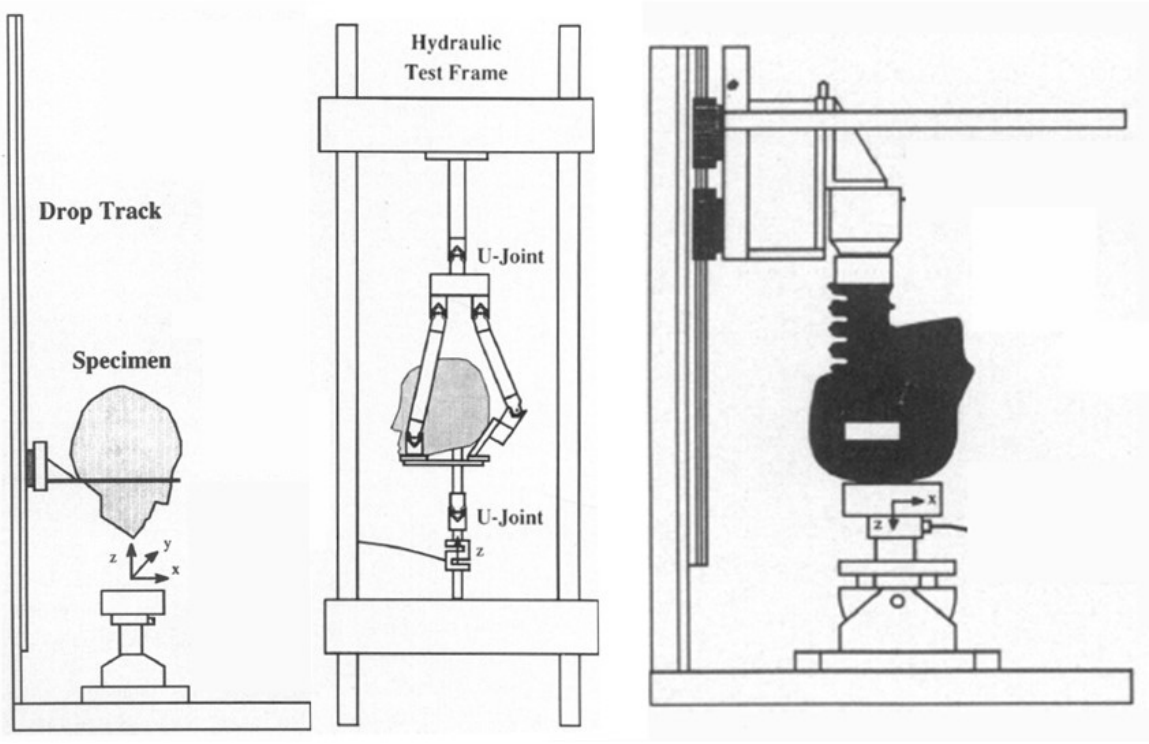

Figure 2-9 Experimental tests to identify mechanisms of BSF, Left: mandibular impact, middle: temporomandibular loading in conjunction with tensile neck loading, right: compressive neck load [14].

2.1.1. Head injury criteria

The head injury predictors are usually based on the acceleration response of the head. These criteria have been developed based on cadaveric tests. Moreover, recently numerical models of the head have been introduced in order to predict the head response, therefore, they can be used to measure the risk of head injuries. Some of these criteria are described in this chapter.

2.1.1.1. Head Injury Criterion (HIC)

Head injury criterion (HIC) is the most widely used injury criterion for head injuries. It has been developed based on Wayne State Tolerance Curve (WSTC) [49]. However, the currently used form of HIC, which has been developed later by Versace [50], is as follows:

$$HIC = max\left[\frac{1}{t_2-t_1}\int_{t_1}^{t_2} a_{(t)}dt\right]^{2.5}(t_2-t_1) \qquad \text{Eq. 2–1}$$

where t_2 and t_1 are any two arbitrary time points during the acceleration pulse. Acceleration is measured in multiples of the acceleration of gravity (g) and time is measured in seconds. The resultant acceleration is used for the calculation. The limit of 1000 of HIC is defined as 16% probability of life threatening injury, whereas a limit of 3000 as 99% [51].

Even though, HIC is widely used as an indicator of the head injury it does not consider the effect of rotational acceleration of the head which has been known as an important cause of brain injuries [52–54].

2.1.1.2. Generalized Acceleration Model for Brain Injury Threshold (GAMBIT)

This injury criterion has been proposed by Newman [55] in order to combine the translational and rotational acceleration for predicting the risk of head injury. The following equation was proposed to calculate GAMBIT:

$$GAMBIT = \left[\left(\frac{a_{(t)}}{a_c}\right)^n + \left(\frac{\ddot{\varphi}_{(t)}}{\ddot{\varphi}_c}\right)^m\right]^{\frac{1}{k}} \quad \text{Eq. 2–2}$$

where $a_{(t)}$ and $\ddot{\varphi}_{(t)}$ are translational (often called 'linear') and rotational accelerations respectively, a_c and $\ddot{\varphi}_c$ are related critical values and *n*, *m* and *k* are constant parameters. Kramer [56] calculated the constants in the Eq. 2-2 using statistical methods and proposed the following equation:

$$GAMBIT = \left[\left(\frac{a_{(t)}}{250}\right)^{2.5} + \left(\frac{\ddot{\varphi}_{(t)}}{25}\right)^{2.5}\right]^{\frac{1}{2.5}} \quad \text{Eq. 2–3}$$

in which $a_{(t)}$ and $\ddot{\varphi}_{(t)}$ are given in [g] and [krad/s^2], respectively. The curve for a GAMBIT of 1.0 was determined to represent a probability of 50 % for irreversible head injury (see Figure 2-10).

Even though, GAMBIT includes both translational and rotational accelerations in order to predict the head injury, it has not been included in any regulation since it still lacks proper validation [29].

2.1.1.3. Tissue level head injury criteria

Evolution of computational methods led to development of head virtual models which helped researchers to propose tissue level head injury criterion based on the use of finite element models of the head and the brain [57]. Figure 2-11 shows a finite element model of the human head with high fidelity [58], which has been developed recently. However, during the last years, different human head models have been developed by different researchers [59] and different parameters were used as the injury criterion, as well. Intracranial pressure [60], Von-Mises stress [61] shear stress [62], strain [63] and strain rate [64] are quantities which have been used to describe the tissue level injuries by means of the finite element method.

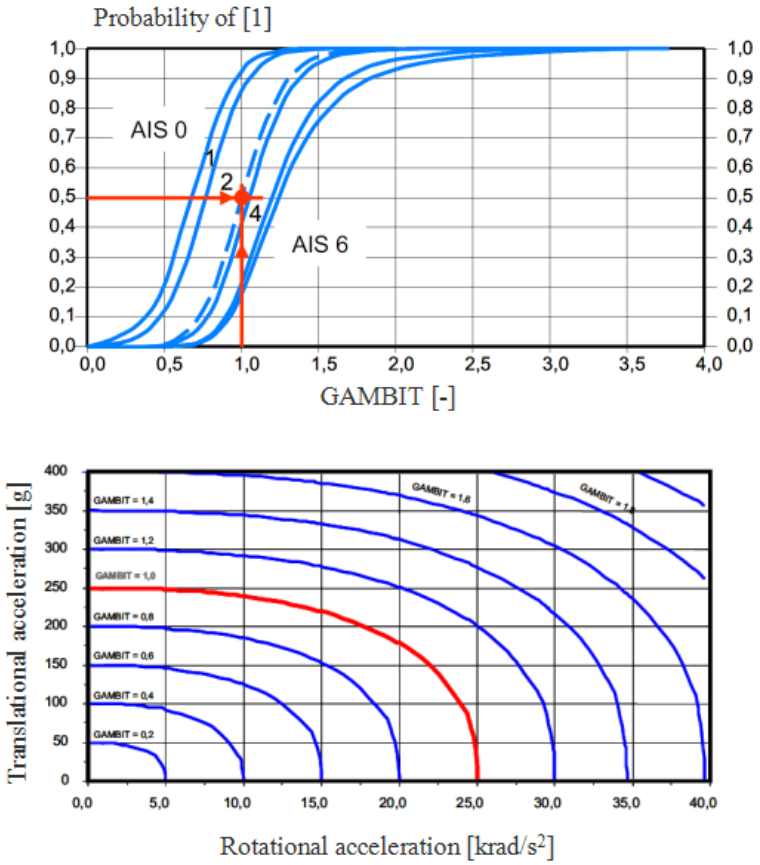

Figure 2-10 Upper: GAMBIT VS. injury risk level

Lower: GAMBIT curves for different values of translational and rotational accelerations [56].

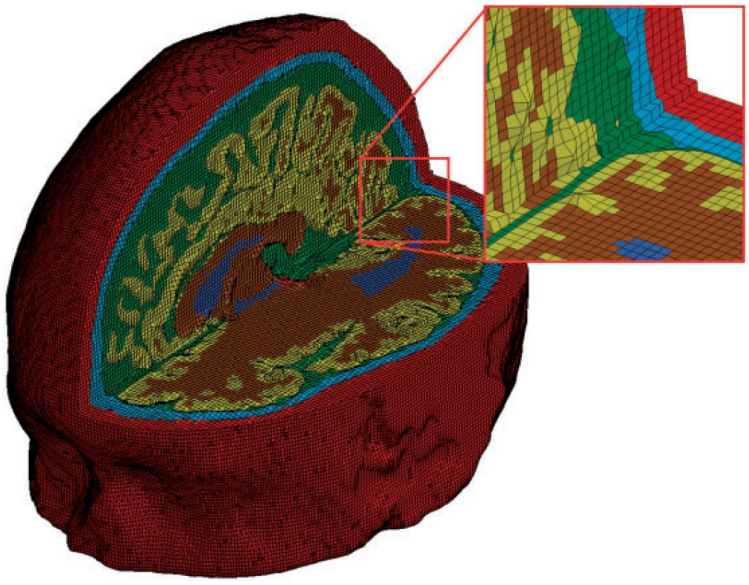

Figure 2-11 A high fidelity 3D finite element model of the head [58].

2.2. Neck Injuries

Neck is made of seven cervical vertebrae, intervertebral discs and a complex muscular system (Figure 2-12), which supports the head and provides the capability of the four basic movements of the head-neck system, namely flexion, extension, lateral bending and rotation [20,21].

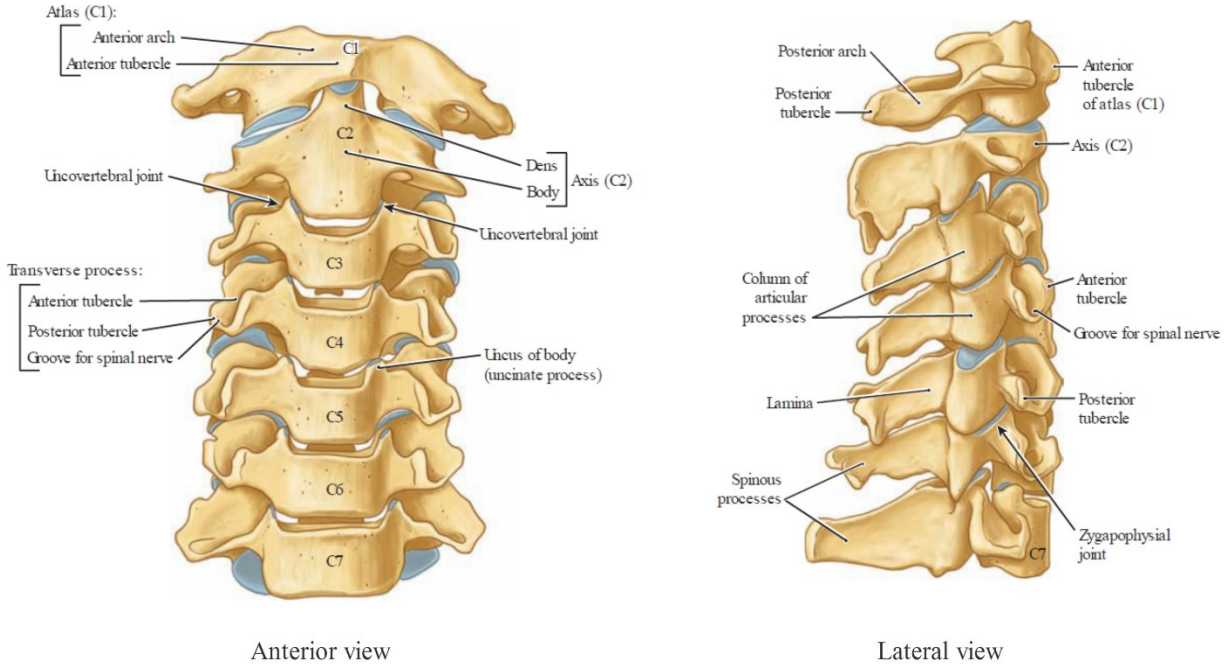

Figure 2-12 Cervical spine [32].

The cervical spine can be considered as four sections, i.e. the atlas, the axis, the C_2-C_3 junction and the remaining typical cervical vertebrae, each section of cervical spine has a unique morphology. The atlas is connected to the occiput and generates a strong joint called atlanto-occipital joints. The head and atlas move and function as one unit except for nodding movement between them. The lower face of atlas is connected to axis and provides a large range of axial rotation. This rotational movement is provided by means of a pivot joint, which is called atlanto-axial joint, between the axis and the atlas thanks to odontoid process (see Figure 2-13). C_2-C_3 joint is commonly known as the beginning of the typical spine where all segments share a similar morphology and kinematics. However, C_2-C_3 junction is different from the other segments. The difference can be realized in a pillar view of the cervical spine[1] in which, the body of the axis looks like a deep anchoring root that holds and moves the head, into the typical cervical spine (see Figure 2-14). Moreover, an operational difference between C_2-C_3 and other segments is that during axial rotation of the neck, the direction of coupling with lateral flexion at C_2-C_3 is opposite to that seen at lower segments and instead of bending towards the same side as rotation, C_2 rotates away from that side, on the average. The rest of the cervical spine can be considered as

[1] A pillar view is obtained by beaming X-rays upwards and forwards through the cervical spine, essentially along the planes of the zygapophysial joints.

the typical segment of the cervical vertebrae which are stacked on one another and provides the fundamental capability of flexion-extension motion of the neck [20].

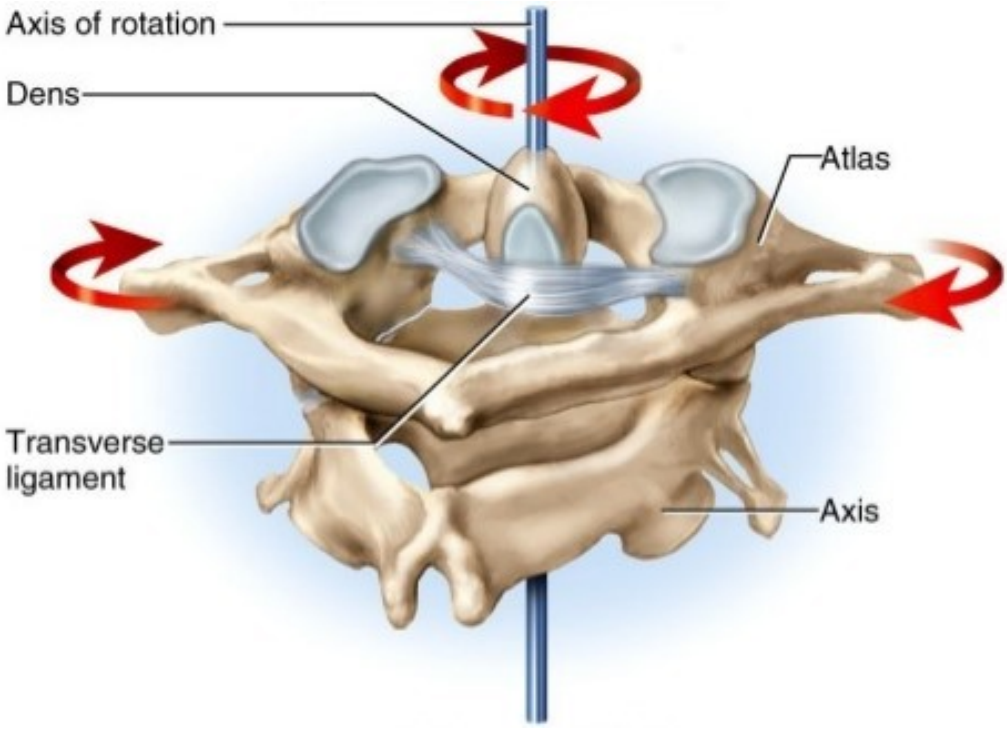

Figure 2-13 Atlanto-axial joint [65].

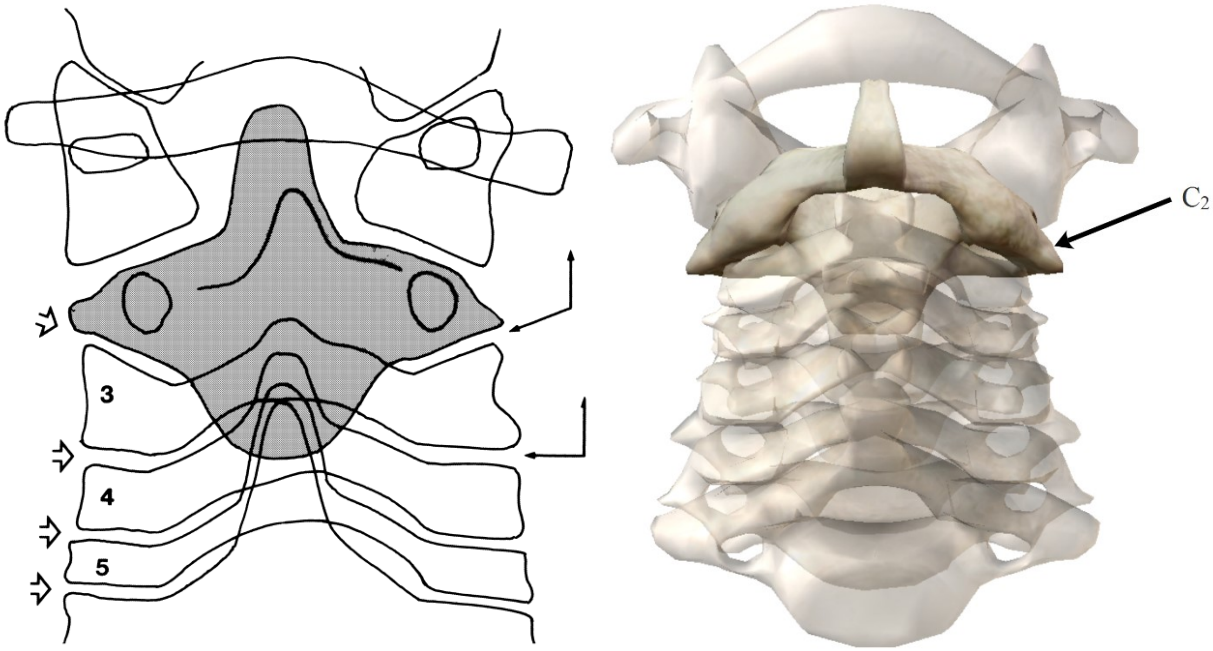

Figure 2-14 A tracing of a pillar view of the upper cervical spine, showing the unique morphology of C_2 (shaded) [20].

A wide range of injuries can occur at the cervical musculoskeletal system. Some types of neck injuries are vertebral fracture, intervertebral disk rupture, ligament disruption, vertebral dislocation, joint disruption, spinal cord laceration and vertebral artery laceration [11,22–27]. Usually cervical spine injuries are due to indirect violence e.g. falling on the head or violent movements transmitted from the skull. Cervical injuries can be categorized according to the motion of the head-neck assembly associated with them and to the relevant mechanical loading i.e. hyperflexion, hyperextension, lateral flexion, compression and rotation [9,29] as shown in Figure 2-15. These injury mechanisms can cause different types of injuries, however, some injuries may be due to combination of them. Table 2-1 lists some cervical injuries and their mechanisms (motions).

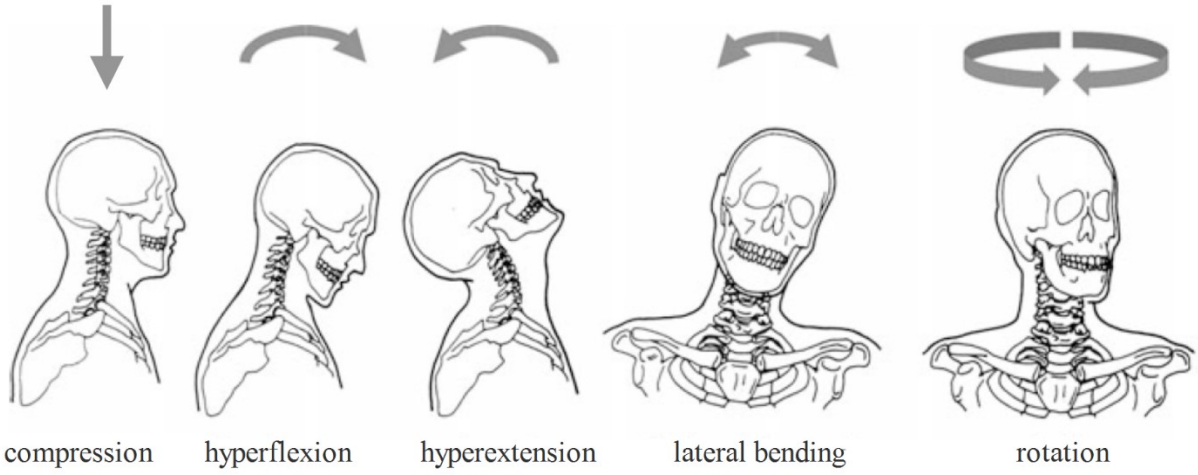

Figure 2-15 Neck injury mechanisms [9,29].

Table 2-1 Some cervical injuries and their mechanisms [9].

Injury types	Cervical motion
Hyperflexion sprain Bilateral interfacetal dislocation Simple wedge (compression) fracture Flexion teardrop fracture	Flexion
Unilateral interfacetal dislocation	Flexion-rotation
Odontoid fracture	Extension-lateral shear/compression
Burst (bursting, dispersion, axial loading) fracture	Vertical compression
Hyperextension dislocation Fracture of posterior arch of atlas Laminar fracture Hyperextension fracture-dislocation Inter-vertebral subluxation	Hyperextension
Uncinate process fracture	Lateral flexion

Shear in anteroposterior and axial torsion may result in dislocation of the atlanto-occipital joint and large compression may lead to fracture of the atlas (Jefferson's fracture). Axial compression in conjunction with extension of the neck may cause C_2 fracture, which is known as hangman's fracture. However, when the load is transmitted from a head contact to the neck, five main load combination can be considered, i.e. compression-flexion, compression-extension, tension-flexion, tension-extension and lateral bending [29].

The combination of axial compression and flexion can result in wedge fracture of the anterior vertebral bodies, burst fracture, fracture and dislocation of the facets. It may also lead to spinal cord disruption or injury due to unstable mechanical condition of the neck structure [29]. Fracture of the posterior structures of the neck may be produced due to compression-flexion loading which is usually due to head frontal impact and is common in motorcyclists accidents [12,66,67]. Neck flexion may also occur in conjunction with tension, which can result in bilateral facet dislocation. Tension-extension is another type of common loading condition in motorcycle accidents [12] which may lead to several injuries e.g. hangman's fracture and soft tissue neck injuries [68]. Lateral bending can also cause different neck injuries like lateral wedge fracture of the vertebral body or fracture of the posterior structure of the cervical column. Lateral bending may occur with torsional load which can result in unilateral facet dislocation or unilateral locked facets [29,69].

2.2.1. Neck injury criteria

There are several injury criteria for neck injury, which have been mostly proposed for the whiplash injury for car passengers and have been mostly developed for sled test using dummies. Since cervical injuries among motorcyclists are usually due to direct impacts on the head the result of an assessment using such cervical injury criteria might not be accurate and reliable for motorcycle accidents [29]. However, this section addresses few available neck injury criteria and presents and discusses use of stress (and strain) distribution as an indicator for risk assessment of cervical injuries.

2.2.1.1. Neck Injury Criterion [NIC]

This injury criterion addresses the pressure gradient of the fluid compartment of the cervical spine as the cause of neck injuries. The criterion has been validated based on animal testing and correlated to the head acceleration and velocity as follows:

$$NIC_{(t)} = 0.2a_{(t)}^{rel} + \left(v_{(t)}^{rel}\right)^2 \qquad \text{Eq. 2–4}$$

Where, $a_{(t)}^{rel}$ and $v_{(t)}^{rel}$ are relative acceleration and velocity of the centre of gravity of the head with respect to the first thoracic vertebra, respectively [70]. The threshold for sustaining minor neck injuries is 15 m^2/s^2. However, if the head rotation exceeds 20-30° due to a considerable error of $NIC_{(t)}$ curves, this criterion might not be suitable for injury prediction [29].

2.2.1.2. N_{ij} Neck Injury Criterion

This injury criterion has been proposed by US national highway traffic safety administration (NHTSA) for neck injury assessment in frontal impacts [71,72] according to the crash tests

performed using animal surrogates which had been carried out before [73]. This criterion proposes a linear combination of normalized axial force and bending moments of the neck as follows:

$$N_{ij} = \frac{F_z}{F_{int}} + \frac{M_y}{M_{int}} \quad \text{Eq. 2–5}$$

in which, F_z is neck axial force and M_y is the neck bending moment in sagittal plane[1]. Moreover, F_{int} and M_{int} refers to critical values of axial force and bending moment, respectively, which have been established and validated for three-year-old Hybrid III dummy based on experimental tests using piglets as child surrogates and have been scaled up for other dummy sizes. The critical values for axial force and bending moment are indicated in Table 2-2 for different sizes of Hybrid III dummies.

Table 2-2 Intercept values for calculating N_{ij} [74].

Dummy	M_y (flexion/extension) [Nm]	F_z (compression/tension) [N]
Hybrid III 50%	310/135	6160/6806
Hybrid III 5%	155/67	3880/4287
Hybrid III 5% (out of position)	155/61	3880/3880
Hybrid III 6-year	93/37	2800/2800
Hybrid III 3-year	68/27	2120/2120

2.2.1.3. Stress (or strain) distribution

In the last years, the Finite Element Method (FEM) has been used as a powerful tool to study human body response during accidents and to design protection equipment [5]. Moreover, since developed neck injury criteria may not be valid for all loading conditions, especially in case of direct impact to the head which induces a high range of motion on head-neck assembly, the stress distribution or strain level of the cervical vertebrae, intervertebral discs or spinal cord may be used as an indicator [75–78]. In addition, in a recent study, researchers from TOYOTA R&D centre, who have been developing one of the most widely used human body models (THUMS: Total HUman Model for Safety), showed a high correlation between the stress distribution and strain level of spinal vertebrae of THUMS with a real life accident in which the driver sustained fracture of the spinal vertebrae [79].

[1] The sagittal plane is a plane parallel to the sagittal suture and divides the body into left and right.

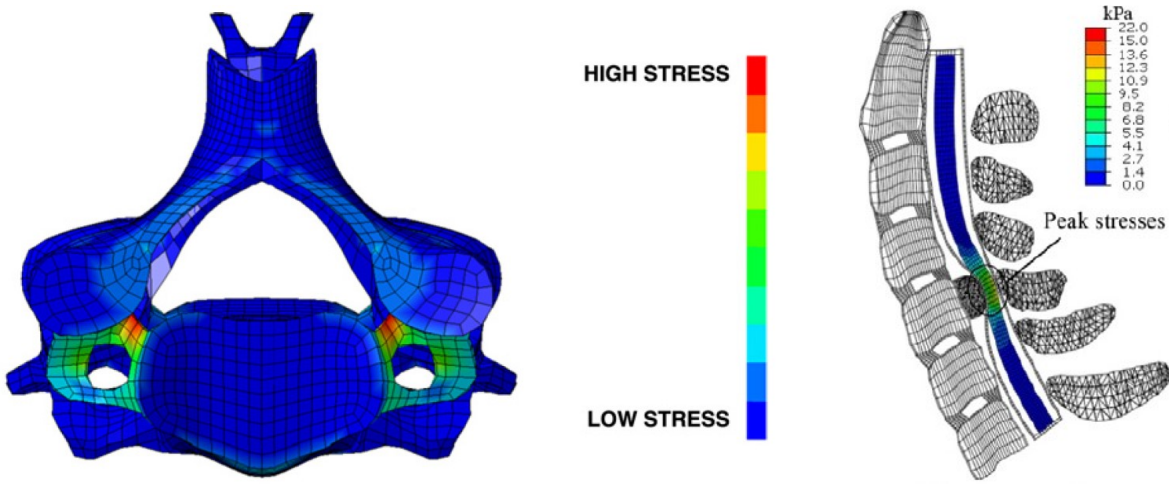

Figure 2-16 Assessing the risk of cervical vertebra fracture (left) and spinal cord injury (right) by means of FEM [75,76].

3. Personal Protective Equipment (PPE)

3.1. Helmet

Helmets are the most common and best protective headgear for motorcycle riders [80]. The primary form of helmets was used just to protect the head against weapons' strikes and had no energy absorbing liner [4]. In 1943, Holbourn showed that the non-penetrating head injuries are due the short-duration acceleration which can be induced to the head during an accident [81]. The induced acceleration on the head is the cause of the most common and dangerous type of injuries for motorcycle riders [82]. In 1953, Charles and Roth introduced the modern form of the crash helmets using an energy absorbing liner, as shown in Figure 3-1 [83].

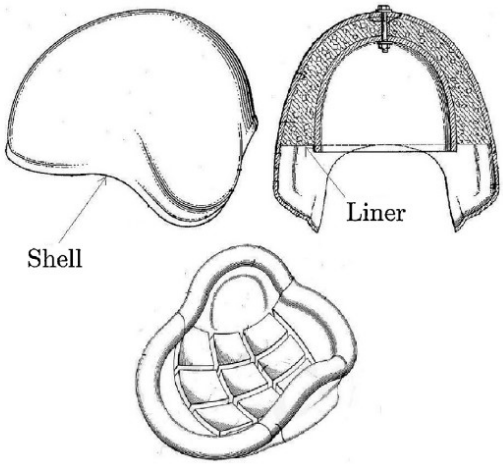

Figure 3-1 Crash helmet [83].

Nowadays, motorcycle helmets mainly consist of a stiff shell, which is usually made of plastics or composite laminates, energy absorbing liners, comfort padding liner, visors and the retention strap, as shown in Figure 3-2. These parts are common in all kinds of motorcycle helmets. Two main parts which contribute to head protection are the outer shell which distributes the impact energy and the energy, absorbing liner, which dissipates the energy of the impact [84].

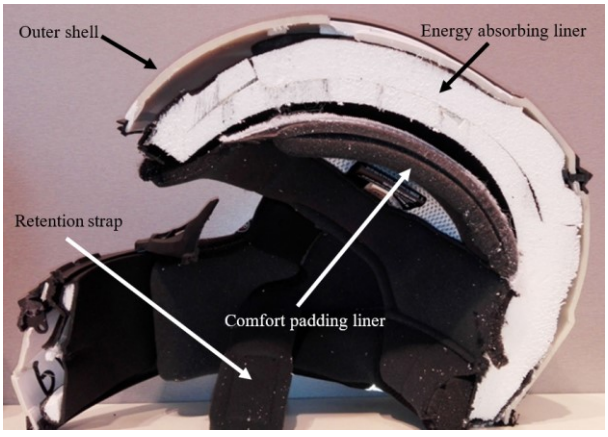

Figure 3-2 Motorcycle helmets (visor is removed) [85].

In the last decades, researchers introduced innovative energy absorbing liners in order to reduce the head acceleration due to the impact. Caserta et al. introduced a composite liner which was made of a common type of liner and layers of aluminium honeycomb (as shown in Figure 3-3) and could improve the energy absorption of the helmet [18].

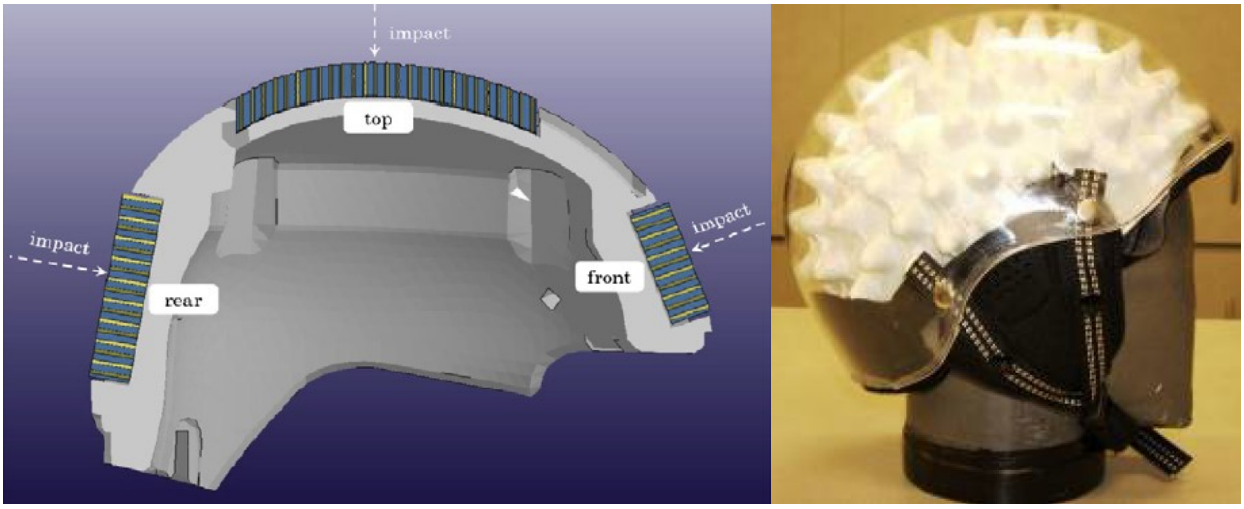

Figure 3-3 Left: Schematic section of the prototype liner proposed by Caserta et al. [18],
Right: Prototype of the innovative liner proposed by Blanco et al. [86].

In another study, Blanco et al. proposed an innovative liner, which could dissipate the impact energy better than conventional pads. Their proposed liner was made of ABS lamina with deformable cones as shown in Figure 3-3 [86].

Moreover, other innovative designs have been introduced in order to reduce both translational and rotational accelerations of the head. One of these innovative helmets, is called MIPS (Multi-direction Impact Protection System) and is designed to reduce the rotational acceleration of the head in case of an oblique impact, by means of a low friction layer between the energy absorbing liner and the outer shell of the helmet as shown in Figure 3- 4 [87].

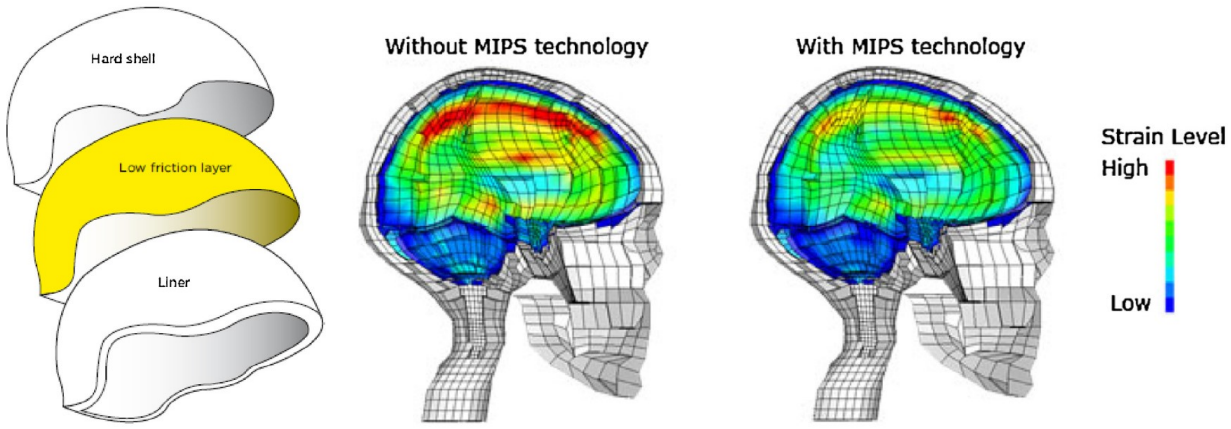

Figure 3- 4 Left: Multi-direction Impact Protection System (MIPS),
Right: Results of oblique impact simulation with KTH FEHM [87].

Halldin et al. showed that MIPS could reduce the peak rotational acceleration and consequently the strain level of the brain [88], as shown in Figure 3- 4.

3.2. Neck Brace

In the last years, motorcycle gear manufacturers have introduced a new item of protective equipment in order to mitigate the risk of neck injuries in motorcyclists. This protective equipment is a brace, which has been designed to restrict the neck movement of the helmeted user, in order to reduce the risk of hyperextension, hyperflexion and lateral bending of the neck and distribute the energy of impact on the shoulders as shown in Figure 3- 5.

Figure 3- 5 Top: Few samples of neck braces, Bottom: Load transfer to the shoulder [89–93].

Since this type of protective equipment has been introduced recently, there are few studies about its effect on reduction of the risk of neck injuries. Leatt et al. introduced their neck brace concept and studied the effect of using it in reducing the risk of neck injuries using Hybrid III dummy [94]. Gorasso and Petrone [95] studied the effect of using the neck brace on neck movements and

muscles activation. However, there is no standard criterion for design and manufacture of such devices yet.

The neck brace that has been considered in the present study, shown in Figure 3- 5, has three main components: the outer shell, which is a composite laminate, the padding liner, that is made of polyurethane foam, and the strap to keep the brace on its position.

3.3. Neck Airbag

The neck airbag is a protective device, which has been designed to protect the neck by restricting the range of motion of the head-neck assembly. The rider can put on this device in the folded condition and in case of accident, the airbag gets inflated in order to provide the protection.

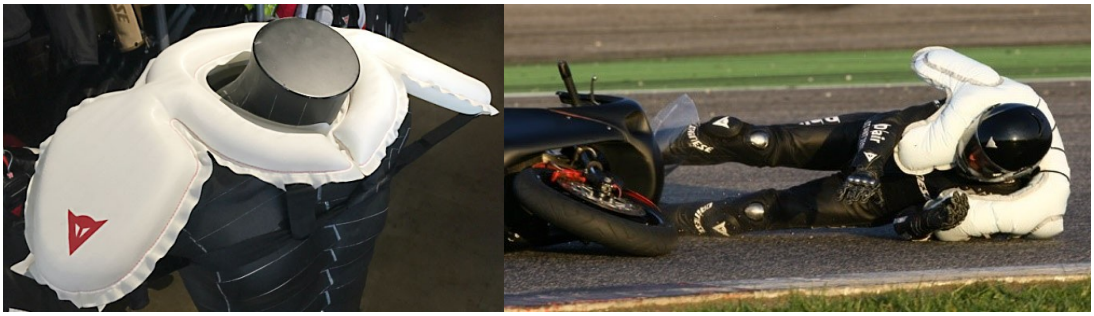

Figure 3- 6 A sample of neck airbag [89].

3.4. Other items of Personal Protective Equipment

Beside helmet and neck protective devices, motorcycle gear manufacturers also provide other types of personal protective equipment for other parts of the body, like chest and back protectors, ankle and elbow protectors etc. Figure 3- 7 shows some of these items of personal protective equipment.

Figure 3- 7 A sample of upper body protective gear including chest, back, shoulder and elbow protectors [89].

The present thesis focuses on the head and neck protection and related protective devices.

4. Standards

The main concern of this thesis is head and neck protection, therefore in this chapter the relevant standards are presented and issues related to head and neck protective devices discussed,other standards are just mentioned briefly.

4.1. Helmet standards

Helmet standards assess the helmet performance considering their mechanical, chemical and optical properties. This thesis only addresses the mechanical properties of helmets, which are assessed by means of impact attenuation test. There are several standards for helmet assessment which have been developed by different associations in different countries. Here, ECE 22.05 (which is adopted in Europe) is mainly described.

4.1.1. ECE 22.05 helmet impact test

This test is used to assess the energy absorption capability of the helmet by measuring the acceleration induced to the centre of gravity of the helmeted headform. Tests are carried out by making use of a drop tower, helmets are subjected to impacts at different points. Figure 4- 1 shows the impact test set-up and the medium size headform used for such a test [96].

Figure 4- 1 Left: helmet's impact test set-up [97]; right:Iso headform used for testing helmets [98].

The test set-up shall be made of the following parts:

1. **Base:** it shall be made of steel, concrete or both and weigh at least 500 kg. Natural frequencies of the base or its parts shall not influence the impact results.

2. **Anvils:** two anvils are used in impact tests; flat and kerbstone. The flat anvil shall have a circular impact area with a diameter of 130 mm. The kerbstone anvil shall have two sides forming an angle of 105°, each of them with a slope of 52.5 towards the vertical and meeting along a striking edge with a radius of 12 mm. The height must be at least 50 mm and the length not less than 125 mm.
3. **Mobile system and the guide:** the mobile system shall provide a free fall for helmeted headform and the guide shall be such that the impact velocity is not less than 95% of the theoretical velocity.
4. **Accelerometers**.

The impact points are described in Figure 4- 2 and Table 4-1.

Table 4-1 The definitions of the impact points for motorcycle helmet.

Point	Definition
B	in the frontal area, situated in the vertical longitudinal plane of symmetry of the helmet and at an angle of 20° measured from Z above the AA' plane.
X	in either the left or right lateral area, situated in the central transverse vertical plane and 12.7 mm below the AA' plane.
R	in the rear area, situated in the vertical longitudinal plane of symmetry of the helmet and at an angle of 20° measured from Z above the AA' plane.
P	in the area with a radius of 50 mm and a centre at the intersection of the central vertical axis and the outer surface of the helmet shell.
S	in the lower face cover area, situated within an area bounded by a sector of 20° divided symmetrically by the vertical longitudinal plane of symmetry of the helmet.

The drop height shall be equal to that required to achieve an impact speed of 7.5 m/s for both flat and kerbstone anvils and 5.5 m/s for tests at point S (for full-face helmets). The linear acceleration of the centre of gravity of the headform shall be recorded versus time. A helmet can be certified by standard if the resultant linear acceleration of the headform does not exceed 275 g, and HIC does not exceed 2400.

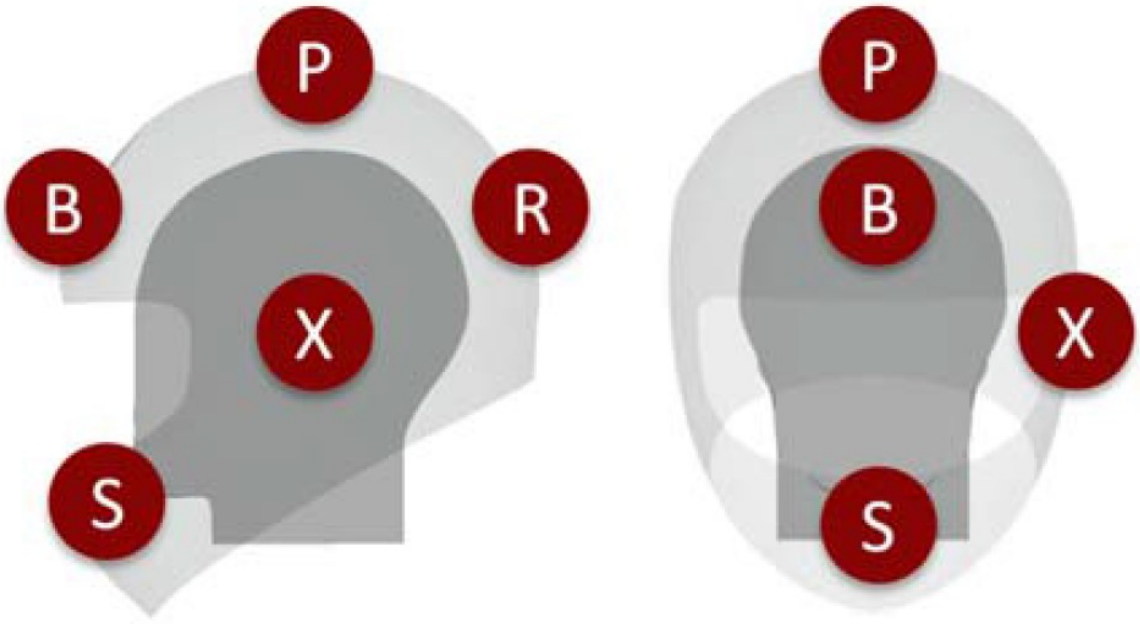

Figure 4- 2 Illustration of impact points for tesing a full face helmet according to ECE 22.05.

4.1.2. Other helmet standards

Although ECE 22.05 is probably the most widely accepted standard for manufacturing helmets and visors in the world [28], there are other standards, which are used to assess the energy absorption capability of motorcycle helmets. The British standard (BS6658, 1985), the U.S. Department of Transportation's Federal Motor Vehicle Safety Standard No. 218 (FMVSS218, 1997), Snell M2010 (2010) that is issued by Snell Memorial Foundation, and the Australia and New Zealand standard (AS/NZS1698, 2006) are some of the currently adopted standards. Testing according to the mentioned standards, generally, requires similar test. However, ECE 22.05 is the only standard which refers to a non-constrained helmeted headform fall. In other mentioned standards the helmeted head must be attached to the mobile system through a ball joint which, allows for rotation and vertical translation, but constraints horizontal translations. Moreover, all these standards adopt different anvil geometries, initial velocity and pass/fail threshold. These differences are shown in Table 4-2.

All mentioned standards assess helmets according to the acceleration to the centre of gravity of the headform and none of them clearly address BSF which is the most common type of injury in motorcycle accidents [12,34]. Even though, testing according to Snell and ECE 22.05 requires impacts on the chin bar of the helmet, it is not clear how the adopted injury criterion can measure the risk of BSF [99]. Therefore, a numerical method has been developed in order to optimize the chin bar of a composite-shell helmet with respect to BSF. The detailed information about this method and the relevant results are presented in Section 8.1.

Table 4-2 Comparison between different standards for testing helmets [28].

	ECE 22.05	Snell M2010	AS/NZS 1698	BS 6658	FMVSS 218
Anvil types and dimensions					
flat	D[1] = 130 mm	D≥127 mm	D≥127 mm	D = 130 mm	D = 127 mm
hemispherical	---	R = 48 mm	R = 48 mm	R = 50 mm	R = 48 mm
kerbstone	χ = 105° H ≥ 50mm r = 12 mm	---	χ = 90° H = 85 mm r ≤ 0.5 mm	---	---
edge	---	L = 180mm W = 6.3 mm H = 35mm	---	---	---
Initial conditions					
flat/1st[2]	7.5 m/s	7.75 m/s	1830 mm	6.5 m/s	6 m/s
flat/2nd	---	A[3]-E: 7.09 m/s J: 6.78 m/s M: 5.73 m/s O: 5.02 m/s	1830 mm	4.6 m/s	6 m/s
hemispherical/1st	---	same as flat anvil	1385 mm	6 m/s	5.2 m/s
hemispherical/2nd	---		1385 mm	4.3 m/s	5.2 m/s
Kerbstone/1st	7.5 m/s	7.75 m/s			
Relevant criteria and their limits					
Criterion 1	PLA ≤ 275 g	A-J: PLA ≤ 275 g M: PLA ≤ 264 g O: PLA ≤ 243 g	PLA ≤ 300 g	PLA ≤ 300 g	PLA ≤ 400 g
Criterion 2	HIC ≤ 2400	---	3 ms at 200 g	---	2 ms at 200 g
Criterion 3	---	---	6 ms at 150 g	---	4 ms at 150g

4.1.3. Proposal of a new test method

Several researchers who have been studying the head and brain injuries have suggested that the current helmet standard criteria should be revised in order to assess helmet's energy absorption in a more realistic way [58,60,88,100]. According to studies, which have been carried out about head/brain injury mechanisms, one of the most important issues, which should be addressed by helmet standards, is the effect of the component of the impact force tangential to the helmet. The tangential force on the helmet induces a rotational acceleration to the head which is known as the main cause of brain injuries like diffuse axonal injury [52–54]. Moreover, several researchers have also suggested that experimental tests in conjunction with numerical methods like finite element analysis, may provide the possibility of measuring the risk of injuries in a more accurate

[1] D: diameter, R: radius, χ: vertex angle, H: height, r: fillet radius, L: length, W: width.
[2] Snell M2010 and BS6658 require a second impact at the same site, but at lower impact velocities.
[3] A, E, J, M and O are different sizes of headforms.

way [58,100]. Therefore, new proposals for helmet standards have been presented in the last few years to include the effect of rotational acceleration due to oblique impacts and use of FE model based injury criteria [101,102]. The new proposal addresses different oblique impacts on helmets as shown in Figure 4- 3 and suggests using numerical analysis (Figure 4- 4) in conjunction with currently used head injury criteria e.g. HIC.

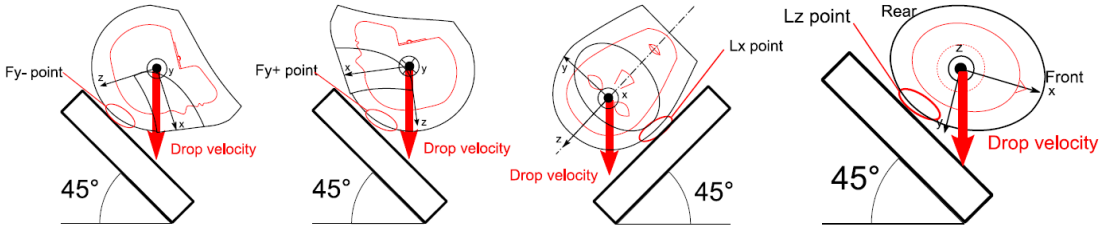

Figure 4- 3 Proposed impact conditions introducing angular acceleration [102].

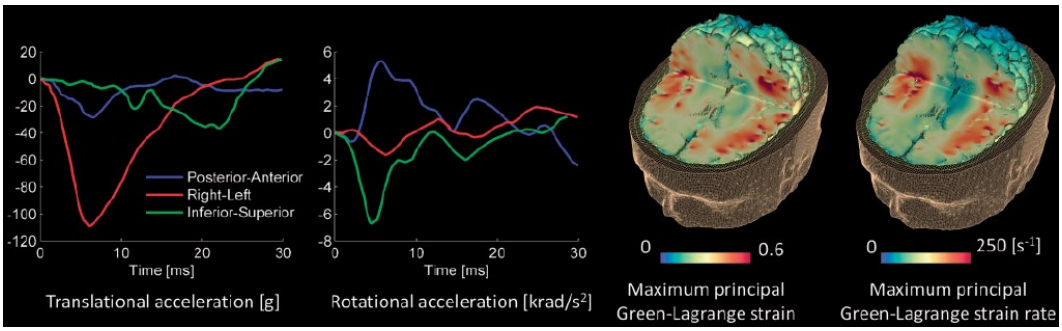

Figure 4- 4 Computational results for a real case head impact [58].

4.2. Neck protective device standards

There is no specific standard criterion to assess the capability of neck protective devices for motorcycle riders yet (until the date of present dissertation), therefore in this thesis finite element analysis (FEA) has been used to assess the capability of a neck protective device. The detailed information about this assessment will be described in Section 7.

4.3. Standards for other types of PPE

Even though, other types of PPE are beyond the scope of the present thesis, relevant standards for protection against impact loading for these types of PPE are mentioned in Table 4-3.

Table 4-3 Comparison between different standards for testing helmets [103].

Standard Number	Standard Name
EN 1621-1	Motorcyclists' protective clothing against mechanical impact, Part 1: Requirements and test methods for impact protectors.
EN 1621-2	Motorcyclists' protective clothing against mechanical impact, Part 2: Motorcyclists' back protectors – Requirements and test methods.
EN 1621-3	Motorcyclists' protective clothing against mechanical impact, Part 3: Motorcyclists' chest protectors – Requirements and test methods
EN 1621-4	Motorcyclists' protective clothing against mechanical impact. Motorcyclists' inflatable protectors. Requirements and test methods

5. Energy Absorbing Materials and Systems

5.1. Introduction

Energy absorbing or energy dissipative materials and structures are used in a wide range of applications like aerospace, defense and automotive industries, packaging, building construction, sports etc. They protect vulnerable and fragile products during shipment and human body parts during road accidents or dynamic sports against shock waves and isolate machine parts from destructive vibrations.

Different energy absorbing materials use different energy absorption mechanisms, which will be described in this chapter, they deform in order to absorb the energy. Their deformation might be elastic, visco-elastic or plastic according to their molecular or cellular structure.

The capability of energy absorption is called toughness [mostly used for metals] and could be calculated by the following equation, which calculates the area under the stress-strain curve [Figure 5-1]:

$$\frac{Energy}{Volume} = \int_0^{\varepsilon_R} \sigma . d\varepsilon \qquad \text{Eq. 5–1}$$

in which:

ε is strain

ε_R is the rupture (fracture) strain and

σ is stress.

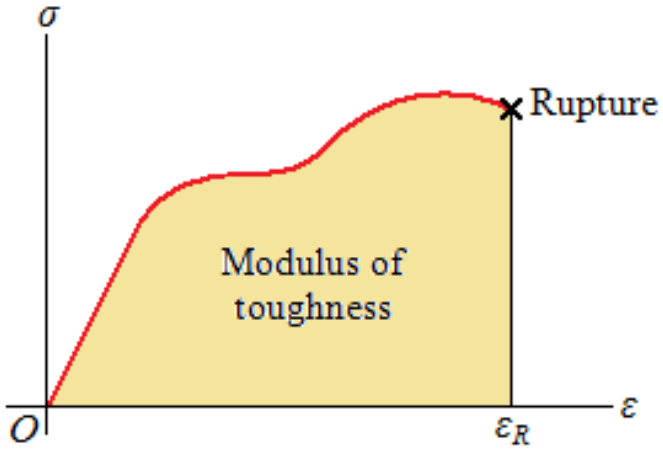

Figure 5-1 – Toughness, the area under the stress-strain curve [104].

Thanks to technology evolution, transports are becoming increasingly fast and impacts due to various accidents are more severe as well, moreover higher levels of safety are required for transported goods, therefore new energy absorbing materials are required by the market to improve the protective capability of both personal equipment and packaging systems. This chapter collects information on currently used protective devices and on several innovations in

the field of energy absorbing materials and systems with different applications with a particular attention to PPE for motorcycle riders.

5.2. Energy Absorbing Materials and Systems

This section provides a brief review of conventional energy absorbing materials and systems which are commercially available and are commonly used to mitigate shock waves due to impact loading.

5.2.1. Cellular Solids

A solid material which is made of an interconnected network of struts and/or surfaces can be called "Cellular solid" [105]. Figure 5-2 illustrates different examples of cellular solids.

A wide range of materials could be categorized as cellular solid. These materials are used every day in different shapes and forms. Usually, there is a foam liner inside shoes so we wear them and use their properties to feel more comfortable, and since bread is some kind of foam, we even eat them almost every day. Bones are some sort of cellular material, therefore, cellular materials are also a part of our body.

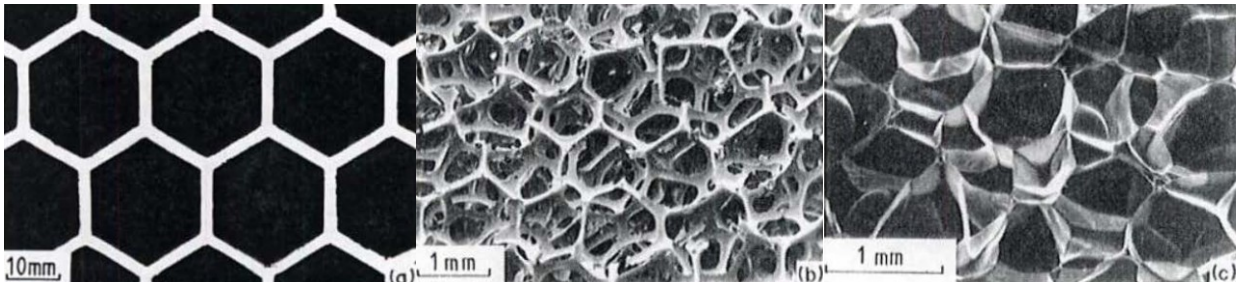

Figure 5-2 – Examples of Cellular Solids: (a) a two dimensional honeycomb, (b) a three dimensional foam with open cells, (c) a three dimensional foam with closed cells [105].

Cellular solids are mainly used in following fields:

- Thermal insulation
- Packaging
- Personal Protective Equipment (PPE)
- Structural use
- Marine Industry

The most important property of a cellular material is the ratio of cellular material density (ρ^*) per solid material density which the cellular solid is made from (ρ_s) and is called relative density [105]:

$$Relative\ Density = \frac{\rho^*}{\rho_s} \qquad \text{Eq. 5–2}$$

A common method for material characterization, which is used for cellular solids is a compression tests. A typical response of a cellular solid obtained from a compression test is

illustrated in Figure 5-3. There are usually three main regions in the cellular solid's stress-strain curve: 1 Elastic region, 2 Plateau region and 3 Densification. The second region is the most important for energy absorption, in which, material can deform significantly with a small stress variation [105].

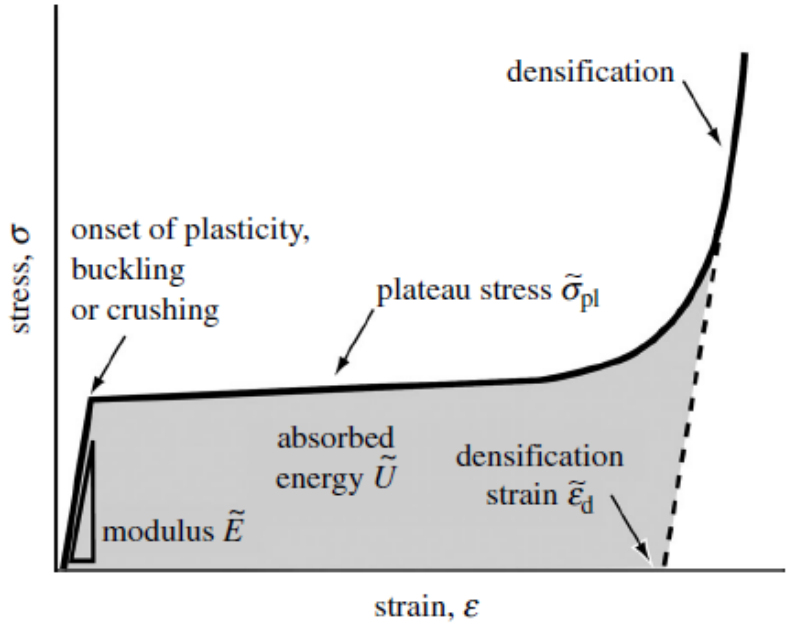

Figure 5-3 – A typical stress-strain curve of a cellular solid [106].

5.2.1.1. Foams

Foams can be produced in different ways according to their base material. Polymeric foams can be produced by introducing the blowing agent into the liquid or hot base material and then by cooling the cells will be formed. The metal foams can be produced by injecting foaming agent (similar to the polymeric foams) and also by casting (See Figure 5-4 and Figure 5-5) [105].

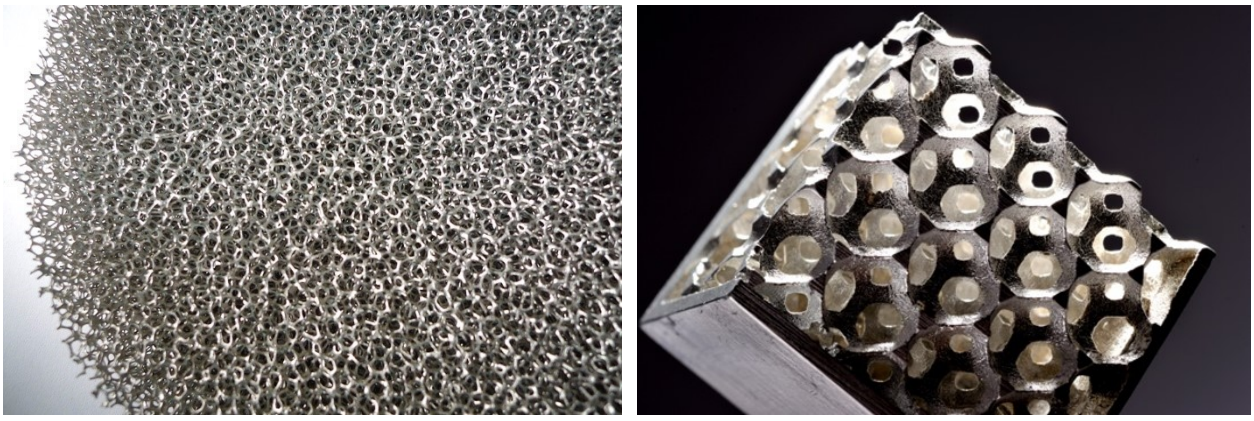

(a) (b)

Figure 5-4 – Metal foams: a. Produced by foaming agent [107], b. Produced by casting [108].

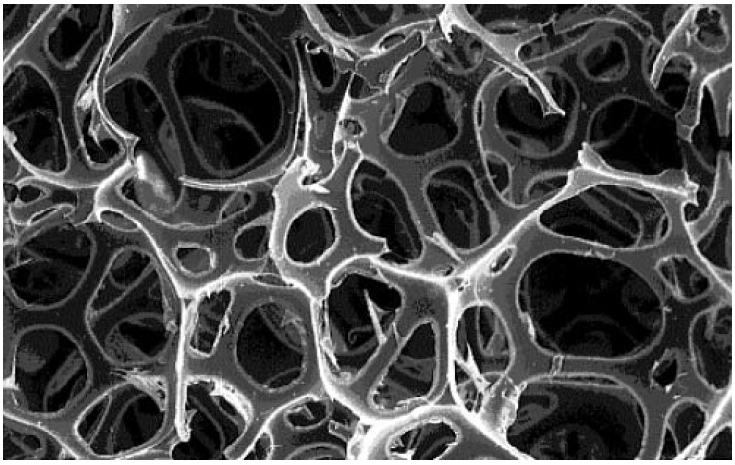

Figure 5-5 – Polyurethane open cell foam produced by gas injection [109].

5.2.1.1.1 Open Cell Foams

Open cell foams are made of an interconnected network of struts. Figure 5-6, schematically shows different samples of regular open cell structures for a single unit, and their interconnected network.

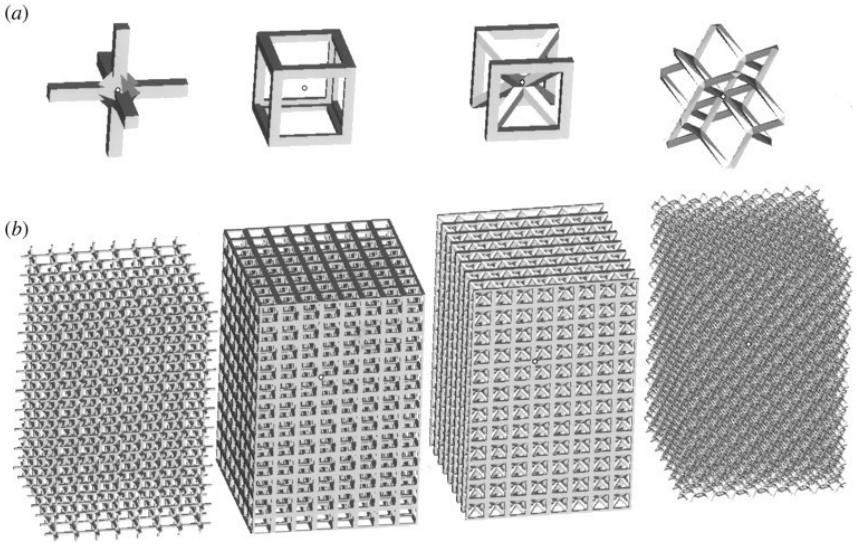

Figure 5-6 – Open Cell Foam, a: a cell structure, b: bulk structure (an interconnected network of struts) [110].

Energy Absorption Mechanism of Open Cell Foams

Open cell foams can absorb energy thanks to the deformation of the struts, which construct the foam structure. As it is illustrated in Figure 5-7, the open cell foam absorbs energy by elastic deformation (cell edge bending) and goes on with buckling of the cell edges and at the end the cell will bottom out by generating the plastic hinges.

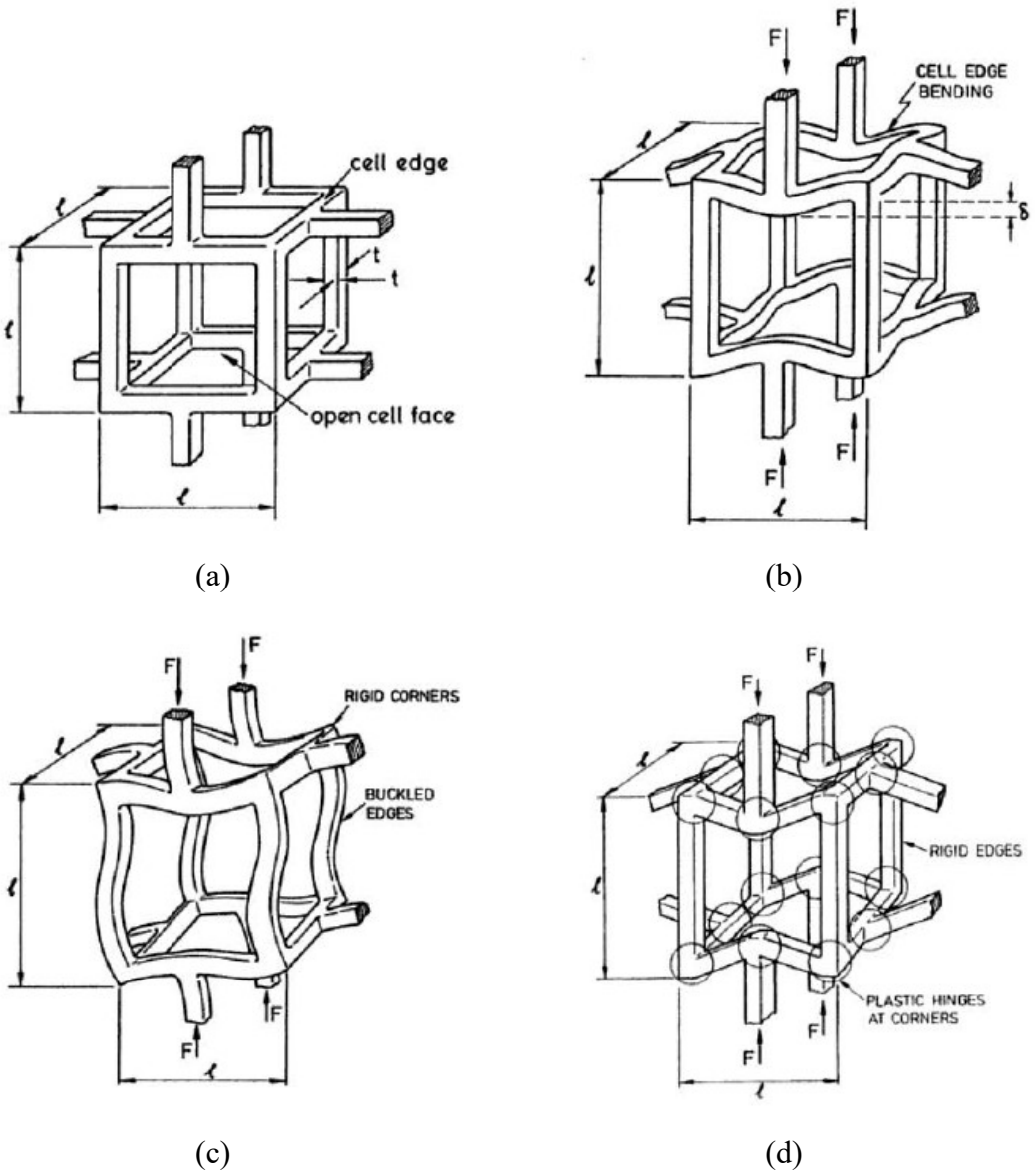

Figure 5-7 – A cell of an open cell foam: a. Schematic cell structure, b. elastic deformation of the cell, c. buckling of the cell edges, d. plastic hinges and the corners [105].

5.2.1.1.1 Closed Cell Foams

Closed cell foams are made of an interconnected network of struts and surfaces. They may have a wide range of arrangements based on their cell configuration. Figure 5-8 shows two different ideal cell geometries and their space filling patterns for closed cell foams. The main difference between closed cell foams and open cell foams is the fact that the gas which is trapped inside the closed cells cannot go out of the cell before cell rupture. In open cell foams instead the gas within the foam can move more freely.

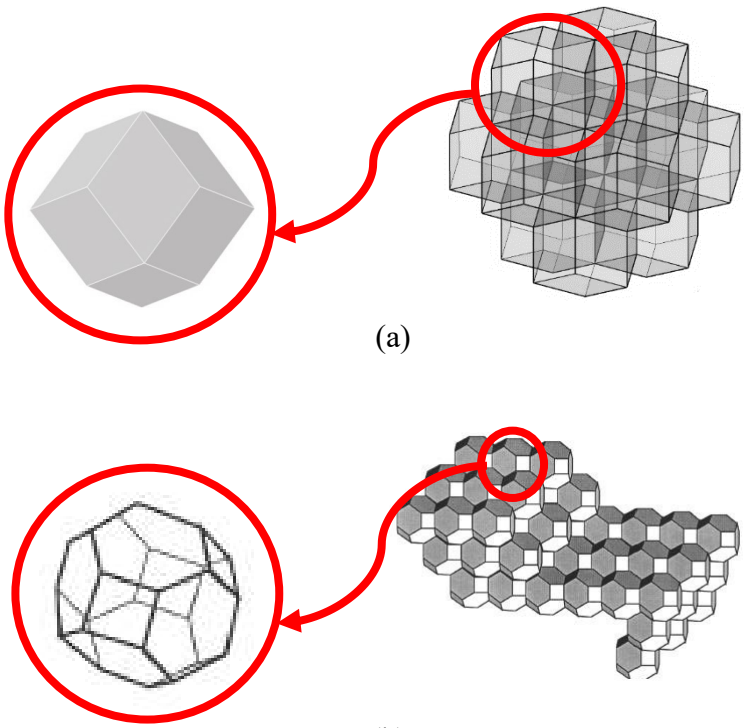

Figure 5-8 – Examples of closed cell structures and their space filling pattern, a: rhombic dodecahedra [111,112], b: truncated octahedron [113].

Energy Absorption Mechanism of Closed Cell Foams

Closed cell foams can absorb energy in the same way as open cell foams but as depicted in Figure 5-9, the surface of the cells can deform and absorb some amount of energy as well. Therefore, they have more mechanisms to dissipate energy.

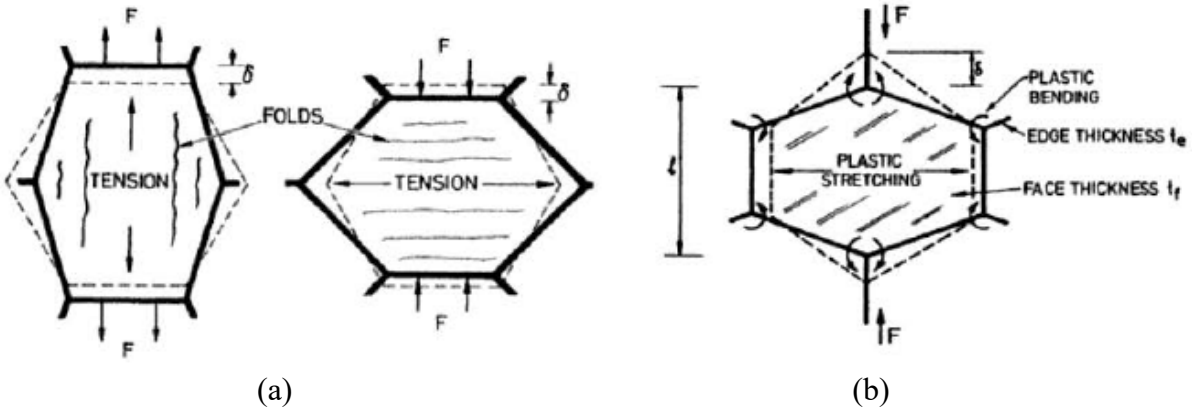

Figure 5-9 – Deformation of the faces of a closed cell foam:
a. Elastic deformation, b. Plastic deformation [105].

In addition, the entrapped gas inside the structure of closed (Figure 5-10) cell foams can influence their mechanical behavior [114]. It was found that the entrapped gas can stiffen and increase the stability of closed cell foams [115].

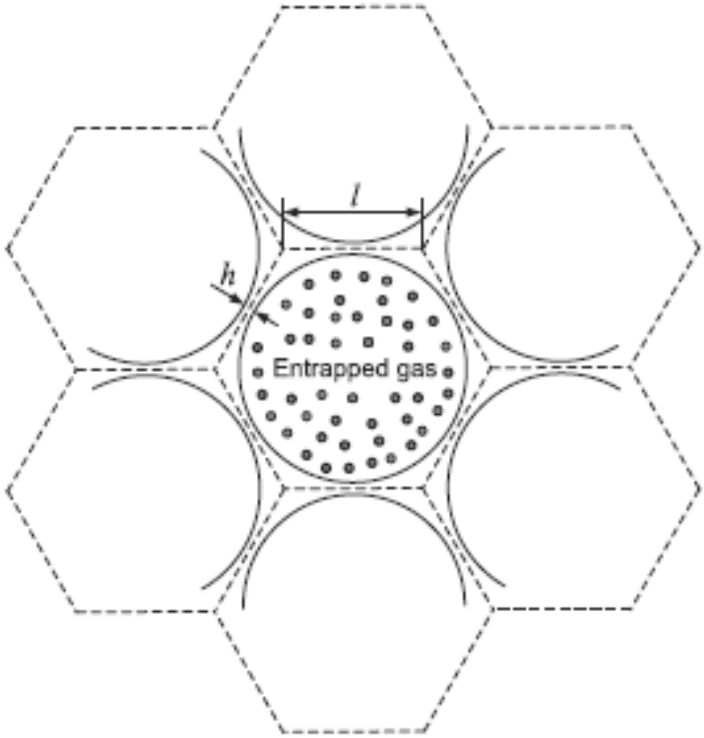

Figure 5-10 – Entrapped gas inside closed cell foams [114].

5.2.1.2. Honeycombs and Similar Structures

Bee's honeycomb is the perfect example of a naturally optimized honeycomb structure by its regular prismatic hexagonal cell, but any structures, which are constructed by nesting any array of prismatic cells can be called honeycomb structure. The cells can be triangular, square, rhombic, hexagonal (like honeycomb bee) etc. Figure 5-11 shows three different types of honeycomb panels.

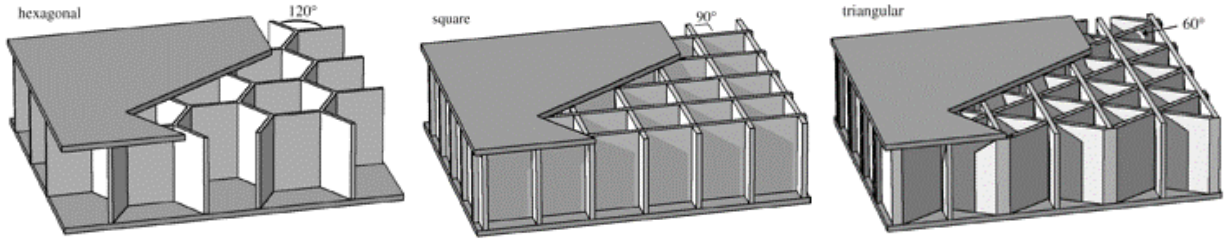

Figure 5-11 – Honeycombs with different cell geometry [116].

Energy Absorption Mechanism

Honeycomb structures can absorb energy thanks to elastic deformation, buckling and plastic hinges as it is shown in Figure 5-12.

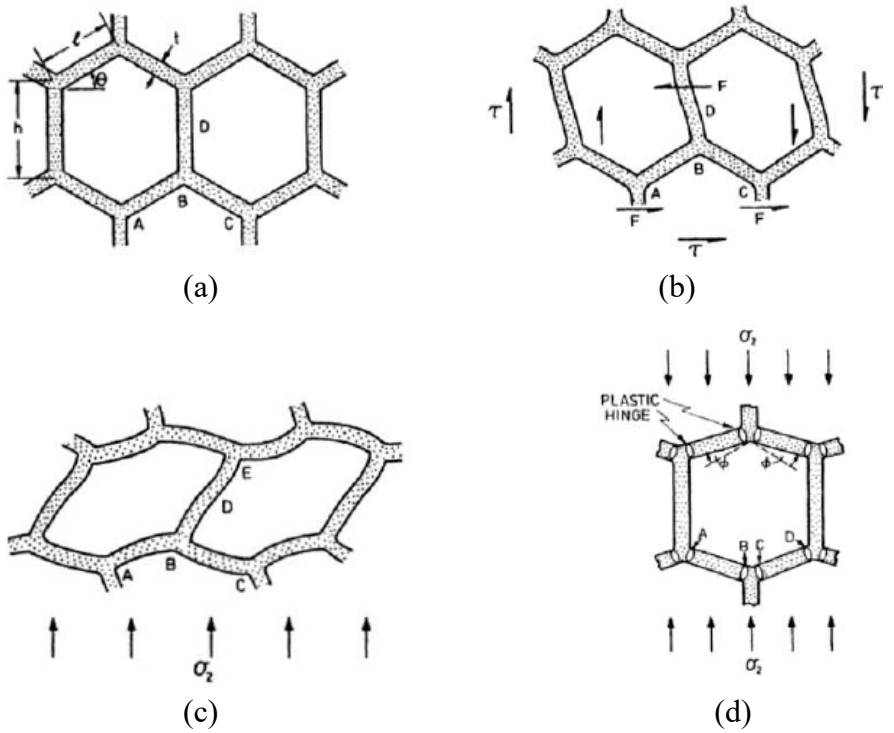

Figure 5-12 – Honeycomb cell: a. Before loading, b. Elastic Deformation, c. Buckling and d. Plastic hinges [105].

Since the stiffness of the honeycomb cell is different in longitudinal and transversal direction, the mechanical properties of honeycombs depend on the loading direction [117]. Figure 5-13 depicts a honeycomb structure and its principal directions and the mechanical properties for directions T, L and W, are illustrated in Figure 5-14.

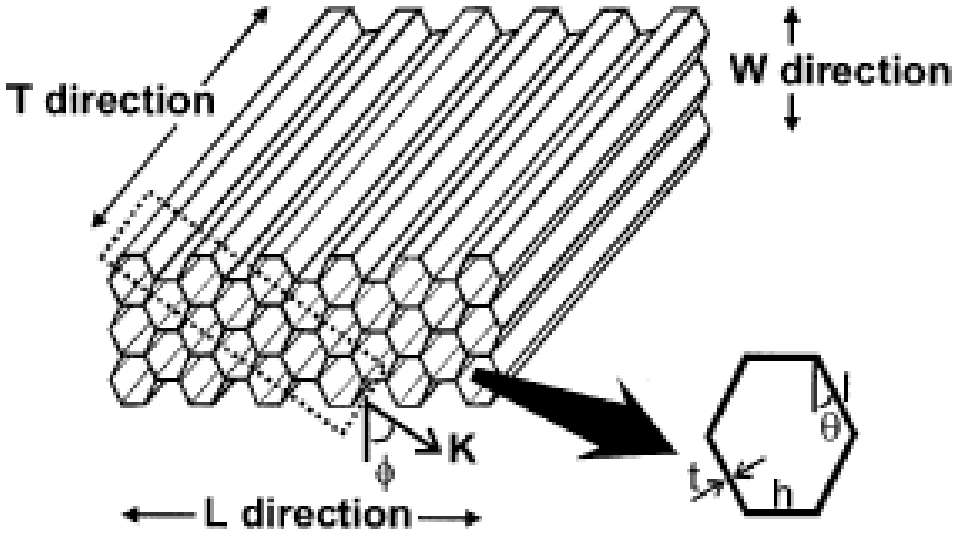

Figure 5-13 – Honeycomb cell principal directions [118].

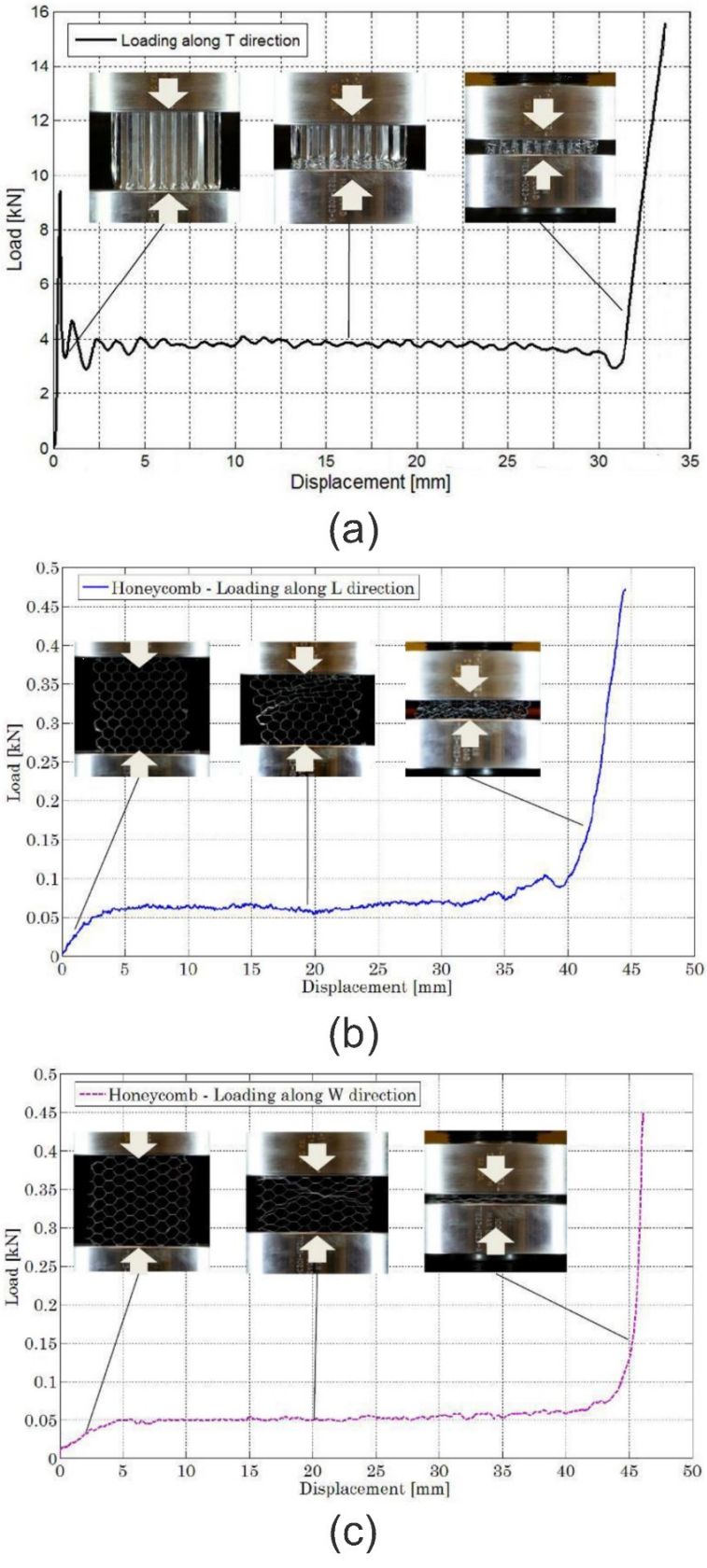

Figure 5-14 – Honeycomb load-displacement curve along a: T direction, b: L direction and c: W direction [117].

5.2.2. Composite Laminates

Composite materials are widely used in various industries like automotive, aeronautics, defense etc. They are light and stiff and often exhibit high energy absorption and dissipation [119,120]. Composite laminates are made by stacking of several laminae, which are bonded together, as shown in Figure 5-15.

In order to compare their energy absorption capability, several authors introduced specific energy absorption, e.g. [119,120], which is defined as the energy which can be absorbed during deformation per unit of mass of the material and can be calculated as:

$$E_s = \frac{W}{m} = \frac{W}{\rho A L_d} \qquad \text{Eq. 5–3}$$

in wich, W is the absobed energy, m is the crushed material mass, ρ is the material density, A is the area of the material cross section and L_d is the crushed material length.

The absorbed energy (W) is:

$$W = \int_{\delta_1}^{\delta_1+\Delta\delta} F.dx \qquad \text{Eq. 5–4}$$

where F is the applied force and δ_1 and $\delta_1+\Delta\delta$ are the displacement at the beginning and the end of loading (See Figure 5-16) [121].

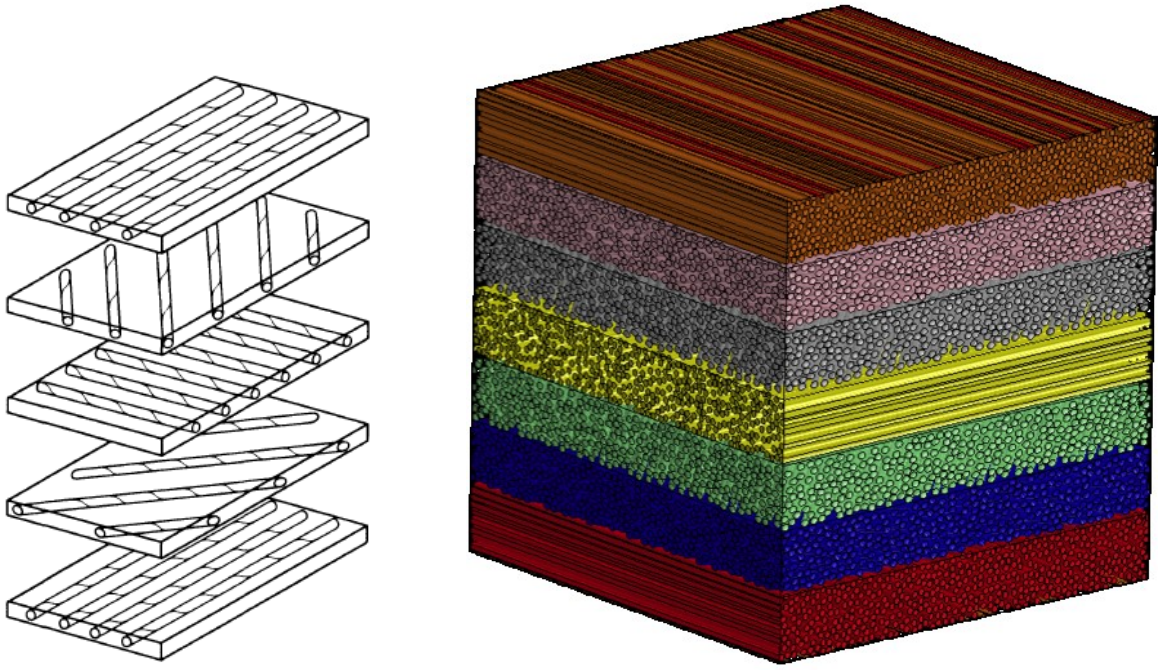

(a) (b)

Figure 5-15 – A laminate construction: a. Un-bonded view [122], b. Bonded view [123].

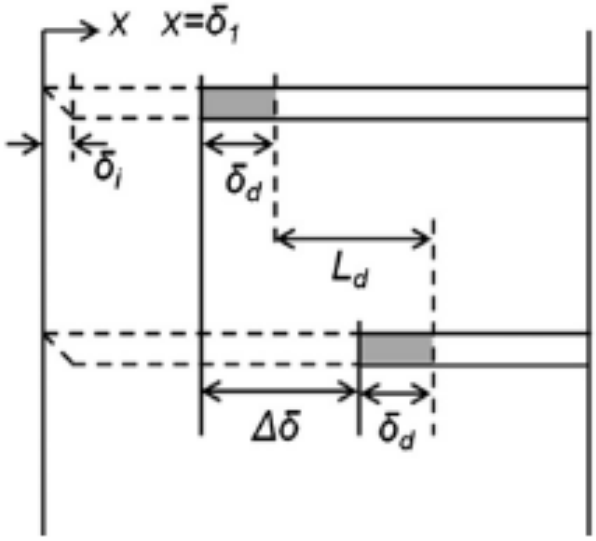

Figure 5-16 – Schematic drawing of a specimen crushed to displacements δ_1 (upper part) and $\delta_1 + \Delta\delta$ (lower part), with L_d indicating the advance of the crush front [121].

Energy Absorption Mechanisms

Composite laminates can be crushed in different ways because of their intrinsic properties and structures and by crushing, they can absorb energy. On the other hand, composite materials fail through a sequence of failure mechanisms which can involve the following possibilities [119]:

- Fiber fracture
- Matrix crazing and cracking
- Fiber-Matrix de-bonding
- Delamination and
- Inter-ply separation

Figure 5-17 illustrates different failure modes of a composite laminate.

The failure mechanisms of a composite structure depends on the following factors [119]:

- Structure geometry
- Lamina orientation
- Type of trigger
- Crush speed

The aforementioned parameters can be used to design or optimize the composite structure in order to achieve the maximum energy absorption capacity.

The progressive crushing of a composite structure leads to a load-displacement curve like that shown in Figure 5-18 in which, zone II is related to the progressive crushing and the largest amount of energy is absorbed in this phase.

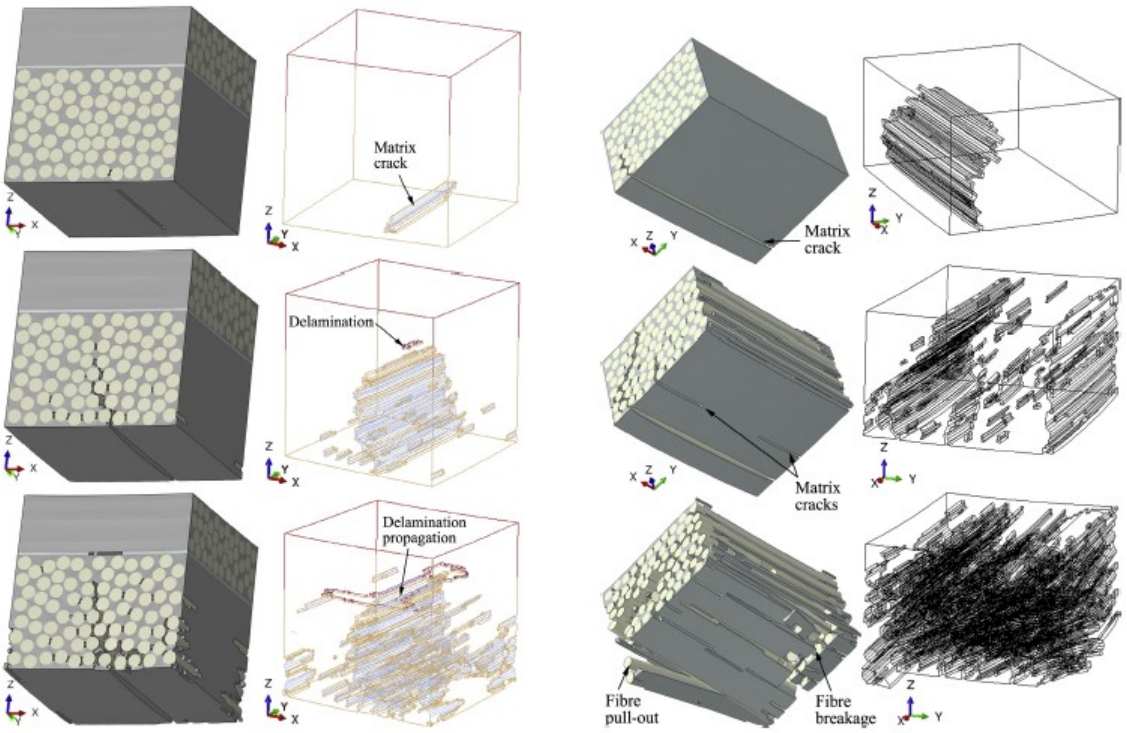

Figure 5-17 – Different fracture modes of a composite laminate [124].

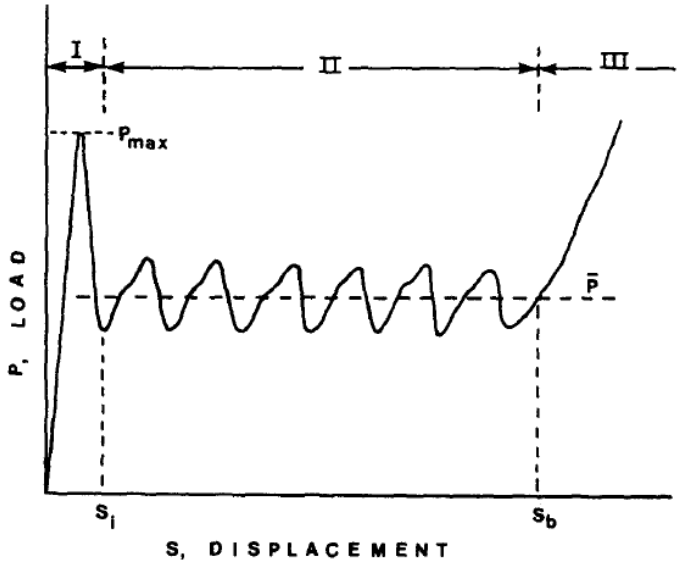

Figure 5-18 – Typical load-displacement curve for progressive crushing of a composite laminate [125].

5.2.3. Airbags

The airbag is an energy dissipative system which has been registered in 1953 as an occupant safety device which could mitigate the energy of collision [126], and has evolved up to now in different industries in order to absorb the impact energy. They are especially used in the car industry to protect car occupants. They come in different shapes and sizes based on their use. Figure 5-19 shows some different types of airbags.

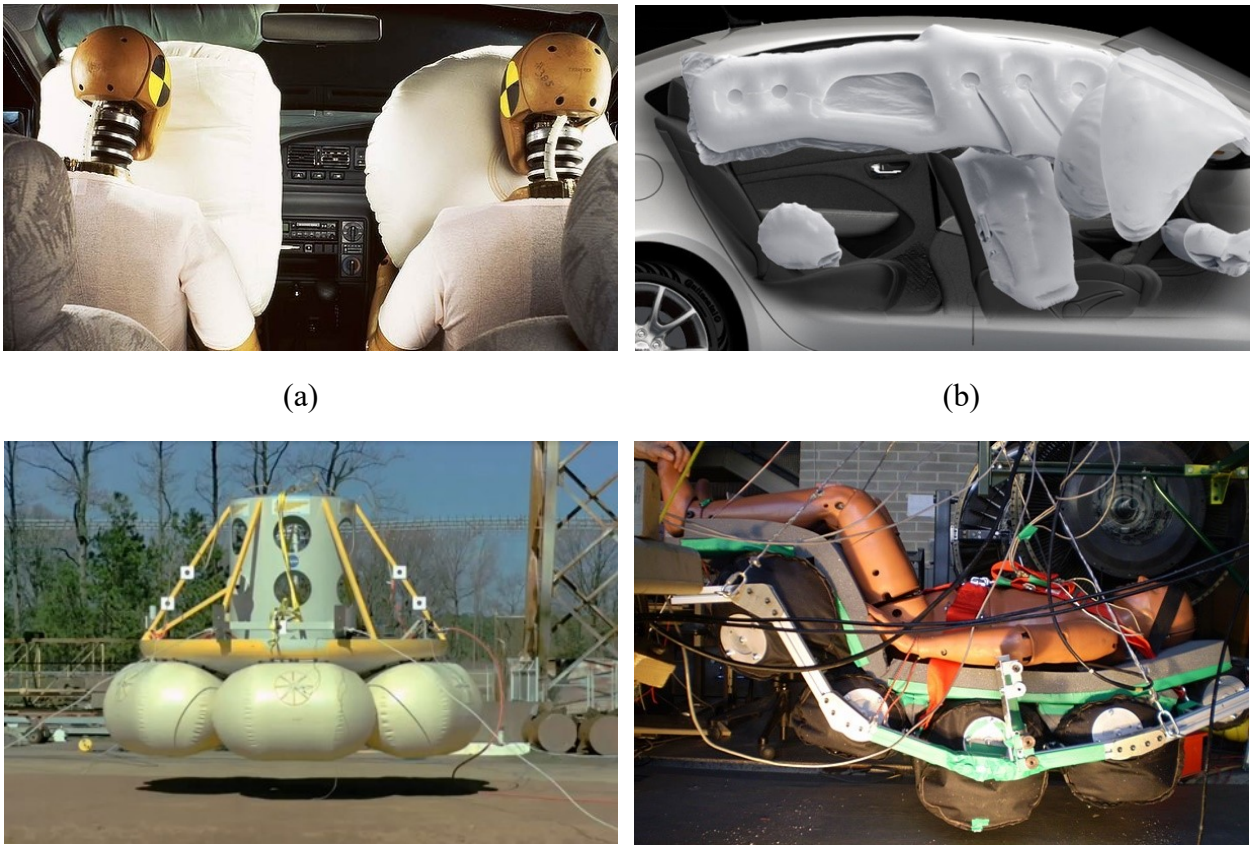

Figure 5-19 – Different type of airbags: a: Car frontal Airbag [127], b: Car side airbag [128] c: Landing airbag [129] d: Occupant landing airbag [130].

Energy Absorption Mechanism

Basically the air bag mitigates the impact load by converting the kinetic energy of the impactor into the potential energy of the airbag gas, by pressurizing it, and dissipates this energy by venting the gas [131]. Therefore, the airbag operates with an internal pressure which is greater than atmospheric pressure in order to decelerate the impactor [132].

Airbag can be considered as a nonlinear spring which can dissipate the dynamic loading, the force equilibrium equation for an ideal airbag (Figure 5-20) and the stiffness of such an equivalent spring could be written as follows, Eq. 5-5 and Eq. 5-6 respectively [131]:

$$m\ddot{x} + \left(P_{bag}(x) - P_{atm}\right)A_{FP}(x) = mg \qquad \text{Eq. 5–5}$$

$$k(x) = \frac{1}{x(t)}\left(P_{bag}(x,t) - P_{atm}\right)A_{FP}(x) \qquad \text{Eq. 5–6}$$

in which:

m: is the mass of the impactor or the subject which should be decelerated

x: is the displacement of the impactor

$\ddot{x}$: is the acceleration of the impactor

P_{bag}: is the inner pressure of the airbag

P_{atm}: is the atmospheric pressure

A_{FP}: is the foot print area of the airbag, as shown in Figure 5-20

g: is the acceleration of gravity

k: is the stiffness of equivalent spring, and

t: is the time

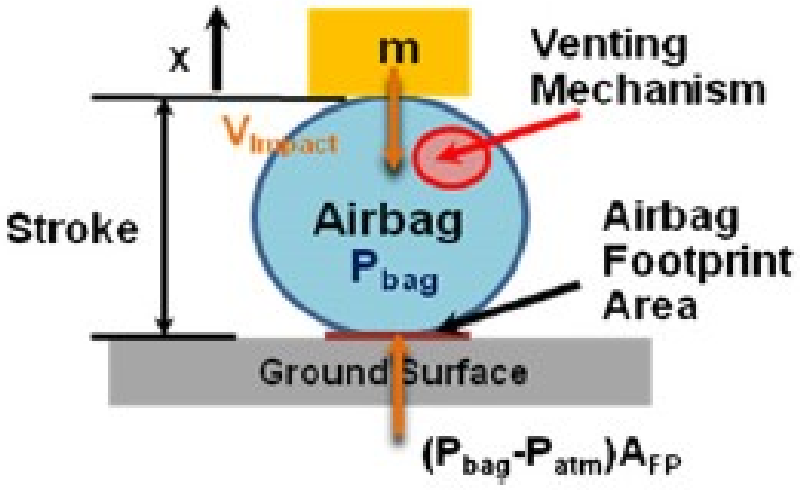

Figure 5-20 – Ideal airbag system [131].

The airbag behavior and response is a function of its geometry and pressure (Eq. 5-6), so by choosing the best combination of these variables the best energy dissipation can be achieved.

5.3. New Energy Absorbing Materials and Systems

After an introduction about energy absorbing materials and systems in Chapter 5.2, this Chapter aims at introducing more recently developed energy absorbing materials and systems.

5.3.1. Cellular Solids

Cellular solids, as it has been mentioned in Chapter 5.2, exhibit a wide range of mechanical properties and their mechanical properties depend on their relative density and the shape of the cell, therefore researchers try to modify the relative density of the foam and its cell shape according to their demands. The materials and systems which are presented here are mostly developed to be used in the field of safety and PPE.

5.3.1.1. Foams

Like other types of cellular structures, mechanical properties of foams depend on their relative density and the shape of the cell. In this section some newly developed foams have been introduced, some of them are still under development and are far from mass production and commercial exploitation.

5.3.1.1.1 Open-Closed Cell Foams

In a classic way, foams are classified as open or closed cell but by controlling the manufacturing process it is possible to have a mixed state of open-closed structure [109] as it is shown in Figure 5-21.

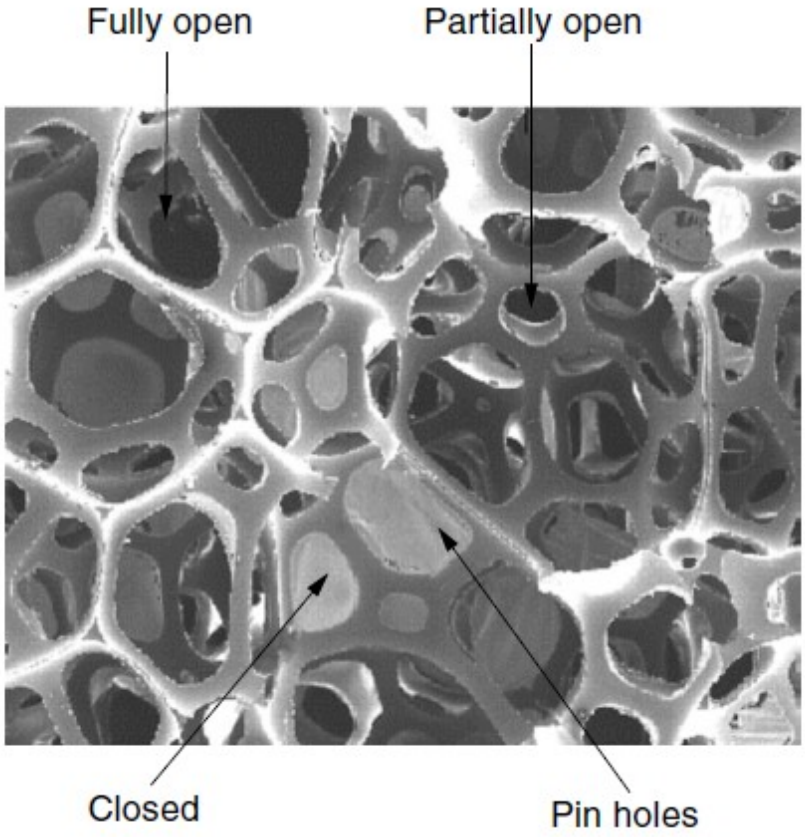

Figure 5-21 – Different states of a foam's cell windows [109].

By controlling the state of the foam's cell windows, the air that flows out of the cell and flows in to the cell can be controlled as well. Therefore, smart materials, which have a low stiffness under static loads and high stiffness at higher strain rate, can be developed. Since at low loading rate, the gas has time to exit the cell, the stiffness of the material is just provided by the cell walls and edges, but at higher loading rates the gas will be trapped inside the cell and the cell internal pressure will increase, hence the stiffness of the cell will increase, as well. D3O® [133] is a typical example of such foams having different mechanical response according to the loading rate.

Another newly developed commercial brand is PORON® [134], which is produced in different densities for a wide range of applications. PORON® is a visco-elastic foam which recovers its original size and properties some time after the impact. The PORON® manufacturer provided some samples for testing to the MOTORIST project. Using the provided samples, mechanical tests were conducted using a compressive test machine in the Department of Industrial Engineering at University of Padova. Three different densities of PORON® have been tested and part of the results are shown in Figure 5-22. Even though, PORON® has a reasonably good energy absorption, it is not light enough to be used as a helmet's liner. Since the present thesis is focused on head-neck protection and studying the use of PORON® for other types of PPE devices would be out of scope of this thesis, no more study was carried out on this material.

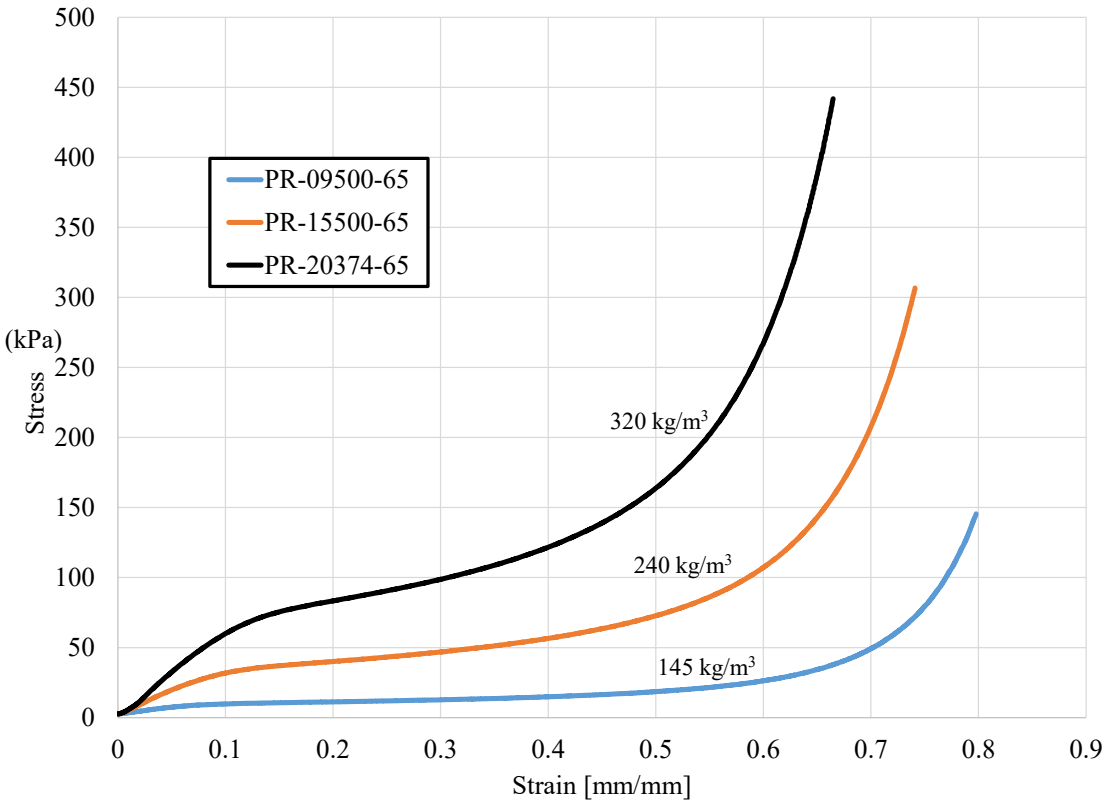

Figure 5-22 – Stress-Strain Curves of PORON® with three different densities.

5.3.1.1.2 Functionally Graded Foams (FGF)

Crushable foams like EPS are very common for packaging and for protective equipment like helmets. They are light and cheap materials and they have suitable energy absorption capability. However, a thick layer of a crushable foam like EPS cannot be usually crushed completely under impact loading, and that means that not all the energy absorption capacity of the foam can be used. Figure 5-23 approximately shows how different layers of a foam like EPS behave under compressive loading.

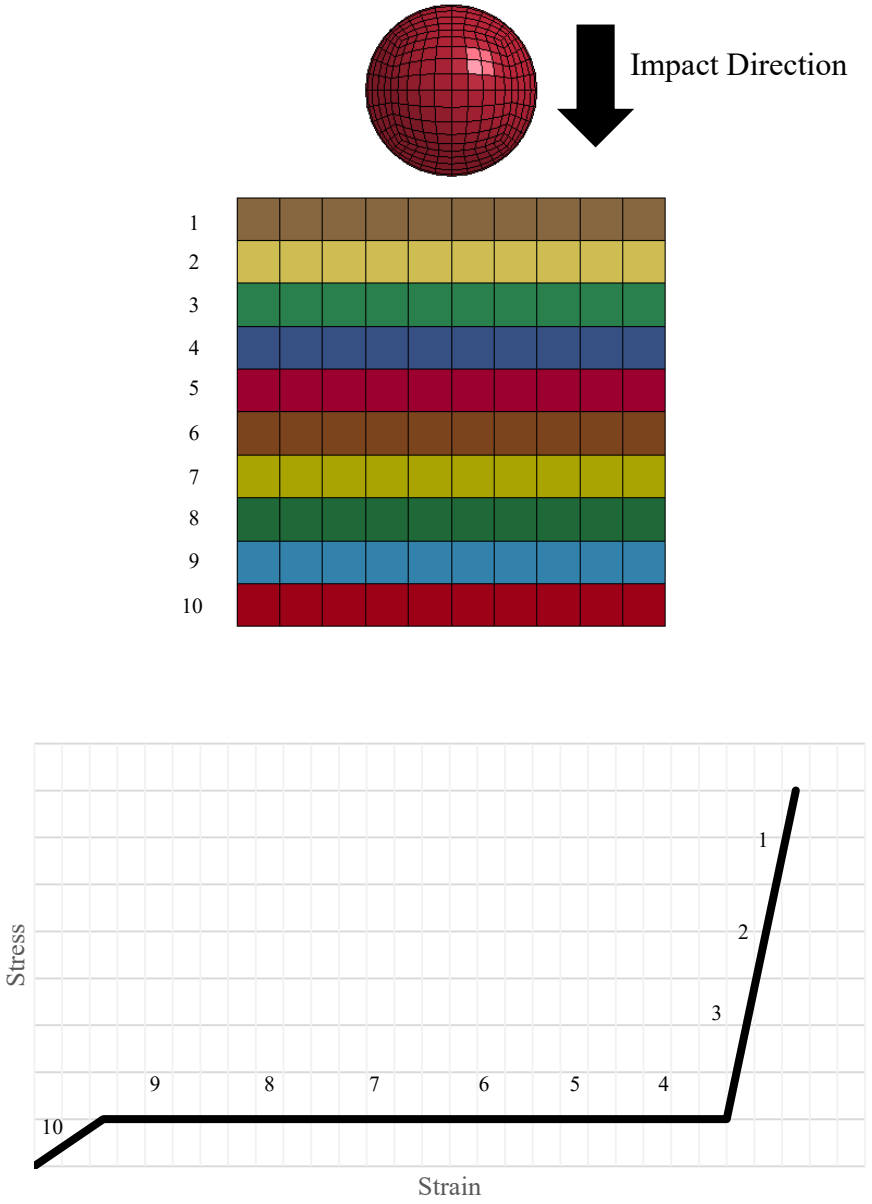

Figure 5-23 – (top) Different layers of foam and (bottom) their related location on the stress-strain curve.

If the mechanical properties of the foam can be modified in a way that almost all layers of foam respond to the external load in the region between point number 4 to 6 on the stress-curve (Figure 5-23) or at least in the plateau zone of the stress-strain curve, an ideal foam would be obtained capable to take full advantage of the whole energy absorption capacity.

L. Cui et al. [135] showed that functionally graded foams have better energy absorption properties in comparison with the uniform ones. Attia et al. [136] also studied the crush behavior of a reinforced column with a core with varying properties through thickness and showed that by using FGF core instead of uniform core energy absorption could be increased by 12%.

Since the main property of a foam is its density, the most commonly accepted idea to produce functionally graded foams assumes that they should be characterized by a controlled density distribution.

5.3.1.2. Honeycomb-shaped Structures

A wide range of honeycomb-shaped structures has been introduced in order to modify conventional honeycombs. They can be manufactured in a controlled way with different properties.

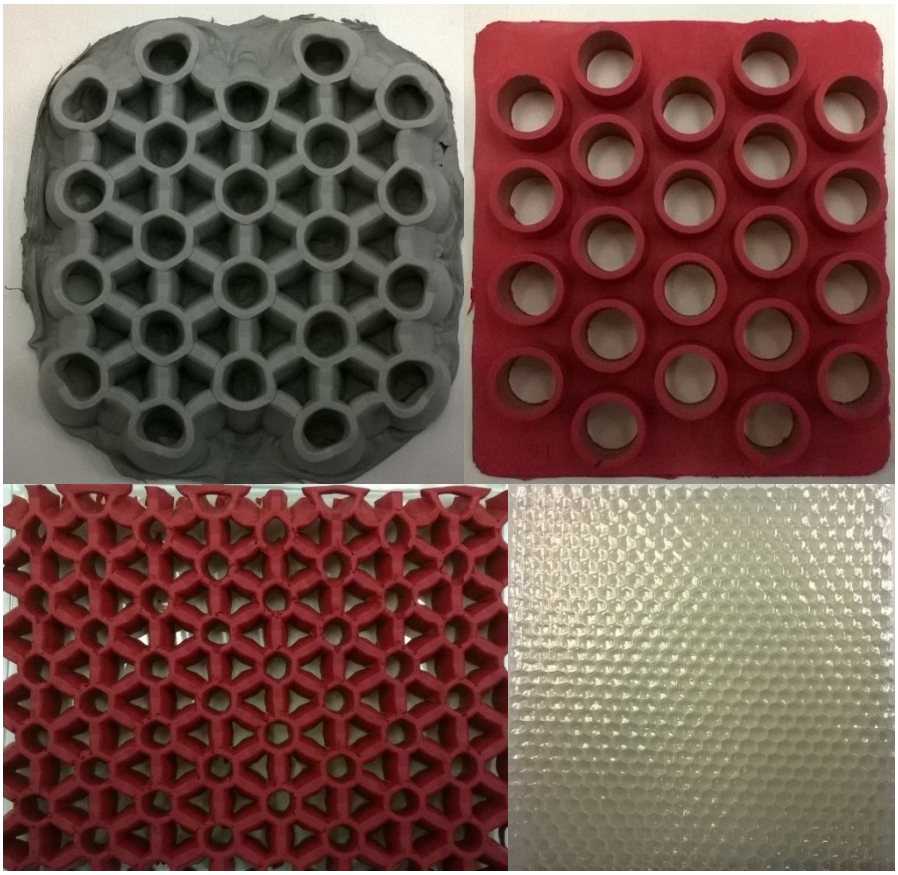

Figure 5-24 – Honeycomb-shaped structures [from Dainese S.p.A. material resources].

Figure 5-24 shows four different types of honeycomb-shaped materials which were designed in order to increase the energy absorption capability and to have an elastic or visco-elastic recovery after loading.

Another honeycomb shaped structure which has been introduced recently is called KOROYD®. Figure 5-25 shows KOROYD® and its mechanical behavior which is compared to its competitor in order to be used as the core of snow boards. The stress-strain curve (Figure 5-25) shows how the proposed core can reduce the stress in comparison with the conventional material.

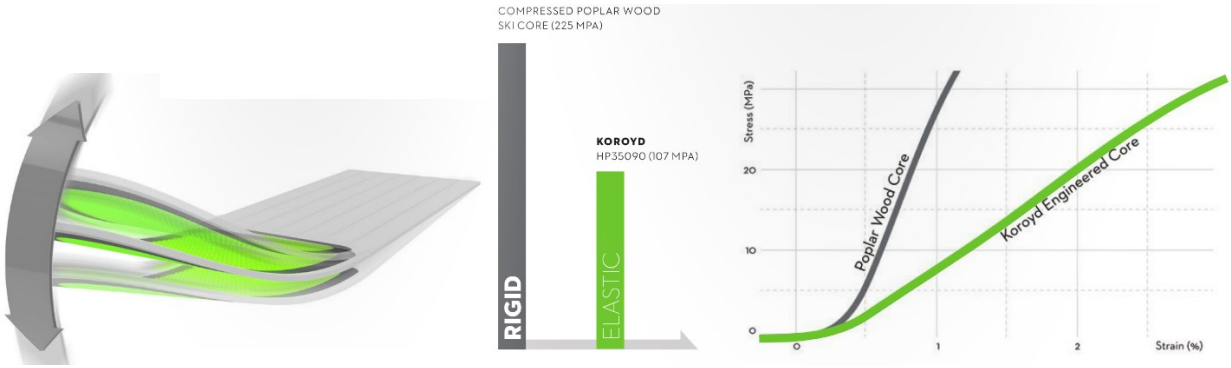

Figure 5-25 – KOROYD and its mechanical properties [137].

5.3.1.3. Adaptive Energy Absorbing Materials

Materials which exhibit coupling between multiple physical domains are called smart materials [138]. According to this coupling, materials can be designed in order to respond in different ways depending on the loading condition. Deshmukh and McKinley [139] have introduced an adaptive type of cellular material which changes its mechanical behavior by controlling the magnetic field strength. This material has been obtained by impregnation of a porous material with a field responsive fluid (Figure 5-26).

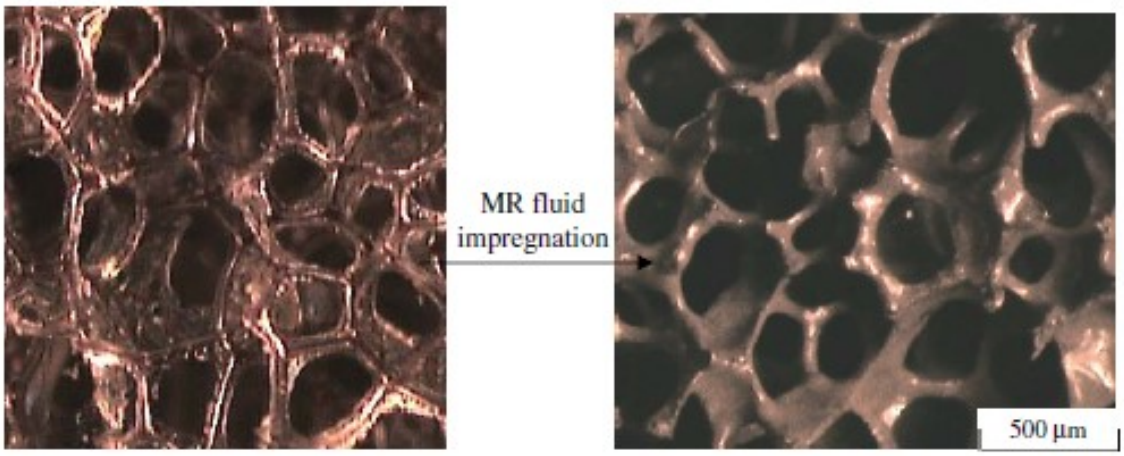

(a) (b)

Figure 5-26 – Optical micrograph of a dry low-density reticulated foam, a: before and b: after impregnation [139].

The cellular material has been impregnated with different fluid volume fractions and their capability to absorb energy has been compared by inducing a magnetic field with strength of 0.18 T. The result showed that energy absorption capability had been increased by utilizing this method (Figure 5-27).

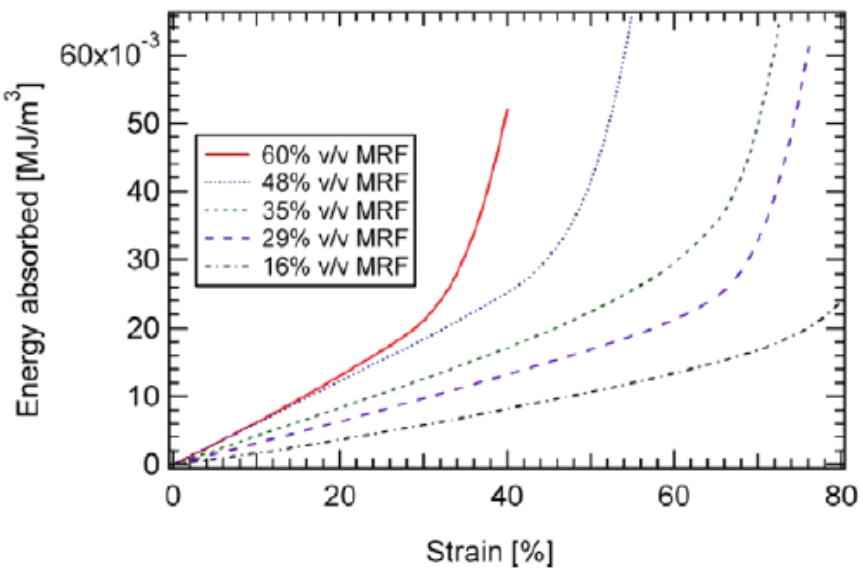

Figure 5-27 – Energy absorption curves for MR fluid-impregnated foam at 0.18 T [139].

5.3.1.4. Architected Materials

Architected materials (also called Architectured Materials) like metallic microlattice have been recently introduced and thanks to the controlled structural network, they have a high stiffness per weight ratio and high energy absorption capability [140]. Figure 5-28 shows that this type of materials can be designed in different scales according to the objective of their use. Based on their lattice structure, they can have different energy absorption capability [141,142] as shown in Figure 5-29.

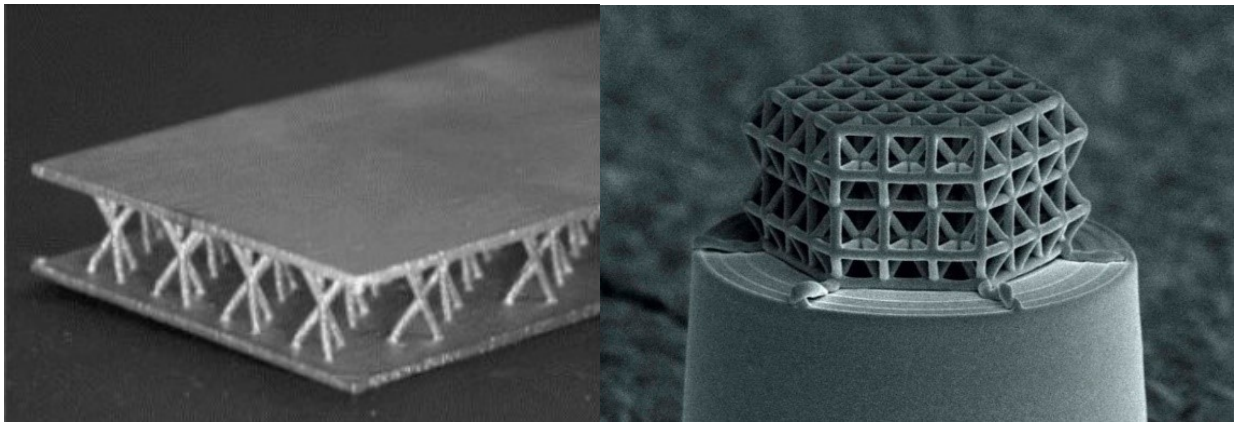

(a) (b)

Figure 5-28 – Lattice Structures: a. mm scale [140], b. µm scale (Photo: J. Bauer / KIT) [143].

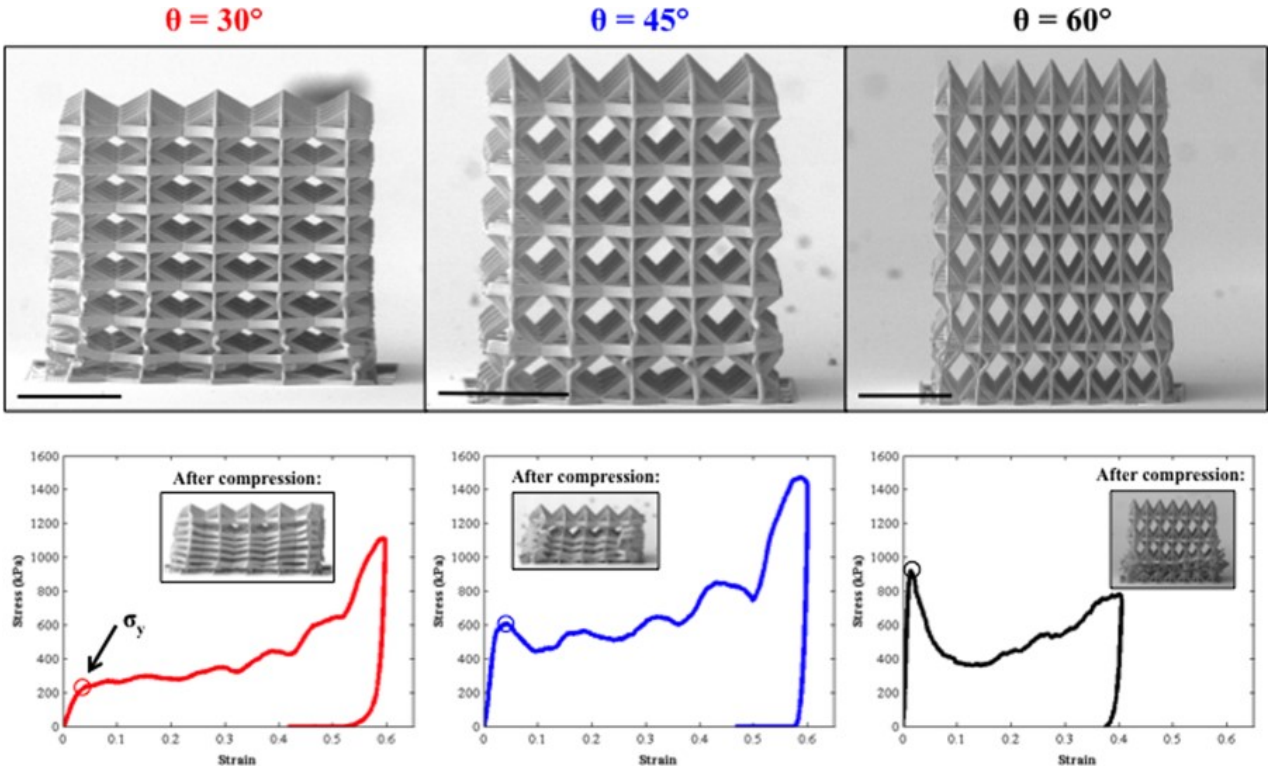

Figure 5-29 – Stress-strain curve for three different lattice structure [141].

Lattice structures can be designed not only to absorb energy, but also to attenuate the stress wave in a predetermined pattern [144].

5.3.2. Composite Laminates

5.3.2.1. Laminate Optimization

Figure 5-30-a shows the effect of fibre orientation on the load-displacement curve of a reinforced beam and Figure 5-30-b illustrates the results of a study about the effect of fiber orientations on the energy absorption capability of composite tubes. As it is shown, mechanical properties of composite materials which are reinforced by means of long fibers can be easily modified by changing the fiber direction and lay-up [145–147]. Hence, by optimizing the lay-up and fiber orientation of a composite laminate a new material with new mechanical properties can be produced according to their use. According to this capability of composite laminates, a numerical method has been developed in order to partially optimize the outer shell of a composite helmet with respect to the induced neck force (section 2.1). The method is presented in section 8.1.

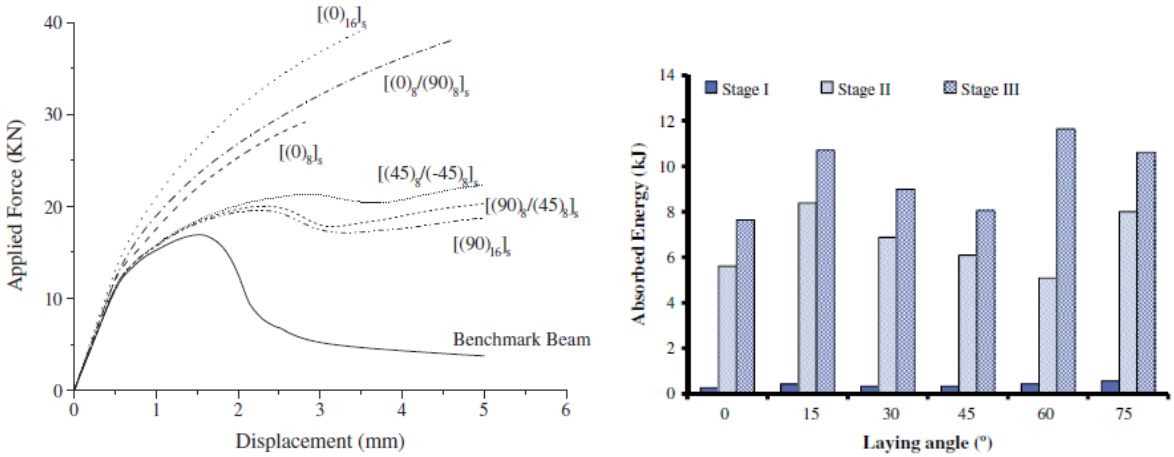

Figure 5-30 – a. Force-Displacement curves for a reinforced beam with different fiber orientations [146], b. Bar chart of total energy absorbed during various stages of axially crushed composite tubes with different fiber orientation [148].

5.3.2.2. High Performance Fibres

High performance polymeric fibers e.g. SPECTRA® and Dyneema® can increase the energy absorption capability of a composite laminate. Their Free Breaking Length (FBL) is more than twice that of carbon fibers [147]. Laminates making use of SPECTRA® fibers are mainly used for ballistic protections as shown in Figure 5-31.

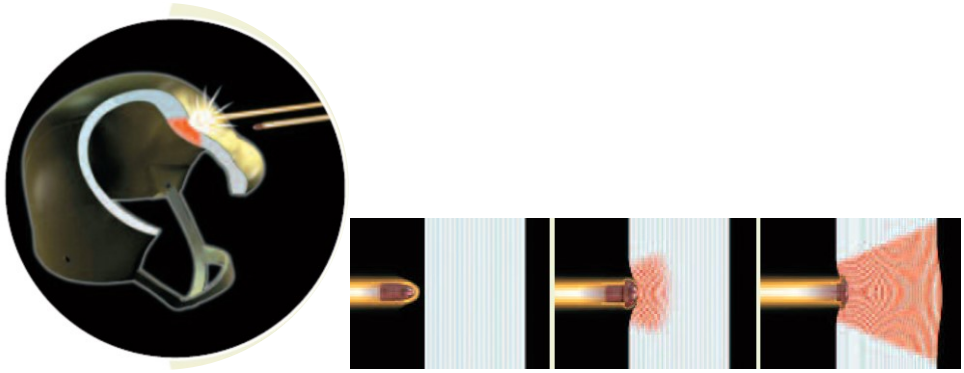

Figure 5-31 – A helmet made with Spectra Shield® material is shown stopping a 9mm round and defeating [149].

Tsampas et. al. [150] tested SPECTRA shield in case of projectile impact and compared the result with composite laminate made of aramid fibers. The projectile couldn't penetrate the SPECTRA shield at velocity of 442 m/s but it penetrated the aramid composite laminate at velocity of 386 m/s. According to their study, SPECTRA shield can absorb energy of impact much more than aramid composite laminates at high velocity impacts. Figure 5-32 shows the difference between the SPECTRA shield and the aramid fiber composite and shows how much the SPECTRA shield can deform, hence, it can absorb energy in this way. SPECTRA fabric was kindly provided by HONYWELL Co. for feasibility study of using it for helmet's outer shell. The testing procedure and the obtained results are presented in section 8.2.

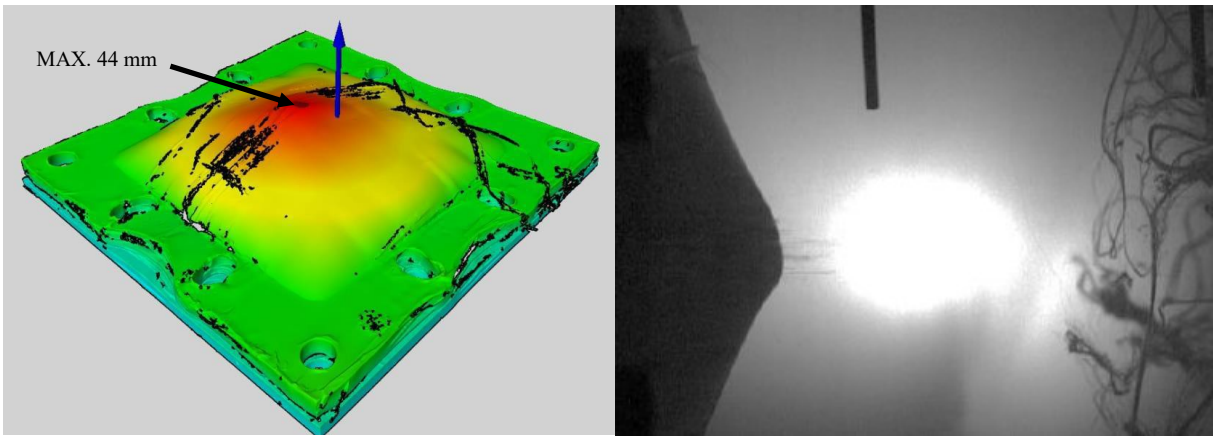

a. Contour plot of the deformation (left), Snapshot from high speed camera shows the maximum deflection (right); projectile velocity 442 m/s.

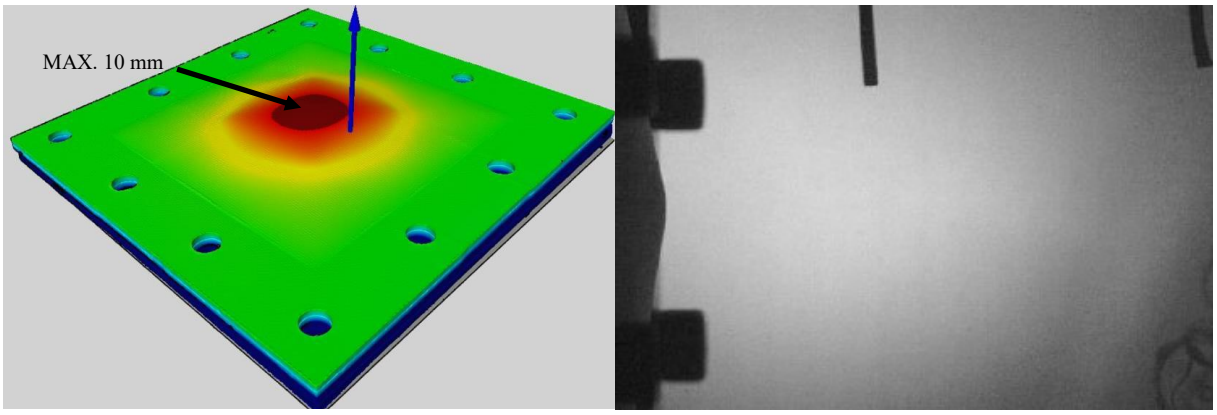

b. Contour plot of the deformation (left), Snapshot from high speed camera shows the maximum deflection (right); projectile velocity 305 m/s.

Figure 5-32 –a. Spectra Shield®, b. Aramid fiber composite laminate [150].

5.3.2.3. Stiffness-Modifiable Composites

Novel composites materials have been developed [151] in order to have stiffness-reduction due to external stimulations [152]. By reducing the stiffness, they can deform more and absorb more energy in comparison with normal condition. The external stimulation is usually electrical current, which can control the stiffness of the structure. These types of composites can be produced by coating the carbon fibers by a thermoplastic material and using a thermoset matrix [153]. Figure 5-33 shows the schematic behavior of a composite panel with active stiffness control capability. The coating softens upon an electrical impulse, the fibers are able to glide within the matrix and the stiffness of the composite decreases [151].

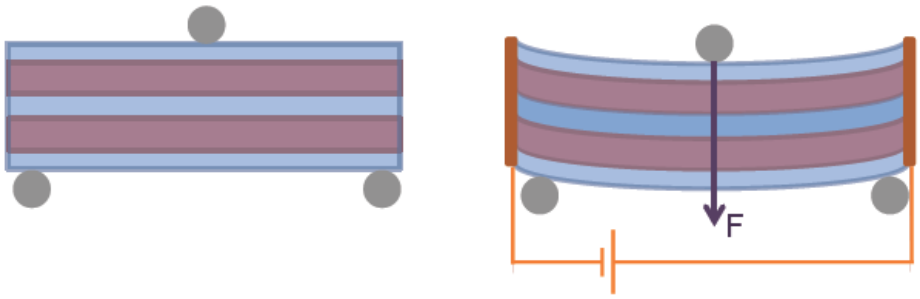

Figure 5-33 – Schematic behavior of a composite with active stiffness control according to [151].

5.3.3. Airbags

The airbag use has spread in recent years; the mechanism of energy absorption has not been modified but evolved actuation systems and new shapes and bags' material have often been adopted. Airbags have been recently used as an exterior safety system for road accidents to reduce the risk of head injury for pedestrian [154] and bicyclists. Figure 5-34 shows crash tests against a car which is equipped by means of exterior airbag.

Figure 5-34 – Exterior Airbag [154,155]

Airbags have been proposed as well to save electronic devices like smart phones [156]. Figure 5-35 shows a device for smartphones impact protection which has been recently proposed.

Figure 5-35 – Smartphone case with airbags [157].

In the field of motorcycle safety airbags are part of recently developed protection systems that detect dangerous situations and automatically inflate the bags around the rider's body. A deployment algorithm analyses data from various sensors and decides whether to deploy the system or not [89].

5.4. Realistic test method for energy absorbing materials

As it has been mentioned in Section 5.2.1, typical behavior of cellular solids can be obtained by means of compression test. However, in reality energy absorbing materials may experience load conditions different from pure compression. Especially for foams which are used as helmet's liner, it is crucial to underrate the response of the liner accurately. As it was mentioned in Section 4.1.3, numerical simulations will be probably a part of next generation of helmet standards in order to assess the helmet's response in case of oblique impacts, therefore a realistic test method should be used for material characterization of helmet's liner. Fahlstedt et. al. [158] reconstructed three real bicycle accidents by means of finite element method and showed high correlation between the numerical simulation and the real life data. They used two different stress-strain curve (as shown in Figure 5-36) in order to define the helmet's liner behavior, one is the conventional compressive stress-strain curve and the second one is shear stress-strain curve. The mentioned study considered both compressive and shearing response of the helmet's liner in order to obtain the response of the head and the brain more accurately.

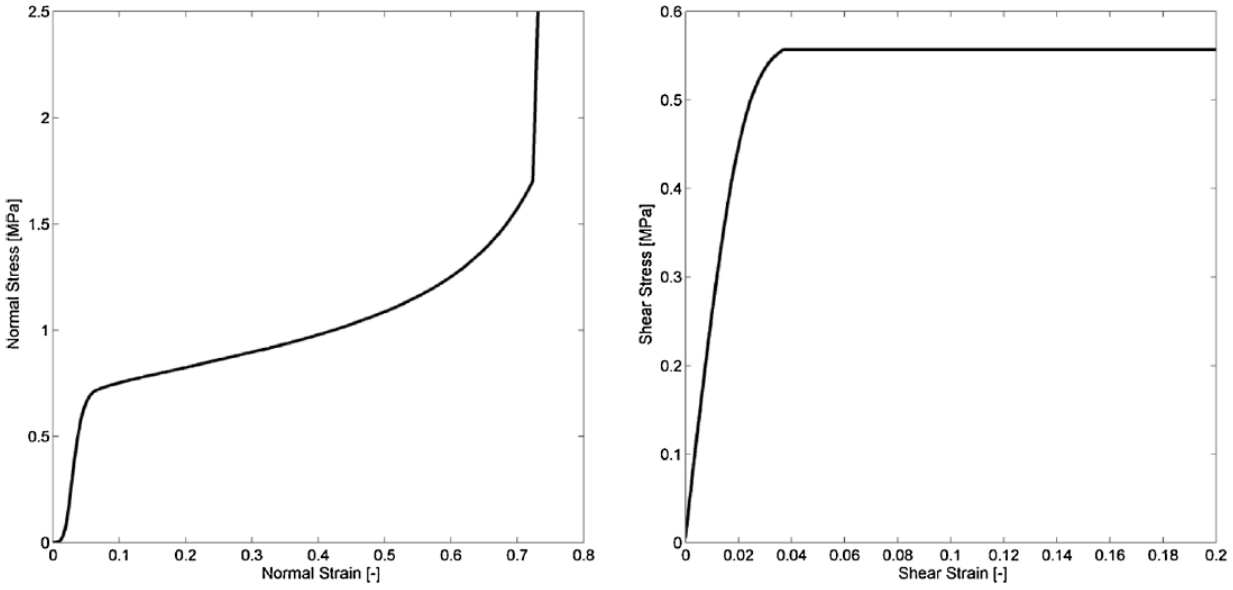

Figure 5-36 – Left: normal stress versus normal strain for the foam, Right: the shear stress versus shear strain for the EPS liner [158].

However, the shear stress-strain curve which has been used in the mentioned paper, was obtained by following an unclear procedure which has not been described in the paper. Conventional shearing test method (Figure 5-37) represents the material response under pure shearing and does not include the effect of normal stress on the shearing response.

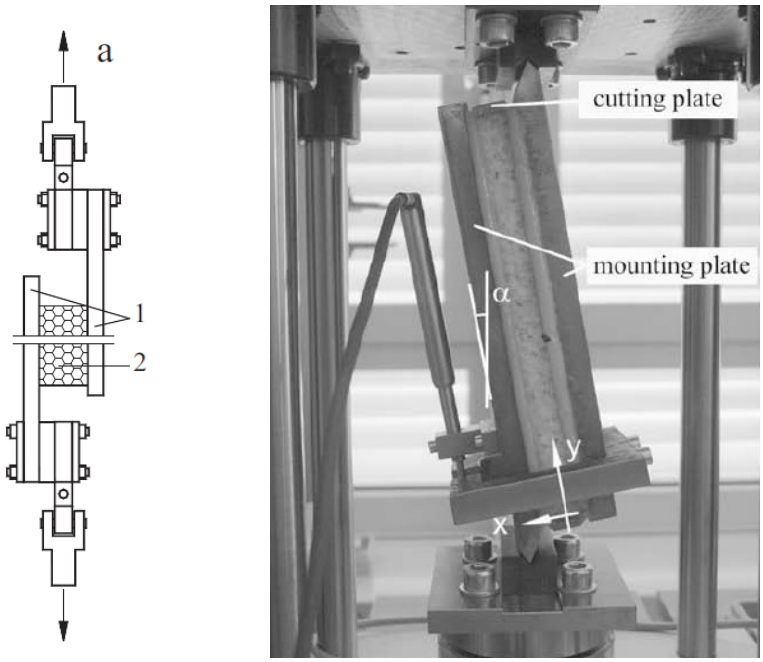

Figure 5-37 – Simple shear testing, 1: metallic parts, 2: Foam specimen [159,160].

Mills and Gilchrist applied shear and compression simultaneously on elastic and crushable foams using test rigs which are shown in Figure 5-38. The tests were carried out on PU [161] and PP [162] and the results were not explicitly reported in term of shear stress-shear strain.

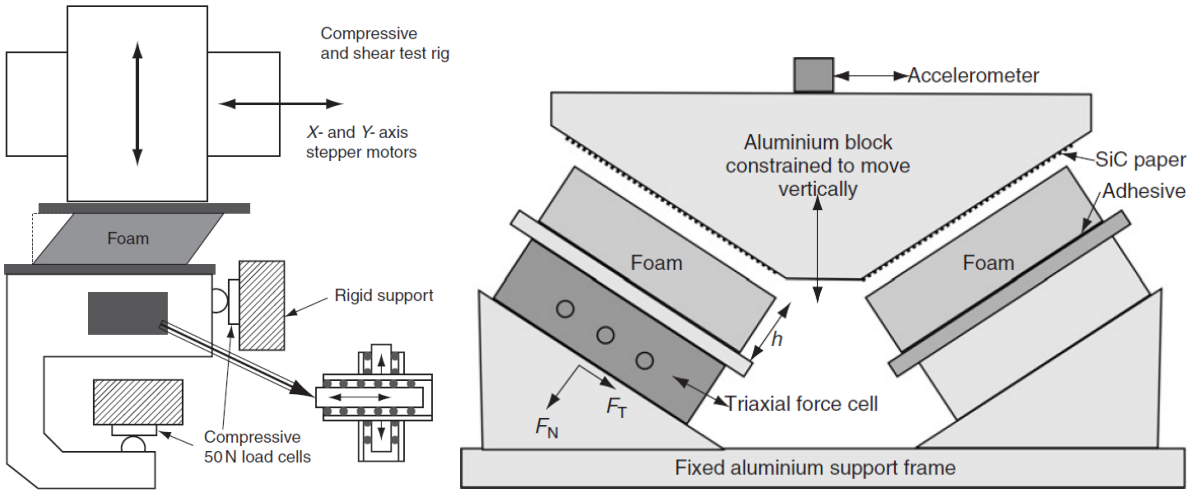

Figure 5-38 – Test rigs for shearing plus compressive loading, Left: used for testing elastic foams, Right: used for testing crushable foams [161,162].

Moreover, another method which was used to study the compression and shear response of foams is using a cylindrical specimen and applying compression and torsion at the same time as shown in Figure 5-39. Gdoutos et. al. used such a method in order to study multiaxial response of Divinycell foams [163].

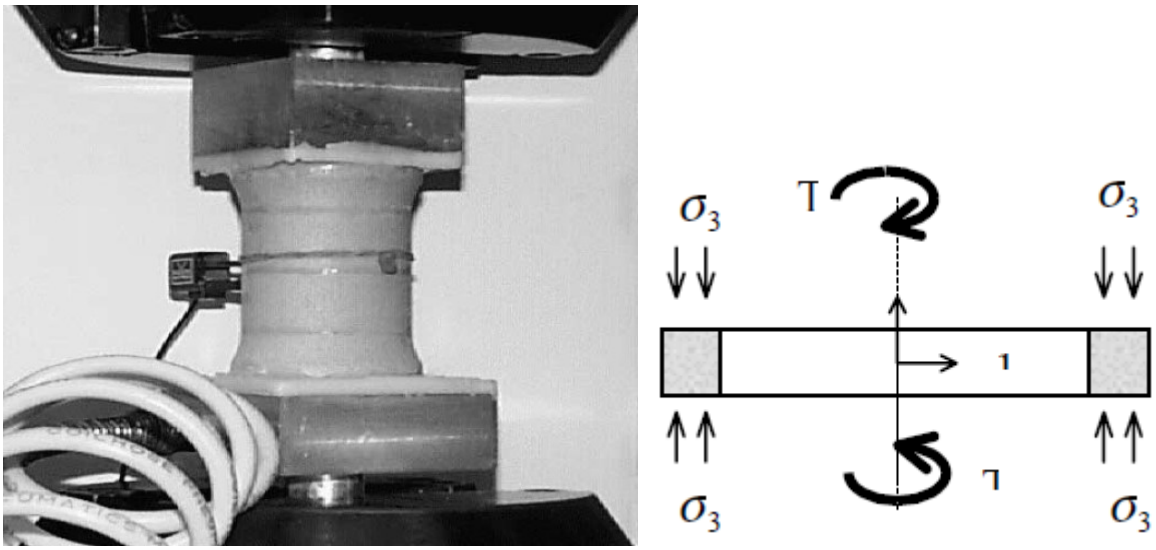

Figure 5-39 – Cylindrical specimen for shearing plus compressive loading [163].

The result of testing the cylindrical specimen (both shearing stress and compressive stress) was reported vs axial strain as shown in Figure 5-40.

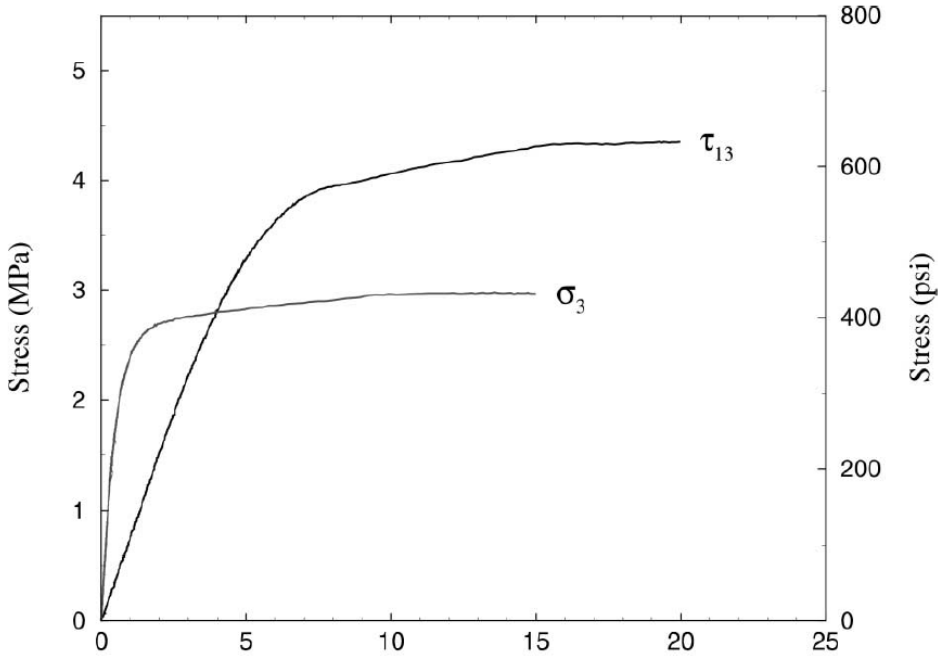

Figure 5-40 – Stress-strain curves for Divinycell H250 [163].

According to the author's knowledge, there is no experimental data in the literature, which represents the response of EPS foam under shearing load in conjunction with axial compression. Therefore, biaxial tests were carried out in order to study the response of the EPS foams under a realistic loading condition. This section describes the test method and presents the results.

5.4.1. Method

A biaxial test rig was used in order to study the response of EPS foams with different densities under compression and shearing force. The tests were carried out at SWEREA-SICOMP which is a member of the MOTORIST EU network and samples were provided by Dainese S.p.A which is another partner of the same network. The test set-up is equipped with a system of transducers in order to measure the axial and two transversal forces. The machine works with displacement controlled actuators in order to generate axial and transversal movement (see Figure 5-41).

The samples were provided as circular molded specimens as shown in Figure 5-42 with dimensions of 90mm×40mmØ. Three different densities of EPS were used for biaxial testing i.e. 25, 40 and 55 kg/m^3. Due to the load-cell's limited capacity, the samples with density of 40 and 55 kg/m^3 were cut to 40mm×40mmØ (Figure 5-42).

The specimens were compressed axially then a transverse load was applied to put the specimen under shear as shown in Figure 5-43. The tests were carried out at different levels of axial strain i.e. 20%, 30%, 40% and 50% in order to study the effect of axial compression on shearing response of the foam. The tests at 20% of axial compression were carried out twice to check the repeatability of the results. A layer of silicon paper was used between the specimen and the machine's contacting surfaces in order to maximize the friction between the specimen and the test set-up (see Figure 5-42). The results were filtered using a Butterworth four-pole filtering function with cut-off frequency of 1000 Hz.

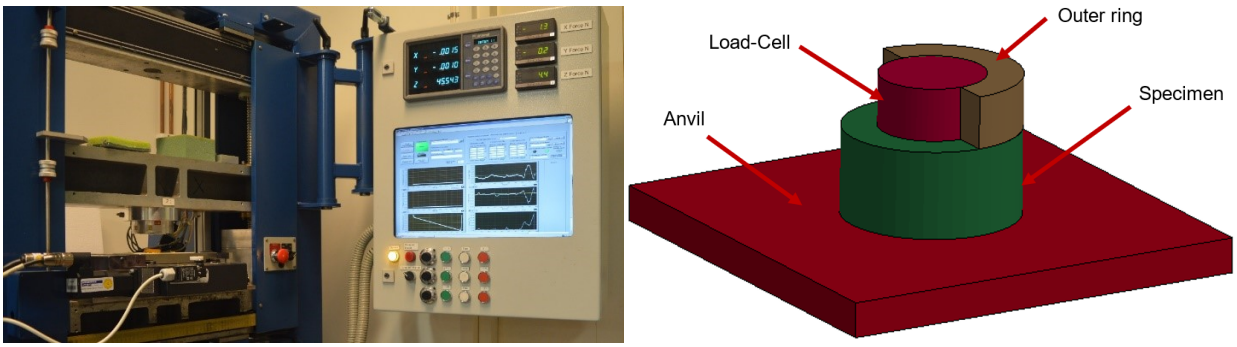

Figure 5-41 –Left: general view of the test rig, Right: description of test rig's parts.

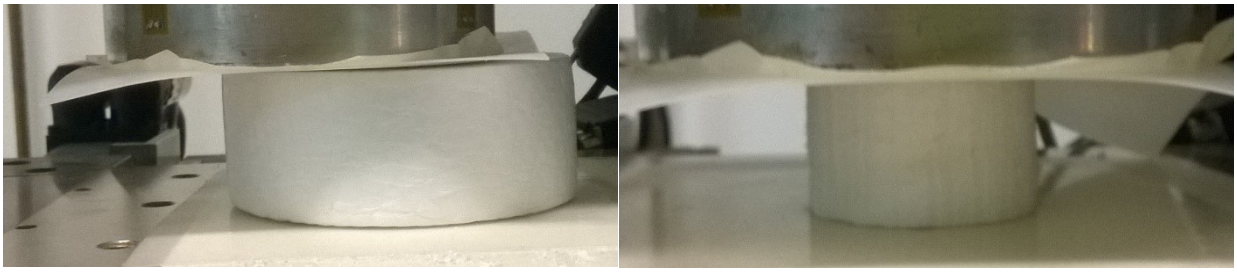

Figure 5-42 –Left: 90mm×40mmØ samples, Right: 40mm×40mmØ samples.

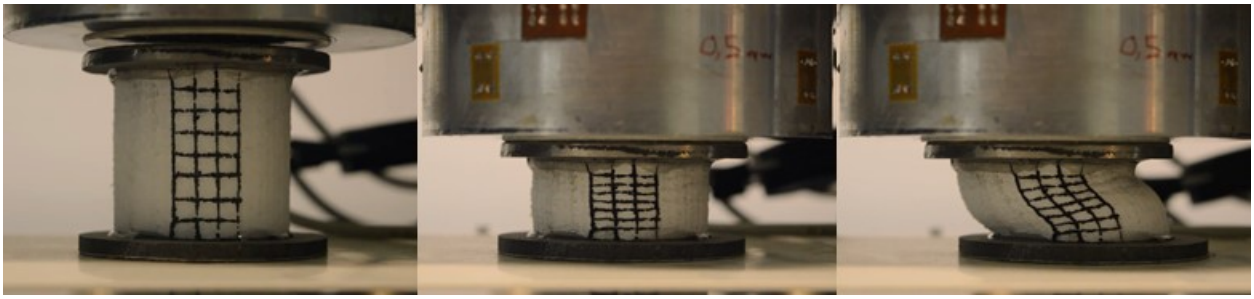

Figure 5-43 – Biaxial test of foams, left: beginning of the test: middle: compressed specimen without shearing load, right: specimen under compression and shear.

By reducing the size of specimens, an undesired rotation was observed which affected the result of the tests (Figure 5-44). This rotation was due to the small ratio of the diameter of the specimen and the test rig's punch (assembly of load-cell and the outer ring which is shown in Figure 5-41) and lead to loose contact.

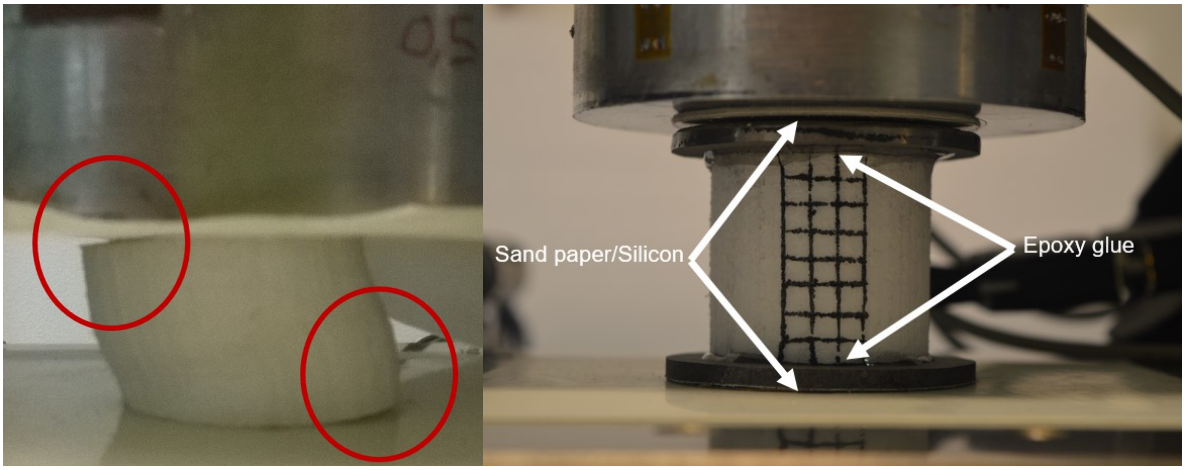

Figure 5-44 – Left: loose contact after applying shear, Right: specimen with ending plates.

In order to solve the problem of rotating specimen, rigid metallic ending plates were attached to the specimens. Ending plates attached to the specimens by means of epoxy glue and covered by sand papers as shown in Figure 5-44 to increase the friction. By using the ending plates, no rotation was observed during the tests but after a certain level of the shearing load the moving part of the test rig started to slide, despite sand and silicon papers were used to avoid such a sliding, therefore the results after sliding were neglected. The tests with ending plates were carried out for three different densities only for 50% of axial strain. The results of the test using ending plates were used as a benchmark in order to correct the result of the tests without the ending plates. The procedure is described in the following chapter.

5.4.2. Results and discussion

As it is shown in Figure 5-45, when the specimen started to rotate the measured force dramatically decreased due to the loose contact. Moreover, Figure 5-46 illustrates the result for the cases with and without the ending plate. Since the stress is calculated according to the cross

section of the specimen, the result for the case with ending plate, which had no rotation, was considered as the reliable one.

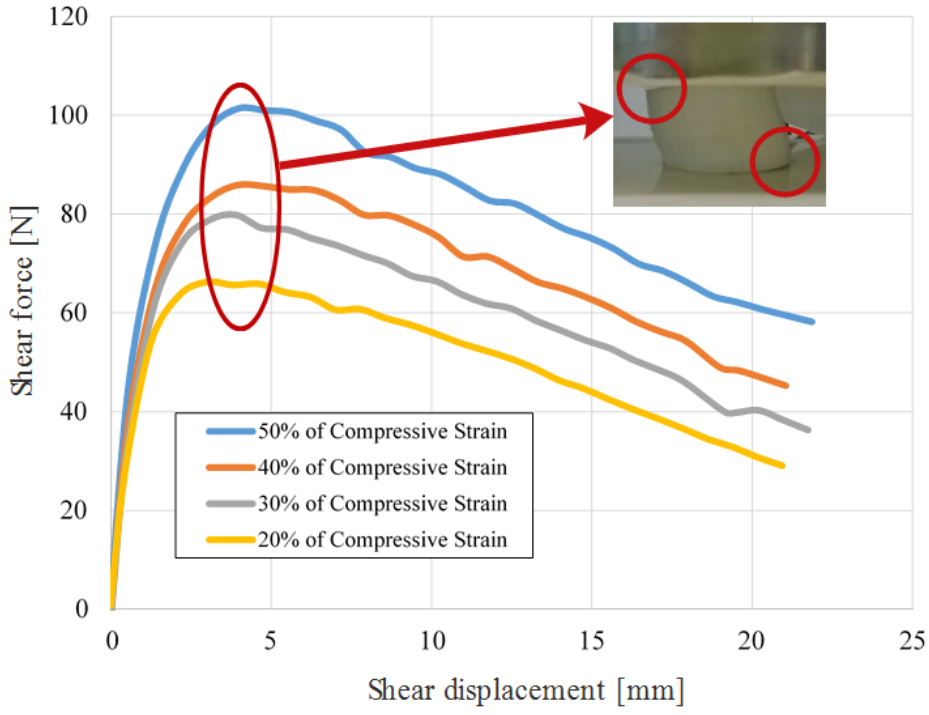

Figure 5-45 – Results for 40 kg/m^3 foam without ending plate.

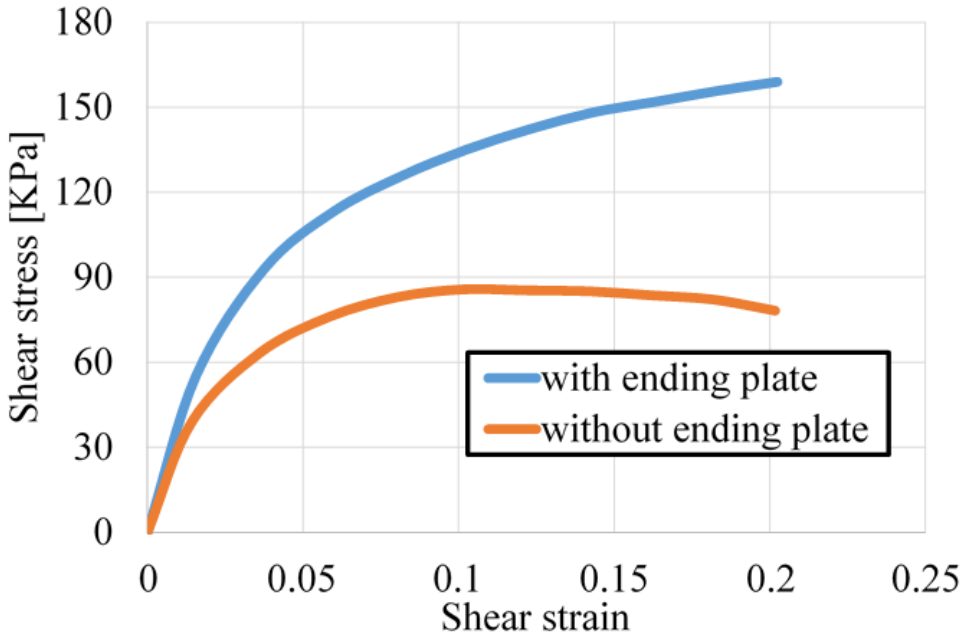

Figure 5-46 – Comparison of the results with and without ending plate for 40 kg/m^3 EPS.

The results of the tests with ending plates were used to correct the shear stress-strain curves obtained from the tests without ending plates. For shear strain less than 20%, it can be assumed

that the shear strain in the center (far enough from the edges) of the specimens with the metallic ending plate and without the metallic ending plate is the same (see Figure 5-47) therefore, the stress should be equal as well. However, as it was shown before, the result for the cases with and without the ending plates are different. The ratio of the stress-strain curve of the case with ending plates over the stress-strain curve for the case without them for the axial compression level of 50% (see Figure 5-46), was used as a correction factor, which could be used to correct the stress-strain curves at other levels of compression (20%, 30% and 40%). This correction factor is not a unique number and is a function of shear strain and foam's density (see Figure 5-48). Since the contact between the specimen and the machine were become loose after a certain level of shearing regardless of the level of compression (Figure 5-45), it was assumed the correction factor is not a function of compressive stress.

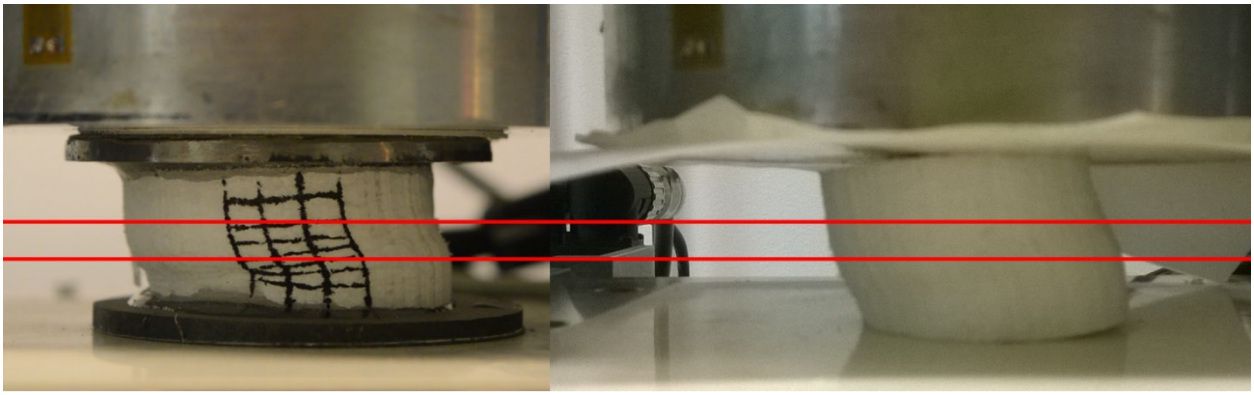

Figure 5-47 – The specimens with and without the ending plate (red lines highlight the core of the specimen).

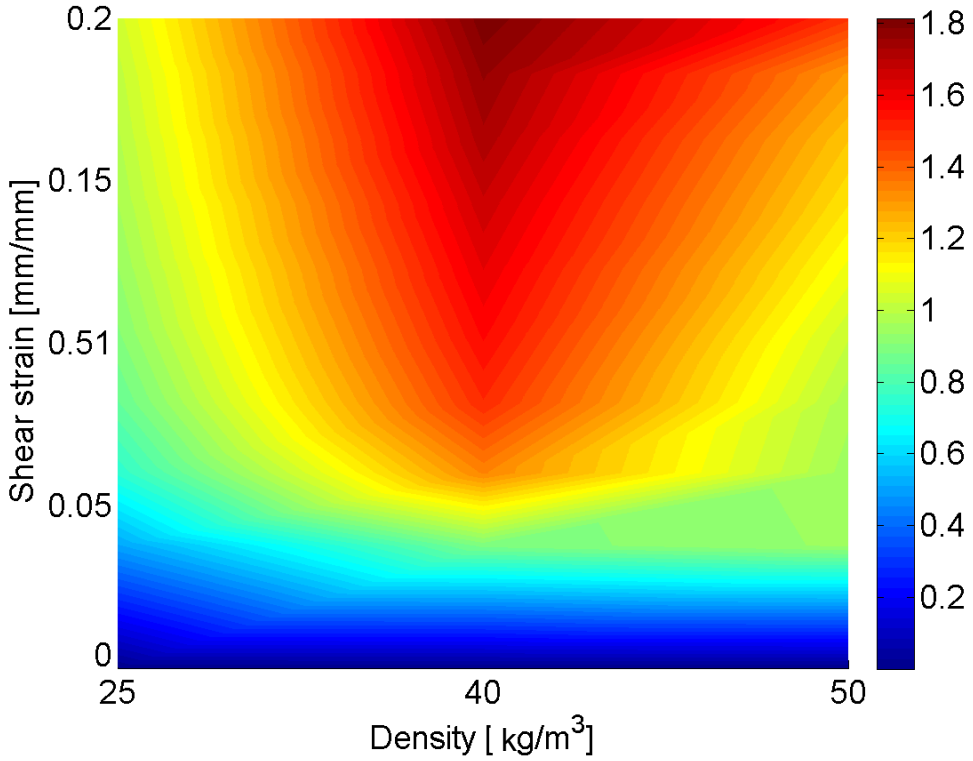

Figure 5-48 – Correction factor in order to mitigate the effect of lose contact.

The results, after applying the correction factor are presented in Figure 5-49 to 51. The results show that the foam responds to the shearing force in a similar way at different levels of compression but the shearing stress was increased by increasing the axial strain. The shearing stress-strain curves show that the shearing response has two main parts, i.e. the linear part and the plateau region. Figure 5-51 shows slightly different response for the heaviest tested foam (55 kg/m^3), however, it is clear that the axial compression affects the shearing response of the foam and shearing stiffness increases as a function of axial compression

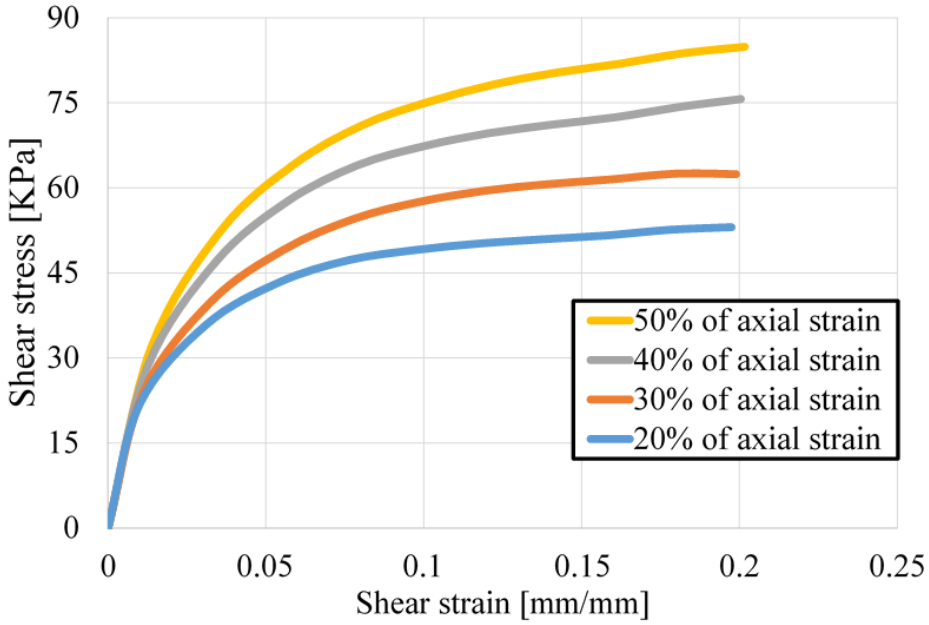

Figure 5-49 – Test results for EPS with density of 25 Kg/m^3.

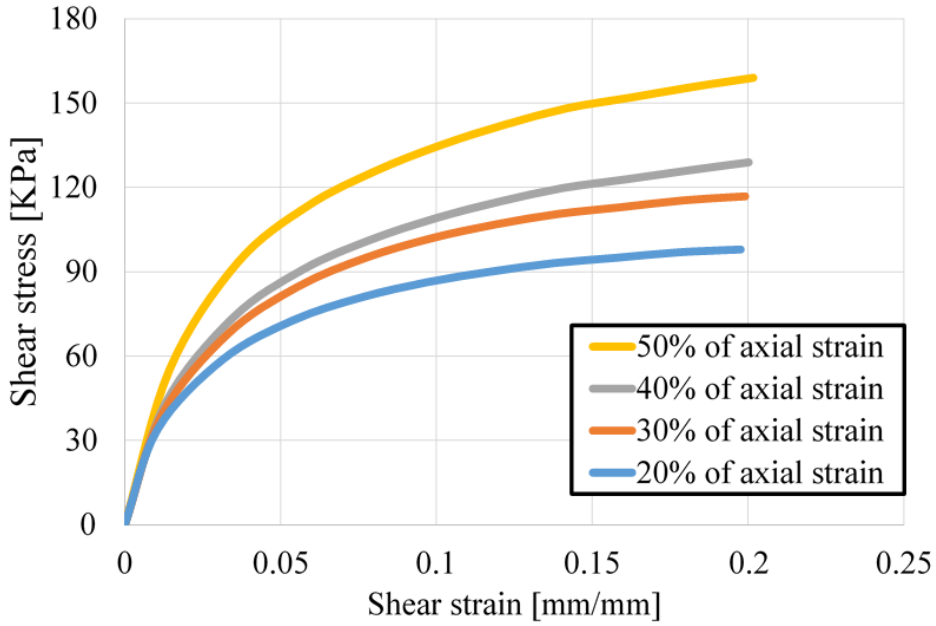

Figure 5-50 – Test results for EPS with density of 40 Kg/m^3.

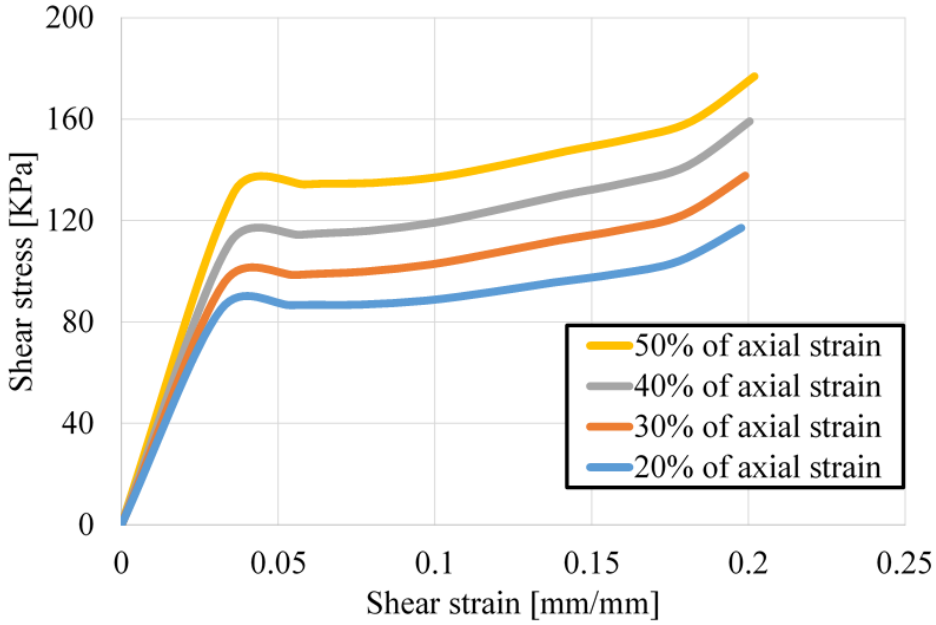

Figure 5-51 – Test results for EPS with density of 55 Kg/m^3.

Three different densities of EPS were tested under biaxial loading condition. The loading condition was a shearing load in conjunction with a compression. The experiments were carried out at different levels of axial strain in order to study the effect of compressive strain on shearing response of the foams.
Even though, the shear hardening effect of the helmets' liner was proposed to be included [162] in finite element analysis of oblique impacts in order to consider its effect on the induced rotational acceleration to the head, there was no experimental data available in the literature about the shear hardening behavior of EPS foams. Therefore, the shear stress vs shear strain curves of EPS foams with different densities are presented explicitly, to be used for simulation of oblique impacts on helmets.

It is shown that by increasing the axial compression the shearing stiffness and yield shear stress increased. Plastic stretching of the foam cell faces provides the major shearing resistance of the closed cell foams [162]. Therefore, the orientation of the cell faces with respect to transverse loading direction influences the shearing resistance [162,164]. The axial strain leads to buckling and inclination of cell faces and such an effect increases by increasing level of axial compression, consequently, the shearing resistance would increase as well.

The tests were carried out to understand the response of helmet's liner under realistic loading condition and provide shearing properties of such materials for more accurate finite element analysis of helmet oblique impacts. As it was mentioned earlier, FE models will be probably a part of standard validation of motorcycle helmets in the next generation of helmet standards and oblique impacts will be included as well, therefore an accurate and proper material characterization method and material properties are highly demanded.

The presented empirical data in this chapter are proposed to be used for FE analysis of helmet oblique impacts, in order to consider the shear hardening phenomena for EPS foams. There are few constitutive material models which could be used for including shear hardening of crushable foams in some available commercial software [165], however they may need some modifications in order to represent the foam material's more accurately.

6. FE models

6.1. Helmet

The finite element model of a size 58 helmet (Figure 6-1), [166] was used for this study. The main parts of the helmet, which are involved in energy absorption, are the composite shell and the foam liner. 4-node quadrilateral shell elements were used to generate the FE model of the composite shell and 4-node tetrahedral solid elements for the liner discretization as shown in Figure 6-1. The chin strap was modeled using 4-node quadrilateral shell elements with a Young's modulus of 1 GPa and a Poisson's ratio of 0.3 [28].

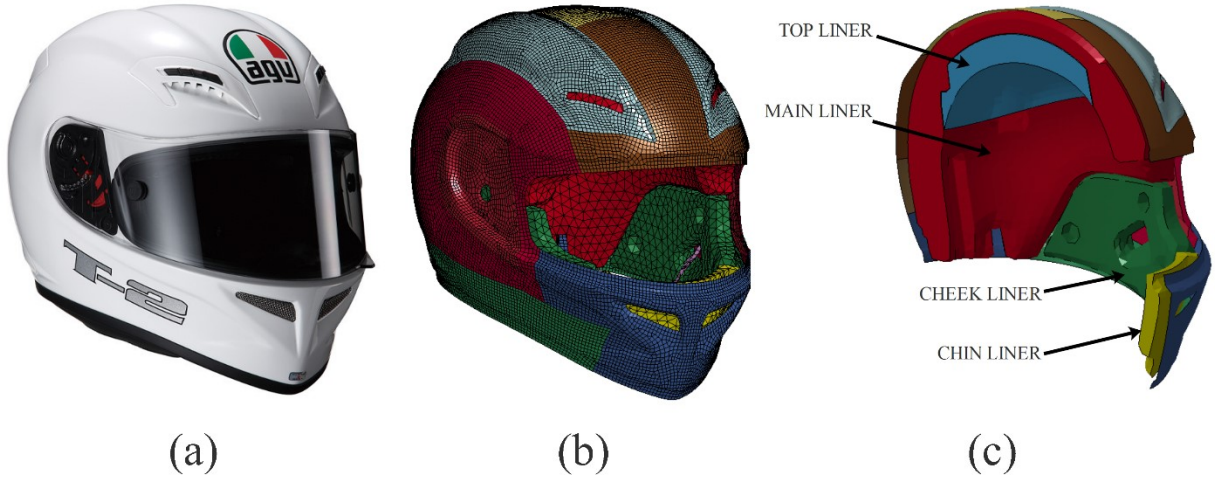

Figure 6-1 – a: AGV T2 Helmet, b: FE model of the helmet, c: foam liners (some parts of the helmet are not shown).

The liner was composed of four sub-parts, i.e. main, top, chin and cheek liners (Figure 6-1), each made of expanded polystyrene (EPS) with a different density (Table 6-1 and Figure 6-2). The Crushable Foam material model (MAT_063 from LS-Dyna material library) was used to model the foam parts [165,166]. This model requires the definition of the compressive stress-strain curve. This curve was obtained using semi-empirical equations provided and explained in [105,167].

Table 6-1 Material properties of foam parts [28].

Part	ρ (kg/m^3)	E (MPa)	v	σ_y (MPa)
EPS; top liner	20	2.9	0.01	0.13
EPS; main liner	40	10.6	0.01	0.36
EPS; cheek and chin liners	60	23.2	0.01	0.66

The shell of the helmet is made of composite laminates with different layups in different regions of the helmet (Figure 6-3). Test coupons were cut from different regions of the helmet in order to identify the ply layups and characterize their mechanical properties [28]. Table 6-2 and

Figure 6-3 show different types of lamina used in the shell and the layups in different regions of the shell, respectively. In the FE model, Laminated Composite Fabric material model (MAT_058 from LS-Dyna material library) was used for the shell [165,166] with the material constants presented in Table 6-3. MAT_058 has the capability of predicting the failure initiation and evolution in composite plies according to the following constitutive equations [168,169]:

$$\begin{bmatrix}\sigma_L\\ \sigma_T\\ \tau\end{bmatrix} = \frac{1}{C}\begin{bmatrix}(1-\omega_L)E_L & (1-\omega_L)(1-\omega_T)v_{TL}E_T & 0\\ (1-\omega_L)(1-\omega_T)v_{LT}E_L & (1-\omega_T)E_T & 0\\ 0 & 0 & C(1-\omega_{LT})G_{LT}\end{bmatrix} \times \begin{bmatrix}\varepsilon_L\\ \varepsilon_T\\ \gamma\end{bmatrix} \quad \text{Eq. 6–1}$$

$$C = 1-(1-\omega_L)(1-\omega_T)v_{LT}v_{TL} \quad \text{Eq. 6–2}$$

where σ, ε, τ and γ are normal stress, normal strain, shear stress and shear strain respectively. The subscripts L and T indicate longitudinal and transverse directions. ω is the damage function which is defined as follows [49]:

$$\omega = 1-\frac{\alpha S_{ut,uc}}{E_{L,T}\varepsilon} \quad \text{Eq. 6–3}$$

where S_{ut} and S_{uc} are ultimate tensile and compressive stresses, respectively, α is the ratio of the limiting stress to the peak stress [169,170] and has been considered equal to 0.1 [28,166] for the present study. In this material model when an element fails, its moduli degrade to near zero but the element will not be deleted in order to avoid instability problems at the interfaces with other parts, like liner and anvil in the present work [28,165].

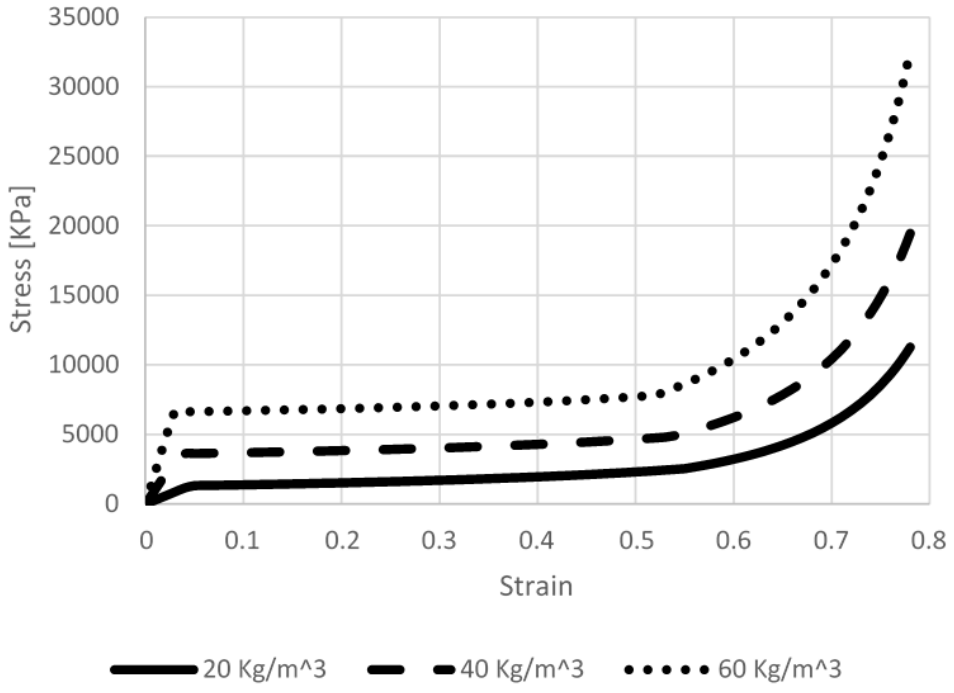

Figure 6-2 – Compressive stress-strain curves used for foam parts [28].

The contact between the shell and the main liner, cheek and chin liner was defined using Automatic Surface to Surface algorithm [165]. The same contact card was used in order to define

the contact between the top liner and the main liner, the chick foams and the main liner and between the chick and the chin liners. The friction coefficient at shell/liners interfaces and between different parts of the liner was set to 0.5 and for the shell/anvil interface was set to 0.23 [6]. The total mass of the helmet was 0.96 kg excluding the visor's mass and the mass of the comfort foams.

The finite element model of the helmet was previously used to simulate the impact attenuation test of the ECE 22.05 standard [28], whole-body drop tests using a Hybrid III dummy [6,28] and oblique impacts using a Hybrid II headform [7]. The head linear and rotational accelerations and the neck forces predicted in these simulations were in good agreement with the experimental data.

Table 6-2 Shell material [28].

Material NO.	Resin	Fibre	Lamina Type	Symbol
1		Carbon	Unidirectional	C
2			Unidirectional	G
3	Epoxy	Glass	Twill Weave	TW,G
4			Plain Weave	PL,G
5		Hybrid (Kevlar/carbon)	Unidirectional	H

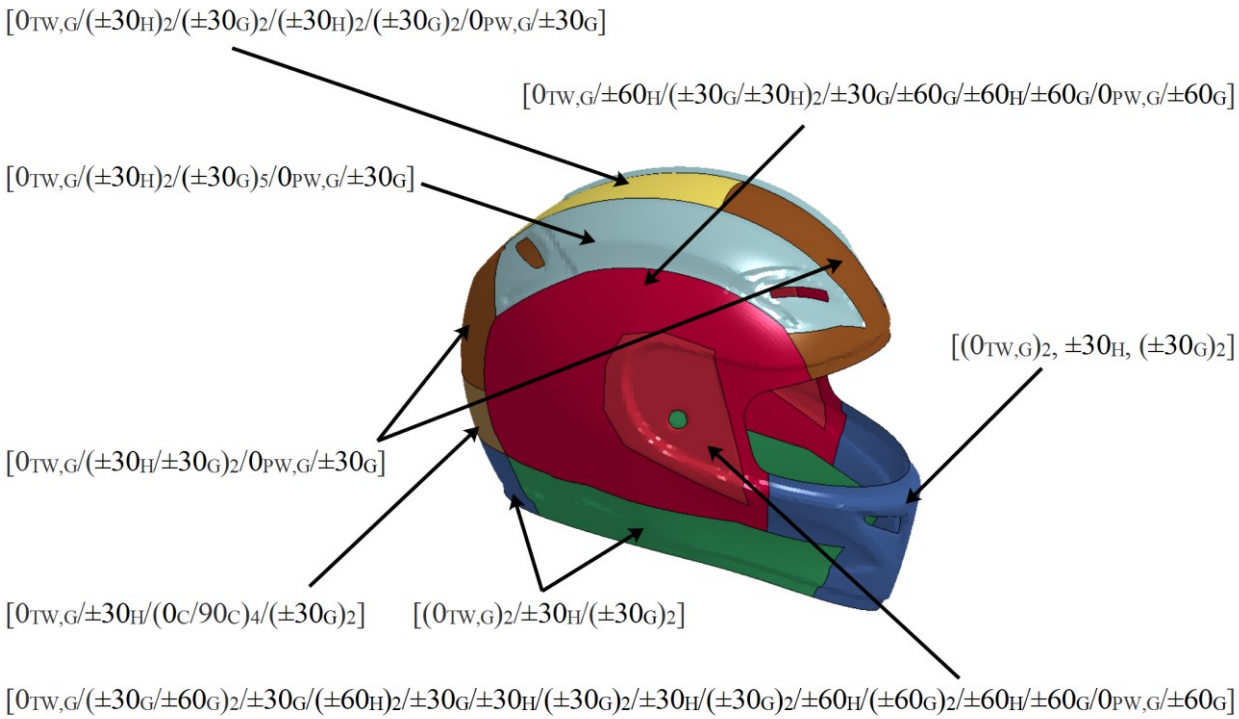

Figure 6-3 – Ply layup for different parts of the shell [28].

Table 6-3 Material properties of the shell used for FE simulations [28].

	Unidirectional Glass/Epoxy	Twill Weave Glass/Epoxy	Plain Weave Glass/Epoxy	Unidirectional Carbon/Epoxy	Unidirectional Hybrid (Carbon/Kevlar)/Epoxy
ρ (kg/m^3)	1984	1950	1266	1455	1400
E_L (GPa)	46	29	34	174	110
E_T (GPa)	16	29	8	9	8
G_{LT} (GPa)	5.8	4.1	1.8	3.9	2.8
v_{LT}	0.28	0.14	0.37	0.29	0.33
$S_{ut,L}$ (MPa)	1280	550	840	2000	1530
$\varepsilon_{ut,L}$	0.028	0.019	0.026	0.014	0.014
$S_{uc,L}$ (MPa)	800	490	126	1420	720
$\varepsilon_{uc,L}$	0.018	0.017	0.02	0.01	0.008
$S_{ut,T}$ (MPa)	40	550	52	42	30
$\varepsilon_{ut,T}$	0.025	0.019	0.014	0.009	0.004
$S_{uc,T}$ (MPa)	145	490	130	130	130
$\varepsilon_{uc,T}$	0.012	0.017	0.016	0.014	0.015
τ_u (MPa)	73	80	60	60	60
γ_u	0.04	0.04	0.051	0.051	0.051

6.2. Neck brace

The neck brace is a collar that is used with a helmet to reduce the amplitude of the displacements of the head-neck system with respect to the torso and it is supposed to reduce the risk of cervical injuries in case of direct impact to the helmet or in case of severe head-whipping. It has three main parts, the composite shell, the liner and the retention strap as shown in Figure 2. The manufacturer provided the CAD model of the device and we developed its finite element model using HYPERMESH V 14.0 [171].

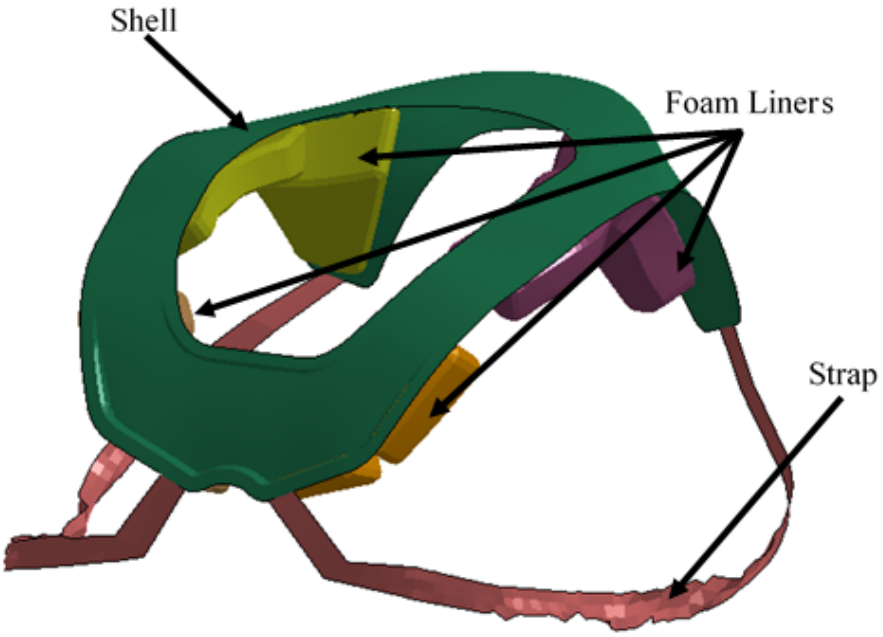

Figure 6-4 – FE model of a neck brace.

The foam liner is composed of four parts, which are connected to the shell and are made of polyurethane with density of 250 kg/m^3. The stress-strain curve of the foam liner was obtained by compression test using a Galdabini universal test machine under quasi-static condition. Polyurethane foam is not rate sensitive at medium level of strain and strain rate [172,173] therefore the result of quasi-static test was used for this study. The test result is shown in Figure 6-5. Low-Density-Foam constitutive material model (MAT-57 from LS-Dyna material Library) was used to simulate the foam parts and 4-node tetrahedral solid elements were used to generate the FE mesh.

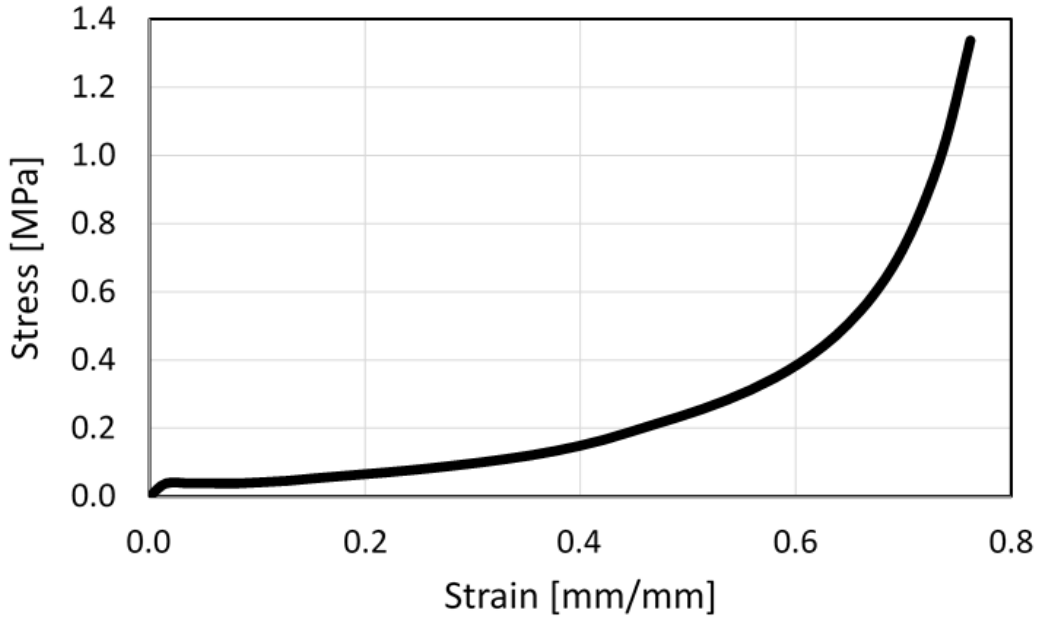

Figure 6-5 – Polyurethane stress-strain curve.

In order to realize the ply configuration of the neck brace's shell, a spare piece of the shell was burnt to melt the resin, unstack the laminate, and understand the number of laminae (Figure 6-6). The shell of the neck brace is a carbon fibre laminate, which is made of four twill weave laminae with total thickness of 3.2 mm. Laminated-Composite-Fabric material model (MAT_058 from LS-Dyna material library) was used to model the shell and material properties were taken from [28] and are mentioned in Table 6-3 . 4-node quadrilateral shell elements were used to generate the finite element model. A dynamic validation was carried out to verify the correctness of the FE model of the shell [174,175]. A piece of the shell's laminate was fixed and an impulse excitation was used in order to record the laminate's response by means of a three axes accelerometer (Figure 6-7). The response was transferred to frequency domain using Fast Fourier Transfer (FFT) function in MATLAB in order to identify the natural frequencies of the laminate. A modal analysis for FE model of the same piece of laminate was carried out. Figure 6-7 shows that the FE simulation can accurately capture five major natural frequencies of the shell.

The neck brace's strap was modeled as an elastic band using 4-node quadrilateral shell elements with a Young's modulus of 1 GPa and a Poisson's ratio of 0.3.

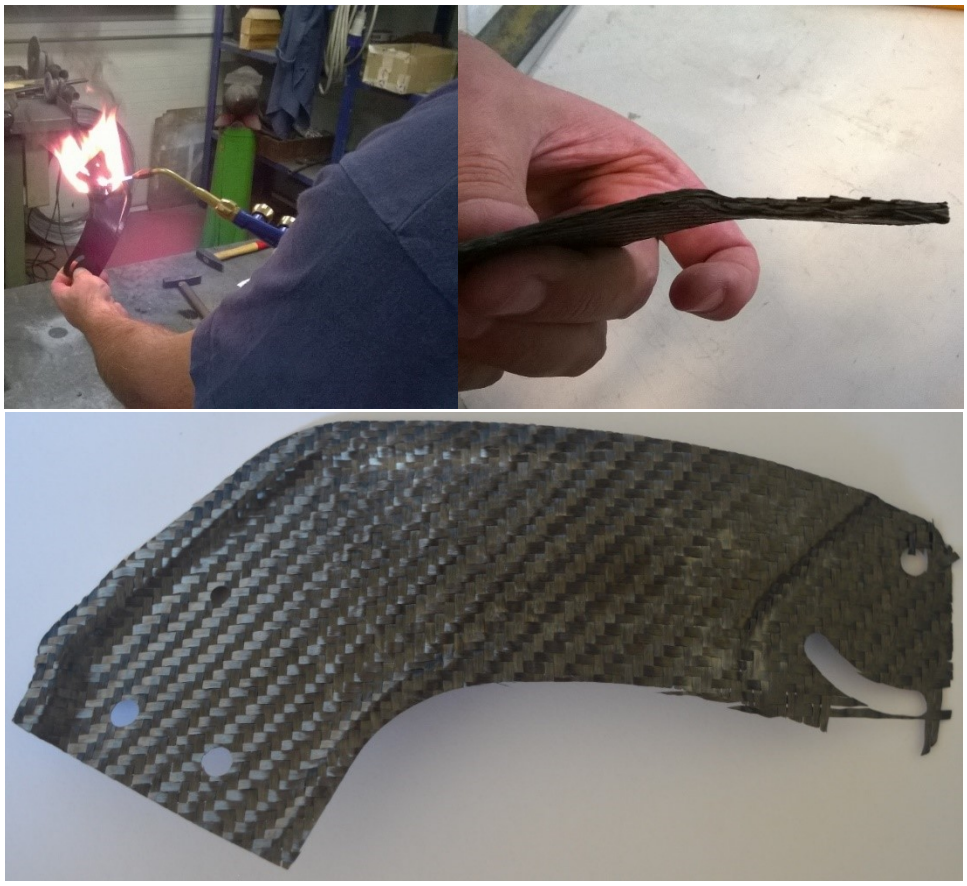

Figure 6-6 – Up and left: Burning the laminate's resin, up and right: stacking of the laminae after burning the resin. Low: a single lamina (carbon fibre twill weave).

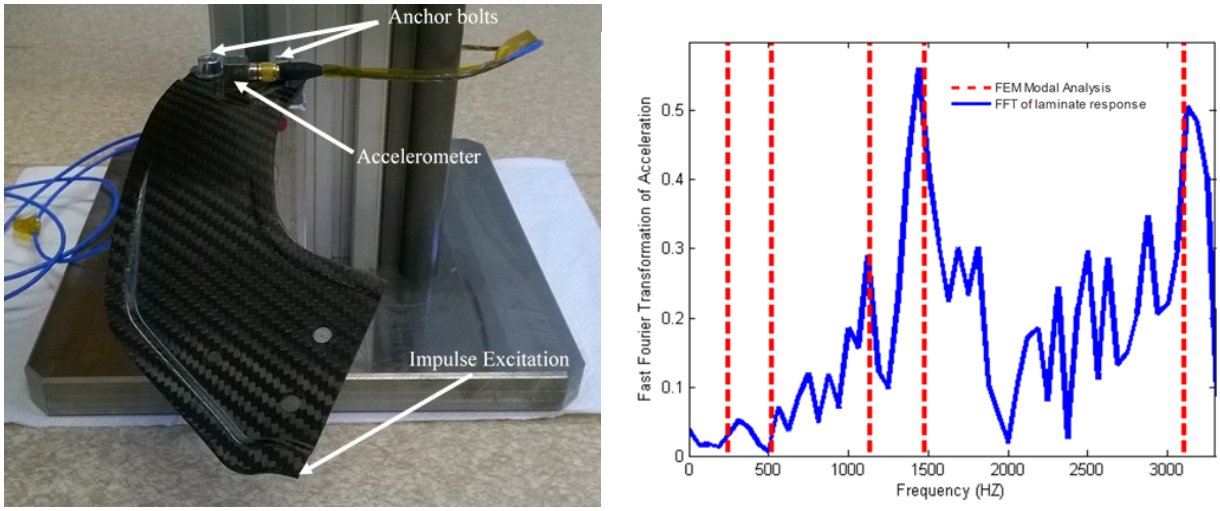

Figure 6-7 – Left: Validation test for the neck brace's shell, Right: Result of validation test for the neck brace's shell.

The neck brace has a locking mechanism and two joints as shown in Figure 6-4. These features have been neglected and in the adopted model it is simply assumed material continuity as shown in Figure 6-4. It is apparent that there are differences between the numerical model and the real

object: in particular not all important frequencies are captured by the numerical model (Figure 6-7) and some limited relative rigid motions between the parts of the neck brace are not present in the numerical model. However, the main focus of the present work is not on a precise assessment of a particular product but on a wider discussion on the properties of neck braces. With that purpose in mind, the numerical model we use realistically represents the behavior of a generic neck brace.

6.3. THUMS (Total HUman Model for Safety)

THUMS V.5 model was used for the present work [176], which is a detailed finite element model of the human body including the skeleton, ligaments, brain, spinal cord etc. as shown in Figure 6-8. The head-brain of THUMS has been validated for translational and rotational loadings and its head-neck complex has been also validated for direct impacts on the head at forehead, maxilla, and middle nasal concha and induced accelerations at T_1 [176,177]. Moreover, in a recent study, researchers showed that the stress level of spinal vertebrae of THUMS is correlated to the risk of fracture of vertebrae [79]. Other body parts of THUMS and the whole body have been validated as well and more details about validations are available in [176].

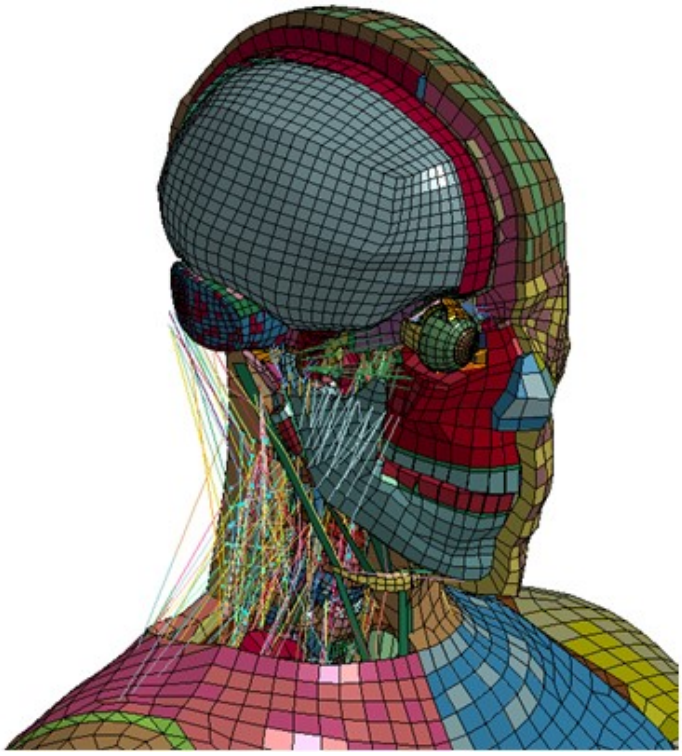

Figure 6-8 – THUMS V.5 head-neck (some parts are not shown).

6.4. Hybrid III head-neck FE model

It is common and computationally cost-effective to use isolated head-neck models to study head and neck injuries [178,179]. In the present work, the finite element model of the head-neck assembly of the Hybrid III 50th percentile male dummy (Figure 6-9) was used for partial optimization of the helmet. This model was provided by Livermore Software Technology Corporation (www.lstc.com) and it has been validated for the neck extension calibration test

[180]. Although the neck of the Hybrid III dummy shows a stiffer response than the human neck under direct head loading, particularly axial loading [181], it is widely used by researchers for testing helmets due to its robustness and the availability of its physical models.

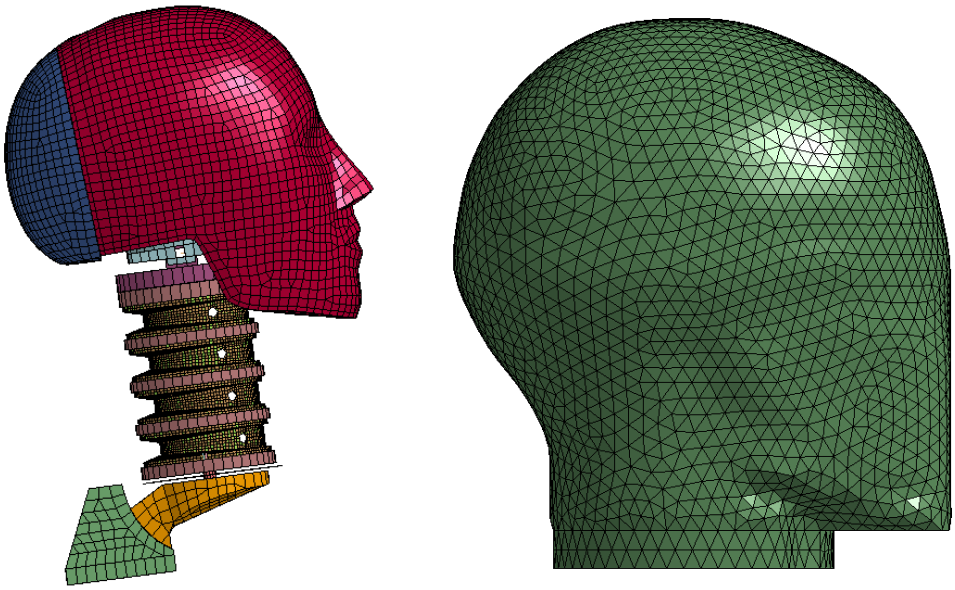

Figure 6-9 – Left: Hybrid III 50th percentile head-neck assembly, Right: ISO headfrom.

6.5. Headform, anvil and impactor

The finite element model of a medium size ISO headform, which was previously developed [28], has been used in the present work (see Figure 6-9). The model meets the requirements of UNECE 22.05 [96] and an accelerometer is defined at its center of gravity.

Moreover, an anvil according to UNECE 22.05 [96] and an impactor according to Snell 2015 [182] have been used in the present work as shown in Figure 6-10.

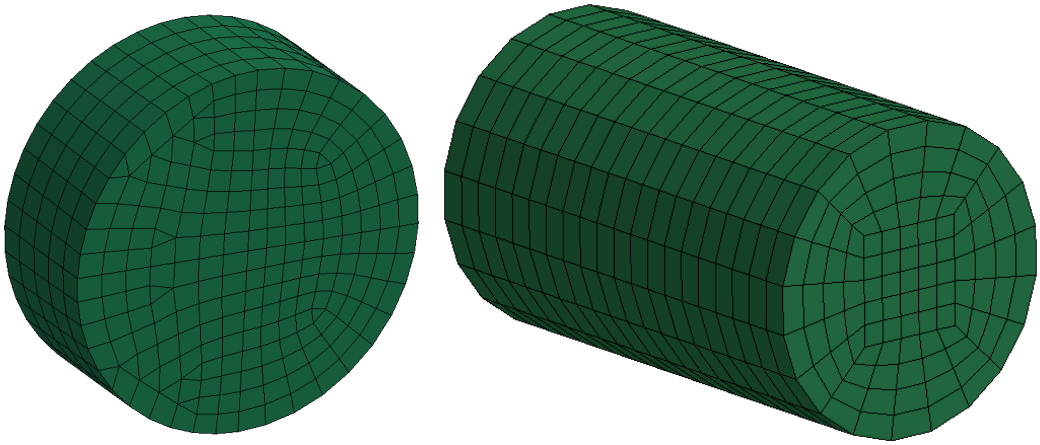

Figure 6-10 – Left: rigid anvil according to ECE 22.05, Right: rigid striker according to Snell 2015.

6.6. Lattice structures

The bending-dominated lattice structures are known to have better mechanical properties regarding energy dissipation and a lattice structure with a cubic unit cell is the simplest 3D lattice structure which has bending-dominated failure mechanism in all three main directions [183]. Moreover, the simplest way to have a varying mechanical properties through the thickness is changing the size of the cells through the thickness by a constant increment. Therefore, a hierarchical structure has been designed in a way that the size of the cells through the thickness follow an arithmetic series (see Figure 6-11). The size of each cell could be calculated according to the thickness and the numbers of the cells through the thickness as follows:

$$l_n = n\Delta l \qquad \text{Eq. 6–4}$$

in which, l_n is the length of the nth cell and Δl is:

$$\Delta l = \frac{2L}{N(N+1)} \qquad \text{Eq. 6–5}$$

where, L is the thickness of the liner and N is the total number of cells through the thickness. A finite element model of a hierarchical lattice structure was developed using a MATLAB code. The code has been developed in order to generate the finite element model of the lattice structures using beam elements. The code has the capability of generating cubic and spherical hierarchical lattice structures as shown in Figure 6-11. Cubic samples were printed out for validation of the FE model.

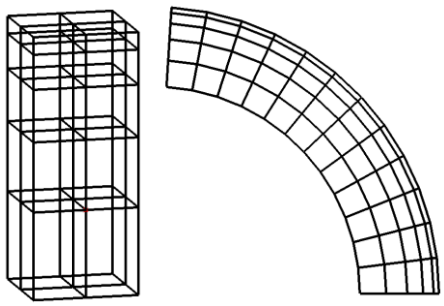

Figure 6-11 – The FE model of cubic (left) and spherical (right, a section of a 3D structure is shown) lattice structures.

Figure 6-12 – The 3D printer used to print out lattice specimens.

A MAKERBOT 3D printer was used in order to print out different structures using PLA and Nylon (see Figure 6-12). The test machine described in Section 5.4 was used to carry out uniaxial compression tests on the printed specimens. The result of the tests showed that the dominant failure mechanism of PLA specimen is a brittle failure and it cannot absorb reasonable amount of the energy, on the contrary, the Nylon specimen could absorb relatively high amount of the energy thanks to its plastic deformation. Figure 6-13 shows the failure of PLA and Nylon specimens under compression and Figure 6-14 compares the response of the two specimens.

Figure 6-13 – Failure mechanism of PLA (left) and Nylon (right) specimens under uniaxial compression.

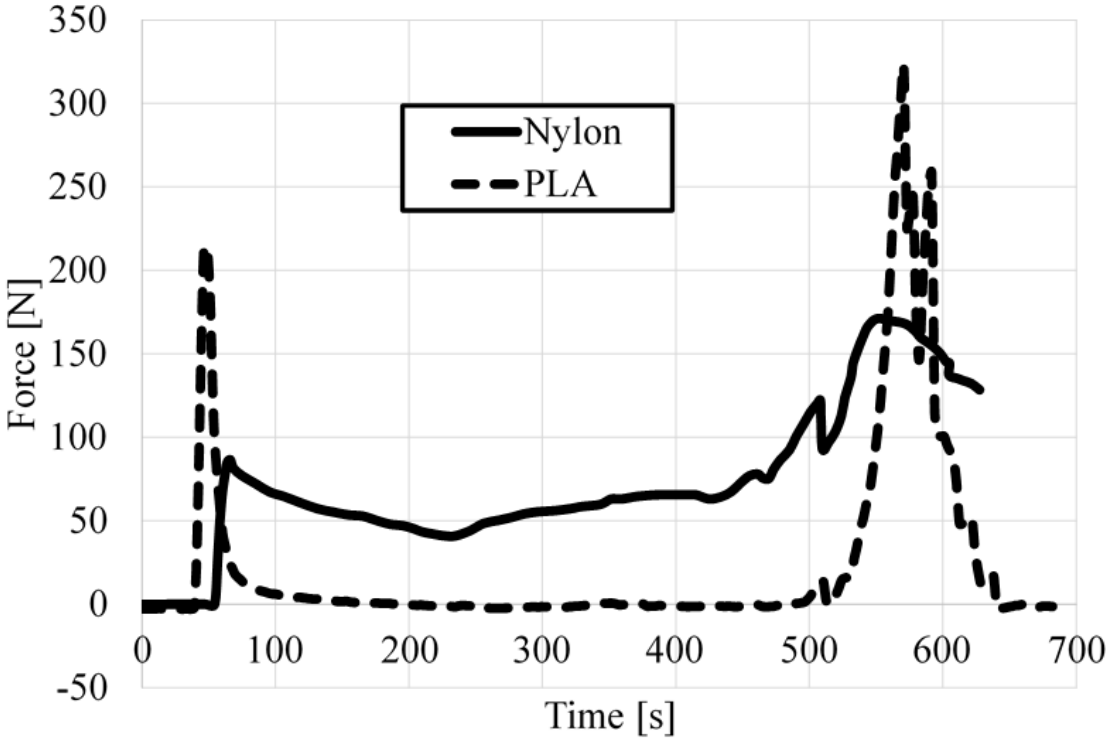

Figure 6-14 – Comparing the reaction force of PLA and Nylon specimen under compression.

As it has been shown, PLA lattice structure could not absorb any reasonable amount of energy because of its brittle behavior, therefore Nylon has been chosen to be assessed as a new energy absorbing liner for helmets. Tensile tests carried out for material characterization using a tensile test machine INSTRON-8501 at SWEREA-SICOPM. The test samples were printed out according to ISO 527 standard, and the result is shown in Figure 6-15 [184]. The result was used for FE simulations. Mat-24-Piecwise-Linear-Plasticity from LS-Dyna material library was used for simulation of the Nylon lattice structure [165]. Moreover, Cowper-Symonds [165] formulation was adopted in order to include the effect of the strain rate. The constants of Cowper-Symonds, C and p, were considered 82 [1/s] and 4.51, respectively [185]. The experimental test (shown in Figure 6-13) was reconstructed by means of finite element method in order to get a validated FE model of the lattice structure (see Figure 6-16). Figure 6-17 and Figure 6-18 show the comparison between the FE simulation and the experimental test. It is shown that the deformation modes of the structure could be predicted by the model and the reaction force predicted is also in a relatively good agreement with the experimental result. However, there are two main differences between the experimental result and numerical simulation, which are the initial pick force and the height of the plateau region. The difference at the initial pick could be due to imperfections of the printed product which may reduce the initial 'strength' of the structure and the difference of the plateau region can be due to the fact that the real structure could have different failure mechanisms like buckling, plastic hinges, etc. at micro and macro levels and the developed FE model may not be able to simulate all failure

mechanisms. Even though the FE model underestimates the energy absorption capability of the real structure it is reliable to be utilized for feasibility study of using lattice structures as helmet liners. The detailed description of this feasibility study is presented in section 8.3.

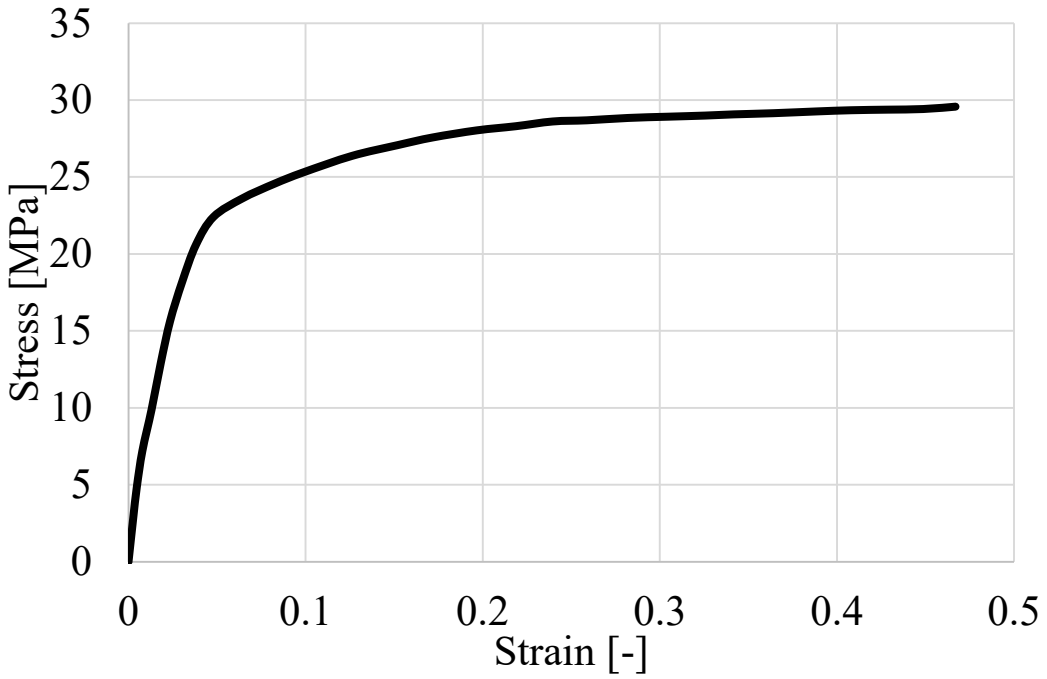

Figure 6-15 – Result of tensile tests using Nylon specimens.

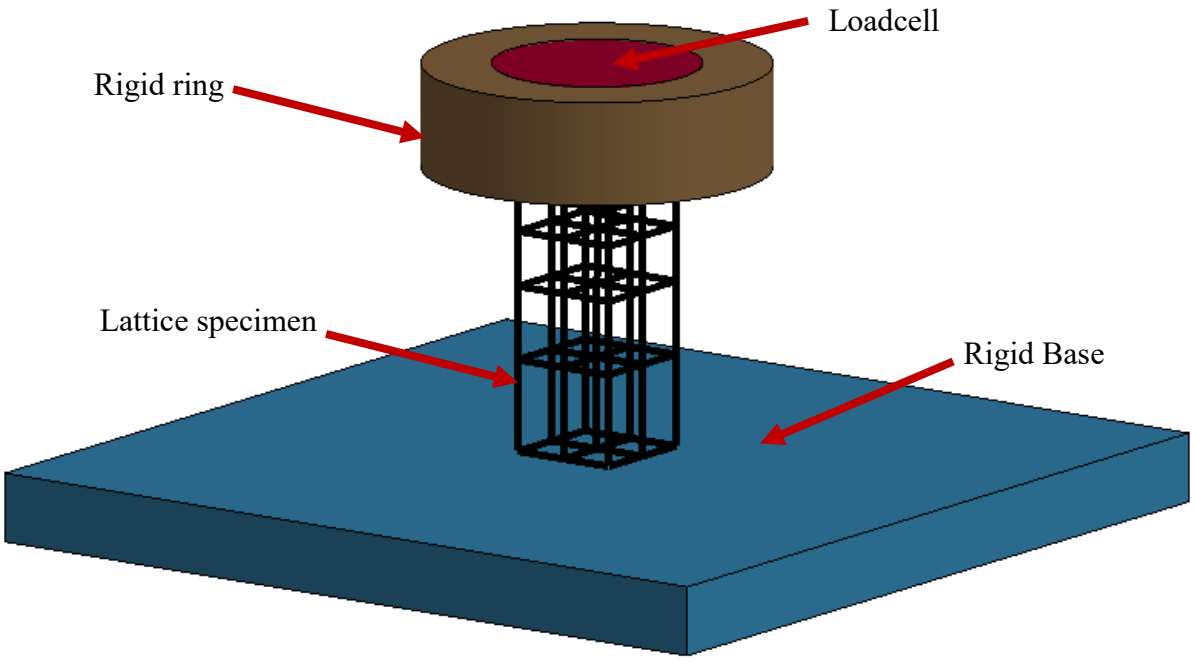

Figure 6-16 –FE model of lattice compression test.

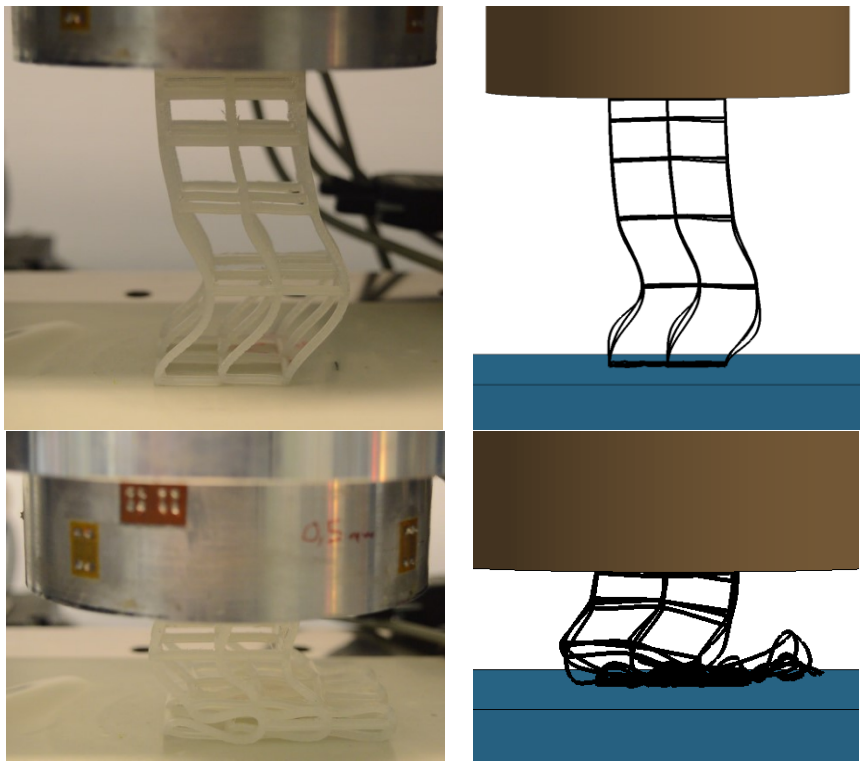

Figure 6-17 –FE model of lattice compression test.

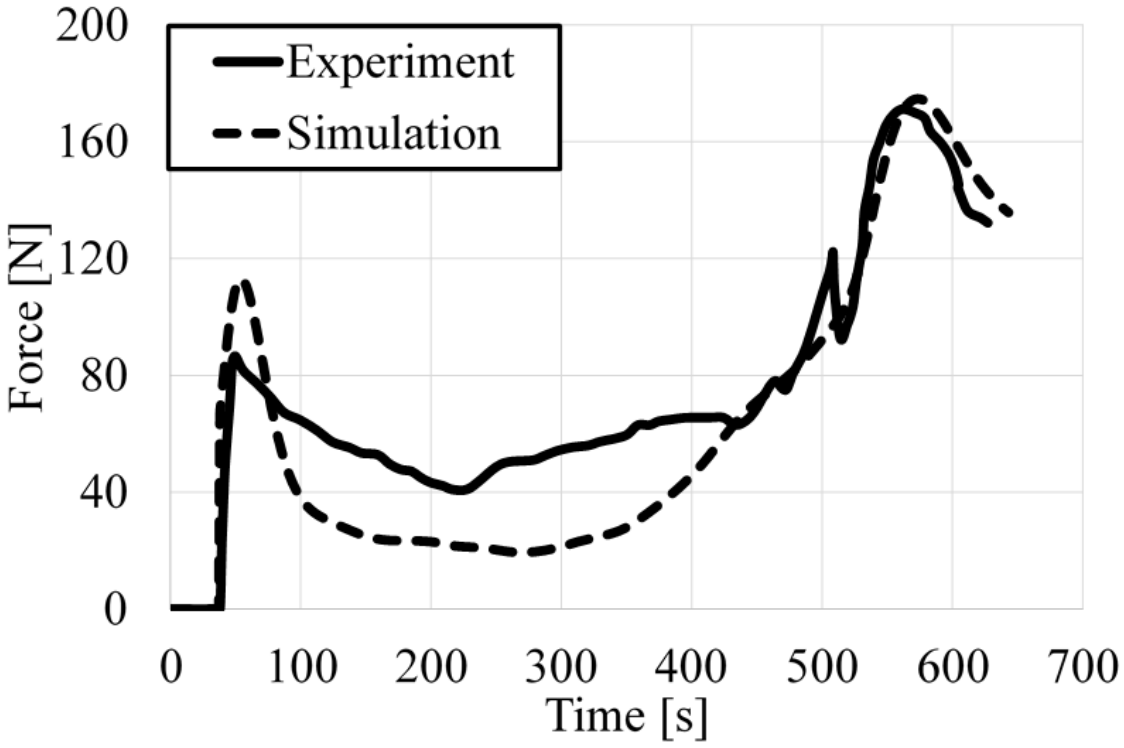

Figure 6-18 –FE model of lattice compression test.

6.7. A simplified helmet with lattice liner

A hemispherical hierarchical lattice structure has been generated using a MATLAB code as a liner of a simplified helmet. The inner radius of the liner was 112 mm and the thickness was 43 mm and the cell sizes through the thickness follow the arithmetic series which was described earlier. The material properties which have been validated in Chapter 6.6 have been used for simulation of this liner. Moreover, 4-node quadrilateral shell elements and an elastic material model with Young's modulus of 7250 MPa, Poisson's ration of 0.3 and density of 1200 kg/m^3 for the hemispherical shell have been considered [186]. In addition, the chin strap was modeled as an elastic band using 4-node quadrilateral shell elements with a Young's modulus of 1 GPa and a Poisson's ratio of 0.3 [166]. Figure 6-19 shows different parts of the finite element model of the concept helmet and its different parts.

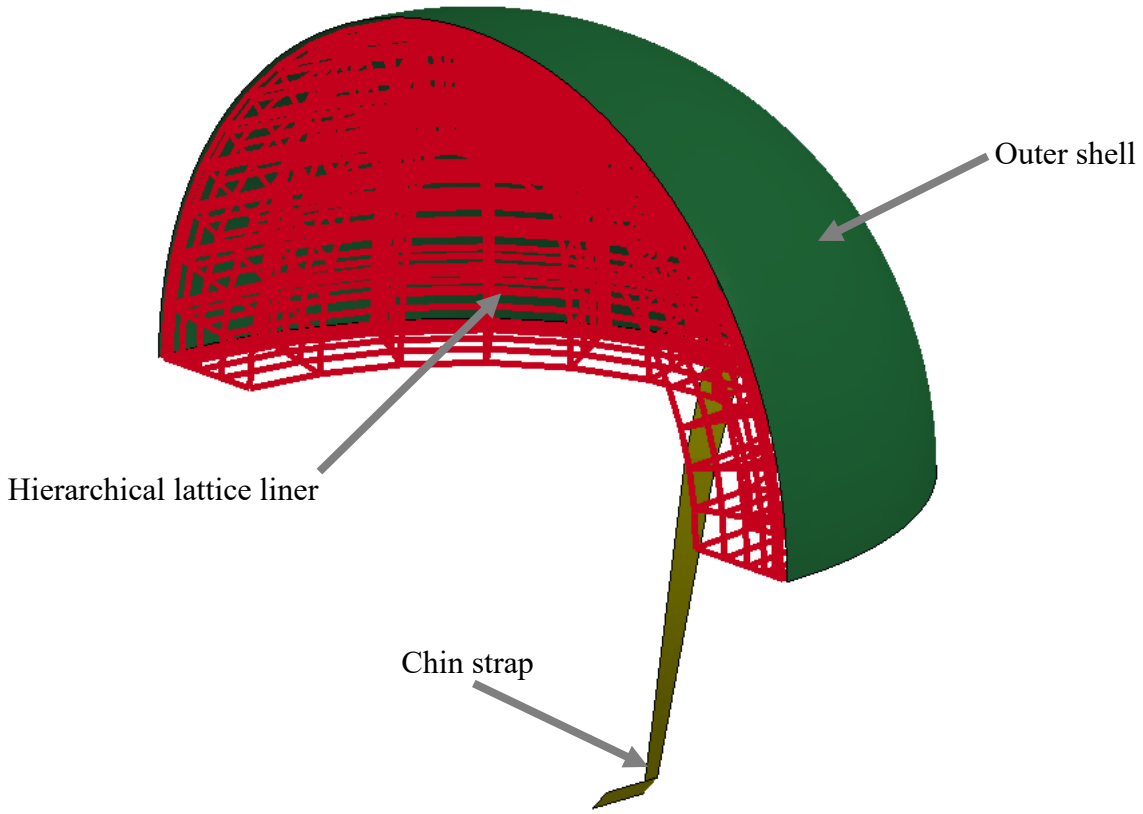

Figure 6-19 –FE model of the simplified helmet with lattice hierarchical liner.

6.8. A simplified helmet with EPS liner

A finite element of a simplified helmet similar to the one which has been described in Chapter 6.7 was generated using EPS liner with density of 110 kg/m^3 in order to compare the result of impact test on the helmet with EPS foam and lattice liner. The material properties of the foam with density of 110 kg/m^3 was calculated according to the following equations [8,28,105,187,188] and is shown in Figure 6-20. This density has been chosen to provide a helmet with a similar total mass, shape and size of the one, which has been described in

Chapter 6.7 in order to provide a reasonable comparison between the foam liner and the liner made of a hierarchical structure.

$$R = \frac{\rho}{\rho_s} \quad \text{Eq. 6–6}$$

$$E = AR^2 + BR \quad \text{Eq. 6–7}$$

$$\sigma_y = RC^{1.5} \quad \text{Eq. 6–8}$$

$$\sigma = \sigma_y + \frac{p_0 \varepsilon}{1-\varepsilon-R} \quad \text{Eq. 6–9}$$

$$\varepsilon_D = 1 - 1.4R \quad \text{Eq. 6–10}$$

in which, ρ and ρ_s are the density of the expanded foam and the density of the solid material which was used to manufacture the foam. Here, ρ_s is the density of polystyrene and is equal to 1050 kg/m^3 [105]. E is the modulus of elasticity of the expanded foam, A and B are material constants and are equal to 6640 MPa and 25.8 MPa, respectively [8]. σ_y is the yield stress and C material constants which is equal to 48.3 MPa [28]. σ and ε are engineering stress and strain at the plateau region of the foam's stress-strain curve. p_0 is the atmospheric pressure (0.1 MPa) and ε_D is densification strain.

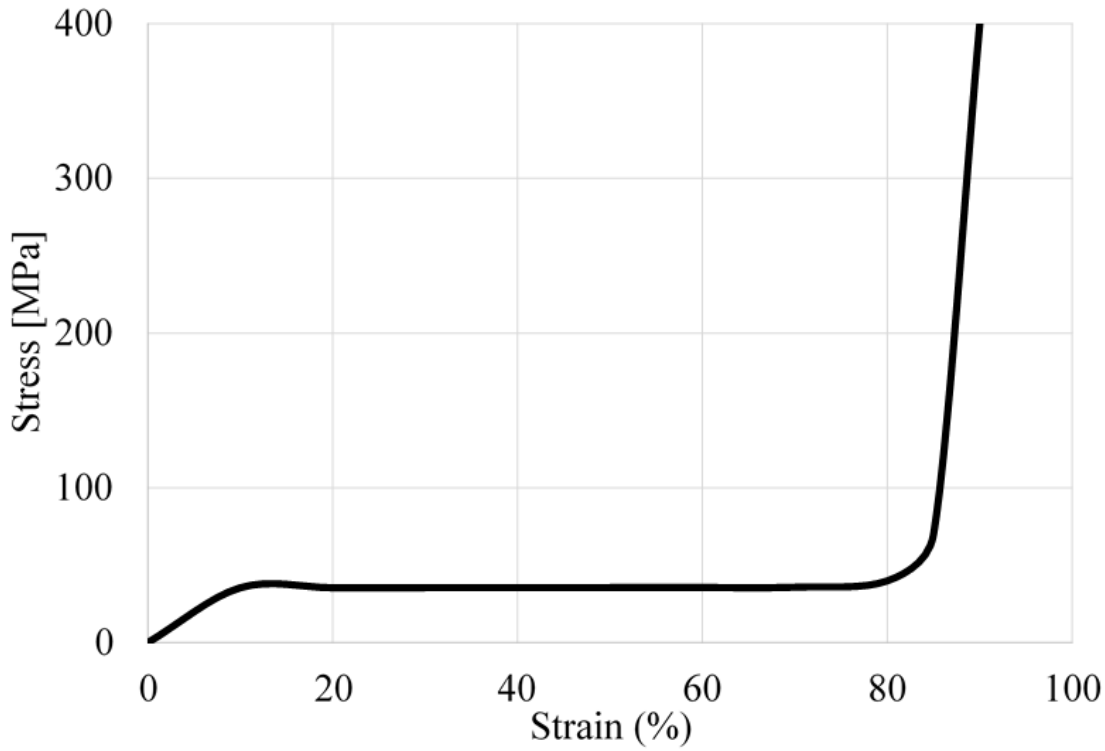

Figure 6-20 – Uniaxial compressive stress-strain curve for the foam with density of 110 kg/m^3.

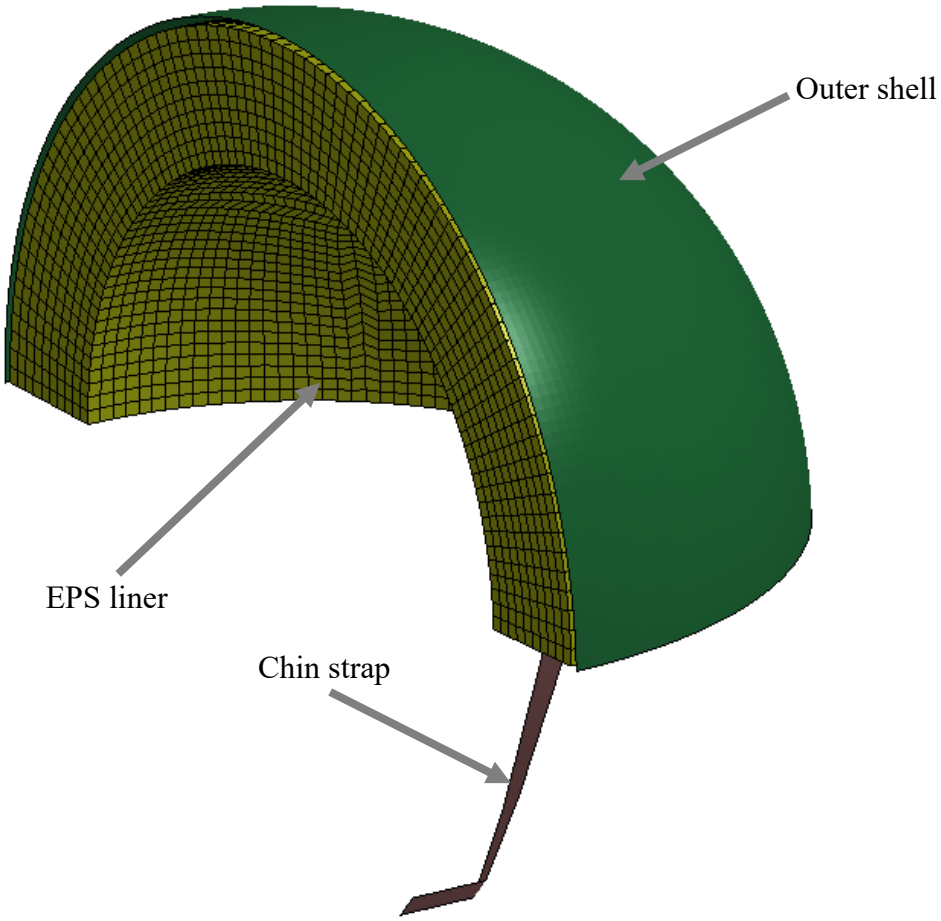

Figure 6-21 – FE model of the simplified helmet with EPS liner.

7. Assessment of a protective neck brace for motorcycle riders

Dowdell et al. [10] studied 200 cases of helmeted rider crashes and reported that almost 20 percent of cases had neck injuries due to impacts on the helmet. Krantz reported that the helmeted motorcycle riders suffered from cervical spine injuries even without any head injury [189]. Ramli et al. [190] studied 177 cases with fatal injuries in motorcycle accidents and reported neck injuries such as cervical vertebra fractures and transection of spinal cord. Badiali [191] studied the induced injuries on hyoid bone due to the hyperextension of the neck. Ouellet et al. [192] studied the probability of increasing the risk of neck injuries by using the helmet and reported that using helmet can increase the risk of neck injuries in the region of C_3 to C_7. Whyte et al. [11] studied 47 cases of fatal motorcyclist accidents and reported 10 cases (21%) with cervical spine fracture and 12 cases (25%) with cervical spine cord injuries due to remote impacts. These surveys show the significant risk of neck injuries of different severity levels in motorcycle accidents and the need for some form of protection for the neck.

As it has been mentioned in Section 3.2, in the last years, motorcycle gear manufacturers have introduced a new item of protective equipment in order to mitigate the risk of neck injuries in motorcyclists. Since this type of protective equipment has been introduced recently, there are few studies about its effect on the reduction of the risk of neck injuries, and there is no standard criterion for assessing the performance of such devices. The Finite Element Method (FEM) has been used as a powerful tool to study human body response during accidents and to design protection equipment [5]. The present chapter aims at studying the effect of a neck brace on reducing the risk of neck injuries. Different types of loading which have been applied to reproduce reasonable accidents scenarios are described in this chapter. Following sections show the results of simulations and discuss the PPE device performance in realistic accidents conditions.

The finite element models of a full-face motorcycle helmet, a neck brace protective device and THUMS, which are described in Section 6, have been used to assess the neck brace.

7.1. Impact conditions

Major mechanisms of neck injuries sustained by motorcycle riders are flexion, extension, lateral flexion and compression, which usually occurs in conjunction with flexion. These mechanisms are correlated to frontal, rear and side impacts and skidding [9]. In order to replicate these injury mechanisms, three different impact configurations were considered, shown in Figure 7-1. These load cases were chosen to reproduce hyperflexion (case No. 1), hyperextension (case No. 2) and lateral bending (case No. 3) of the cervical spine. The helmeted THUMS was launched at the speed of 7.5 m/s, the same speed prescribed in ECE 22.05 [96], towards a rigid flat obstacle with an angle of 45° with the body axis. For all impact conditions, the simulation was carried out for the case with and without the neck brace to study the effects of using it.

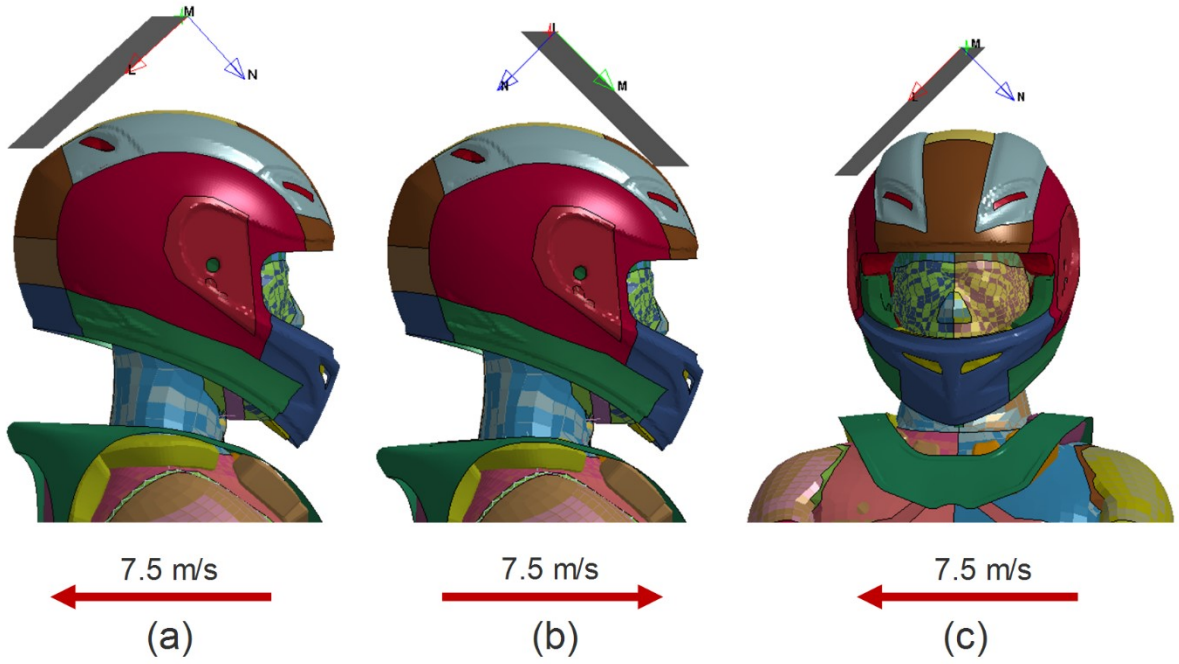

Figure 7-1 – Impact configurations: a) hyperflexion (Load case No.1), b) hyperextension (Load case No.2) and c) lateral bending (Load case No.3).

Moreover, hyperflexion in conjunction with compression which is a more realistic impact condition for motorcycle accidents [9] was considered, as well. In this load case the helmeted THUMS was launched towards the rigid wall as shown in Figure 7-2. For this load case also the simulation was carried out for the case with and without the neck brace.

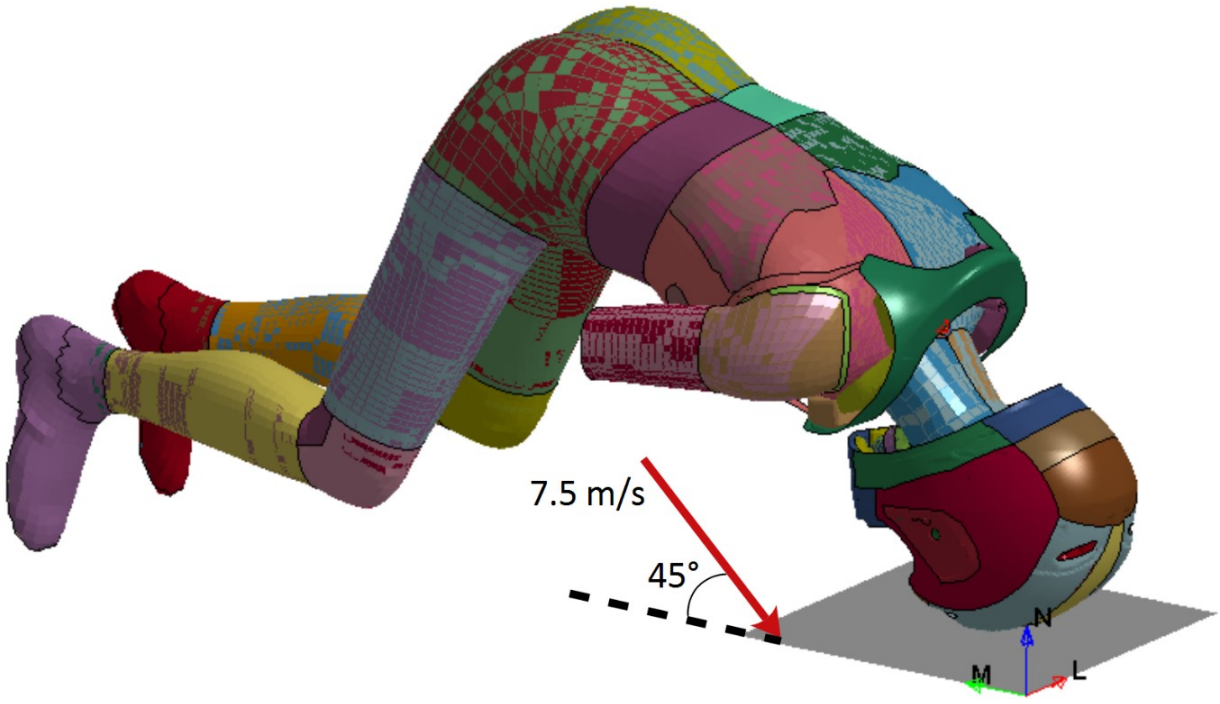

Figure 7-2 – A realistic Impact configurations (some parts of the model are hidden).

7.2. Results

The main focus of this chapter is to assess the effect of using a neck brace instead of evaluating, in absolute terms, the risk of neck injury. There are several injury criteria for neck injury, which have been mostly proposed for the whiplash injury for car passengers and have been mostly developed for sled test using dummies. Since cervical injuries among motorcyclists are usually due to direct impacts on the head, the result of assessment using such cervical injury criteria might not be accurate and reliable for motorcycle accidents [29]. Therefore the maximum stresses in the cervical vertebrae for all load cases have been compared in the two conditions with and without neck brace, an approach that has been used in previous studies, e.g. [75–78]. Figure 7-3 shows the stress distribution in the cervical vertebrae for load case No. 1 and illustrates that the stress distribution is almost the same for the cases with and without the brace during the simulation. Figure 7-4 depicts the stress distribution in the vertebrae for load case No. 2. In the case of using the brace, the stress level of C_4 is increased at 20 ms, the increase of the stress at the spinous process of C_6 and C_7 can be seen at 40 ms as well. The stress distribution in the vertebrae for load case No. 3 is shown in Figure 7-5. It is shown that at 20 ms the stress level at lower vertebrae is higher in case of using the brace. In addition, from 35 to 40 ms the stress at the body of the vertebrae was increased when the brace was used. Figure 7-6 shows the stress distribution of cervical vertebrae for the realistic impact condition. It is shown that using the brace could mitigate the stress at anterior tubercle of Atlas, but the stress was considerably increased at spinous process of C_3 to C_7 between 20 ms and 30 ms by using the brace.

To investigate the effects of the neck brace on neck forces, the shear and axial neck loads for all investigated cases were determined. An approach similar to that adopted in [193] was used, where the difference between the head force and the neck force were used to study the dynamic response of the neck in an experimental study. In the present study, the neck force at C_1 and C_7 were subtracted in axial and transverse directions (see Figure 7-7) to obtain the total neck force:

$$F_T = F_T^{C_1} - F_T^{C_7} \qquad \text{Eq. 7–1}$$

$$F_L = F_L^{C_1} - F_L^{C_7} \qquad \text{Eq. 7–2}$$

where $F_T^{C_1}$ and $F_T^{C_7}$ are the transverse forces at C_1 and C_7 and $F_L^{C_1}$ and $F_L^{C_7}$ are the axial forces at C_1 and C_7, respectively. Shearing neck force (F_T) and axial neck force (F_L) are shown in Figure 7-9 to Figure 7-12. Here, the positive shearing refers to the head-neck rotation when the head is rotating in positive direction of θ, which is shown in Figure 7-8. Moreover, the negative axial load represents compression and the positive axial load is tension.

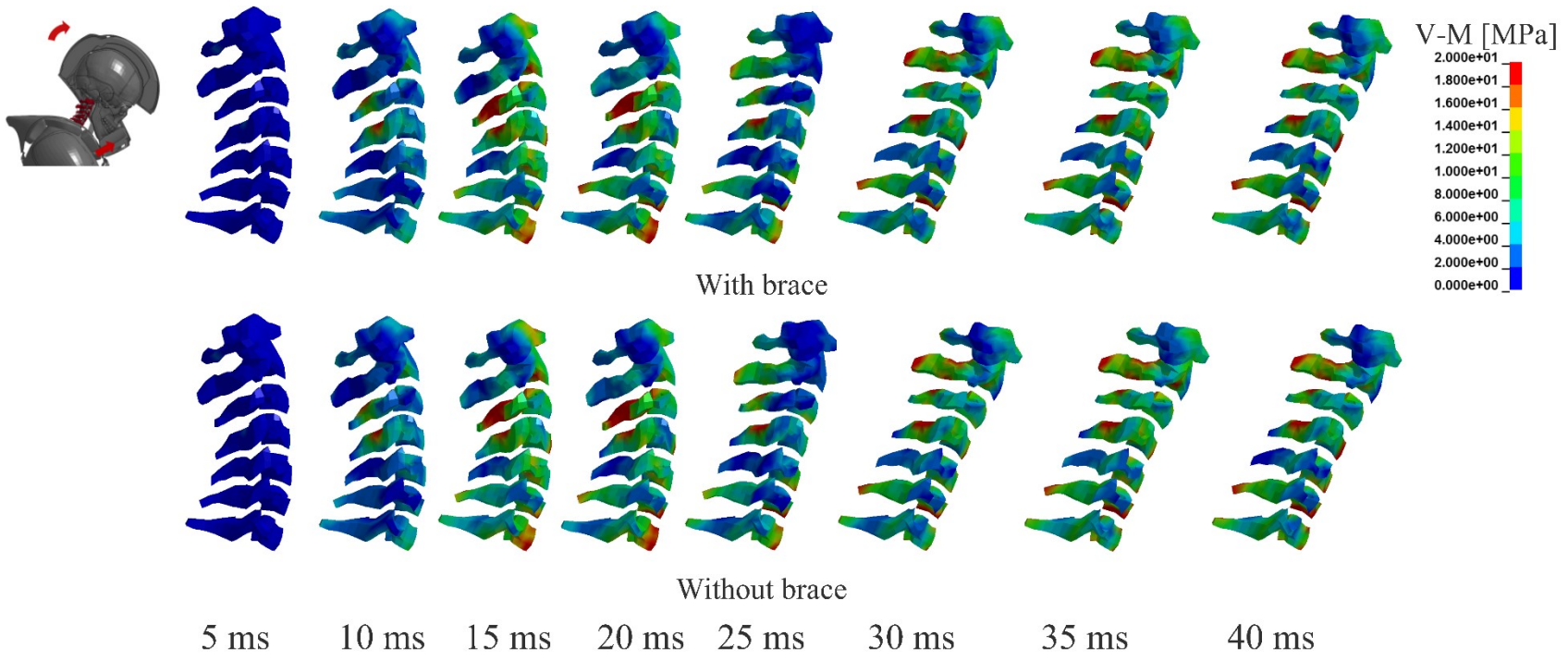

Figure 7-3 – Stress in the cervical vertebrae, for load case No. 1- Hyperflexion. The upper row shows the result for the case with the neck brace and the lower row shows the result for the case without it.

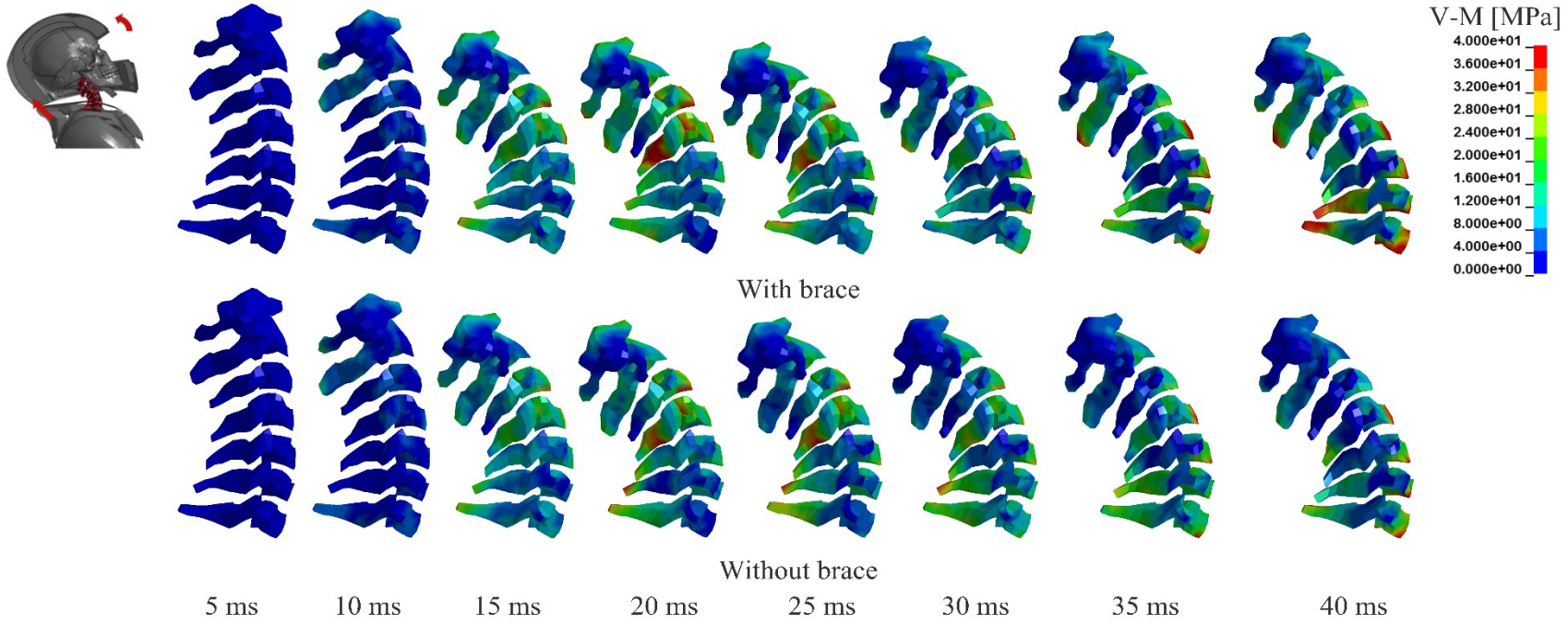

Figure 7-4 – Stress in the cervical vertebrae, for load case No. 2- Hyperextension. The upper row shows the result for the case with the neck brace and the lower row shows the result for the case without it.

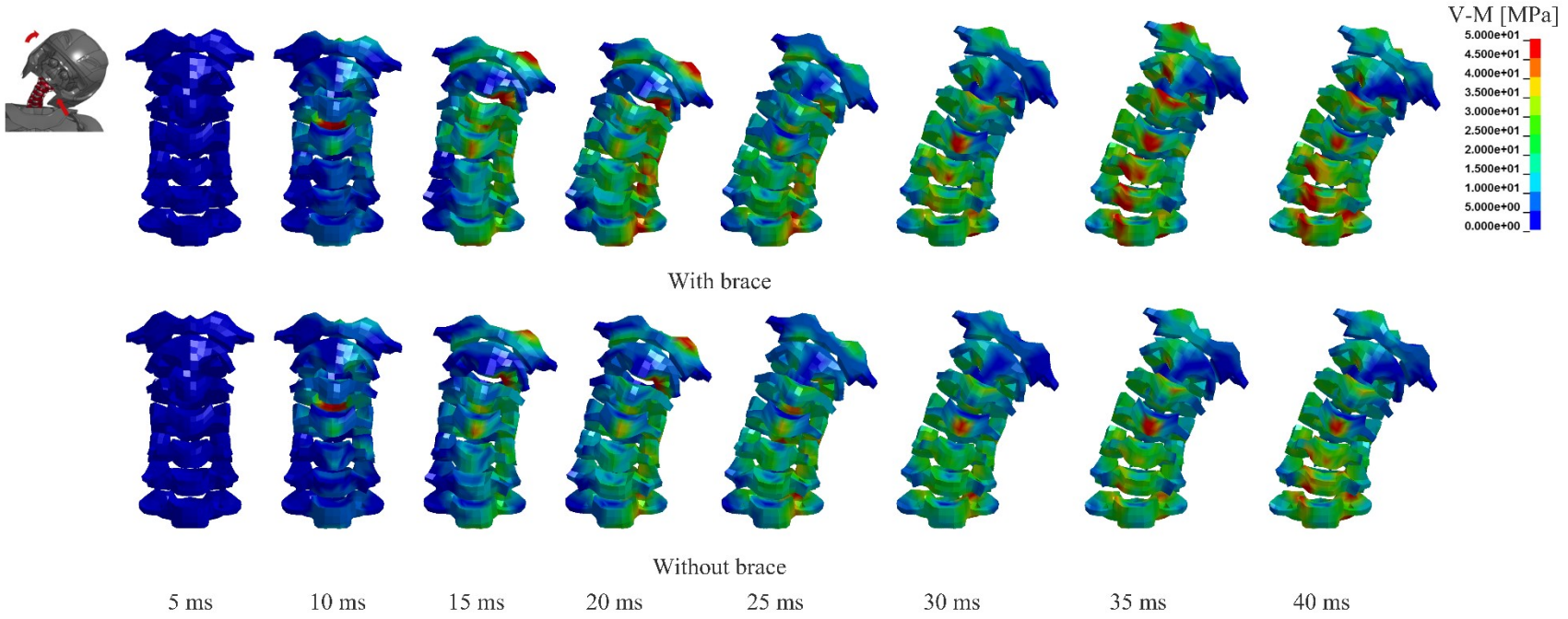

Figure 7-5 – Stress in the cervical vertebrae, for load case No. 3- Lateral bending. The upper row shows the result for the case with the neck brace and the lower row shows the result for the case without it.

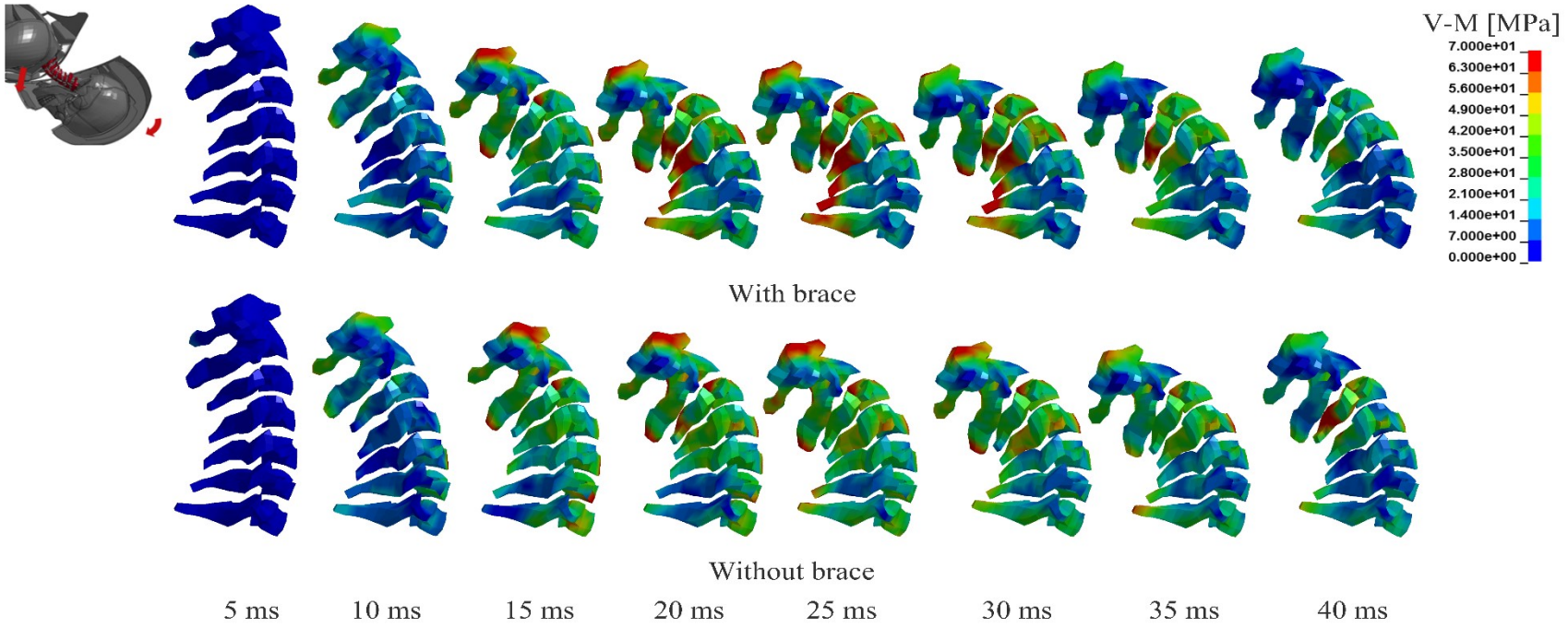

Figure 7-6 – Stress in the cervical vertebrae, for the realistic impact condition. The upper row shows the result for the case with the neck brace and the lower row shows the result for the case without it.

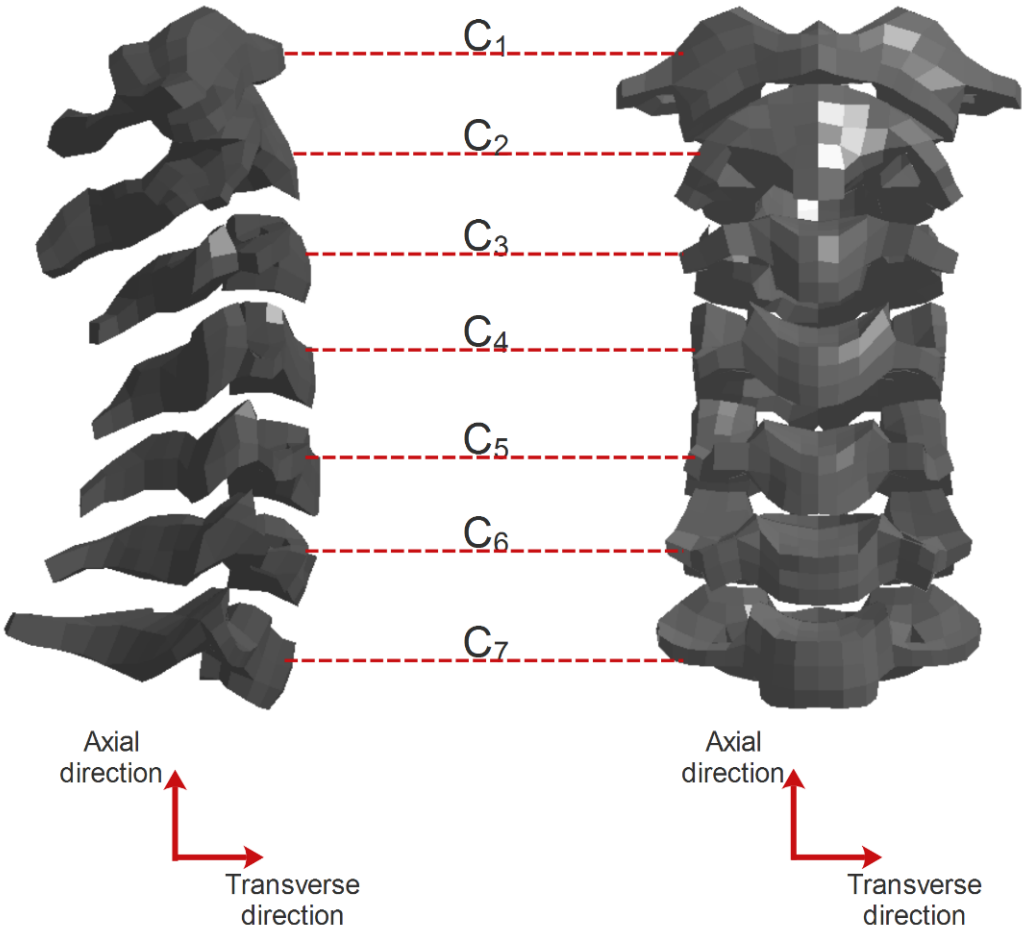

Figure 7-7 – Transversal and axial directions for Hyperflexion and Hyperextension (left) and for lateral bending (right).

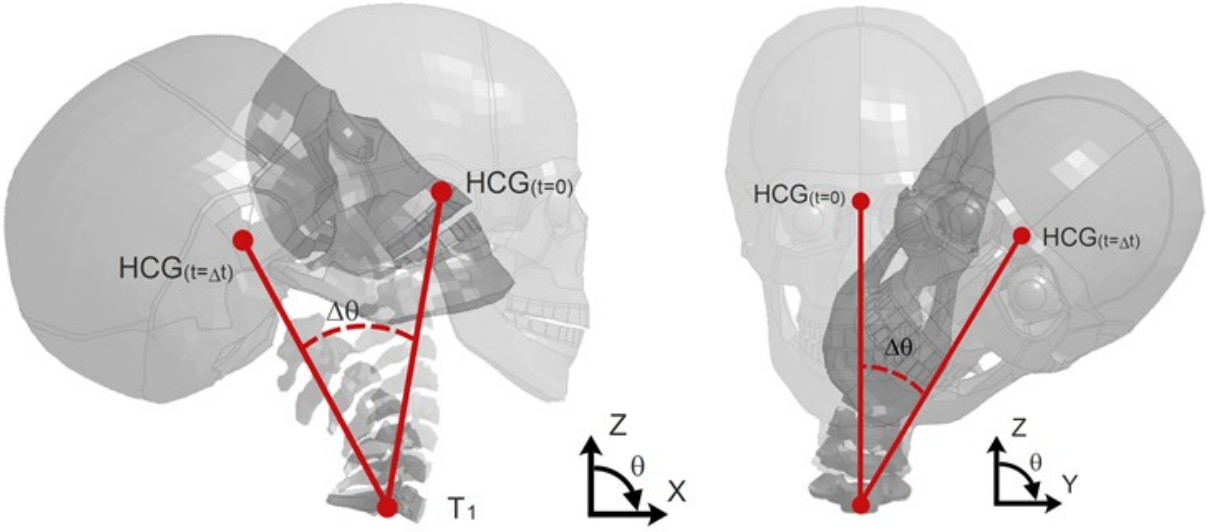

Figure 7-8 – Relative rotation of head with respect to torso (T_1) for Hyperflexion and Hyperextension (left) and for lateral bending (right).

Figure 7-9 shows the result of simulations for the hyperflexion load case (No. 1). The difference between the two cases of using or not using the neck brace are rather small. It is shown that the pick axial and shearing loads were reduced in case of using the brace however, after 23 ms the axial load was higher for the case with the brace.

In Figure 7-10, the results for load case No. 2 (hyperextension) show that the shearing load was reduced at some points by using the brace but at some other points it was increased. Moreover, using the brace reduced the neck axial load between 20 ms and 30 ms but increased the induced axial load on the neck after 35 ms even more than the maximum load, which was induced at neck without using the brace.

In case of lateral bending the results, which have been presented in Figure 7-11, show that using the neck brace increased both shearing and axial induced load at the neck.

Figure 7-12 shows that using the neck brace in a realistic load condition, when there is a mixed mode of loading (flexion-compression), could reduce the axial compressive load at the neck by 19%. However, the direction of the axial force changed after 19 ms from compressive to tensile when the neck brace was used, in contrast to the case without the neck brace. The figure also shows that the direction of the shearing load changed after 19 ms when the brace was used. The change in the neck force direction is due to the contact force between the head and the neck brace after 4 ms (see Figure 7-17). Furthermore, the peak shearing and axial loads happened in a shorter time in case of using the brace. As it is shown for the case without the brace, the axial and shear loads raised to the maximum value from 4 ms to 11 ms and 16 ms respectively and decreased to zero in almost 22 ms after reaching the maximum value. When the brace was included, the axial and shear forces decreased to zero in almost 8 ms.

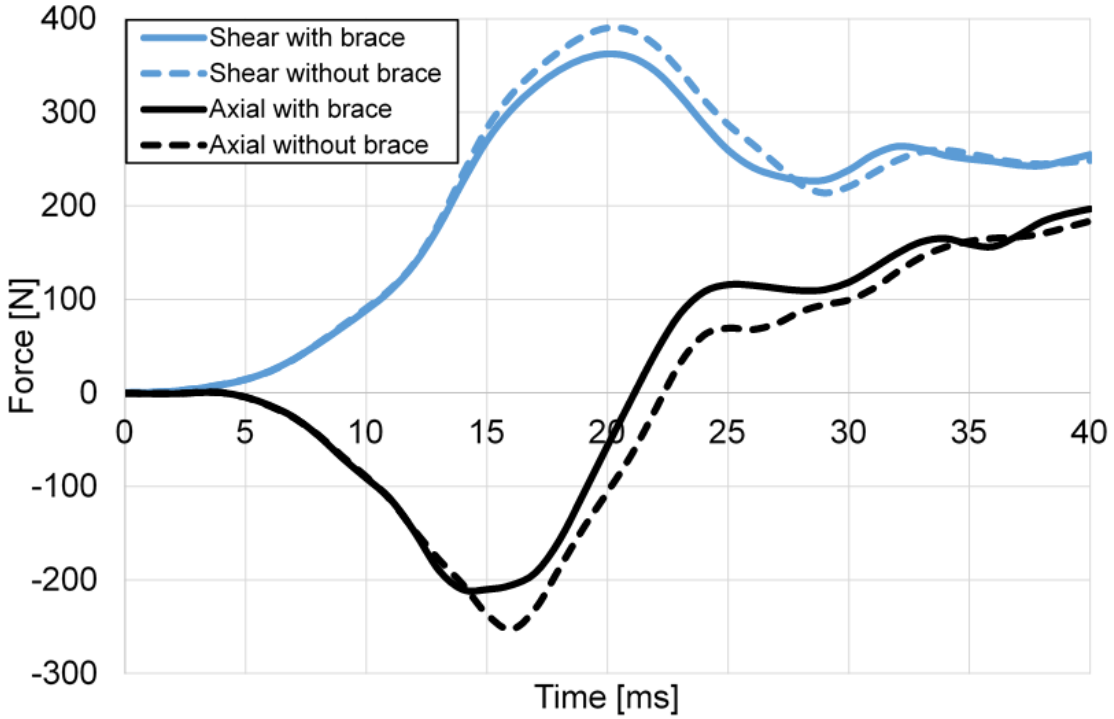

Figure 7-9 – Neck axial and shear forces for load case No. 1- Hyperflexion.

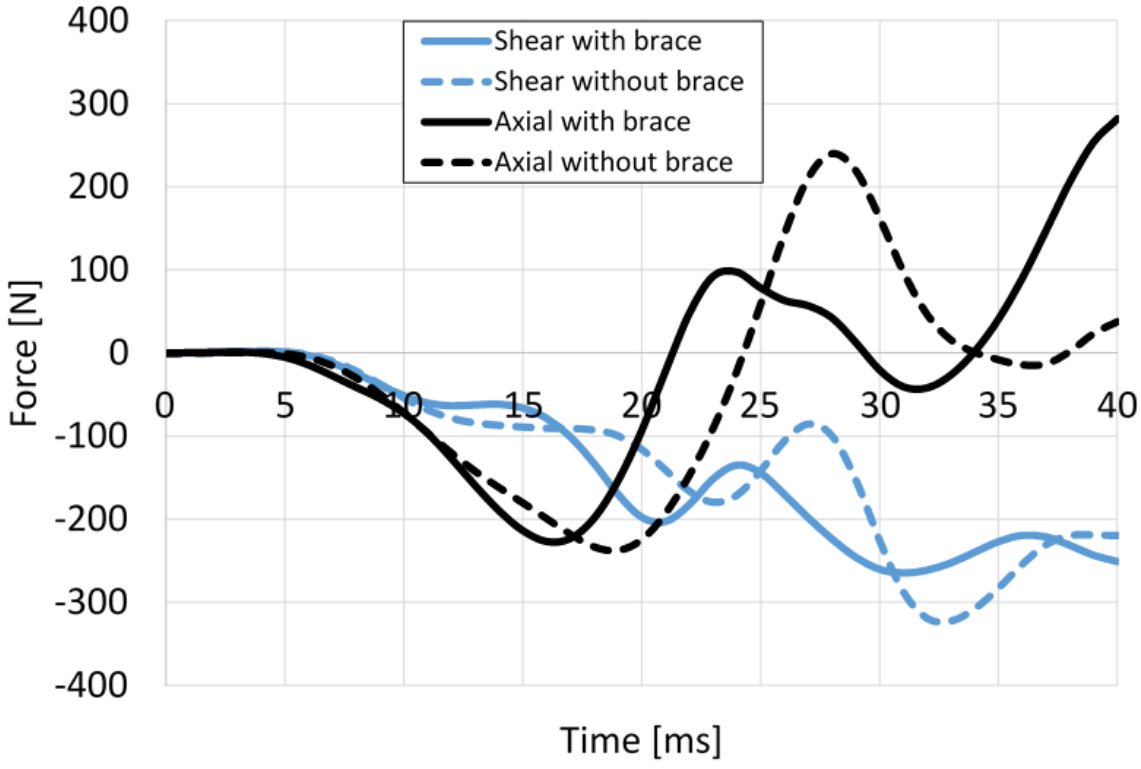

Figure 7-10 – Neck axial and shear forces for load case No. 2- Hyperextension.

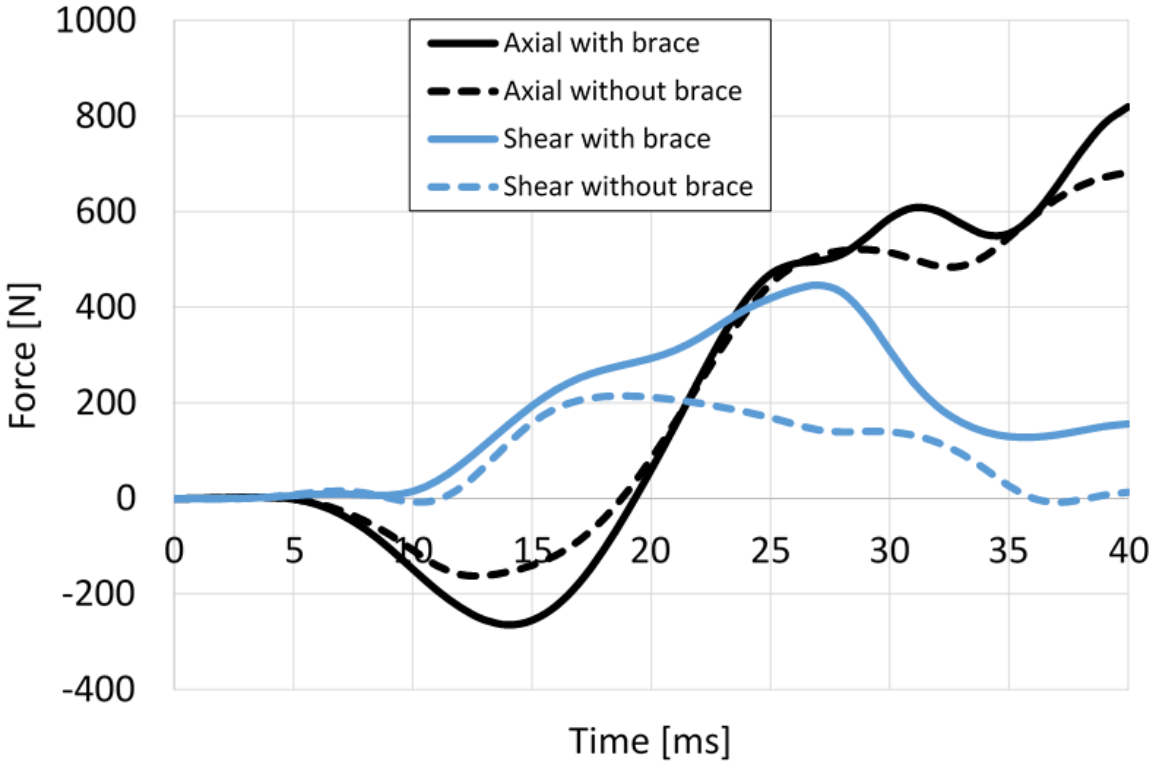

Figure 7-11 – Neck axial and shear forces for load case No. 3- Lateral Bending.

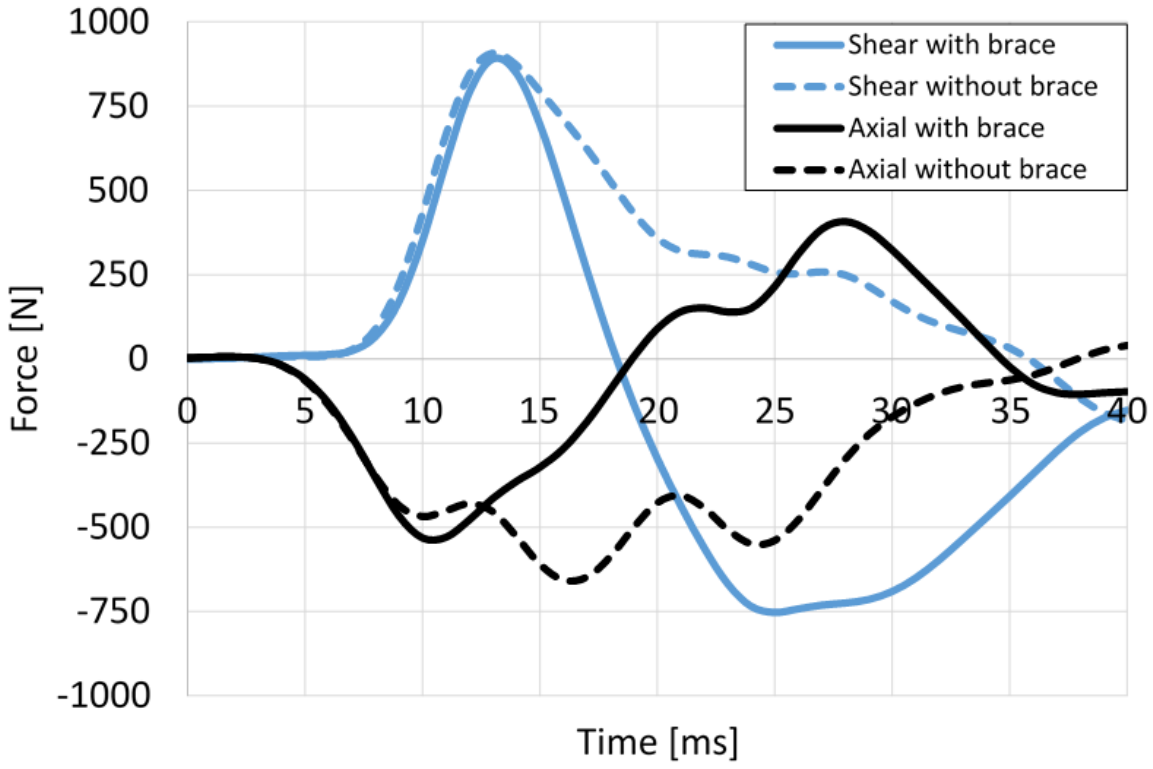

Figure 7-12 – Neck axial and shear forces for the realistic impact condition.

7.3. Discussion

A finite element model of a neck brace was generated and validated experimentally. The neck brace model was coupled with a validated helmet model [6] and a high fidelity human body model [176], and four load cases were simulated to assess the protection capability of the neck brace for hyperextension, hypeflextion, lateral bending and flexion-compression modes of neck deformation.

The results showed that the neck brace increased stress in neck vertebrae for the investigated load cases. It was also shown that although using the neck brace can reduce the induced shear and axial neck loads at some points during the neck deformation, the impact between the neck brace and the helmet can also induce higher loads in the neck (Figure 7-9 to Figure 7-12).

The aim of the neck brace is to reduce the relative rotation of the head with respect to torso. Here the first thoracic vertebra (T_1) addresses the torso [194] (Figure 7-8). Nevertheless, according to FE analyses which have been mentioned before using the neck brace may have a reverse effect. The relative rotation of head-torso was calculated as follows:

$$\Delta\theta_{(t)} = \theta_{(t)}^{HCG} - \theta_{(t)}^{T_1} \qquad \text{Eq. 7–3}$$

where $\theta_{(t)}^{HCG}$ and $\theta_{(t)}^{T_1}$ are the rotational displacement of head and T_1 respectively in global coordinate system as a function of time [195].

Figure 7-13 to Figure 7-16 show the rotation $\Delta\theta_{(t)}$ in time. Figure 7-13 shows that using the brace could reduce the rotation of the head with respect to torso in case of hyperflexion. The results showed that in load cases No.2 (hyperextension) and No.3 (lateral bending) the rotation of HCG with respect to T1 did not change in case of using the brace, however the level of rotation is slightly higher when the brace was used. Figure 7-16 shows that the neck brace could restrict the rotation of HCG at 12 ms but due to a large impact force (see Figure 7-17) between the helmet and the brace changed the rotational movement significantly in rebound.

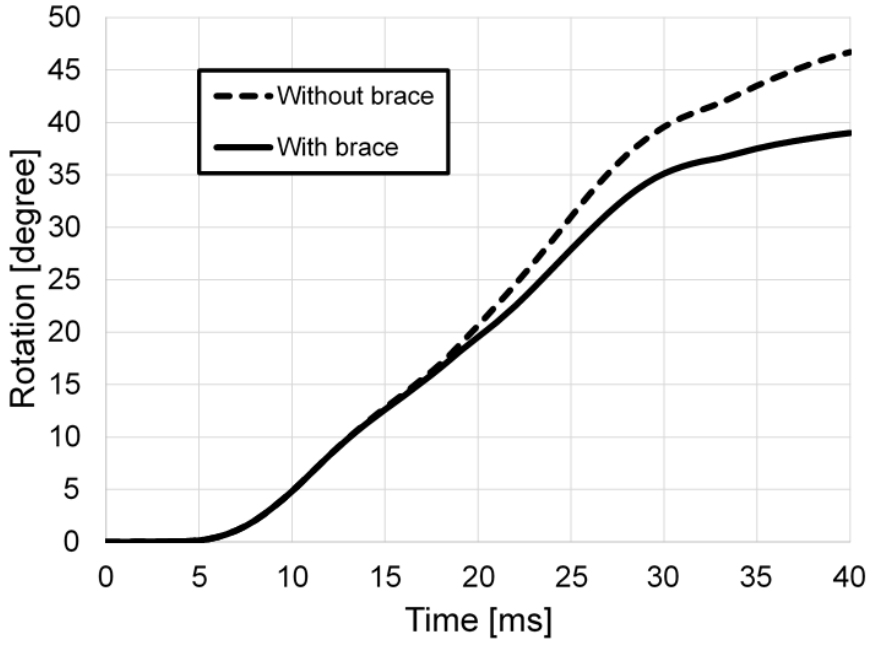

Figure 7-13 – Relative rotation of head-torso around y axis for load case No. 1.

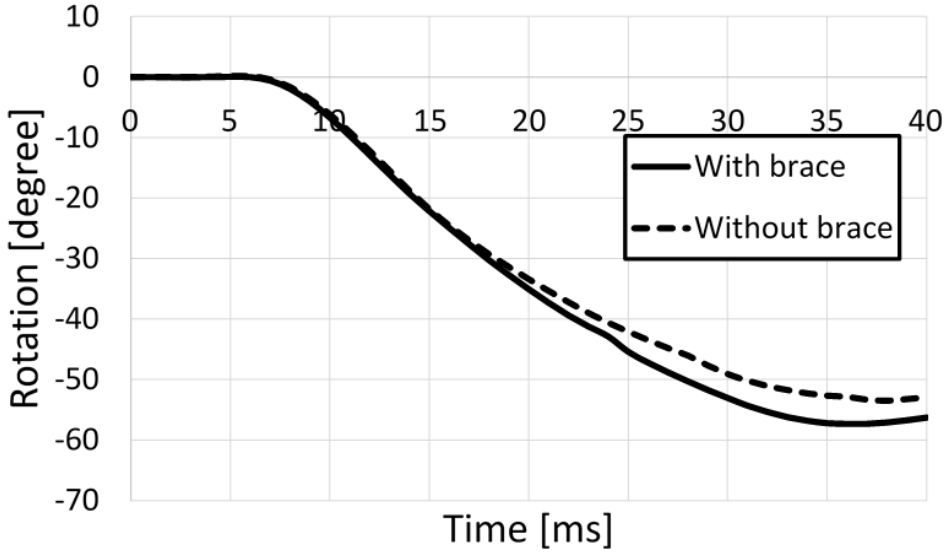

Figure 7-14 – Relative rotation of head-torso around y axis for load case No. 2.

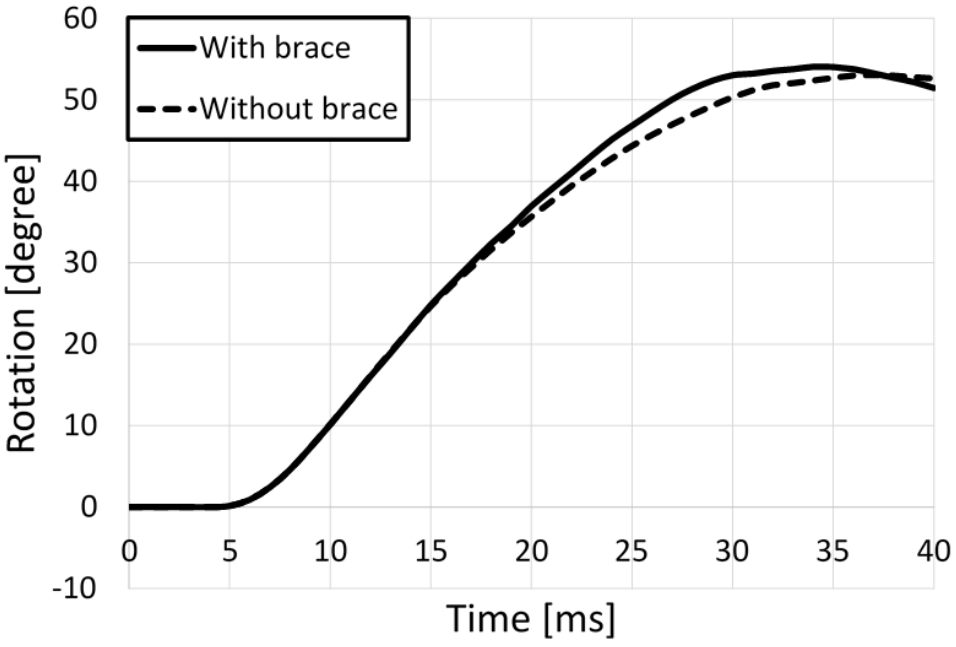

Figure 7-15 – Relative rotation of head-torso around x axis for load case No. 3.

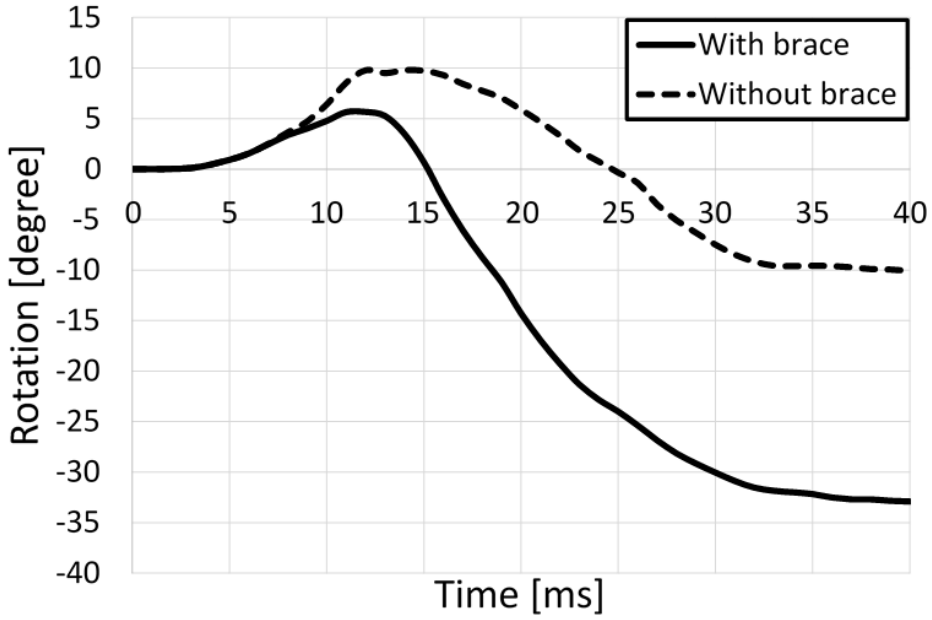

Figure 7-16 – Relative rotation of head-torso around y axis for the realistic impact condition.

Figure 7-17-a shows that both components of contact force between the helmet and the brace opposed the flexion of the head-neck and could reduce the maximum induced shearing and compressive axial load in the neck (Figure 7-9), however, the Z component of the reaction force increased the axial neck force in tension (after 25 ms).

In case of hyperextension (load case No.2), the force applied on the helmet due to its contact with the neck brace increased the neck force as well (Figure 7-10). In this case, the contact took

place while the neck was already under tension and the Z component of the contact force (Figure 7-17-b) induced higher tension at the neck. The X component of the reaction force had the same effect on the neck-shearing load.

Figure 7-17-c shows that the Z component of the contact force between the helmet and the brace induced a tensile load in the neck while the neck was partially under tension so this tensile load induced higher tension on that part of the vertebrae, which were remote from the contact point between the brace and the helmet. The direction of shearing load changed due to the kinematic of the moving parts as shown in Figure 7-17-c, but it increased the total induced shearing neck load (Figure 7-11).

Figure 7-17-d shows the contact force between the helmet and the brace for the realistic impact condition in which the neck was under a mixed mode loading of compression and flexion. The head neck assembly rebounds under axial loading [193] as it is shown in Figure 7-16. Although the neck brace reduced the flexion of the neck, the large reaction force on the helmet due to the contact with the brace caused the rebounding motion (extension) of the head. As a result, the brace increased the axial and shear neck loads and consequently the level of rotation of HCG with respect to T_1. In addition, Figure 7-17 shows that the level of the contact force between the helmet and the brace for the realistic impact condition is significantly higher than the other three load cases. This could be the result of body's inertia in this impact condition [7,196].

The results of this study show that restraining the head-neck motion by the investigated neck brace may increase the induced load at the neck and stress level at cervical vertebrae and consequently can increase the risk of neck injuries. This is in agreement with findings from experiments on cadavers. Yogonanadan et al. showed that dropping cadavers with the restrained head-neck caused more spinal injuries comparing to un-restrained specimens [197]. Alike, Nightingale et al. studied the effect of different end conditions on neck injuries and showed that increasing the constraints on the head could increase the risk of cervical injuries [198]. The cervical spine angulation is known as an energy dissipation mechanism and therefore, restraining the head-neck motion may increase the risk of cervical injury.

This study has limitations, which should be considered when interpreting the results. First, the effects of friction between shoulder/brace and helmet/brace were not considered. A large friction coefficient at these interfaces was assumed. Quantifying the friction coefficient and studying its effect is a future work. Four impact conditions that are likely to represent common impact conditions [9] were studied, but accidents can occur in different conditions. However, this work shows that in the simulated conditions, a realistic neck brace model can induce neck forces that are higher than those generated when the neck brace is not used. Therefore, developing a standard procedure for assessing the performance of neck protective devices is crucial for the safety of motorcycle riders.

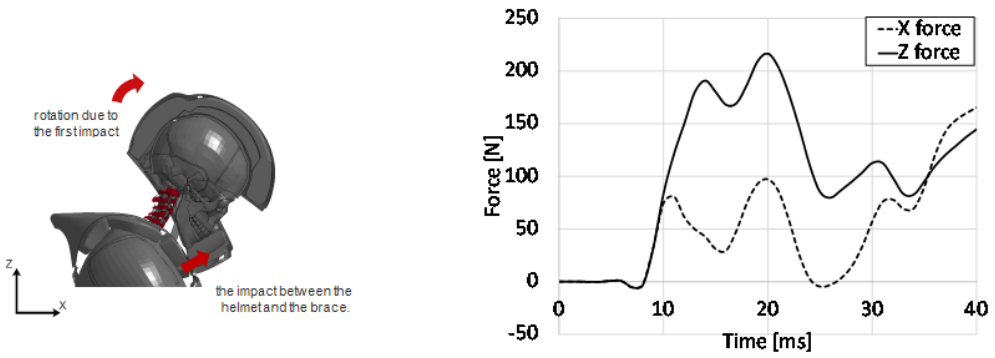

(a) Hyperflexion

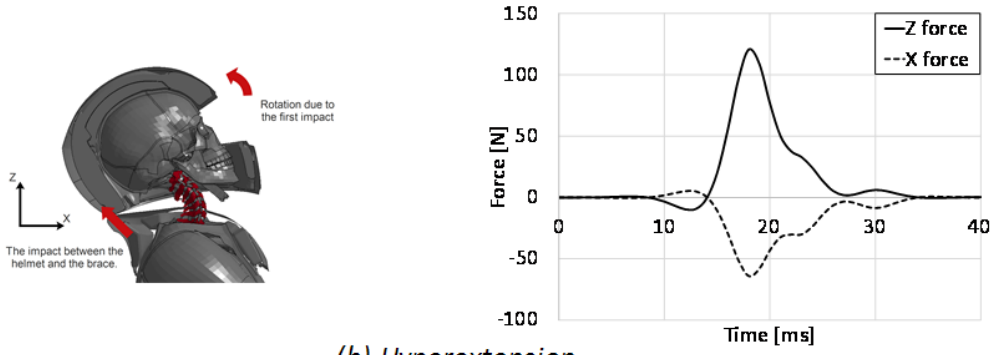

(b) Hyperextension

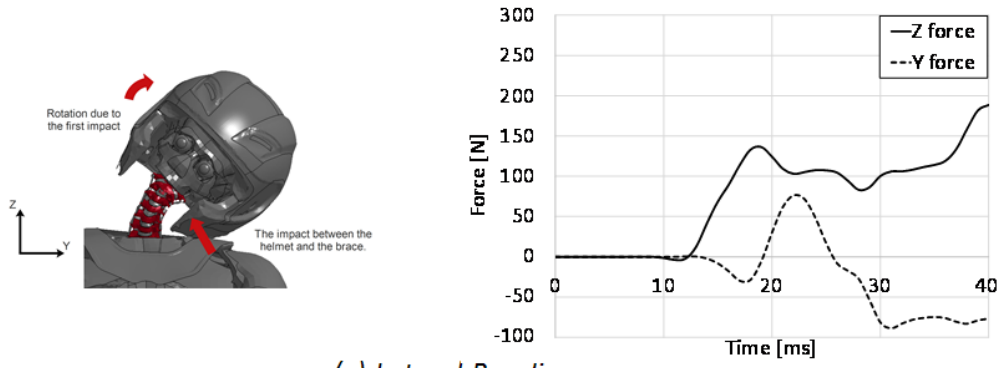

(c) Lateral Bending

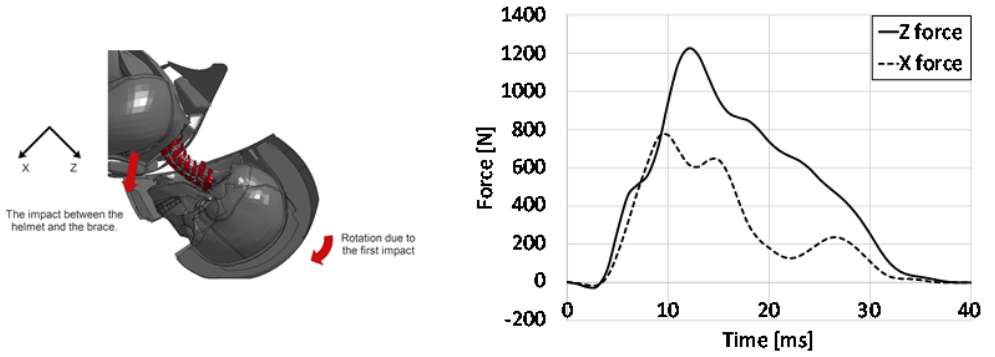

(d) Realistic impact condition

Figure 7-17 – The force induced on the helmet due to the impact between the helmet and the brace (Some parts of the model are not shown). Time zero is the instant of the impact beween the helmet and the obstacle.

8. Using New Energy Absorption Materials in PPE

8.1. Composite laminate optimization

In this chapter a human head/neck surrogate, Hybrid III, is used to test whether it is possible to decrease the upper neck tensile force (a possible indicator of BSF) by altering the ply orientation of a composite chin bar, while meeting standard requirements. This work is the first step of an attempt to consider the neck load in the design process of the helmet chin bar by means of computational methods.

The stiffness and energy absorption capability of composite laminates are functions of fibre orientations in each lamina [199,200]. Hence, by carefully selecting ply orientations of the composite chin bar of the helmet, thus keeping the mass of the helmet constant, it may be possible to reduce the force transmitted to the neck by chin impacts. The chin bar of the AGV-T2 helmet has a $[(0_{TW,G})_2, \pm 30_H, (\pm 30_G)_2]$ configuration and is made of pairs of three different plies: glass/epoxy twill weave, unidirectional Kevlar/carbon/epoxy hybrid and unidirectional glass epoxy (see chapter 6.1), where glass/epoxy twill weave is the external ply (see Figure 8-1). The orientation of ply pairs, i.e. θ_1, θ_2 and θ_3 shown in Figure 8-1, were the design variables in this study.

The chapter is organized as follows. In the following section, the design variables, objective function and the search algorithm are described. Then, the results, including the optimal chin bar lay-up, are presented and the mitigation mechanisms are discussed. Finally, some concluding remarks with directions for future work are provided.

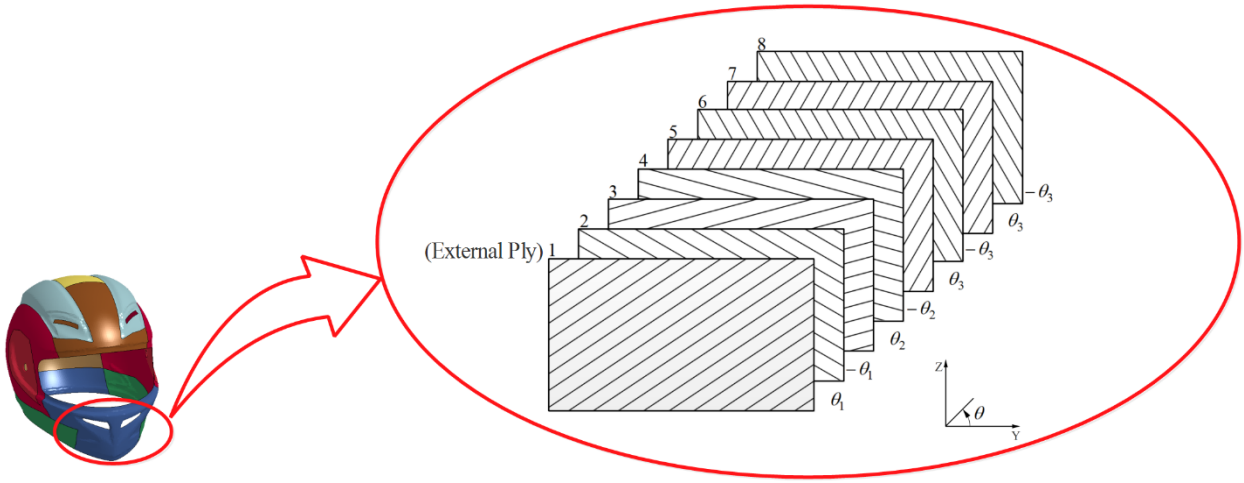

Figure 8-1 – The chin bar ply lay-up.

8.1.1. Method

Finite element models of a full-face composite-shell motorcycle helmet, the 50th percentile male hybrid III dummy and the medium size ISO headform for this study are used. A computational approach developed to perform several iterations within the design space to search for the optimal solution. In the following section impact conditions and search algorithm have been described.

8.1.1.1. Impact conditions and the search algorithm

Impacts during accidents can occur in many different conditions but standards have to prescribe a few more likely impact conditions for testing helmets. For the chin bar impacts using the head/neck assembly, the impact conditions prescribed in the Snell standard [182] has been adopted. A 5kg cylindrical impactor with an initial speed of 3.5 m/s hits the chin bar of the helmet positioned on the Hybrid III head-neck (Figure 8-2). The neck bracket of the dummy was fixed as suggested in [178,179]. During simulations, the neck axial force was recorded.

To find a ply lay-up that transmits the minimum axial force to the neck, θ_1, θ_2 and θ_3 were varied from zero to 90 degrees with an interval of 15 degrees. By considering this variation as a permutation problem with repetition, 7^3 (=343) possible lay-ups had to be searched for the minimal neck axial force. A MATLAB code was developed to change the angles, modify and run LS-Dyna input files, store the maximum neck axial force during the impact as the output and generate a dataset of ply lay-up (θ_1, θ_2 and θ_3) versus neck axial force. After running all simulations for the entire design space, the code sorted the dataset from the minimum to the maximum value of the neck axial force (Figure 8-2).

In order to ensure that the helmet with an optimal ply lay-up for the chin bar can also pass the standard chin bar impact test, the ECE 22.05 standard test [96] was simulated. The helmet positioned on the FE model of the ISO headform was propelled towards a rigid anvil at a 5.5 m/s speed (Figure 8-2). The MATLAB code started from the ply configuration that induced the minimum neck axial force, read the ply configuration and modified the LS-Dyna input file of the ECE virtual test. After running the simulation, the code filtered head accelerations using a Butterworth filter [201] and calculated the Head Injury Criterion (HIC) and Peak Linear Acceleration (PLA). The code continued checking the configurations from the sorted dataset in order to find the one which passed the requirements of the ECE 22.05 standard, i.e. HIC < 2400 and PLA < 275 g.

Figure 8-2 shows the flowchart of the search algorithm. The entire simulations lasted 221 hours using a PC with an Intel Core I7 3.6 GHZ processor and 32 GB RAM. All the simulations terminated correctly with no convergence or stability problems.

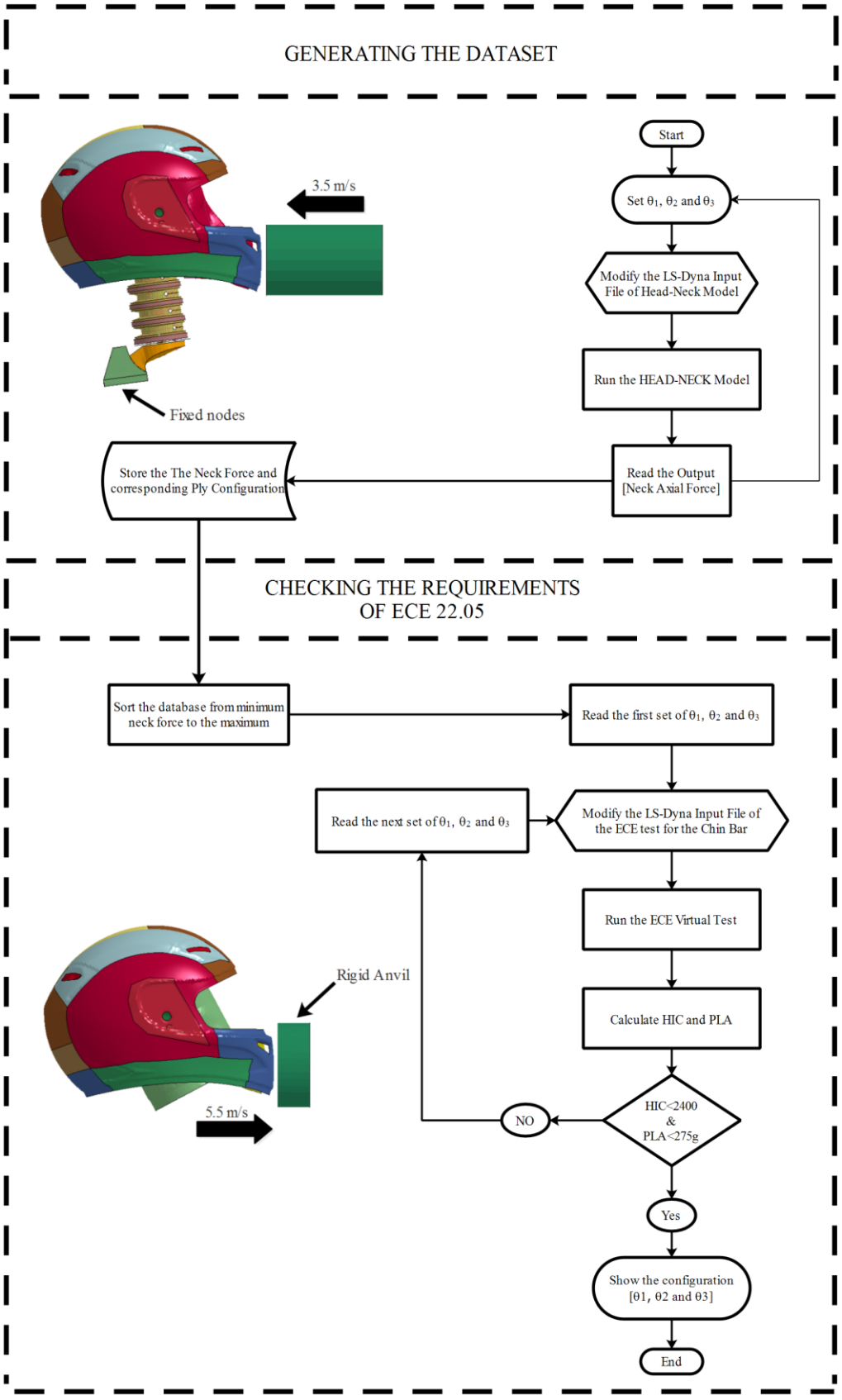

Figure 8-2 – Flowchart of the search algorithm.

8.1.2. Results and discussion

The first 20 ms of the impacts were simulated. In all simulations, the peak neck force occurred during the first 15 ms of the impact. As can be seen in Figure 8-3, the impact deforms the chin bar shell and foam and reduces the distance between the chin liner and the chin. The chin liner did not touch the chin in any of the simulations using head/neck assembly. Instead, the chin strap transmitted the impact force from the helmet shell to the chin, leading to a large neck tensile force (Figure 8-4).

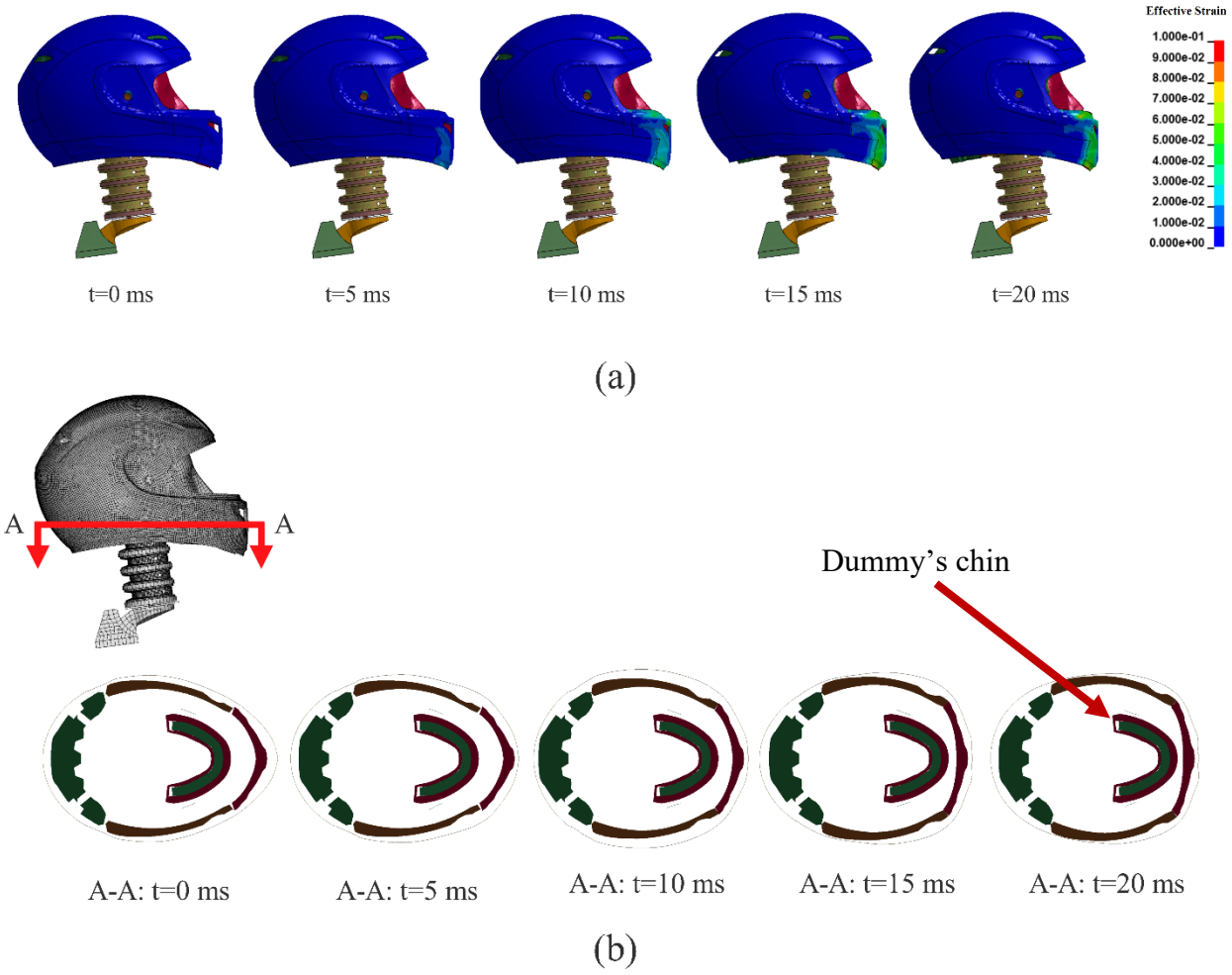

Figure 8-3 – (a) Deformation of the helmet chin bar at different time points (some parts of the helmet are not shown). (b) Sectional view of the helmet, showing the deformation of the chin bar (both shell and liner) at different time points.

The peak value of the predicted neck force in the dummy varied between 0.712kN and 1.037 kN, with a 0.928 kN mean and a 0.060 kN standard deviation. For all cases the largest neck force was tensile. A multiple linear regression analysis was used to test how changing the angles influence the predicted neck force. The adjusted R^2 was 0.13 showing large variability but the F-test showed a significant linear trend ($F=18$, $p<0.001$) [202]. The analysis results for the influence of each ply angle show that both θ_2 and θ_3 have significant influence on the neck force in the

dummy ($p<0.001$ for both) but the influence of θ_1 was not significant ($p>0.9$), probably because θ_1 is the angle of the twill weave plies, which have the same properties in longitudinal and transverse directions (Table 6-3).

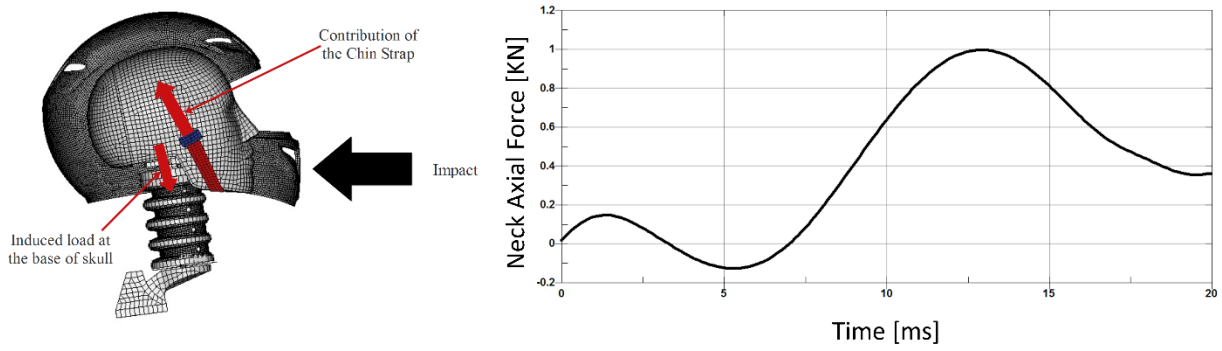

Figure 8-4 – Left: The load transmission mechanism in a chin bar impact, (some parts of the helmet are not shown); Right: time history of the neck axial load induced by facial impact on the helmet chin bar.

The predicted peak neck axial force versus ply angles is shown in Figure 8-5 for all 343 chin bar impact simulations. Figure 8-5(a) shows that the ply configurations with θ_1, θ_2 and θ_3 equal to 0° or 90° induce the lowest neck axial forces. According to Figure 8-5(b), there is also a local minimum if θ_1, θ_2 and θ_3 are equal to 45°. The minimum neck force, 711.5 N, was predicted for the $[(0)_2, (90)_2, (90)_4]$ chin bar laminate, but this helmet did not pass the ECE 22.05 test because the predicted HIC and PLA for the standard chin bar test were 1218 and 335 g respectively, with PLA being greater than its limit set in the standard. The helmet with the lowest neck force (724 N) that passed the standard chin bar test with HIC = 850 and PLA = 272 had a $[(0)_2, (90)_2, (0)_4]$ chin bar lay-up. Hereafter we call this configuration the optimum ply lay-up or optimum ply configuration. The chin bar with a $[\pm75, \pm60, (\pm15)_2]$ lay-up induced the maximum neck force (1037 N), but it passed the standard chin bar test with HIC = 479.1 and PLA = 125.5. This analysis shows that by only changing the ply angles of the chin bar laminate, thus keeping the mass of the helmet constant, the neck force can be reduced by 30% while still meeting the requirement of the standard.

The deformation of the chin bar shell under impact loading led to damage propagation in its layers, a mechanism for energy absorption and subsequent reduction of the neck force. Figure 8-6 shows the damage distribution in different plies of the chin bar that induced the highest neck force and that in the optimised chin bar. As can be seen, for the optimal lay-up, damage is better distributed between plies and it is spread across a wider area in each ply. As a result, the optimized chin bar absorbs more energy during the impact leading to a lower neck force. The absorbed energy was determined from the FE simulations by measuring the internal energy of the chin bar after the impact. The energy absorbed by the chin bar shell with the optimum lay-up was 9.2 J, which was 40% larger than the energy absorbed by the stiffest chin bar shell, confirming that energy absorption during impact is a key to the reduction of the neck force.

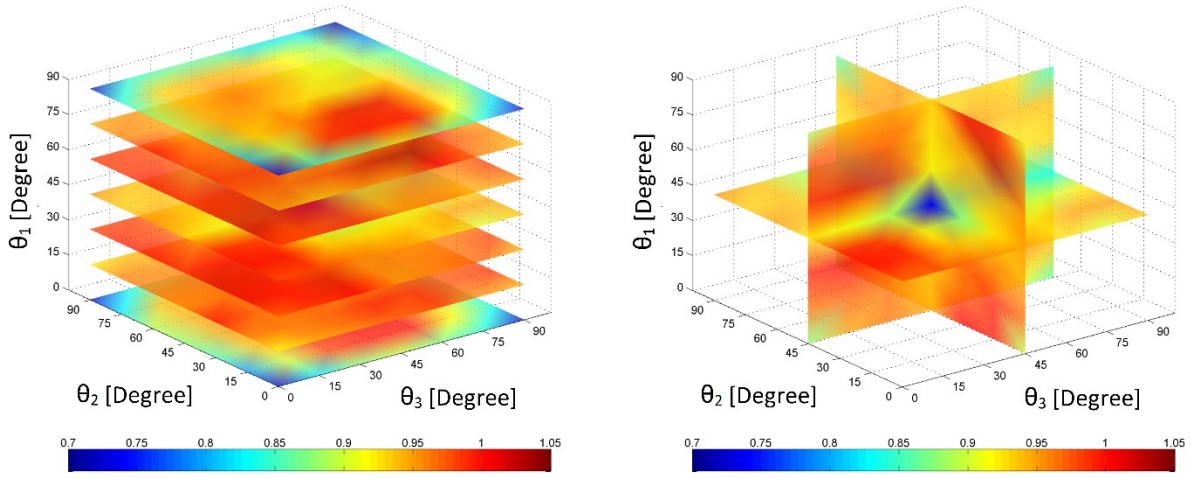

Figure 8-5 – Iso surface plot of Neck Axial Force (kN): (a) Slice surface at θ_1=0, θ_1=15, θ_1=30, θ_1=45, θ_1=60, θ_1=75, θ_1=90. (b) Slice surface at θ_1=45°, θ_2=45°, θ_3=45°.

Basilar skull fracture can take place in direct or indirect impacts, such as pedestrians accidents, falls and vehicle accidents [203], where the base of the skull is exposed to complex loading conditions that can cause BSF [204], but the mandibular loading in conjunction with the neck tensile load, a common loading condition during motorcycle accidents [10], has the highest risk of basilar skull fracture [14]. The present work focused on the optimization of the helmet chin bar and introduced a numerical approach to optimize the stiffness of the chin bar laminate, which is correlated to the transmitted neck load due to the blow on the chin bar [34], in order to minimize the upper neck force due to such an impact.

Results of this study show that the neck axial force in the Hybrid III dummy reduces by reducing the stiffness of the chin bar laminate, but the chin bar stiffness reduction may increase the value of HIC and PLA during the ECE test. This is due to the further compression of the chin liner, producing larger force on the isolated headform thus increasing PLA. This effect can be compensated by including the chin liner in the optimisation [205], which is out of the scope of the present work. The focus of this work is on testing whether the chin bar design can be improved to mitigate the neck force, while ensuring that the requirements of standards are met.

One of the limitations of this work is using the Hybrid III head/neck system. Using a neck was necessary to measure the neck tensile force, a possible indicator of BSF, but the Hybrid III neck is known for its low fidelity particularly under head axial loading [206,207]. However this is not the load condition of interest in the present study. Previous work has shown that as the angle between the neck axis and the loading direction approaches ninety degrees, the performance of the Hybrid III neck converges to the performance of a high fidelity computational model of the human neck, THUMS [28]. A direction for future work will be to use higher fidelity neck models to test the protection that different chin bar designs offer with respect to high neck forces.

A precise evaluation of the neck force is beyond the scope of the present thesis: it is apparent that neck morphology varies greatly in the human race according to sex, age, muscular mass etc. The

induced neck force would not only depend on the above mentioned features, but also on the relative stiffnesses of the various elements: chin bar, chin strap, neck and … so the aims of the present section are mainly two:

1. Highlight the risk of inducing excessive neck forces due to the impact on a stiff chin bar;

2. Propose a procedure to optimize the chin bar structure with respect to such a risk.

Moreover, according to the idea and the results presented in the present chapter, a research proposal with cooperation of Dainese S.p.A. and Imperial College London was funded by the Veneto region to develop an experimental set-up to evaluate the effect of different chin bars on the induced neck load due to the facial impacts.

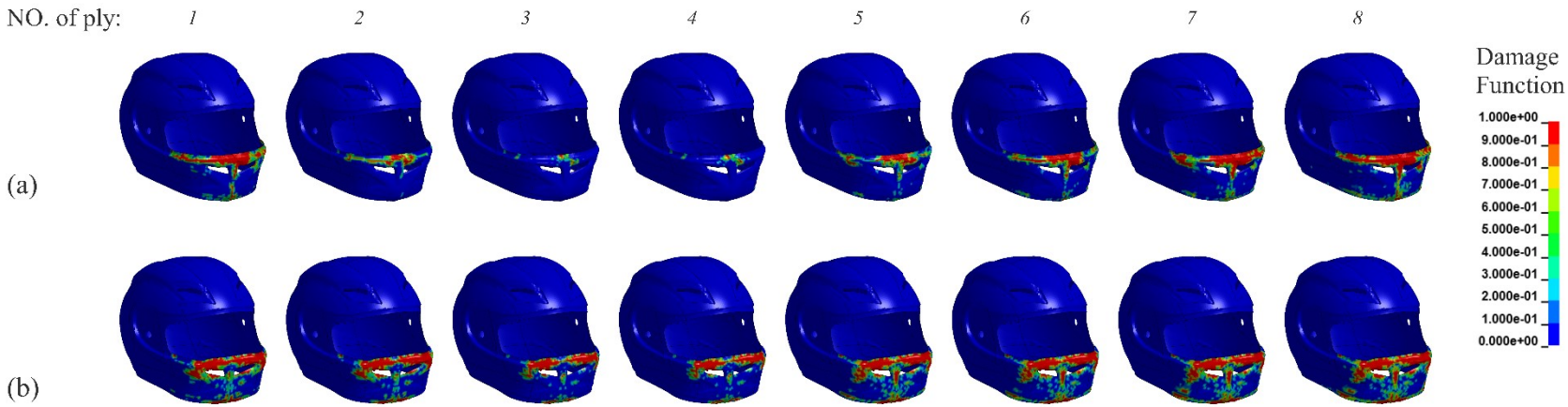

Figure 8-6 – Damage distribution in the shell of the helmet in different plies. (a) china bar, which induced the maximum neck load, 1037 N, (b) optimum chin bar, which induced a neck tensile load of 724 N.

8.2. SPECTRA

As it has been mentioned in Chapter 5.3.2.2, SPECTRA is a high performance fibre, which has a high capability of energy absorption and is lighter than carbon fibres, which are currently used for manufacturing helmet's shell. The specific weight of SPECTRA and carbon fibre that used here are 240 and 600 gr/m^2, respectively. Three different types of tests were carried out to compare SPECTRA with carbon fibres to assess if SPECTRA could be used as a substitute for carbon fibres to improve helmet's level of protection and make them lighter, two quasi-static tests and one impact test. These tests were carried out according to the recommendations given by a helmet manufacturer, DAINESE S.p.A. [a partner of the MOTORIST project] and are presented in this chapter. The SPECTRA fabric which were used for molding the samples were provided by HONEYWELL Co.

8.2.1. Tensile test

Rectangular samples molded using both SPECTRA fabric and carbon fibres and aluminum tabs were attached to the specimens for tensile tests in order to neglect the edge effect close to the test rig grippers as shown Figure 8-7. Tests were carried out for specimens with fibres along the longitudinal and transverse axes and with fibres oriented 45° with respect to longitudinal and transverse axes (see Figure 8-8). A Schenk universal test machine in the laboratory of Industrial Engineering Department of University of Padova was used for tensile tests as shown in Figure 8-9.

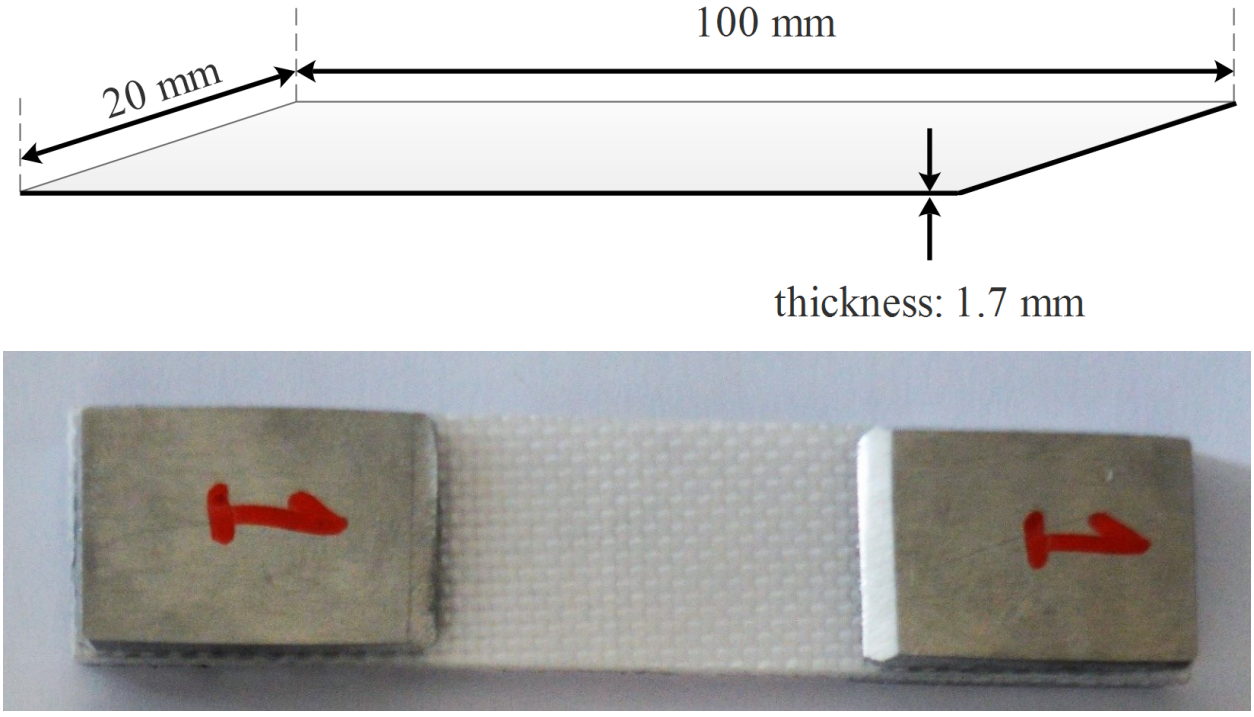

Figure 8-7 – The size of rectangular specimens made of SPECTRA and carbon (top); SPECTRA specimen with aluminum tabs (bottom).

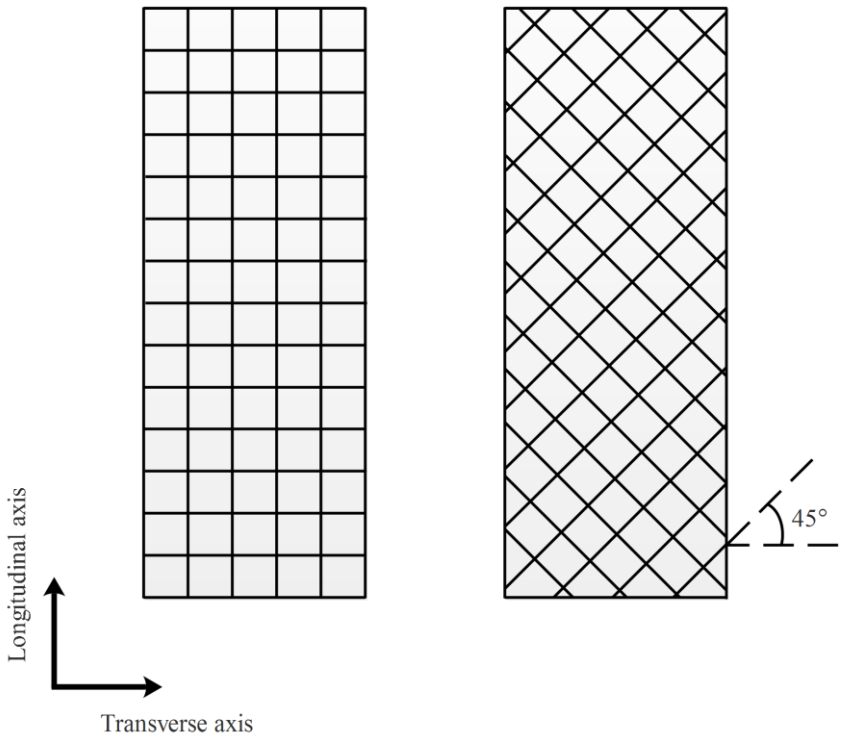

Figure 8-8 – Fibres' orientation.

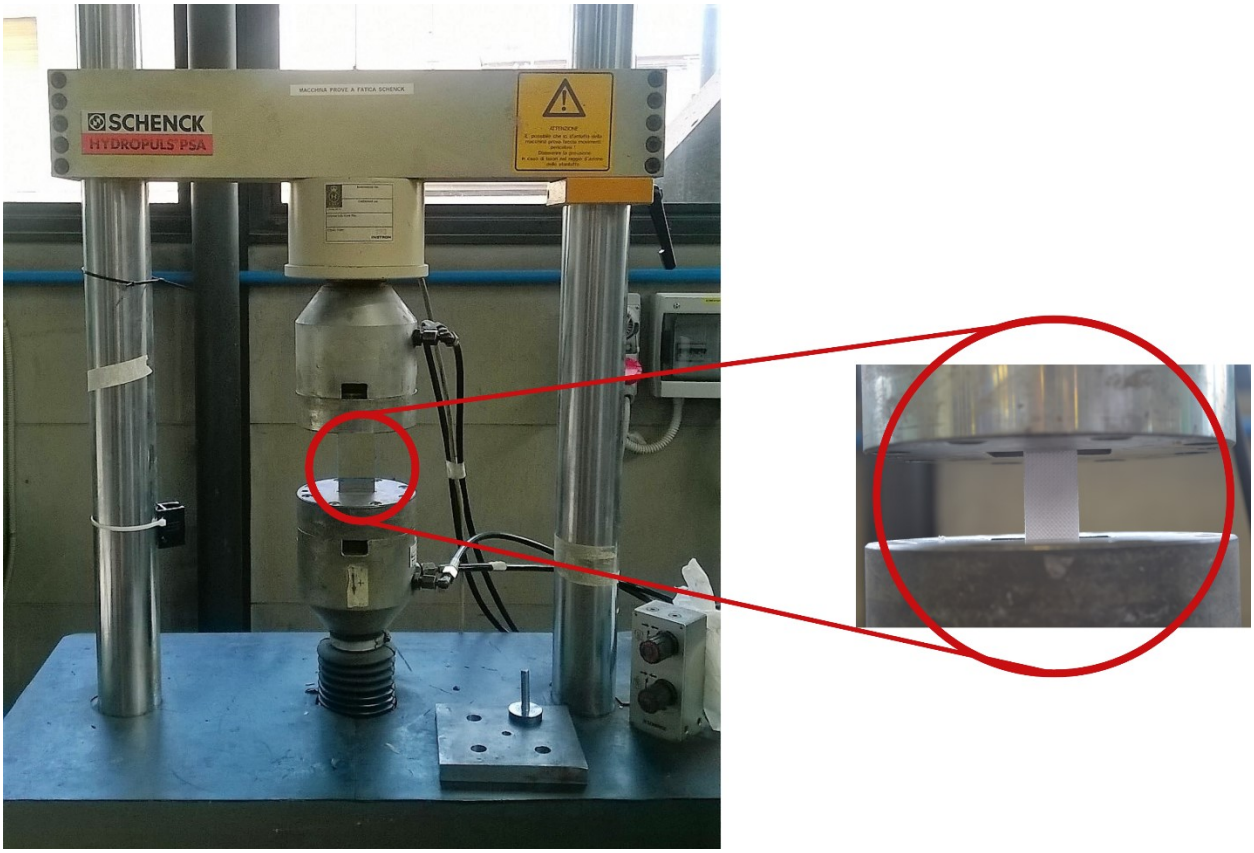

Figure 8-9 – Test set-up used for tensile tests, at DII-UniPd.

8.2.2. Three point bending test

Specimens similar to those described in Chapter 8.2.1 but without tabs, were used for three point bending tests. A MTS universal test machine, which was equipped with special fixtures for three point bending tests, was used for this type of tests as shown in Figure 8-10. A span length of 90 mm was considered.

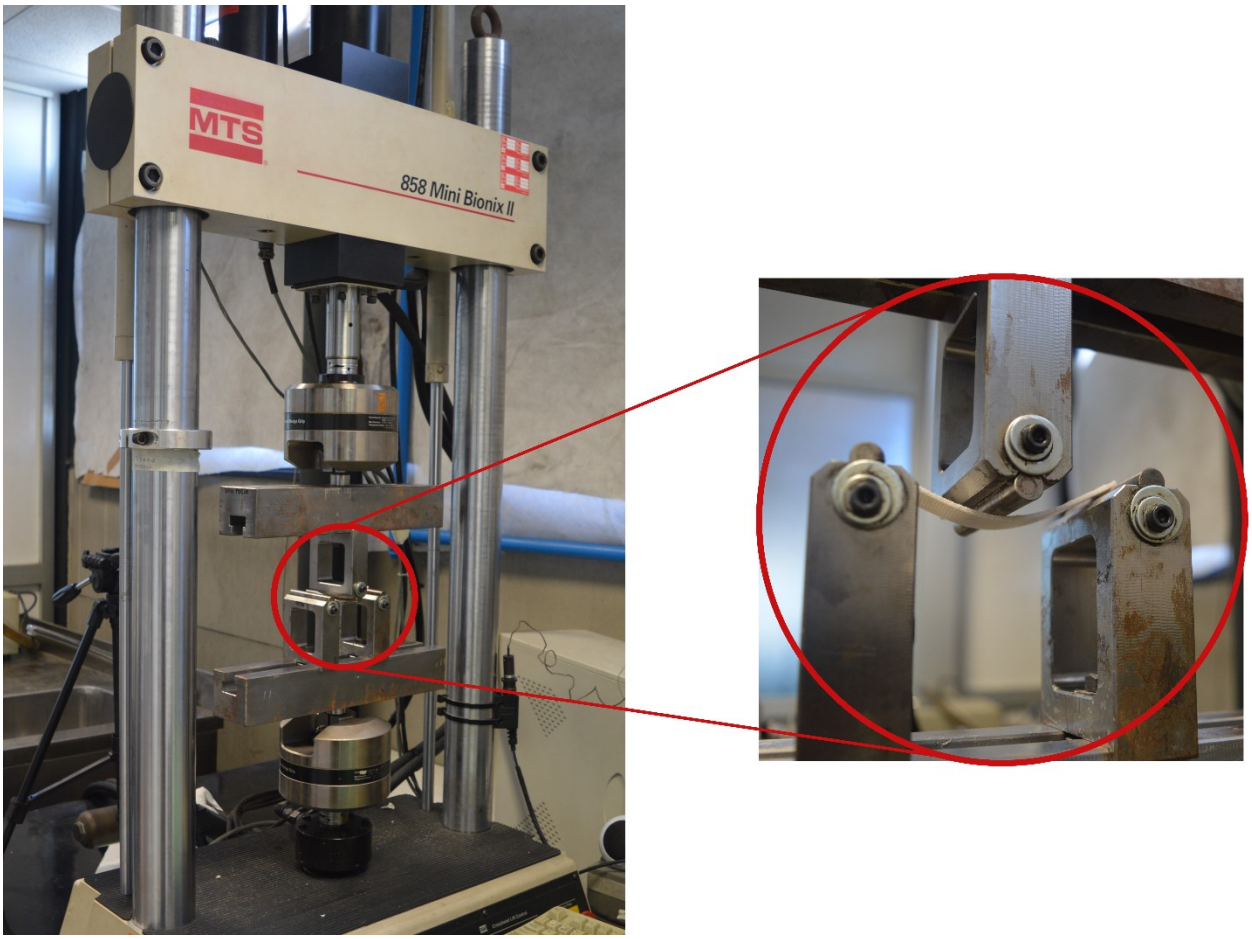

Figure 8-10 – Test set-up used for three point bending tests, at DII-UniPd.

8.2.3. Impact tests

Impact tests were carried out on circular specimens with diameter of 100 mm by means of a drop tower test set-up at DAINESE S.p.A. as shown in Figure 8-11. Two different impactors were used to impact the samples: one was a spherical impactor with diameter of 30 mm and the other was a conical impactor with tip angle of 60° (see Figure 8-11). The tests were performed both on specimens made of SPECTRA and carbon fibres. All specimens were supported by an EPS foam cylinder with diameter of 90 mm, thickness of 40 mm and density of 30 kg/m^3 as shown in Figure 8-11. Since in reality, the outer shell and the energy absorbing liner of the helmet would be hit together, the foam support was used in order to replicate a realistic boundary condition for tests according to the impacts that may take place on a helmet.

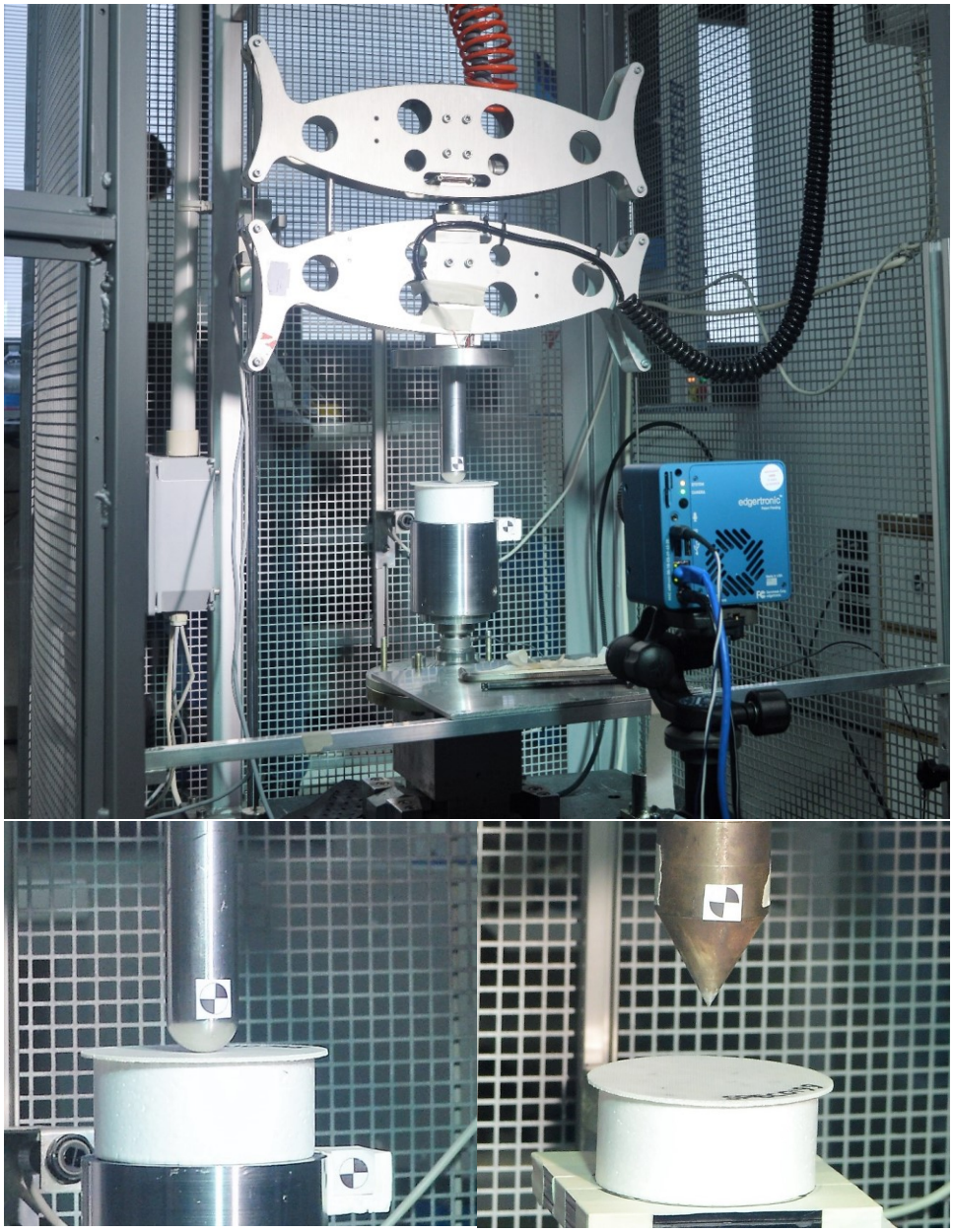

Figure 8-11 – Impact test set-up at Dainese S.p.A. (top), spherical impactor (bottom - left) and conical impactor (bottom - right).

8.2.4. Results

The results of the tensile tests are shown in Figure 8-12 and Figure 8-13. It is shown that the specimens made of carbon fibres were stiffer than SPECTRA and failed at higher forces but they failed at lower level of elongation. In case of using specimens with fibres along the longitudinal and transverse directions (see Figure 8-12), the specimens made of carbon failed at 24.4 kN which was 31% higher than the failure force of SPECTRA but the SPECTRA's elongation at failure was 4 mm which was 272% higher than carbon's elongation. Similar results obtained from the specimens with fibres oriented -45°/+45° with respect to loading direction. In this case, carbon fibre laminate failed at 3.47 kN which was 46% more than the failure force of SPECTRA

but SPECTRA's elongation at failure point was 6.49 mm that was 271% more than the elongation of specimens made of carbon fibres (Figure 8-13).

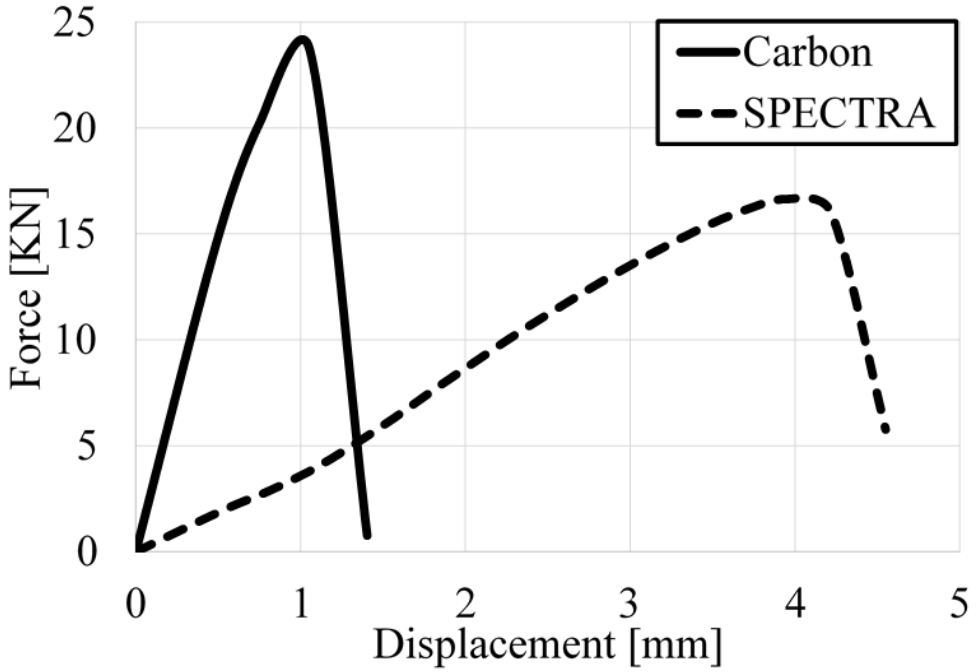

Figure 8-12 – Results of the tensile tests for specimens with fibres along longitudinal axis.

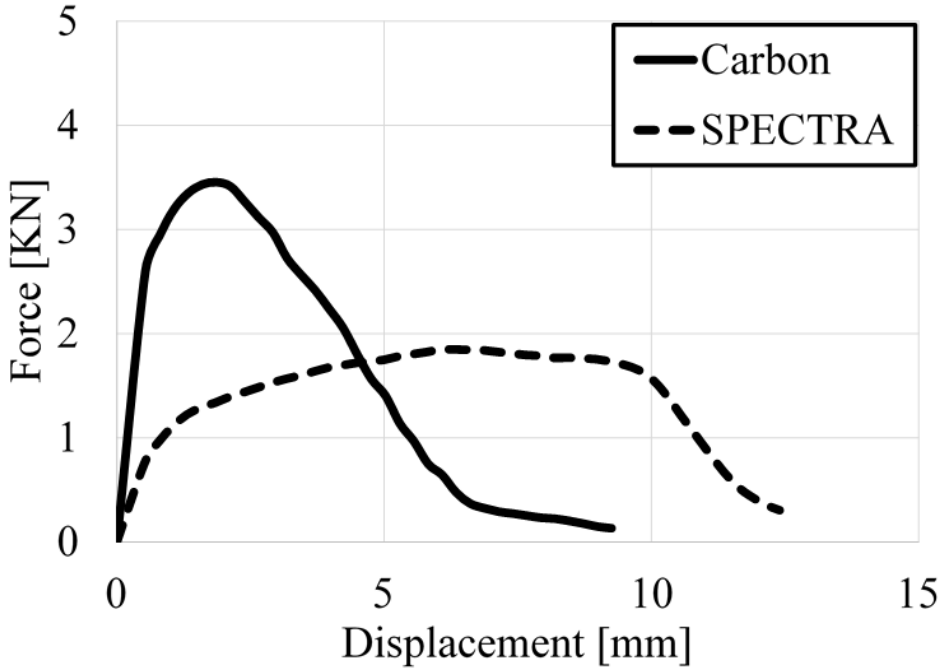

Figure 8-13 – Results of the tensile tests for specimens with fibres oriented 45° with respect to longitudinal axis.

Figure 8-14 and Figure 8-15 show the result of 3-point bending tests for (0/90) and (-45/+45) specimens, respectively. According to these results, the specimens made of SPECTRA were very

compliant in comparison with those made of carbon laminate and showed very low resistance under bending loading.

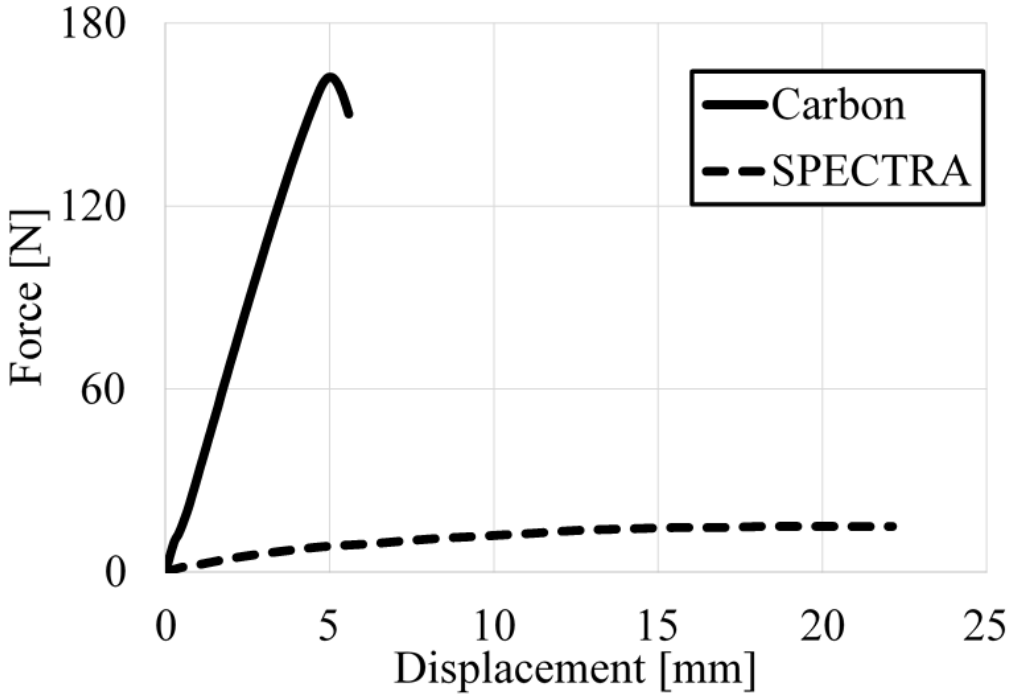

Figure 8-14 – Results of the three point bending tests for specimens with fibres along longitudinal axis.

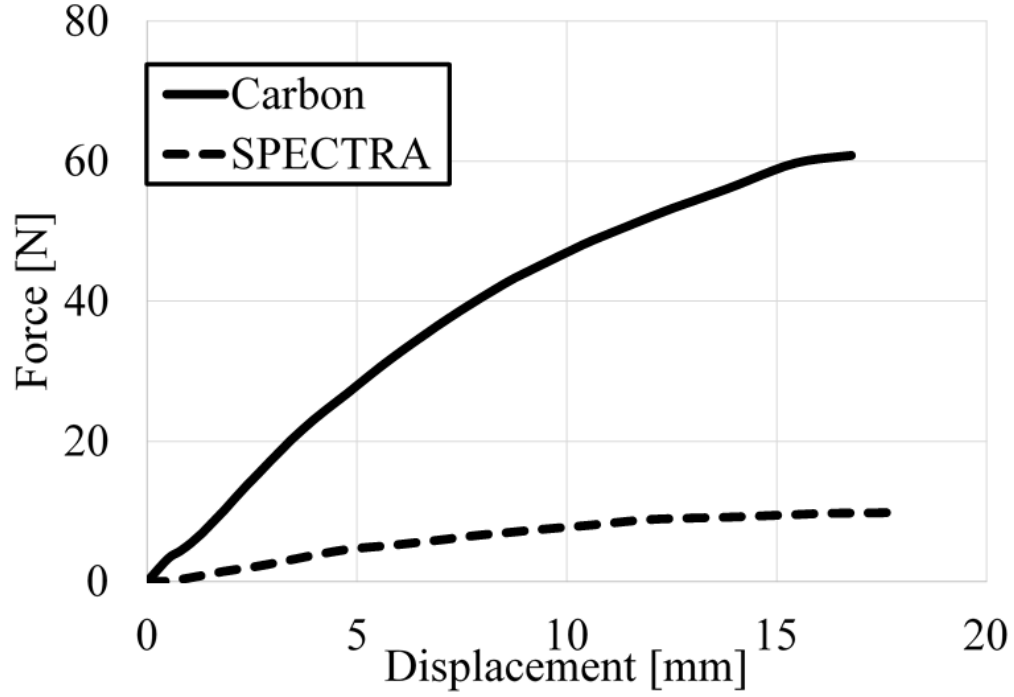

Figure 8-15 – Results of the three point bending tests for specimens with fibres oriented 45° with respect to longitudinal axis.

Results of impact tests for cases of using spherical and conical impactors are shown in Figure 8-16 and Figure 8-17, respectively. The transmitted acceleration to the anvil acquired in order to compare the capability of energy absorption of laminates made of carbon fibres and SPECTRA supported by EPS foam. The results of impact tests showed that the specimen made of SPECTRA transmitted a peak acceleration equal to 92 g which was 14.5% more than the peak acceleration transmitted by carbon laminate (Figure 8-16). On the contrary, in case of using conical impactor, a higher peak acceleration was transmitted by the laminate made of carbon fibres. The specimen made of carbon fibres transmitted a peak acceleration equal to 77 g that was 9% higher than what was transmitted by the laminate made of SPECTRA (Figure 8-17). Moreover, the size of the penetration in the laminate made of carbon (13.6 mm) was more than three times larger than the one in the laminate made of SPECTRA (3.9 mm), as shown in Figure 8-18. However, the laminate made of carbon fibres deformed more locally, whereas the laminate made of SPECTRA had a wider deformed area (Figure 8-19).

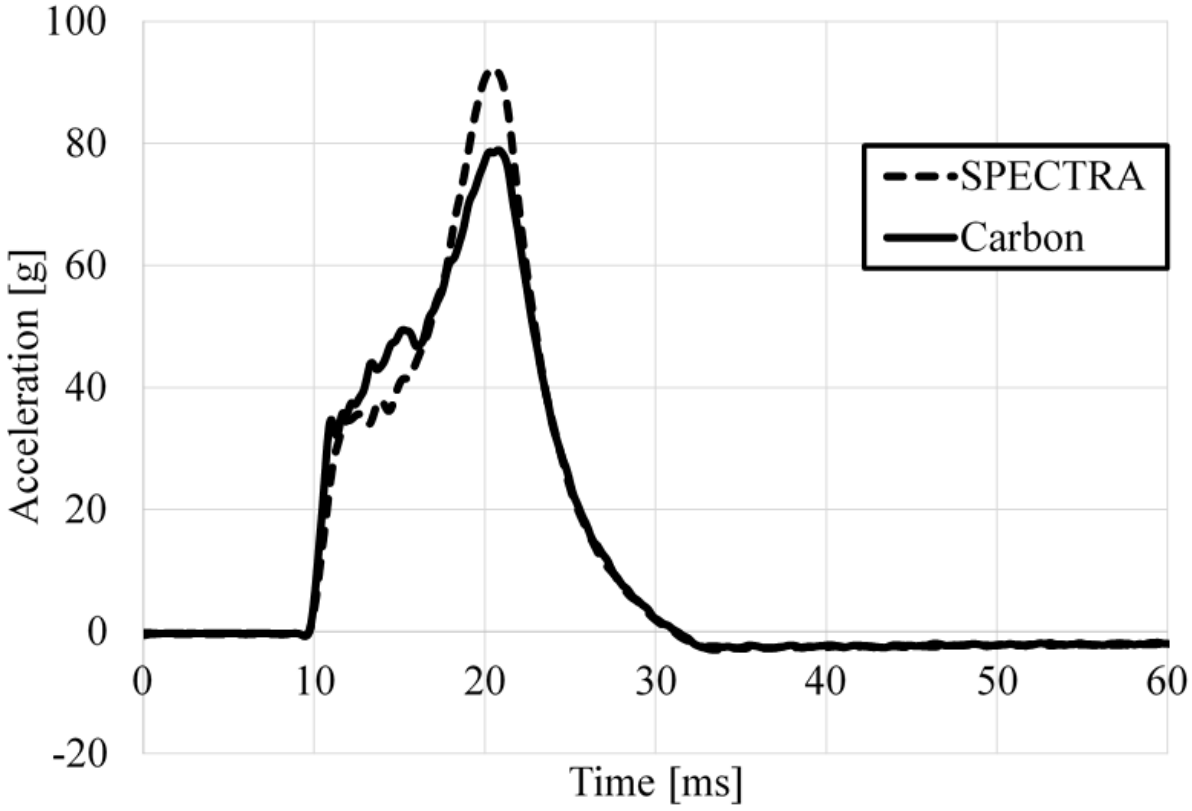

Figure 8-16 – Results of the impact test with spherical impactor.

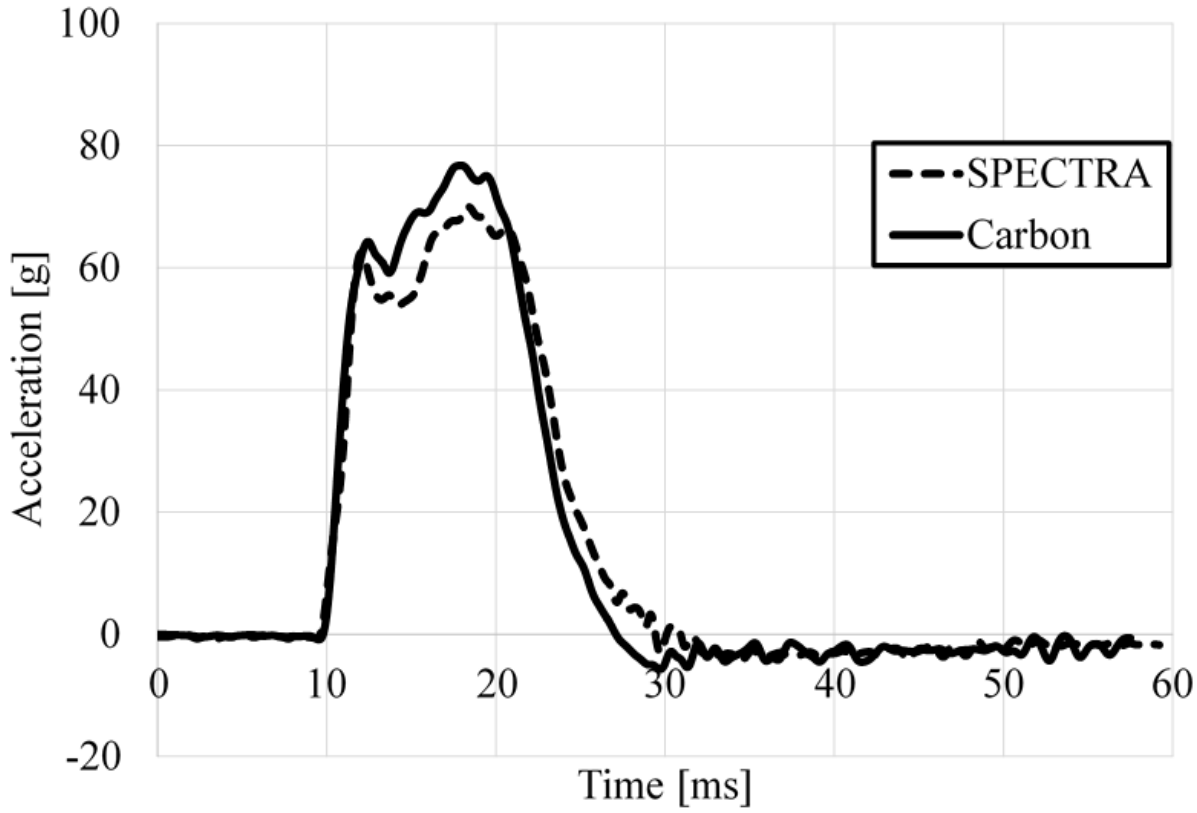

Figure 8-17 – Results of the impact test with conical impactor.

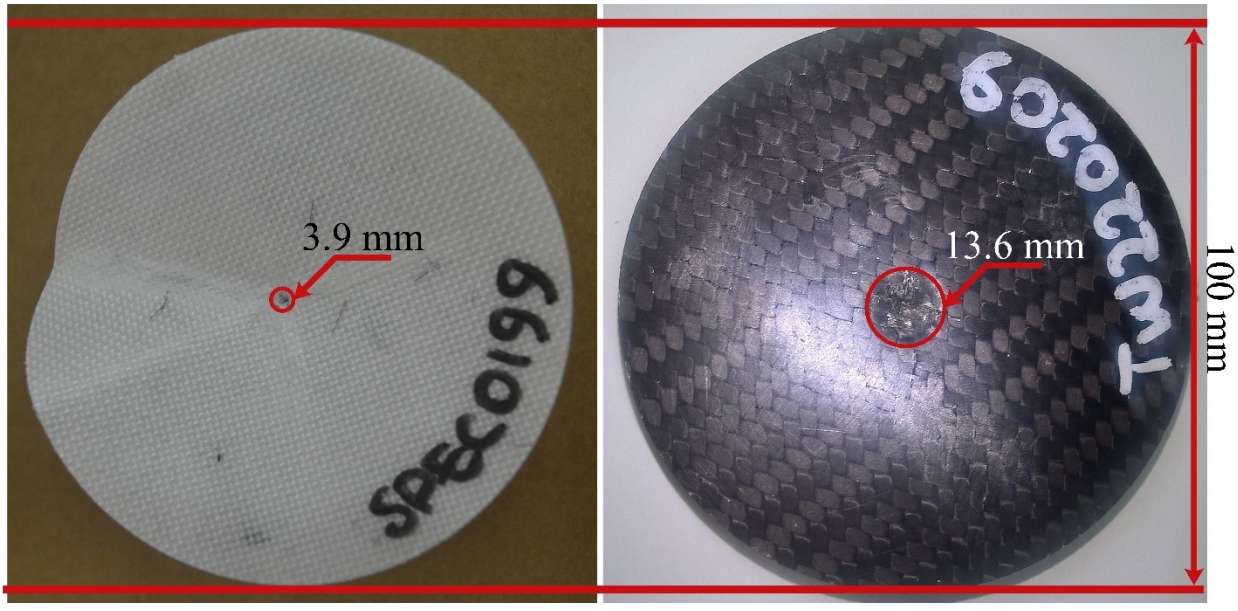

Figure 8-18 – Size of penetration in tested laminates made of SPECTRA (left) and carbon (right) using a conical impactor.

The results of this study show that laminates made of carbon fibres had higher strength against tensile and bending loading. Moreover, the result of impact tests showed that the laminates made

of carbon fibres transmitted lower force to the anvil, in case of using a spherical impactor. On the contrary, they transmitted higher force when a conical impactor was utilized. In general, carbon fibres, which are already used for manufacturing the outer shell of the helmet, showed a better mechanical response. However, SPECTRA showed also a fairly good mechanical response under impact loading. In addition, the mass of the SPECTRA fabric that has been used for this study is 240 gr/m^2 and the mass of the carbon fabric is 600 gr/m^2. Therefore, according to the result of the present work molding a hybrid laminate made of carbon fibres and SPECTRA fabric may provide an optimized compromise in order to minimize the mass of the outer shell and maximize the capability of energy dissipation of the outer shell of the helmets.

8.3. Lattice structures as the helmet liner

Researchers showed that energy absorption capacity of pad liners could be designed by using functionally graded foams [135] and helmets' protection capability could be optimized by means of such materials, however, manufacturing such materials is not straightforward [16]. It is known that the EPS foams, which are currently used as the helmet's liner, crush almost at a constant stress (see chapter 5.2.1.1). According to this, a simplified analytical formulation has been derived in order to predict the induced load at the center of gravity of a helmeted headform as shown in Figure 8-19 as follows [208]:

$$F_i = 2\pi\sigma_y\sqrt{R_{i1}R_{i2}}u_i \qquad \text{Eq. 8–1}$$

in which R_{i1} and R_{i2} are equivalent curvature of the contact between the head and the foam liner along and across the impacted object axis, σ_y is the yeild stress (or platue region's stress) of the foam and u_i is the foam's intentention. This analytical model shows that by increasing the foam's indentation the trasmitted force to the headform increases. Moreover, it shows that by using a material with varying yield stress the transmitted force might be optimized. Therefore, in this chapter, the use of a liner with a varying yield stress has been assessed in order to reduce the risk of head injuries. Here the feasiblity of using a hierarchical lattice structure as a helmet liner has been studied.

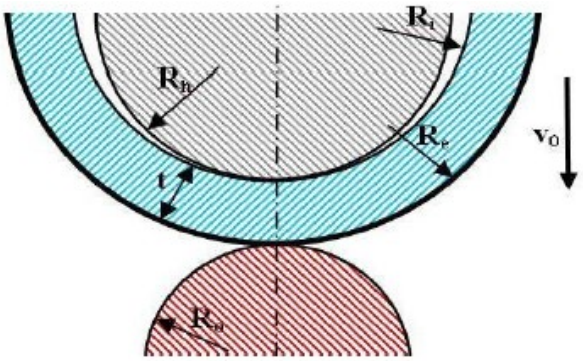

Figure 8-19 – Unidimensional helmet model with head (grey), foam liner (cyan) and impacted object (red) [208].

8.3.1. Method

The finite element model of the concept helmet which was described in Chapter 6.7 was put on the headform as shown in Figure 8-20 and lunched towards an inclined rigid anvil with

inclination of 45° at speed of 7.5 m/s. This oblique impact condition was adopted in order to induce linear and rotational acceleration simultaneously [102]. Similar impact was simulated using the helmet model which was described in Chapter 6.8 in order to compare the capability of EPS and the lattice structure in reduction of the risk of head injuries. These simulations were carried out in order to calculate the induced linear and rotational acceleration at the center of gravity of the headform and Head Injury Criterion (HIC).

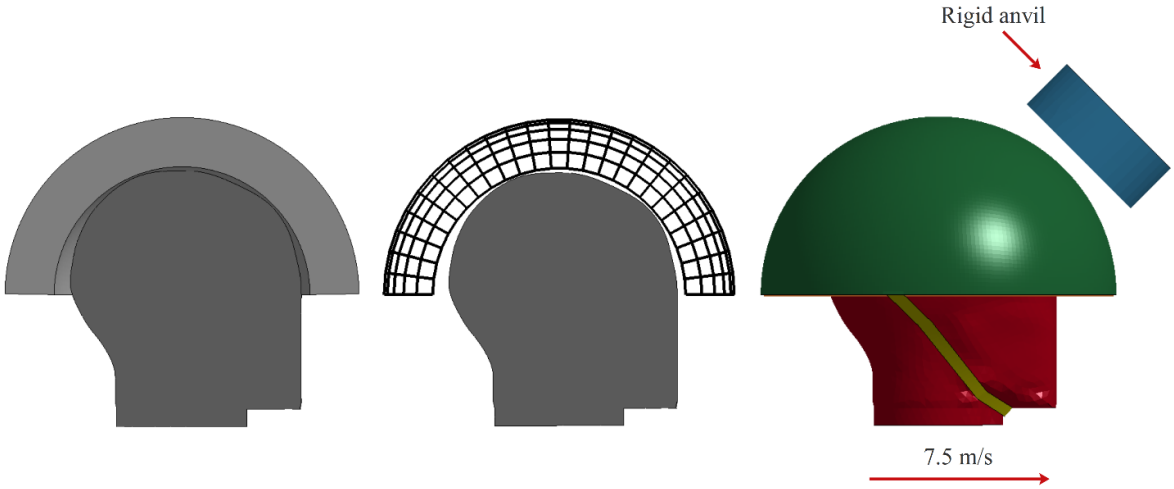

Figure 8-20 – Section view of the headfrom and EPS liner (left), Section view of the headfrom and the lattice liner (middle) and impact condition for assessment of the concept helmet (right).

Moreover, as an exercise which would provide very useful information in case the brain model of THUMS had been fully validated, other simulations were carried out using THUMS model. In these simulations, the helmeted human body model was lunched towards a rigid wall as shown in Figure 8-21. The same impact condition was considered using a helmet with EPS liner in order to compare the stress field of the brain for two different helmets with EPS and hierarchical lattice structure liners. The impact velocity and configuration were adopted from a recent proposal for motorcycle's helmet standard [102].

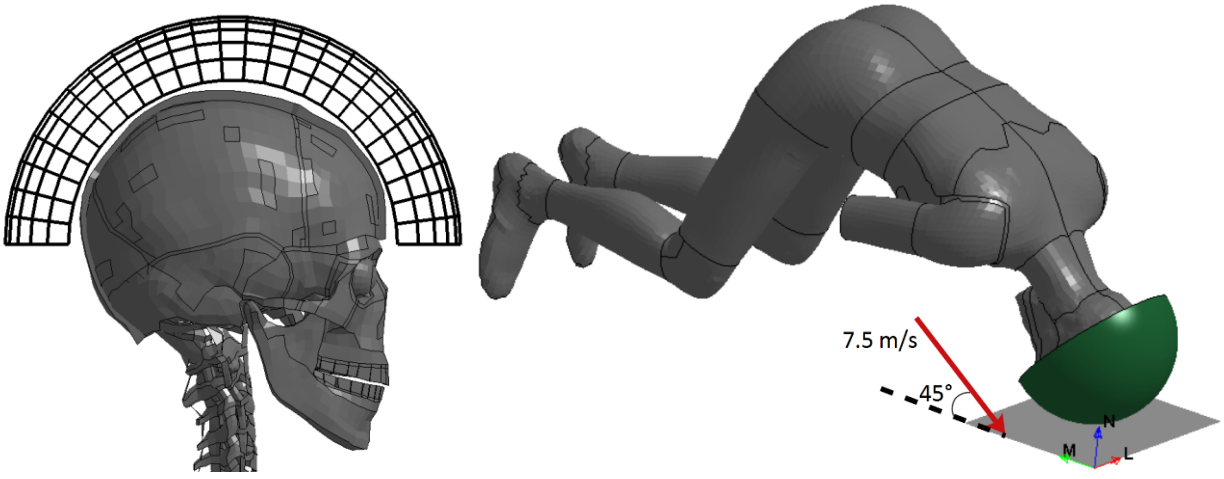

Figure 8-21 – Left: Section view of the lattice liner on THUMS. Right: Impact condition of the helmeted THUMS (some parts of the model are not shown).

8.3.2. Results and discussion

Figure 8-22 and 23 show the deformation of the helmet's liner in case of using EPS and hierarchical lattice structure, respectively. The results showed that both liners would crush and deform plastically however, their failure mechanisms were different as discussed in Chapter 5.

The resultant linear acceleration, which was induced to the headform's center of gravity due to the impact, is shown in Figure 8-24. It is shown that the Peak Linear Acceleration (PLA) was reduced by almost 50% and the duration of the peak acceleration was increased when the hierarchical lattice structure was used instead of the foam liner. Moreover, rotational acceleration of the headform's around the coronal axis[1] was reduced by 52% as shown in Figure 8-25 and its duration was increased in the case of using the hierarchical lattice liner. Head Injury Criterion (HIC) has been calculated for both cases and is shown in Table 8-1. HIC was decreased by 42% while the lattice liner was used.

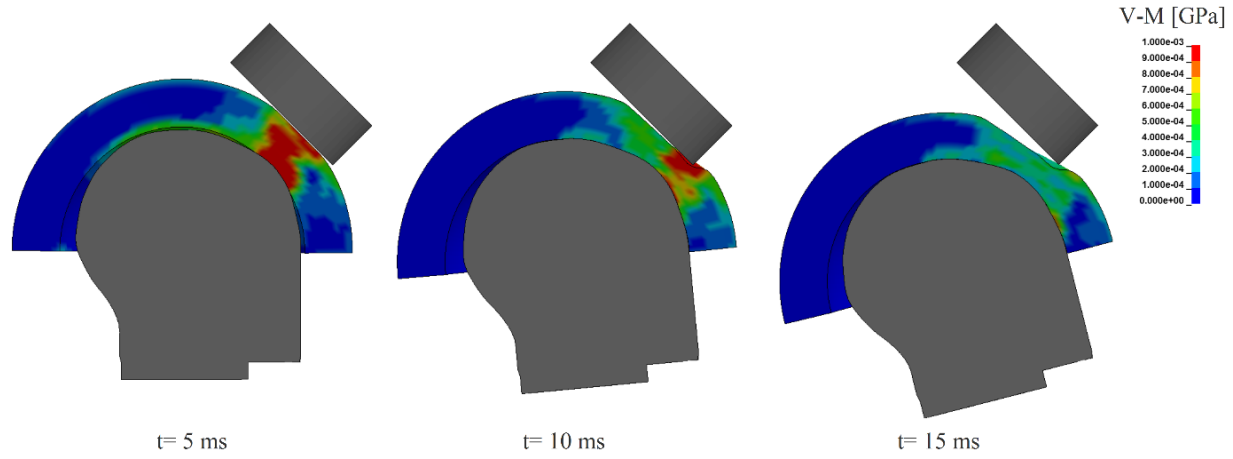

Figure 8-22 – Stress distribution of EPS liner during the impact (some parts are not shown).

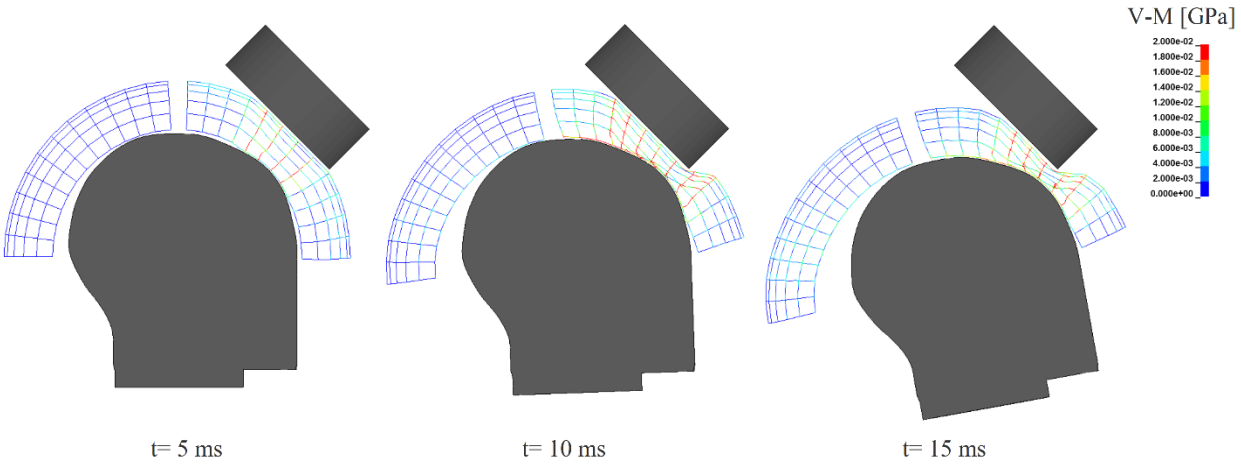

Figure 8-23 – Stress distribution of lattice liner during the impact (some parts are not shown).

[1] Coronal axis is the one which is perpendicular to the sagittal plane.

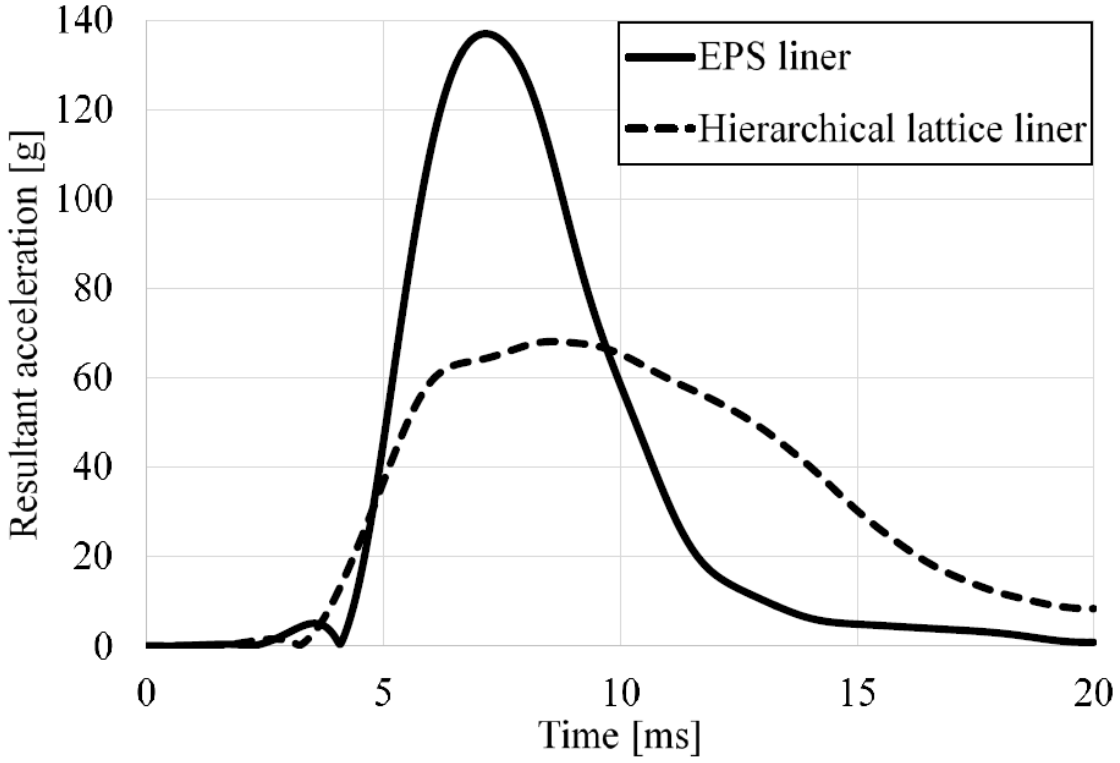

Figure 8-24 – Resultant linear acceleration of the headform's center of gravity.

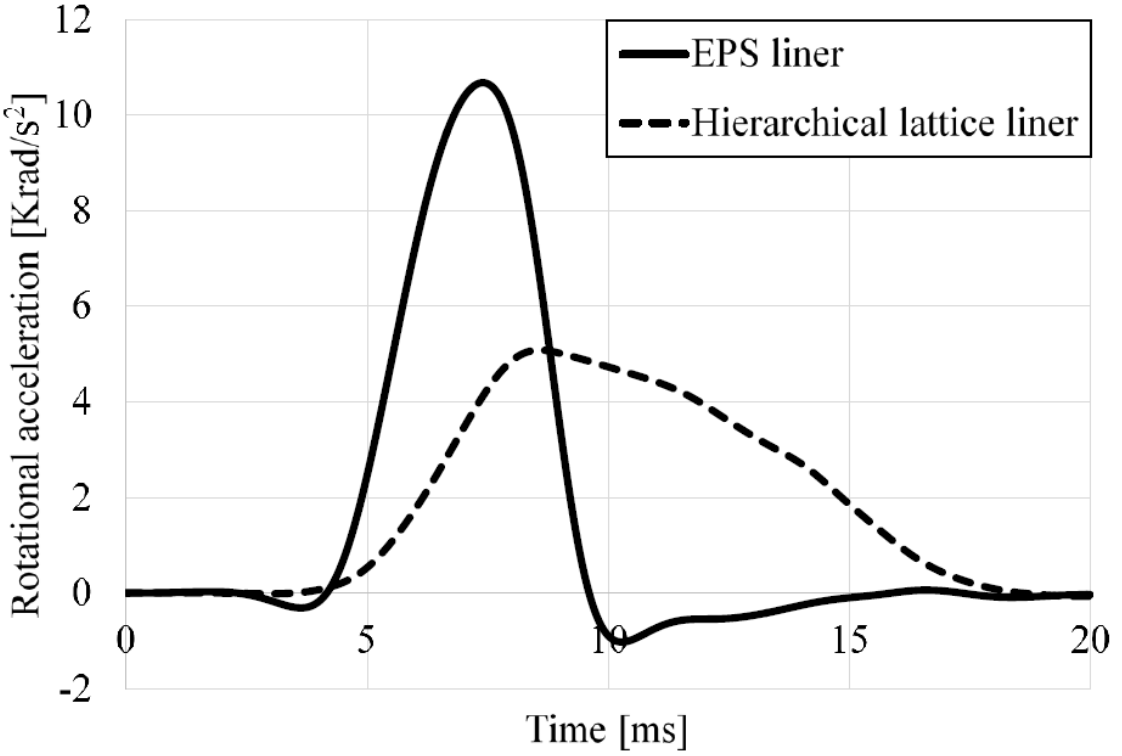

Figure 8-25 – Rotational acceleration of the headform's center of gravity around coronal axis.

Table 8-1 Comparing EPS and lattice liner for oblique impact using the headform.

Model	HIC	PLA [g]	Max. Rot. Acceleration [krad/s^2]
Helmet with EPS liner	603	137	10.7
Helmet with hierarchical lattice liner	347	68	5.1

Finite element simulations were carried out using THUMS as well. Using such a model provides the ability of comparing the stress and strain field of the brain for different cases. Bain et. al. [63], Newman et. al. [61] and Kang et. al. [62] used the strain, Von-Mises stress and shear stress of the brain, respectively, as an indicator for assessing the risk of brain injury. Therefore, these quantities have been compared for cases of using EPS and lattice liner, in order to realize the effect of using a hierarchical lattice as the helmet liner on risk of brain injury.

Figure 8-26 shows the changes of the brain's effective strain during the impact which has been described in Chapter 8.3.1. It is shown that using the lattice liner could reduce the strain in the brain during the impact at different points of the section which is shown in this figure. Moreover, Figure 8-27 and Figure 8-28 show that both effective stress and maximum shear stress of cerebrum, cerebellum and brainstem were reduced in case of using the lattice liner.

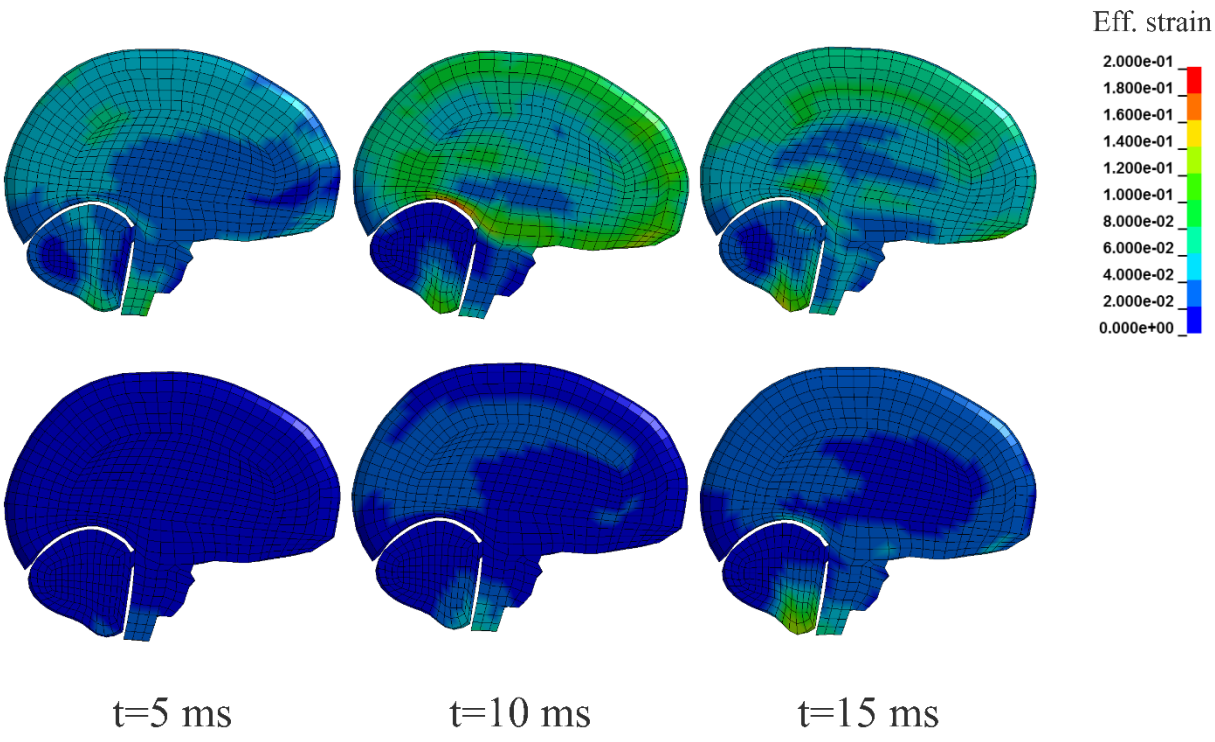

Figure 8-26 – Section view of brain's effective strain (the top row is for the helmet with EPS liner and the bottom row is for the helmet with hierarchical lattice liner).

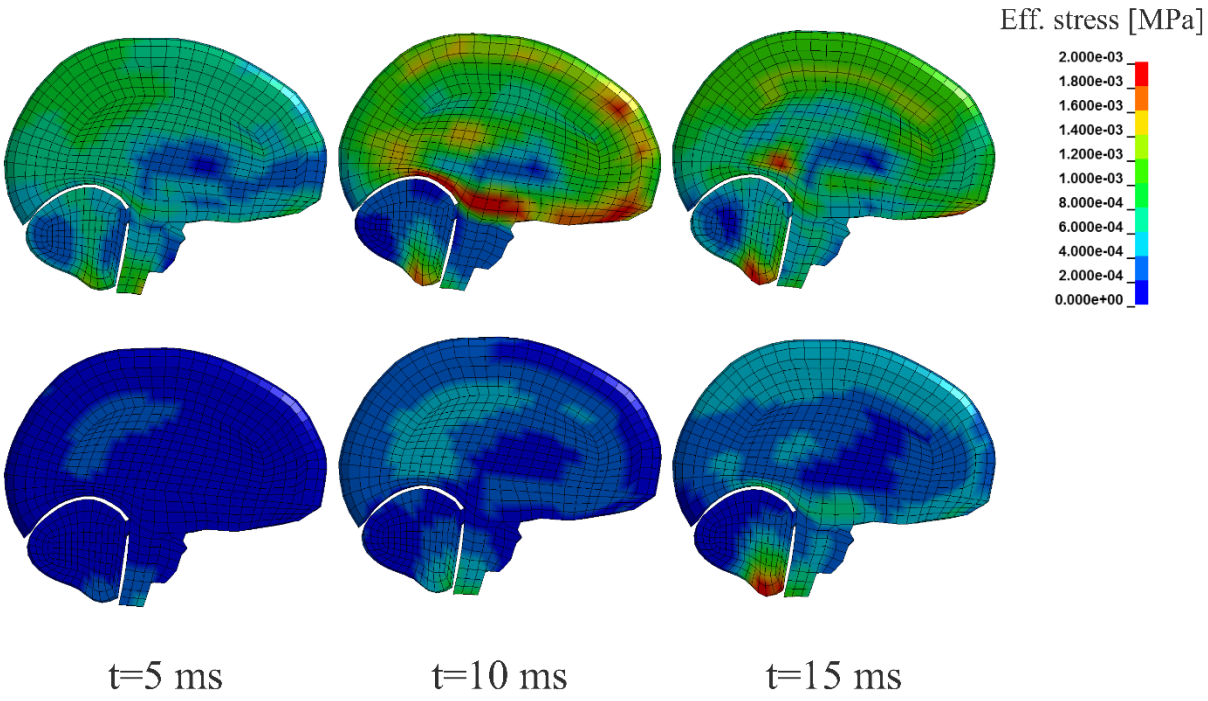

Figure 8-27 – Section view of brain's effective stress (the top row is for the helmet with EPS liner and the bottom row is for the helmet with hierarchical lattice liner).

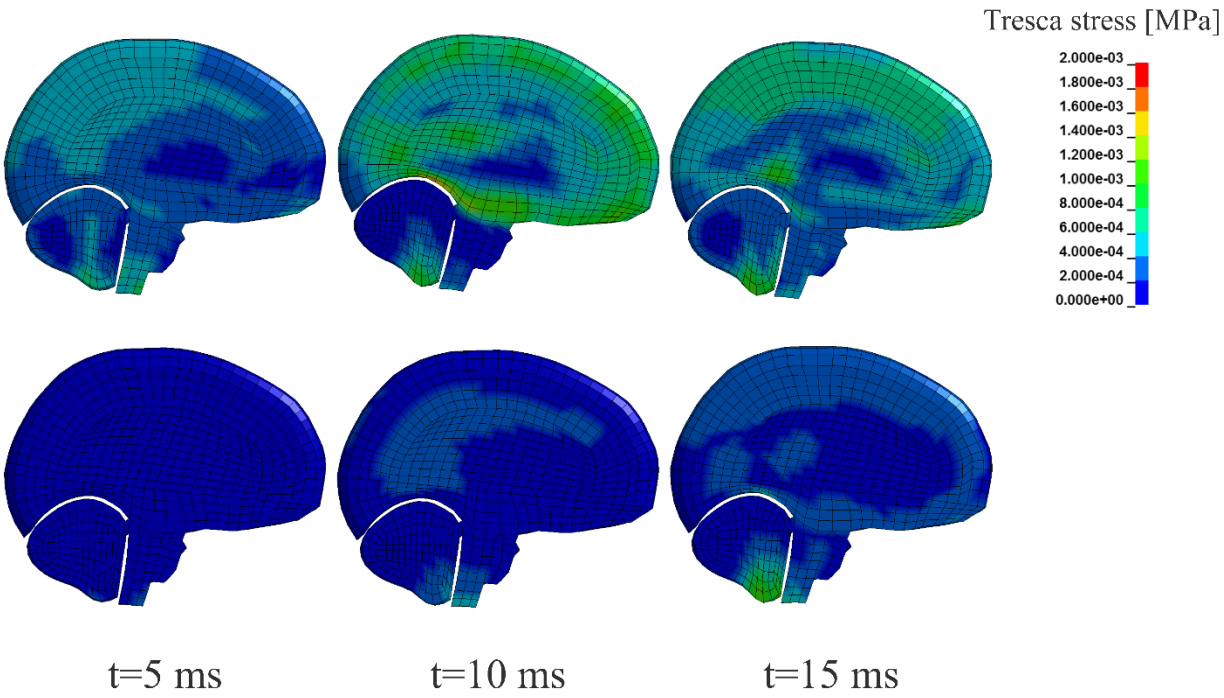

Figure 8-28 – Section view of brain's maximum shear stress (the top row is for the helmet with EPS liner and the bottom row is for the helmet with hierarchical lattice liner).

Di Landro et. al. [15] concluded that using functionally graded materials could be an alternative for optimization of helmet's liner in order to increase the energy absorption. In another experimental study, Gupta [209] showed that a functionally graded structure could increase the energy absorption up to 500% comparing to a structure with uniform material properties through the thickness. Moreover, Cui et. al. [16] showed that the protection capability of helmets could be improved by means of using liners with varying mechanical properties through the thickness. These studies were dedicated to functionally graded foams while manufacturing helmet liners made of such foams is still in concept phase [16]. However, thanks to the advances in field of additive manufacturing, complex lattice structures can be manufactured nowadays. Therefore, here the feasibility of using a hierarchical lattice structure has been studied in order to realize how such a structure could be used in order to improve the energy absorption capability and protection level of the helmets. A hierarchical lattice structure has varying cell sizes at different rows as shown in Figure 6-11 and each cell size provides particular mechanical properties, therefore, the entire structure has varying mechanical properties through the thickness. As it is shown in Figure 8-29 a material like EPS crushes uniformly through thickness unlikely, a lattice structure with varying mechanical properties through the thickness starts to crush from the weakest layer and all layers would crush one after the other from the weakest layer to the strongest one. Such a structure provides a varying yield stress (σ_y) through the thickness, therefore a helmet's liner with such a mechanical properties would reduce the transmitted force to the head center of gravity according to Eq. 8.1.

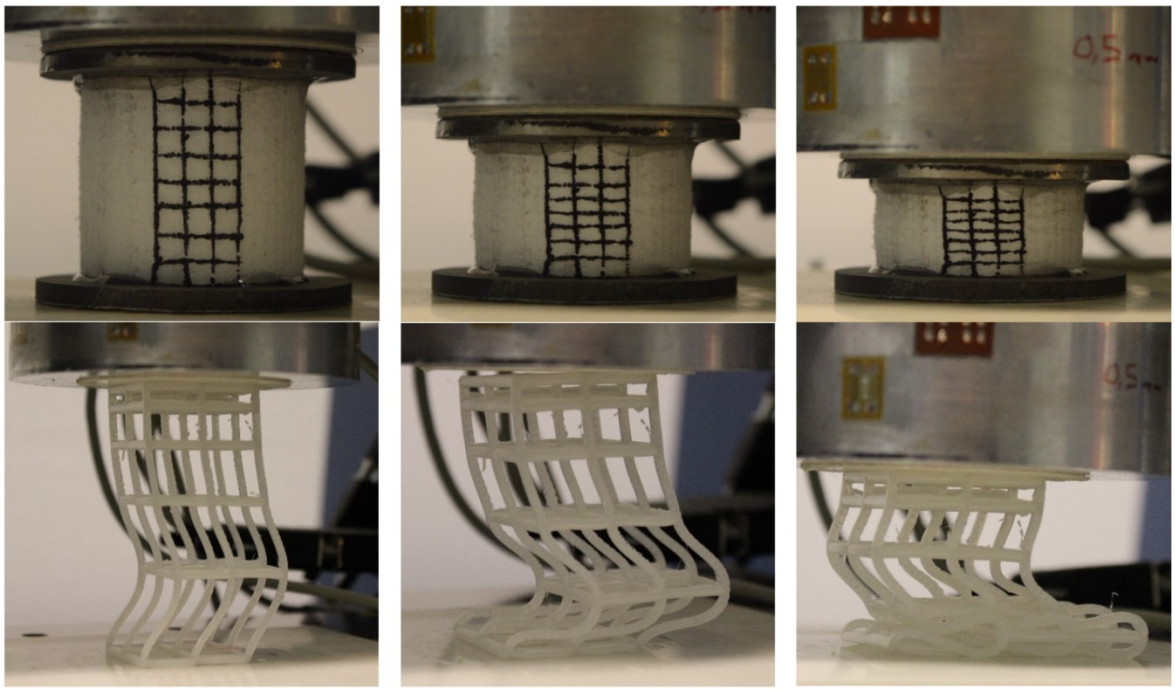

Figure 8-29 – Difference in crushing of uniform material (top row) and a hierarchical lattice structure (bottom row) [compression is increasing from left to right]; EPS crushes uniformly through thickness unlikely, the lattice structure starts to crush from the weakest layer and all layers would crush one after the other from the weakest layer to the strongest one.

9. Summary and Conclusions

9.1. Biaxial behavior of EPS

The results of the tests showed that the response of EPS under shearing loading is a function of compression level. Similar conclusion was presented for other types of foams however the results were not presented explicitly in terms of shear stress and shear strain. Moreover, the increase of shear stiffness by increasing the normal stress should be included in simulation of helmeted headforms (head) in case of oblique impacts in order to provide a realistic evaluation of helmets.

9.2. Assessment of the neck brace

We studied the response of the cervical spine in case of using neck protective devices and compared the results with the case in which the neck brace was not used. We carried out a finite element analysis using validated FE models of the helmet, the neck protective device and the human body model. The simulations were carried out for four common types of load cases in motorcycle accidents. The simulations were performed for cases with and without the neck protective device in order to realize the effect of using such a device on the neck's response. The results show that using such devices may increase the stress level at cervical spine and consequently can increase the risk of neck injury. The results show that design of such devices requires better understanding of mechanisms of neck injury mitigation.

9.3. Composite laminate optimization

We presented possible improvements in chin bar design procedures. We used a computational approach to optimize the ply orientation of a composite chin bar to reduce the neck force, a parameter linked to basilar skull fracture in real accidents, while satisfying the requirements of the ECE22.05 standard. The optimal chin bar ply configuration reduced the neck axial force by 30% compared to the chin bar configuration that led to the maximum neck axial force, with the key protection mechanism being more energy absorption due to larger damage distributed within the plies of the chin bar laminate, while still satisfying the standard requirements. Our results show that the design of helmets can be improved to protect motorcyclists against different types of head injuries, without compromising their capability to meet current requirements of standards. This can be achieved by adopting computational approaches to provide the possibility of including different biomechanical criteria in the design process and reducing the design cost by decreasing the number of experimental iterations. This approach can be adopted by helmet manufacturers to improve their products, while they are waiting for new helmet testing standards.

9.4. Spectra

Three different types of tests were carried out in order to compare the mechanical properties of carbon fibre laminates which are already used for molding outer shell of the motorcyclist's helmets and laminates made of SPECTRA. The specific weight of SPECTRA is less than half of the carbon. SPECTRA can deform plastically while carbon specimens showed brittle failure.

Specimens made of carbon fibres showed higher mechanical resistance against quasi-static tensile and bending loading. However, in case of impact testing the response of the specimens were similar. Since SPECTRA is much lighter than carbon, molding a hybrid laminate using both carbon fibre and SPECTRA fabric may provide and optimized laminate considering the mass and the stiffness.

9.5. Lattice structures as the helmet liner

The feasibility of using a hierarchical lattice liner for helmets were assessed by means of FEM. The results showed that a hierarchical lattice structure could reduce the peak linear acceleration, HIC and maxim rotational acceleration of the helmeted headform in comparison with the liner made of EPS which had the same mass of the hierarchical lattice liner. Moreover, THUMS model was used to compare the risk of brain injuries in case of an oblique impacts for the helmets with a hierarchical lattice and EPS liner according to three different biomechanical criteria which have been introduced in order to assess the risk of brain injuries i.e. effective strain, effective stress and maximum shearing stress. The results showed that using hierarchical lattice liner could reduce the mentioned parameters in the brain. Moreover, according to the advances in field of additive manufacturing, printing lattice structures with varying cell sizes thought the thickness might be used for mass production in the near future and such structures could be used instead of conventional foams in personal protective equipment.

9.6. Future works

Biaxial behavior of EPS

The presented empirical data about biaxial behavior of EPS are proposed to be used for FE analysis of helmet oblique impacts to consider the shear hardening for EPS foams. There are few constitutive material models which could be used for including shear hardening of crushable foams in commercially available FE packages, however they may need some modifications in order to represent the foam material more accurately. Therefore, the next step of this part of the work would be including the presented results in FE simulation of helmet oblique impacts.

Assessment of the neck brace

Currently available neck protective devices for motorcycle riders have been developed to restrict the movement of the head/neck assembly. The result of the present study show that limiting the movement of the head/neck assembly may increase the risk of cervical injuries in some load cases. Therefore, design of such devices requires better understanding of mechanisms of neck injury mitigation. Thus, further researches on mechanisms of cervical injury mitigation toward development of a standard for neck protective devices would be the next step of this aspect of the work.

Composite laminate optimization

The computational method adopted here could successfully include the induced neck axial load due to the facial impacts in design of the helmets. This approach could be used for further researches to include more biomechanical criteria in the design of helmets which are not clearly

addressed in the standards. Moreover, developing an experimental set-up to test and compare different geometries of helmets' chin bar could be the next step, as well. Moreover, according to the idea and the results presented in chapter 8.1, a research proposal with cooperation of Dainese S.p.A. and Imperial College London was funded by the Veneto region to develop an experimental set-up to evaluate the effect of different chin bars on the induced neck load due to the facial impacts.

SPECTRA

This material could be used to reduce the total mass of helmets, however the results of this work showed that pure SPECTRA may not be the best option for molding helmets' outer shell laminates. Therefore, the future work will be developing a hybrid laminate using SPECTRA and carbon fibers to find the optimized laminate for the helmets with respect to total mass and stiffness.

Lattice structures as the helmet liner

The feasibility of using a simple hierarchical lattice structure has been studied in the present work and the results show that using such structures can improve the protection level of the helmets. Even though, using a hierarchical structure could reduce the risk of head injuries the design of the lattice can be optimized further. Therefore, the next step of this work will be the optimization of the lattice structure to minimize the risk of head injuries and the investigation of the best manufacturing procedure.

10. References

[1] M. Koornstra, J. Broughton, R. Esberger, C. Glansdrop, W. Koppel, F. Taylor, J.-P. Cauzard, A. Evans, L. Hantula, M. Piers, W. Vanlaar, Transport safety performance in the EU - A statistical overview, Brussels, 2003.

[2] M. Peden, R. Scurfield, D. Sleet, D. Mohan, A. A. Hyder, E. Jarawan, C. Mathers, World report on road traffic injury prevention, Geneva, n.d.

[3] M.-R. Lin, J.F. Kraus, Methodological issues in motorcycle injury epidemiology., Accid. Anal. Prev. 40 (2008) 1653–60.

[4] F.A.O. Fernandes, R.J. Alves de Sousa, Motorcycle helmets—A state of the art review, Accid. Anal. Prev. 56 (2013) 1–21.

[5] R. Miralbes, Design of motorcycle rider protection systems using numerical techniques, Accid. Anal. Prev. 59 (2013) 94–108.

[6] M. Ghajari, U. Galvanetto, L. Iannucci, R. Willinger, Influence of the body on the response of the helmeted head during impact, Int. J. Crashworthiness. 16 (2011) 285–295.

[7] M. Ghajari, S. Peldschus, U. Galvanetto, L. Iannucci, Effects of the presence of the body in helmet oblique impacts., Accid. Anal. Prev. 50 (2013) 263–71.

[8] A. Cernicchi, U. Galvanetto, L. Iannucci, Virtual modelling of safety helmets: practical problems, Int. J. Crashworthiness. 13 (2008) 451–467.

[9] S.S. Ooi, S. V Wong, R.S. Radin Umar, A.A. Azhar, M.M.H.M. Ahmad, Cervical spine injuries sustained by motorcyclists in road crashes in Malaysia, Int. J. Crashworthiness. 10 (2005) 295–303.

[10] B. Dowdell, G.J. Long, J. Ward, M. Griffiths, A Study of helmet damage and rider head/neck injuries for crash involved motorcyclists, Roads and Traffic Authority, Road Safety Bureau, New South Wales Australia, 1988.

[11] T. Whyte, T. Gibson, R. Anderson, D. Eager, B. Milthorpe, Mechanisms of head and neck injuries sustained by helmeted motorcyclists in fatal real-world crashes: Analysis of 47 in-depth cases., J. Neurotrauma. (2016).

[12] S. Piantini, M. Pierini, M. Delogu, N. Baldanzini, A. Franci, M. Mangini, A. Peris, Injury Analysis of Powered Two-Wheeler versus Other-Vehicle Urban Accidents, in: IRCOBI Conf., Malaga, Spain, 2016.

[13] C.P. Chee, A. Ali, Basal skull fractures. A prospective study of 100 consecutive admissions., Aust. N. Z. J. Surg. 61 (1991) 597–602.

[14] J.H. McElhaney, R.H. Hopper, R.W. Nightingale, B.S. Myers, Mechanisms of basilar skull fracture., J. Neurotrauma. 12 (1995) 669–78.

[15] L. Di Landro, G. Sala, D. Olivieri, Deformation mechanisms and energy absorption of polystyrene foams for protective helmets, Polym. Test. 21 (2002) 217–228.

[16] L. Cui, M.A. Forero Rueda, M.D. Gilchrist, Optimisation of energy absorbing liner for equestrian helmets. Part II: Functionally graded foam liner, Mater. Des. 30 (2009) 3414–3419.

[17] C. Brandstaetter, G. Yannis, P. Evgenikos, E. Argyropoulou, P. Papantoniou, M. Reurings, M. Vis, J. Broughton, J. Knowles, J.-F. Pace, E. López-de-Cozar, P. Pérez-Fuster, J. Sanmartín, M. Haddak, Annual Statistical Report, Deliverable D3.9 of the EC FP7 project DaCoTA, 2012.

[18] G.D. Caserta, L. Iannucci, U. Galvanetto, Shock absorption performance of a motorbike helmet with honeycomb reinforced liner, Compos. Struct. 93 (2011) 2748–2759.

[19] R.M. Coelho, R.J. Alves de Sousa, F.A.O. Fernandes, F. Teixeira-Dias, New composite liners for energy absorption purposes, Mater. Des. 43 (2013) 384–392.

[20] N. Bogduk, S. Mercer, Biomechanics of the cervical spine. I: Normal kinematics, Clin. Biomech. 15 (2000) 633–648.

[21] H. Chen, L. Zhang, Z. Wang, K.H. Yang, a I. King, Biomechanics of the neck, Theor. Biomech. (2011) 386–402.

[22] A.T. Dibb, R.W. Nightingale, J.F. Luck, V.C. Chancey, L.E. Fronheiser, B.S. Myers, Tension and combined tension-extension structural response and tolerance properties of the human male ligamentous cervical spine, J. Biomech. Eng. 131 (2009) 81008.

[23] P.C. Ivancic, Neck injury response to direct head impact, Accid. Anal. Prev. 50 (2013) 323–329.

[24] G. Schippinger, E. Spork, A. Obernosterer, F.J. Seibert, F. Schweighofer, Injury of the cervical spine associated with carotid and vertebral artery occlusion: case report and literature review, Injury. 28 (1997) 315–318.

[25] D.C. Viano, C.S. Parenteau, Analysis of head impacts causing neck compression injury, Traffic Inj. Prev. 9 (2008) 144–152.

[26] H.F. Yeh, C.J. Seak, T.F. Chiu, Y.C. Chang, Traumatic vertebral artery dissection and Wallenberg syndrome after a motorcycle collision, Am. J. Emerg. Med. 27 (2009) 3–5.

[27] E.M. Yliniemi, J. a Pellettiere, E.J. Doczy, D.J. Nuckley, C.E. Perry, R.P. Ching, Dynamic tensile failure mechanics of the musculoskeletal neck using a cadaver model., J. Biomech. Eng. 131 (2009) 51001.

[28] M. Ghajari, The Influence of the Body on the Response of the Helmeted Head during Impact, Imperial College London, 2011.

[29] K.-U. Schmitt, P.F. Niederer, D.S. Cronin, M.H. Muser, F. Walz, Trauma biomechanics : an introduction to injury biomechanics, Forth, Springer, 2014.

[30] Pearson education, 2009. http://www.pearsoned.com.

[31] www.compelvisuals.com.

[32] A.M.R. Agur, A.F. Dalley, Grant's atlas of anatomy, Wolters Kluwer, 2017.

[33] L.B. Rawling, The Surgery of the Skull and Brain, Oxford Medical Publication, London, 1912.

[34] T.J. Gibson, K. Thai, Helmet protection against basilar skull fracture, ATSB research and analysis report, research grant report 2007-03, Canberra, 2007.

[35] A.A. Wani, A.U. Ramzan, T. Raina, N.K. Malik, F.A. Nizami, A. Qayoom, G. Singh, Skull base fractures: An institutional experience with review of literature, Indian J. Neurotrauma. 10 (2013) 120–126.

[36] F.H. Harvey, A.M. Jones, "Typical" basal skull fracture of both petrous bones: an unreliable indicator of head impact site., J. Forensic Sci. 25 (1980) 280–6.

[37] R.D. Cooter, D.J. David, Motorcyclist craniofacial injury patterns, in: Proc. Int. Mot. Saf. Conf., Orlando, 1990.

[38] L.E. Thibault, T.A. Gennarelli, Biomechanics and Craniocerebral Trauma, Central Nervous System Trauma Research Status Report, Bethesda, 1985.

[39] M.J. Shkrum, D.A. Ramsay, Forensic Pathology of Trauma, Humana Press, 2007.

[40] C.M. Shaw, E.C. Alvord, Injury of the basilar artery associated with closed head trauma., J. Neurol. Neurosurg. Psychiatry. 35 (1972) 247–57.

[41] S. Sprogøe-Jakobsen, E. Falk, Fatal thrombosis of the basilar artery due to a minor head injury., Forensic Sci. Int. 45 (1990) 239–45.

[42] E. Shaqiri, G. Vyshka, A. Sinamati, B. Ymaj, Z. Ismaili, Fatal basilar thrombosis possibly related to minor cervical trauma: a case report., Case Rep. Med. 2010 (2010).

[43] www.kramestudios.com.

[44] A.M. Nahum, J.W. Melvin, Accidental Injury : Biomechanics and Prevention, Springer New York, 2002.

[45] E.R. LeCOUNT, J. HOCKZEMA, SYMMETRICAL TRAUMATIC FRACTURES OF THE CRANIUM; SYMMETRICAL FRAGMENTATION, Arch. Surg. 29 (1934) 171.

[46] B.M. VANCE, E.R.. and A.C.W. LeCount, C.W. Apfelbach, FRACTURES OF THE SKULL, Arch. Surg. 14 (1927) 1023.

[47] A.R. Moritz, The pathology of trauma, Henry Kimpton, London, 1954.

[48] S. WERNE, Studies in spontaneous atlas dislocation., Acta Orthop. Scand. Suppl. 23 (1957) 1–150.

[49] Gadd, C. W., CRITERIA FOR INJURY POTENTIAL, in: Impact Accel. Stress Symp. Natl. Acad. Sci., National Research Council, Washington, 1961: pp. 141–144.

[50] J. Versace, A Review of the Severity Index, in: 1971.

[51] T.J. Horgan, A finite element model of the human head for use in the study of pedestrian accidents, University College Dublin, 2005.

[52] T.A. Gennarelli, Head injury in man and experimental animals: clinical aspects., Acta Neurochir. Suppl. (Wien). 32 (1983) 1–13.

[53] K. Ueno, J.W. Melvin, Finite element model study of head impact based on Hybrid III head acceleration: the effects of rotational and translational acceleration., J. Biomech. Eng. 117 (1995) 319–28.

[54] S.S. Margulies, L.E. Thibault, A proposed tolerance criterion for diffuse axonal injury in man, J. Biomech. 25 (1992) 917–923.

[55] J.A. Newman, A geheralized acceleration model for brain injury threshold (GAMBIT), in: IRCOBI, 1986: pp. 121–131.

[56] F. Kramer, Passive sicherheit von kraftfahrzeugen, Vieweg+Teubner Verlag / GWV Fachverlage, Wiesbaden, 2009.

[57] K. Ueno, J.W. Melvin, L. Li, J.W. Lighthall, Development of Tissue Level Brain Injury Criteria by Finite Element Analysis, J. Neurotrauma. 12 (1995) 695–706.

[58] M. Ghajari, P.J. Hellyer, D.J. Sharp, Computational modelling of traumatic brain injury predicts the location of chronic traumatic encephalopathy pathology, Brain. 140 (2017) 333–343.

[59] H. Samaka, F. Tarlochan, Finite element (FE) human head models - literature review, Int. J. Sci. Technol. Res. 2 (2013) 17–31.

[60] S. Kleiven, Predictors for traumatic brain injuries evaluated through accident reconstructions., Stapp Car Crash J. 51 (2007) 81–114.

[61] J. Newman, M. Beusenberg, E. Fournier, N. Shewchenko, C. Withnall, A. King, K. Yang, L. Zhang, J. McElhaney, L. Thibault, G. Mcginnis, A new biomechanical assessment of mild traumatic brain injury. Part I: Methodology, Proc. 1999 Int. Ircobi Conf. Biomech. Impact, Sept. 23-24, 1999.

[62] H.-S. Kang, R. Willinger, B.M. Diaw, B. Chinn, Validation of a 3D anatomic human head model and replication of head impact in motorcycle accident by finite element modeling, in: 1997.

[63] A.C. Bain, D.F. Meaney, Tissue-level thresholds for axonal damage in an experimental model of central nervous system white matter injury, J. Biomech. Eng. 122 (2000) 615.

[64] L. Zhang, K.H. Yang, A.I. King, A proposed injury threshold for mild traumatic brain injury, J. Biomech. Eng. 126 (2004) 226.

[65] www.slideshare.net/cervical vertebra.

[66] F.A. Pintar, N. Yoganandan, L. Voo, J.F. Cusick, D.J. Maiman, A. Sances, Dynamic Characteristics of the Human Cervical Spine, in: 1995.

[67] R.W. Nightingale, J.H. McElhaney, D.L. Camacho, M. Kleinberger, B.A. Winkelstein, B.S. Myers, The Dynamic Responses of the Cervical Spine: Buckling, End Conditions, and Tolerance in Compressive Impacts, in: 1997.

[68] R. Ferrari, The whiplash encyclopedia : the facts and myths of whiplash, Jones and Bartlett Publishers, 2006.

[69] E. Moffatt, A. Siegel, D. Huelke, Nahum A., The biomechanics of automotive cervical fractures, in: Am. Assoc. Automot. Med. Annu. Conf., 1978: pp. 151–168.

[70] O. Boström, M.Y. Svensson, B. Aldman, H.A. Hansson, Y. Häland, P. Lövsund, T. Seeman, A. Suneson, A. Säljö, T. Örtengren, A new neck injury criterion candidate based on injury findings in the cervical spinal ganglia after experimental neck extension trauma, in: IRCOBI, 2016.

[71] K.D. Klinich, R.A. Saul, G. Auguste, S. Backaitis, M. Klienberger, Techniques for developing child dummy protection reference values, 1996.

[72] M. Kleinberger, E. Sun, R. Eppinger, S. Kuppa, R. Saul, Development of improved injury criteria for the assessment of advanced automotive restraint systems, 1998.

[73] P. Prasad, R.P. Daniel, A biomechanical analysis of head, neck, and torso injuries to child surrogates due to sudden torso acceleration, in: 28th Stapp Car Crash Conf., 1984.

[74] Occupant crash protection, FMVSS NO. 208.

[75] J.A. DeWit, D.S. Cronin, Cervical spine segment finite element model for traumatic injury prediction, J. Mech. Behav. Biomed. Mater. 10 (2012) 138–150.

[76] B. Khuyagbaatar, K. Kim, W.M. Park, Y.H. Kim, Influence of sagittal and axial types of ossification of posterior longitudinal ligament on mechanical stress in cervical spinal cord: A finite element analysis, Clin. Biomech. 30 (2015) 1133–1139.

[77] T. Mustafy, M. El-Rich, W. Mesfar, K. Moglo, Investigation of impact loading rate effects on the ligamentous cervical spinal load-partitioning using finite element model of functional spinal unit C2–C3, J. Biomech. 47 (2014) 2891–2903.

[78] K. Wang, H. Wang, Z. Deng, Z. Li, H. Zhan, W. Niu, Cervical traction therapy with and without neck support: A finite element analysis, Musculoskelet. Sci. Pract. 28 (2017) 1–9.

[79] T. Katsuhara, Y. Takahira, S. Hayashi, Y. Kitagawa, T. Yasuki, Analysis of Driver Kinematics and Lower Thoracic Spine Injury in World Endurance Championship Race Cars during Frontal Impacts, SAE Int. J. Transp. Saf. 5 (2017) 2017-01–1432.

[80] L. Chang, G. Chang, J. Huang, S. Huang, D. Liu, C. Chang, Finite element analysis of the effect of motorcycle helmet materials against impact velocity, J. Chinese Inst. Eng. 26 (2003) 835–843.

[81] A.H.S. Holbourn, Mechanics of head injuries, Lancet. 242 (1943) 438–441.

[82] H.L.. Van Den Bosch, Crash helmet testing and design specifications, 2006.

[83] L. Charles, H.. Roth, Crash helmet, US 2625683, 1953.

[84] F.M. Shuaeib, A.M.S. Hamouda, R.S. Radin Umar, M.M. Hamdan, M.S.J. Hashmi, Motorcycle helmet - Part II. Materials and design issues., J. Mater. Process. Technol. 123 (2002) 406–421.

[85] http://bikegear.co.za.

[86] D.H. Blanco, A. Cernicchi, U. Galvanetto, FE modeling of innovative helmet liners, in: 11th Int. LS-DYNA Conf., 2010.

[87] MIPS, www.mipsprotection.com.

[88] P. Halldin, A. Gilchrist, N.J. Mills, A new oblique impact test for motorcycle helmets, Int. J. Crashworthiness. 6 (2001) 53–64.

[89] www.dainese.com.

[90] www.mcmfactory.com.

[91] Neck Brace Adventure - Sport - REV'IT!.

[92] EVS Sports, evs-sports.com/snow/race-collars.

[93] MoveoBrace Carbon, www.moveosafety.com/en/moveobrace-carbon.

[94] C. Leatt, C. de Jongh, P.A. Keevy, White paper: Research and development efforts towards the production of the Leatt-Brace® Moto GPX unrestrained torso neck brace, Cape Town, 2012.

[95] L. Gorasso, N. Petrone, On-track measurements of neck movements and muscle activity during motocross sessions with or without neck brace, Procedia Eng. 60 (2013) 337–342.

[96] ECE 22.05, Uniform provisions concerning the approval of protective helmets and of their visors for drivers and passengers of motorcycles and mopeds, E/ECE/324 & E/ECE/TRANS/505 Addendum 21, Regulation No. 22, Revision 4, Geneva, 2002.

[97] www.mavet.it.

[98] www.davida-helmets.com.

[99] S. Farajzadeh Khosroshahi, M. Ghajari, U. Galvanetto, Assessment of motorcycle helmet chin bar design criteria with respect to basilar skull fracture using FEM, in: 10th Eur. LS-DYNA Conf., Wurzburg, Germany, 2015.

[100] R. Willinger, C. Deck, Model Based Head Injury Criteria for Head Protection Optimization, in: Helmet Perform. Des., London, 2013.

[101] IRCOBI - TBI Workshop, (2015).

[102] N. Bourdet, S. Mojumder, S. Piantini, C. Deck, M. Pierini, R. Willinger, Proposal of a new motorcycle helmet test method for tangential impact, in: Int. IRCOBI Conf. Biomech. Impacts, 2016: pp. 503–504.

[103] M. Nasim, M. Brasca, A. Cernicchi, E. Silani, Standards in PPE,a survey, 2016.

[104] Modulus of Toughness, www.engineeringarchives.com.

[105] L.J. Gibson, M.F. Ashby, Cellular Solids, Structure and Properties, 2nd ed., Cambridge Solid State Science Series, 1999.

[106] M.. Ashby, The properties of foams and lattices, Philos. Trans. R. Soc. A Math. Phys. Eng. Sci. 364 (2006) 15–30.

[107] N. Lloyd, K. Fletcher, CSM Library.

[108] ALVEOTEC - Innovation, www.alveotec.fr.

[109] Shau-T. Lee, N.S. Ramesh, Polymeric foams : mechanisms and materials, CRC Press, 2004.

[110] L.E. Murr, S.M. Gaytan, F. Medina, H. Lopez, E. Martinez, B.I. Machado, D.H. Hernandez, L. Martinez, M.I. Lopez, R.B. Wicker, J. Bracke, Next-generation biomedical implants using additive manufacturing of complex, cellular and functional mesh arrays, Philos. Trans. R. Soc. London A Math. Phys. Eng. Sci. 368 (2010).

[111] The Rhombic Dodecahedron, www.kjmaclean.com/Geometry/rhombicdodeca.html.

[112] Rhombic dodecahedra filling space, commons.wikimedia.org/wiki/File:Rhombic_ dodecahedra _ filling _ space.jpg.

[113] R.A. Freitas Jr., Nanomedicine, volume I: basic capabilities, Landes Bioscience, Georgetown, TX, 1999.

[114] Y. Sun, Q.M. Li, Effect of entrapped gas on the dynamic compressive behaviour of cellular solids, Int. J. Solids Struct. 63 (2015) 50–67.

[115] O. Lopez-Pamies, P.P. Castañeda, M.I. Idiart, Effects of internal pore pressure on closed-cell elastomeric foams, Int. J. Solids Struct. 49 (2012) 2793–2798.

[116] H.N.. Wadley, Multifunctional periodic cellular metals, Philos. Trans. R. Soc. A Math. Phys. Eng. Sci. 364 (2006) 31–68.

[117] G. Caserta, The use of honeycomb in the design of innovative helmets, Imperial College London, 2012.

[118] M. Doyoyo, D. Mohr, Microstructural response of aluminum honeycomb to combined out-of-plane loading, Mech. Mater. 35 (2003) 865–876.

[119] G.C. Jacob, J.F. Fellers, S. Simunovic, J.M. Starbuck, Energy absorption in polymer composites for automotive crashworthiness, J. Compos. Mater. 36 (2002) 813–850.

[120] J.J. Carruthers, A.P. Kettle, A.M. Robinson, Energy absorption capability and crashworthiness of composite material structures: a review, Appl. Mech. Rev. 51 (1998) 635.

[121] L. Grauers, R. Olsson, R. Gutkin, Energy absorption and damage mechanisms in progressive crushing of corrugated NCF laminates: Fractographic analysis, Compos. Struct. 110 (2014) 110–117.

[122] R.M. Robert M. Jones, Mechanics of composite materials, Taylor & Francis, 1999.

[123] Materials simulation software for composite materials, www.e-xstream.com/ materials/ composites.

[124] L. Yang, Z. Wu, D. Gao, X. Liu, Microscopic damage mechanisms of fibre reinforced composite laminates subjected to low velocity impact, Comput. Mater. Sci. 111 (2016) 148–156.

[125] D. Hull, A unified approach to progressive crushing of fibre-reinforced composite tubes, Compos. Sci. Technol. 40 (1991) 377–421.

[126] J.W. Hetrick, Safety cushion assembly for automotive vehicles, US patent NO. 2649311 A, 1953.

[127] Subaru Air Bag Recall, Patriot Subaru of North Attleboro Serving Providence, www.patriotsubaruofna.com/subaru-airbag-recall.htm.

[128] New Airbag in the 2013 Dodge Dart | Advanced Extrication, advancedextrication.com.

[129] Space Parachutes - Inflatable Systems | Airborne Systems, airborne-sys.com/experience/space-parachutes-inflatable-military.

[130] NASA - Seat Attenuation Designs for Orion, www.nasa.gov/offices/nesc/home /Feature _ Seat_Attenuation.html.

[131] S. Do, O. de Weck, A personal airbag system for the Orion Crew Exploration Vehicle, Acta Astronaut. 81 (2012) 239–255.

[132] J.K. Cole, D.E. Waye, BAG: a code for predicting the performance of a gas bag impact attenuation system for the PATHFINDER Lander, 1993.

[133] Impact protection | Shock absorption | D3O, www.d3o.com.

[134] PORON Urethanes, www.rogerscorp.com/ems/poron.

[135] L. Cui, S. Kiernan, M.D. Gilchrist, Designing the energy absorption capacity of functionally graded foam materials, Mater. Sci. Eng. A. 507 (2009) 215–225.

[136] M.S. Attia, S.A. Meguid, H. Nouraei, Nonlinear finite element analysis of the crush behaviour of functionally graded foam-filled columns, Finite Elem. Anal. Des. 61 (2012) 50–59.

[137] Koroyd Advanced Engineered Cores & Engineered Protection, koroyd.com/.

[138] D.J. Leo, Engineering analysis of smart material systems, John Wiley & Sons, 2007.

[139] S.S. Deshmukh, G.H. Mckinley, Adaptive energy-absorbing materials using field-responsive fluid-impregnated cellular solids, Smart Mater. Struct. 16 (2007) 106–113.

[140] M.G. Rashed, M. Ashraf, R.A.W. Mines, P.J. Hazell, Metallic microlattice materials: A current state of the art on manufacturing, mechanical properties and applications, Mater. Des. 95 (2016) 518–533.

[141] L.C. Montemayor, J.R. Greer, Mechanical response of hollow metallic nanolattices: combining structural and material size effects, J. Appl. Mech. 82 (2015) 71012.

[142] S. McKown, Y. Shen, W.K. Brookes, C.J. Sutcliffe, W.J. Cantwell, G.S. Langdon, G.N. Nurick, M.D. Theobald, The quasi-static and blast loading response of lattice structures, Int. J. Impact Eng. 35 (2008) 795–810.

[143] Nanoscale lattice is world's smallest, newatlas.com/worlds-smallest-lattice/41633.

[144] J.J. Rimoli, F. Casadei, M. Ruzzene, Multiphase materials for stress wave steering and methods of providing same, US patent NO. 20150285327 A1, 2013.

[145] H.W. Wang, H.W. Zhou, L.L. Gui, H.W. Ji, X.C. Zhang, Analysis of effect of fiber orientation on Young's modulus for unidirectional fiber reinforced composites, Compos. Part B Eng. 56 (2014) 733–739.

[146] B. Krour, F. Bernard, A. Tounsi, Fibers orientation optimization for concrete beam strengthened with a CFRP bonded plate: a coupled analytical–numerical investigation, Eng. Struct. 56 (2013) 218–227.

[147] J.W.S. Hearle, E. Textile Institute (Manchester, High-performance fibres, CRC Press, 2001.

[148] E. Mahdi, A.M.S. Hamouda, T.A. Sebaey, The effect of fiber orientation on the energy absorption capability of axially crushed composite tubes, 2014.

[149] Honeywell Spectra, www.honeywell-spectra.com/.

[150] S. Tsampas, M. Juntikka, M. Willows, D5.5-Technical report on phase 1 tests, with video recordings and measurements, CR15-055 confidential report, 2015.

[151] J. Rössler, Development of a stiffness-modifiable composite, Technical report no 138/2014, Gothenburg, Sweden.

[152] A. Bachinger, E. Marklund, J. Rössler, P. Hellström, L.E. Asp, Stiffness-modifiable composite for pedestrian protection, in: ECCM16 – 16th Eur. Conf. Compos. Mater., Seville, Spain, 2014.

[153] C. Tridech, H.A. Maples, P. Robinson, A. Bismarck, High performance composites with active stiffness control., ACS Appl. Mater. Interfaces. 5 (2013) 9111–9.

[154] L. Jakobsson, T. Broberg, H. Karlsson, A. Fredriksson, N. Gråberg, C. Gullander, M. Lindman, Pedestrian airbag technology – a production system, in: 23rd Int. Tech. Conf. Enhanc. Saf. Veh., Seoul, South Korea, 2013.

[155] Exterior Automobile Airbags, myscienceacademy.org/2013/01/30/exterior-automobile-airbags.

[156] C. Lu, Mobile phone anti-collision safe airbag, CN202354640 U, 2012.

[157] Honda creates smartphone case with air bags, www.phonearena.com/news/Honda-creates-smartphone-case-with-air-bags_id50007.

[158] M. Fahlstedt, P. Halldin, S. Kleiven, The protective effect of a helmet in three bicycle accidents - A finite element study, Accid. Anal. Prev. 91 (2016) 135–143.

[159] I.J. Gnip, S.A. Veyelis, V.I. Kersulis, S.I. Vaitkus, Deformability and strength of expanded polystrene (EPS) under short-term shear loading, Mech. Compos. Mater. 43 (2007) 85–94.

[160] F. Bartl, H. Klaus, R. Dallner, O. Huber, Material behaviour of a cellular composite undergoing large deformations, Int. J. Impact Eng. 36 (2009) 667–679.

[161] N. Mills, A. Gilchrist, Modelling the indentation of low density polymer foams, Cell. Polym. 19 (2000) 389–412.

[162] N. Mills, A. Gilchrist, Shear and compressive impact of PP bead foam, Cell. Polym. 18 (1999) 157–174.

[163] E.E. Gdoutos, I.M. Daniel, K.A. Wang, Failure of cellular foams under multiaxial loading, Compos. - Part A Appl. Sci. Manuf. 33 (2002) 163–176.

[164] Y. Chen, R. Das, M. Battley, Finite element analysis of the compressive and shear responses of structural foams using computed tomography, Compos. Struct. 159 (2017) 784–799.

[165] LS-Dyna keyword user's manual, 2014.

[166] M. Ghajari, C. Deck, U. Galvanetto, L. Iannucci, R. Willinger, Development of numerical models for the investigation of motorcyclists accidents, in: 7th Eur. LS-Dyna Conf., 2009.

[167] N.J. Mills, S. Wilkes, S. Derler, A. Flisch, FEA of oblique impact tests on a motorcycle helmet, Int. J. Impact Eng. 36 (2009) 913–925.

[168] A. Matzenmiller, J. Lubliner, R.L. Taylor, A constitutive model for anisotropic damage in fiber-composites, Mech. Mater. 20 (1995) 125–152.

[169] X. Xiao, M.E. Botkin, N.L. Johnson, Axial crush simulation of braided carbon tubes using MAT58 in LS-DYNA, Thin-Walled Struct. 47 (2009) 740–749.

[170] K. Schweizerhof, K. Weimar, T. Munz, T. Rottner, Crashworthiness analysis with enhanced composite material models in LS-DYNA—merit and limits, in: Fifth Int. LS-DYNA Conf., Southfield, Michigan, 1998.

[171] Altair, HYPERMESH, 14.0.

[172] S. Ouellet, D. Cronin, M. Worswick, Compressive response of polymeric foams under quasi-static, medium and high strain rate conditions, Polym. Test. 25 (2006) 731–743.

[173] D. Whisler, H. Kim, Experimental and simulated high strain dynamic loading of polyurethane foam, Polym. Test. 41 (2015) 219–230.

[174] V. Tinard, C. Deck, N. Bourdet, R. Willinger, Motorcyclist helmet composite outer shell characterisation and modelling, Mater. Des. 32 (2011) 3112–3119.

[175] R. Willinger, D. Baumgartner, T. Guimberteau, Dynamic characterization of motorcycle helmets: Modelling and coupling with the human head, J. Sound Vib. 235 (2000) 611–625.

[176] THUMS, AM50 Occupant Model, Academic Version 5.0, 2015.

[177] A. Chawla, S. Mukherjee, D. Mohan, S. Jain, Validation of the cervical spine model in Thums, Proc. 19th Int. Tech. Conf. Enhanc. Saf. Veh. (2005) 1–11.

[178] J.C. Roberts, T.P. Harrigan, E.E. Ward, T.M. Taylor, M.S. Annett, A.C. Merkle, Human head–neck computational model for assessing blast injury, J. Biomech. 45 (2012) 2899–2906.

[179] K.M. Tse, L. Bin Tan, S.J. Lee, S.P. Lim, H.P. Lee, Investigation of the relationship between facial injuries and traumatic brain injuries using a realistic subject-specific finite element head model, Accid. Anal. Prev. 79 (2015) 13–32.

[180] S. Guha, LSTC_NCAC Hybrid III 50th Dummy Positioning & Post-Processing, 2014.

[181] A. Bartsch, E. Benzel, V. Miele, D. Morr, V. Prakash, Hybrid III anthropomorphic test device (ATD) response to head impacts and potential implications for athletic headgear testing., Accid. Anal. Prev. 48 (2012) 285–91.

[182] Snell 2015, STANDARD FOR PROTECTIVE HEADGEAR For Use with Motorcycles and Other Motorized Vehicles, 2015.

[183] V.S. Deshpande, M.F. Ashby, N.A. Fleck, Foam topology: bending versus stretching dominated architectures, Acta Mater. 49 (2001) 1035–1040.

[184] E. Svensson, Material characterization of 3D-printed energy-absorbent polymers inspired by nature, CHALMERS University of Technology, 2017.

[185] R.T. Moura, L.M. Mazzariol, A.H. Clausen, M. Langseth, M. Alves, Axial Loading of Cylinders Made of Nylon with Nano-particles, Proc. IMPLAST 2010 Conf. (2010).

[186] M.A. Forero Rueda, L. Cui, M.D. Gilchrist, Optimisation of energy absorbing liner for equestrian helmets. Part I: Layered foam liner, Mater. Des. 30 (2009) 3405–3413.

[187] A. Gilchrist, N.J. Mills, Modelling of the impact response of motorcycle helmets, Int. J. Impact Eng. 15 (1994) 201–218.

[188] N.J. Mills, A. Gilchrist, Finite-element analysis of bicycle helmet oblique impacts, Int. J. Impact Eng. 35 (2008) 1087–1101.

[189] K.P. Krantz, Head and neck injuries to motorcycle and moped riders-with special regard to the effect of protective helmets., Injury. 16 (1985) 253–8.

[190] R. Ramli, J. Oxley, F.M. Noor, N.K. Abdullah, M.S. Mahmood, A.K. Tajuddin, R. McClure, Fatal injuries among motorcyclists in Klang Valley, Malaysia, J. Forensic Leg. Med. 26 (2014) 39–45.

[191] G. Badiali, E. Pasquini, O. Piccin, C. Marchetti, Injury risk related to the helmet strap: Mandible and hyoid bone fractures with a hyoepiglottic ligament lesion, 2010.

[192] J. V Ouellet, D.R. Thom, T. Smith, H.H. Hurt, Helmets and neck injuries in fatal motorcycle crashes, in: Int. Mot. Saf. Conf., Orange County, US, 2013.

[193] R.W. Nightingale, J.H. McElhaney, W.J. Richardson, B.S. Myers, Dynamic responses of the head and cervical spine to axial impact loading, J. Biomech. 29 (1996) 307–318.

[194] N. Bourdet, R. Willinger, Coupled head–neck–torso and seat model for car seat optimization under rear-end impact, J. Sound Vib. 313 (2008) 891–907.

[195] J. Östh, M. Mendoza-Vazquez, F. Sato, M.Y. Svensson, A. Linder, K. Brolin, A female head–neck model for rear impact simulations, J. Biomech. 51 (2017) 49–56.

[196] A.M. Hering, S. Derler, Motorcycle helmet drop tests using a hybrid III dummy, in: IRCOBI, Montpellier, France, 2000: pp. 307–321.

[197] N. Yoganandan, A. Sances, D.J. Maiman, J.B. Myklebust, P. Pech, S.J. Larson, Experimental spinal injuries with vertical impact., Spine (Phila. Pa. 1976). 11 (1986) 855–60.

[198] R.W. Nightingale, B.J. Doherty, B.S. Myers, J.H. McElhaney, W.J. Richardson, The influence of end condition on human cervical spine injury mechanisms, in: Proc. 35th Stapp Car Crash Conf., 1991: pp. 391–400.

[199] H.W. Wang, H.W. Zhou, L.L. Gui, H.W. Ji, X.C. Zhang, Analysis of effect of fiber orientation on Young's modulus for unidirectional fiber reinforced composites, Compos. Part B Eng. 56 (2014) 733–739.

[200] E. Mahdi, A.M.S. Hamouda, T.A. Sebaey, The effect of fiber orientation on the energy absorption capability of axially crushed composite tubes, Mater. Des. 56 (2014) 923–928.

[201] SAE J211-1 (1995): Instrumentation for Impact Test, Part 1, Electronic Instrumentation, 2007.

[202] J.D. Jobson, Multiple Linear Regression, in: Springer, New York, NY, 1991: pp. 219–398.

[203] M. Liu-Shindo, D.B. Hawkins, Basilar skull fractures in children., Int. J. Pediatr. Otorhinolaryngol. 17 (1989) 109–17.

[204] G.E. Voigt, G. Sköld, Ring fractures of the base of the skull., J. Trauma. 14 (1974) 494–505.

[205] C.H. Chang, L.T. Chang, G.L. Chang, S.C. Huang, C.H. Wang, Head injury in facial impact--a finite element analysis of helmet chin bar performance., J. Biomech. Eng. 122 (2000) 640–6.

[206] B. Fréchède, A. McIntosh, R. Grzebieta, M. Bambach, Hybrid III ATD in inverted impacts: influence of impact angle on neck injury risk assessment., Ann. Biomed. Eng. 37 (2009) 1403–14.

[207] B. Herbst, S. Forrest, D. Chng, A. Sances, Fidelity of Anthropometric test dummy necks in rollover accidents, in: Proc. 16th Int. Tech. Conf. Enhanc. Saf. Veh., Washington, 1998.

[208] A. Cernicchi, U. Galvanetto, R. Olsson, Virtual testing of composite motorcycle helmets, Int. J. Mod. Phys. B. 22 (2008) 1705–1711.

[209] N. Gupta, A functionally graded syntactic foam material for high energy absorption under compression, Mater. Lett. 61 (2007) 979–982.